

Middlesex University Research Repository:

an open access repository of
Middlesex University research

<http://eprints.mdx.ac.uk>

Cornwell, K J, 1970.
Thermoelectric Generation Using Molten Salts.
Available from Middlesex University's Research Repository.

Copyright:

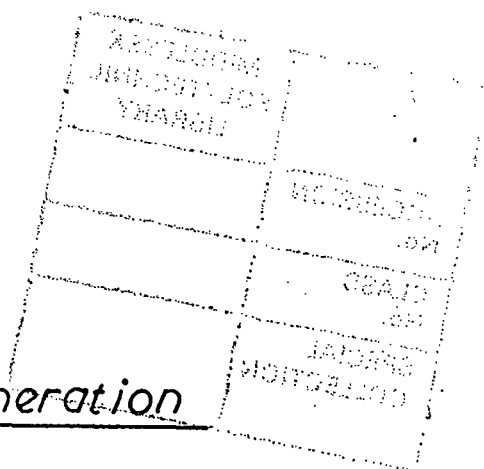
Middlesex University Research Repository makes the University's research available electronically.

Copyright and moral rights to this thesis/research project are retained by the author and/or other copyright owners. The work is supplied on the understanding that any use for commercial gain is strictly forbidden. A copy may be downloaded for personal, non-commercial, research or study without prior permission and without charge. Any use of the thesis/research project for private study or research must be properly acknowledged with reference to the work's full bibliographic details.

This thesis/research project may not be reproduced in any format or medium, or extensive quotations taken from it, or its content changed in any way, without first obtaining permission in writing from the copyright holder(s).

If you believe that any material held in the repository infringes copyright law, please contact the Repository Team at Middlesex University via the following email address:
eprints@mdx.ac.uk

The item will be removed from the repository while any claim is being investigated.



Thermoelectric Generation

using

Molten Salts



A thesis submitted to the Council for
National Academic Awards for the degree
of Doctor of Philosophy, May 1970.

By K.J.Cornwell, B.Sc.

Enfield College of Technology.

Synopsis

Thermoelectric generation of electrical energy from heat energy has been reviewed, the history of the subject has been reassessed, and the materials used for thermoelectric generation have been critically examined. The suitability of a material for thermoelectric generation is determined by the product of the figure of merit, Z , and the absolute temperature, T . The figure of merit of a material depends upon the thermoelectric potential, α , and the ratio of the electrical conductivity, σ , to the thermal conductivity, K :

$$Z T = \alpha^2 T \sigma / K$$

The most suitable semiconductor materials have (dimensionless) ZT values between 0.5 and 1, and the most suitable molten salts developed in this work have ZT values of about 0.5. The advantages of molten salt thermocells over semiconductor thermoelements are the absence of contact junction, doping and thermal expansion problems, and the low cost of the materials. The major disadvantage is the mass transfer between the electrodes, and this caused the failure of many of the initial generation thermocells designed by the author.

Pure molten salts are found to have ZT values ranging up to 0.3 and mixtures of salts have been examined in an attempt to increase the ZT value. The $\text{AgCl} - \text{AgI}$ system has been studied as an example of a common-cation mixture. The thermoelectric potential has been measured up to a temperature of about 1200°C and the thermal conductivity has been measured using a transient hot wire method which was specially adapted for measurements on molten salts at high temperatures. The maximum ZT value is 0.4 for the $\text{AgCl} - \text{AgI}$ eutectic mixture. The $\text{AgCl} - \text{CuCl} - \text{LiCl}$ system has been studied as an example of a common anion mixture. A theory to the thermoelectric potential of common anion mixtures has been developed and partially substantiated by experiment. Some salt mixtures are expected to have ZT values in excess of unity, yielding actual conversion efficiencies of 7 - 10%.

The thermoelectric effect in a molten salt thermocell is due to the flow of ions between the electrodes, and this flow of ions causes an electrochemical mass transfer. In addition there is a mass transfer between the electrodes caused by natural convection currents in the salt. A cell has been developed in which the mass transfer problem has been

overcome by arranging for the mechanisms just described to transfer metal from a molten metal alloy electrode to another electrode situated vertically above it, and allowing gravity to return the metal to the lower electrode. Convection currents have been decreased by inserting a fibrous material in the salt. Theory to the thermoelectric potential of a thermocell with alloy (rather than pure metal) electrodes has been developed and confirmed experimentally.

In order to demonstrate the feasibility of thermocell generation a small generator consisting of up to 44 of these cells has been constructed and has given an open circuit potential of 13 volts and a short circuit current of 0.6 amps. This is believed to be the first thermoelectric generator using a liquid thermoelectric material and also the first utilising the thermoelectric effect of the flow of ions.

Acknowledgments

For general supervision and many valuable suggestions I would like to thank my supervisors, Dr. D. T. Swift-Hook, Ph.D., M.A., M.Sc., F. Inst.P., F.I.E.E., head of electrical research at the Marchwood Engineering Laboratories of the Central Electricity Generating Board, and Dr. B. J. Zaczek, M.Eng., Ph.D, D.I.C., M.I. Mech.E., M.Inst,F., head of the fuel technology section at Enfield College. Gratitude is also expressed to Dr. J. R. W. Warn and Dr. R. W. Dyson, both of Enfield College, for many discussions on the electrochemical and thermodynamic aspects of this work.

The general helpfulness of the Enfield College Laboratory technicians, especially Mr. J. Webster, is acknowledged. Finally I would like to thank my wife for typing the manuscript and for giving encouragement at times when I would have discontinued this work.

The Contents

<u>Introduction and Notation</u>	<u>Page</u>
<u>Chapter 1 Thermoelectric Generator Engineering.</u>	10
1.1. The fundamental principles of thermoelectric generation.	11
1.2. The historical background - a reassessment.	15
1.3. The engineering problems.	21
1.4. Thermoelectric generation today.	25
<u>Chapter 2 Thermoelectric Materials.</u>	32
2.1. Solid metals and semiconductors.	33
2.2. Electronically conducting liquids.	34
2.3. Ionically conducting liquids.	38
<u>Chapter 3 The Thermal and Electrical Conductivity of Molten Salts.</u>	41
Introduction	42
3.1. Correlation between the measurements and the theory on the thermal conductivity of molten salts.	43
3.2. Experimental results using the transient hot wire method.	51
3.3. The electrical conductivity of molten salts.	71
<u>Chapter 4 The Thermoelectric Potential of Pure Molten Salts.</u>	73
4.1. Theory to the thermoelectric potential of pure molten salts.	74
4.2. Literature review of cationic thermoelectric potential measurements.	79
4.3. Methods of measuring the cationic thermoelectric potential.	82
4.4. Methods of estimating the cationic thermoelectric potential.	87
<u>Chapter 5 The Conversion Efficiency and Engineering Problems of Thermocell Generation.</u>	89
5.1. The conversion efficiency of a thermocell and the figure of merit of the salt.	90
5.2. The Z_{gT} values of some pure molten salts.	94
5.3. Configurational and Electrochemical problems of thermocell generation.	96
<u>Chapter 6 Common - Cation Salt Mixtures -- the AgCl - AgI System</u>	104
6.1. The equilibrium diagram.	105
6.2. The thermoelectric potential of the AgCl - AgI eutectic mixture to high temperatures.	107
6.3. The Z_{gT} value of the AgCl-AgI eutectic mixture.	111

	<u>Page</u>
<u>Chapter 7</u> <u>The Thermoelectric Potential of Cells with Alloy</u> <u>Electrodes — The Ag(Bi)_{T_h} AgCl - AgI/T_c Ag(Bi)</u> <u>System.</u>	113
7.1. Theory to the thermoelectric potential.	114
7.2. Experimental results and discussion.	117
7.3. Trial of the 'H' cell configuration for thermoelectric generation.	123
<u>Chapter 8.</u> <u>The Mass Transfer Problem in Generation Thermocells.</u>	127
8.1. Electrochemical mass transfer.	128
8.2. Convective mass transfer.	136
8.3. Trials of various vertical tube configurations for thermocell generation.	141
<u>Chapter 9.</u> <u>Common Anion Salt Mixtures — The AgCl, CuCl,</u> <u>LiCl System.</u>	162
9.1. Introduction.	163
9.2. The theoretical thermoelectric potential.	165
9.3. The experimental results.	169
9.4. The Z _s T values.	175
<u>Chapter 10.</u> <u>Trials of a Continuously Operating Thermocell and</u> <u>Conclusions on the Future Prospects for Thermocell</u> <u>Generation.</u>	177
10.1. Tests on a continuously operating vertical tube thermo- cell.	178
10.2. Tests of a small generator.	180
10.3. The prospects for thermocell generation.	188
10.4. Conclusion.	190
<u>References.</u>	191

Introduction and Notation

(The introduction to the subject matter is given as chapters 1 and 2. The following notes are concerned with the general arrangement and notation used in this thesis).

The object of the research described in this thesis was to find a method of continuously generating electrical energy from heat energy using the thermoelectric effect of the flow of ions in a molten salt. During much of this pioneer work the author had no idea of the type of thermocell which would be suitable for continuous generation, and many of the earlier designs were rejected owing to unforeseen engineering difficulties. Nevertheless knowledge gleaned from these unsuccessful attempts was generally used in subsequent thermocell designs. Some details of these attempts are included in this thesis to show how the final design emerged, and to prevent future researchers from covering the same ground.

After much consideration it was decided to arrange the thesis in a basically chronological manner. Not only are the contents more readable, but the necessity for certain of the tests is more apparent when presented in this way. The contents, (as listed on page 5), are sufficiently sectionalised to give rapid selection of topics. The theory to the thermoelectric potential of molten salts and their mixtures, for example, is given in sections 4.1, 6.2, and 9.2. Reference details are arranged in an author index at the end of the thesis.

Conventional notation is used throughout the thesis and the terms are defined when they are first introduced in the text. It is felt that some apology is necessary for the use of ionic entropy terms with up to five different indicies and sufficies as encountered in chapters 4, 6 and 9. These terms may be clarified to some extent by noting that it is common practice to denote a partial molal quantity by a single bar and a molal transfer quantity by an asterisk. The species to which the quantity relates (such as a metal, an ion or an electron) is always given as a suffix. Hence the term \bar{S}_{Mz+} is the partial molal entropy of a metal ion (with z charges) in a mixture, and Q_x^* is the molal heat of transfer of a uni-valent anion in a mixture. S. I. units are used except in the cases of the electrical

and thermal conductivities where the author has noticed no evidence in recent literature of any departure from units of $\Omega^{-1} \text{ cm}^{-1}$ and $\text{watt cm}^{-1} \text{ K}^{-1}$ respectively. (The centimetre is not strictly allowable in S. I. units as it is not a triplet power of a metre). A summary of the frequently occurring notation follows.

- A Area of the electrode in contact with the electrolyte, or cross-sectional area of a solid thermoelement.
- a_k Activity of species k.
- c Specific heat at constant pressure.
- E Electrical potential, (also V).
- e^- Electron.
- F Faraday, (96 490 coulomb equiv⁻¹).
- G Molal Gibbs free energy.
- h Heat transfer coefficient.
- I Electrical current.
- I_{sc} Short circuit current.
- K Thermal conductivity.
- K_c Thermal equilibrium constant based on concentrations.
- K_a Thermal equilibrium constant based on activities,
- l Length between electrodes in a thermocell, or length of a thermoelement.
- m Mass.
- \dot{m} Mass transfer rate.
- Q or q Heat energy flow.
- Q_k^* Molal heat of transfer of species k.
- R Universal gas constant, (8.314 J g-mole⁻¹ K⁻¹).
- R_c Electrical resistance of cell.
- R_l Electrical resistance of external load.
- S_k Molal entropy of species k.
- S_k^E Excess molal entropy of species k.
- S_k^* Molal entropy of transfer of species k, ($= Q_k^* / T$).
- \bar{S}_k Partial molal entropy of species k.
- \bar{S}_k^- Total transported molal entropy of species k, ($= \bar{S}_k + S_k^*$).
- ΔS_k^f Molal entropy of fusion of k.
- T Temperature.

T_l	Liquidus temperature.
t	Time.
t_k	Transference number of ion k .
V	Electrical potential, (also E).
V_{oc}	Open circuit potential.
V_{cc}	Closed circuit potential.
x_k	Molal concentration of species k .
Z_c	Figure of merit of a thermoelectric couple.
Z_m	Figure of merit of a single material, $(= \alpha^2 \sigma / K)$.
Z_s	Figure of merit of a molten salt, $(= \alpha_s^2 \sigma_s / K_s)$.
α	Thermoelectric potential, $(= dE/dT)$.
σ	Electrical conductivity.
π	Peltier coefficient.
τ	Thomson coefficient.

Chapter 1

Thermoelectric Generator Engineering

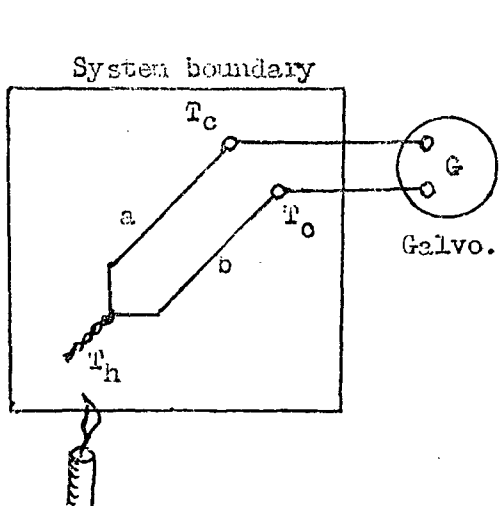
Contents:

- 1.1. The fundamental principles of thermoelectric generation.
- 1.2. The historical background - a reassessment.
 - 1.2.1. Discovery of the thermoelectric effects.
 - 1.2.2. Thermoelectric generation before the second world war.
 - 1.2.3. Thermoelectric generation in the semiconductor age.
- 1.3. The engineering problems.
 - 1.3.1. Thermal and electrical energy transfer problems.
 - 1.3.2. Material property problems.
 - 1.3.3. Design and economic problems.
- 1.4. Thermoelectric generation today.
 - 1.4.1. Fossil - fuel fired generators.
 - 1.4.2. Isotope and reactor generators.
 - 1.4.3. The future of thermoelectric generators.

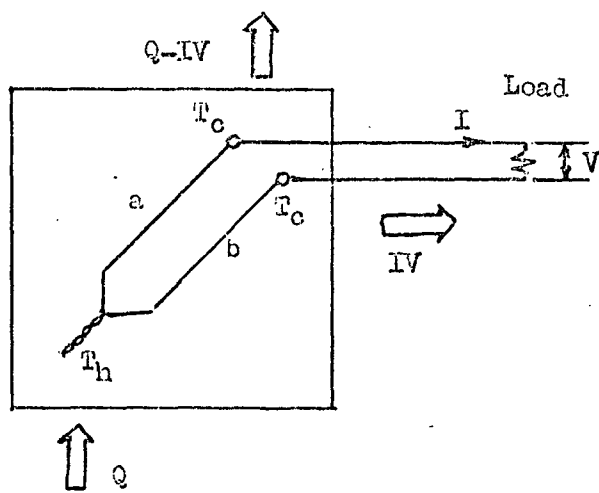
1.1. The fundamental principles of thermoelectric generation.

When one end of a metal wire is heated and the other end is kept cool so that a temperature gradient is established along its length an electrical potential difference is found to exist between the ends. This potential can be measured with respect to another wire of a different material acting over a similar temperature difference as shown below. The pair of wires is then called a thermoelectric couple or more commonly a thermocouple and the voltage developed between the two cool ends is known as the thermoelectric voltage. This voltage depends upon the temperature difference between the hot and cool junctions, and the rate of change of the open circuit voltage E with respect to this temperature difference is called the Seebeck coefficient, the thermoelectric potential for one degree temperature difference or less precisely but more commonly just the thermoelectric potential α . Thus $\alpha = dE/dT$.

A thermocouple is commonly used for measuring temperature difference but it may also be used for conversion of heat energy into work in the form of electrical energy and as such it is a heat engine. The thermal efficiency of this engine η (that is the ratio of the electrical energy output IV and the heat energy input Q) is then some fraction of the efficiency of a reversible engine η_{max} operating between the same maximum and minimum temperatures:



Temperature measurement thermocouple



Thermoelectric engine

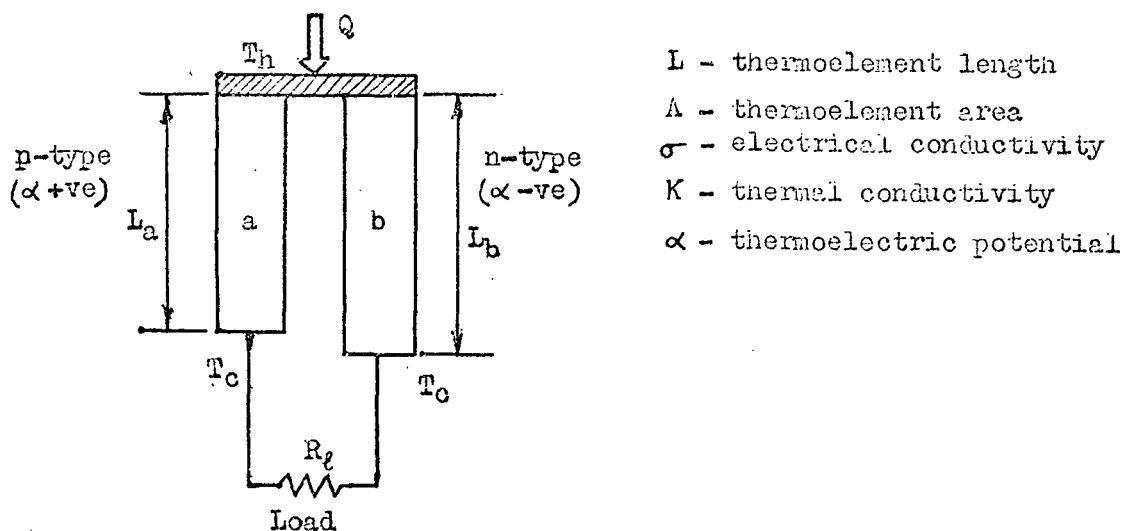
$$\eta_{\max} = \frac{T_h - T_c}{T_h}$$

$$\eta = \frac{IV}{Q} = \phi \frac{T_h - T_c}{T_h}$$

ϕ is termed the material efficiency and by substituting certain semiconductors for the metal wires a material efficiency of about 20% has been obtained .

The converse effect is possible where electrical energy is supplied to the thermoelectric circuit to give cooling of one junction and heating of the other and this is called the Peltier effect. The ratio of the quantity of heat transferred to or from a junction and the current required to transfer this heat energy is termed the Peltier coefficient Π ($= Q/I$). This effect has been used successfully for refrigeration, again using semiconductor materials.

The formula for the theoretical efficiency of a thermoelectric generator is derived in most textbooks on direct energy conversion (such as Spring 1965). For a generator of the following form:



it is found that the optimum geometrical configuration for maximum efficiency is given by:

$$\frac{(L/A)_a}{(L/A)_b} = \left[\frac{\sigma_a K_a}{\sigma_b K_b} \right]^{\frac{1}{2}} \quad \text{--- (1.1)}$$

The optimum efficiency is then found to be the product of the material efficiency and the Carnot efficiency:

$$\eta = \frac{(1 + \overline{Z_c T})^{\frac{1}{2}} - 1}{(1 + \overline{Z_c T})^{\frac{1}{2}} + T_c/T_h} \times \frac{T_h - T_c}{T_h} \quad (1.2)$$

where:

$\overline{Z_c T}$ = mean value of $Z_c T$ over the range from T_c to T_h

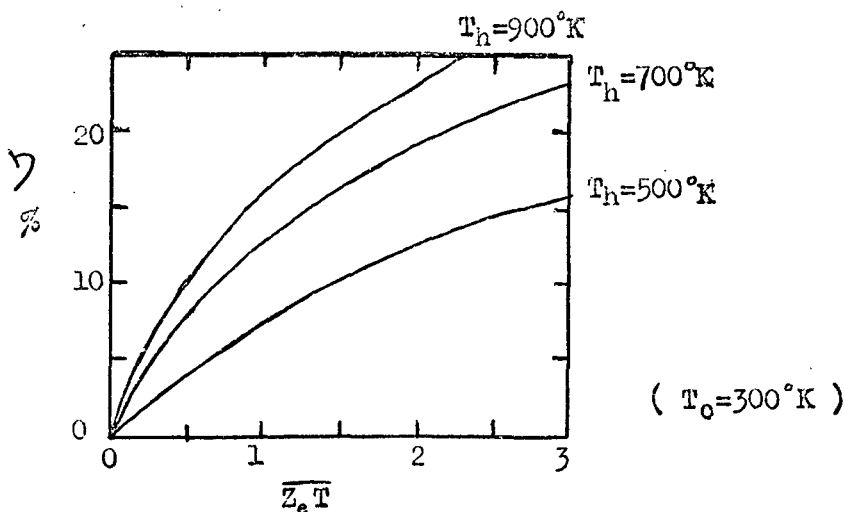
$$Z_c = \frac{(\alpha_a - \alpha_b)^2}{\left[\left(\frac{K_a}{\sigma_a} \right)^{\frac{1}{2}} + \left(\frac{K_b}{\sigma_b} \right)^{\frac{1}{2}} \right]^2} \quad (1.3)$$

Z_c is the only parameter of the efficiency equation which includes properties of the thermoelement materials and it is termed the figure of merit of the couple. The positive and negative semiconductor thermoelement materials are usually selected to have approximately equal values of σ , K and $|\alpha|$ in which case:

$$Z_c = \frac{\alpha^2 \sigma}{K} \equiv Z_m \quad (1.4)$$

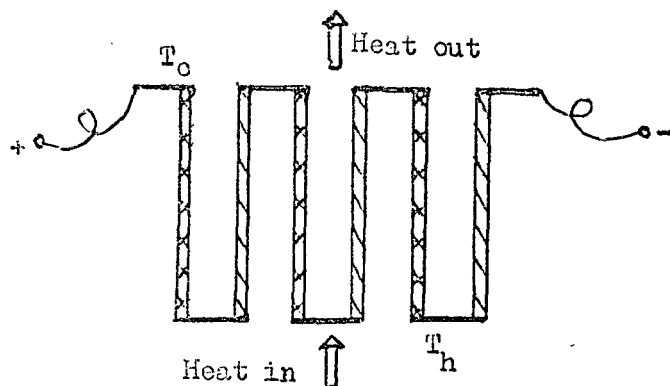
This ratio is used as the figure of merit of a single material Z_m .

The efficiency of the generator then depends on the hot and cold junction temperatures and the dimensionless parameter $\overline{Z_c T}$. The following curves show the variation of the optimum efficiency η with $\overline{Z_c T}$ at a cold junction temperature T_c of 300°K :



The best semiconductor materials for thermoelectric generation have a value of $\overline{Z_c T}$ between $\frac{1}{2}$ and 1.

The voltage obtainable from a single thermoelectric couple acting over a few hundred degrees temperature difference is of the order of 10 mV in the case of a metal and 100 mV in the case of some semiconductors. As early as 1823 Cumming pointed out that if useful voltages were to be obtained a number of couples must be connected electrically in series and thermally in parallel:



This arrangement is called a thermopile and is the basis on which thermoelectric generators are designed.

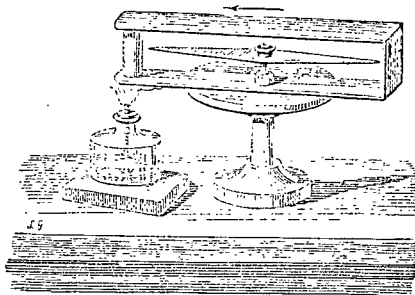
1.2. The historical background - a reassessment.

Popular text books on direct energy conversion generally give the impression that although thermoelectricity was reported by Seebeck in 1822 the effect was not used for practical generation until semiconductor technology was established in the early nineteen-fifties. In this section it is proposed to concentrate especially on thermoelectric generators between these two periods as an attempt to correct this particular misconception.

1.2.1. Discovery of the thermoelectric effects.

On the 21st July, 1820 Professor Oersted communicated his discovery of electromagnetic induction as a treatise to the leading natural philosophers of the day in each European country. This discovery and the subsequent research work it initiated rather overshadowed the observation of thermoelectricity a couple of years later.

During 1821 Thomas Johann Seebeck (1770 - 1831) was studying the results he had obtained using an apparatus consisting of a magnetic needle situated in an electrical circuit made of two different metals as shown below.



(From a wood engraving in Deschanel's 'Natural Philosophy', 1882).

He found that the needle deflected when one of the junctions was heated and he listed a number of metals in order according to the deflection they produced. Bismuth and antimony were correctly placed at the ends of this list. Unfortunately he did not appreciate that this effect related heat energy and electricity but thought that it related heat energy and magnetism (Seebeck 1822-3). He went on to give a rather novel explanation of gravity by asserting that the temperature difference between the equator and the poles produced a magnetic field.

About the same time James Cumming (1777 - 1861) a professor at Cambridge University also performed some experiments on the thermoelectric effect (Cumming, 1823). Although he was aware of Dr. Seebeck's explanation Professor Cumming correctly attributed the effect to a flow of electricity induced by the flow of heat. It would thus appear that this thermoelectric phenomenon which was later named the Seebeck effect should more deservedly have been attributed to Cumming. This possibly would have been the case if Cumming had not published his finds in the Transactions of the Cambridge Philosophical Society which was new and rather obscure at that time. But he was intimately connected with this Journal being one of the founder members and the first president of the Society. It is interesting to note that P. G. Tait (who himself made some notable contributions to thermoelectric theory) in the Rede Lecture at Cambridge on the 23rd May 1873 mentioned that Cumming 'seems in fact to have made an independent discovery of thermoelectricity'. (Tait, 1873).

During the next two years the thermoelectric potentials of metals and a few alloys were studied in greater detail by Seebeck and Cumming and also Antoine César Becquerel (1788 - 1878) in France (Becquerel 1826 and 1829). The work recorded is mainly concerned with the order of the metals in the 'thermoelectric power series' and the theoretical implications of the 'thermoelectric neutral point'. The former term is a misnomer as the power obtained from a thermocouple depends on the electrical resistance of the couple as well as the closed circuit potential, (i.e. V^2/R). In fact it was the open circuit thermoelectric potential which was measured although for the next century it was often called thermoelectric power and even today the term lingers on in some textbooks. The thermoelectric neutral point is the temperature at which some metals such as iron undergo a reversal in the direction of their thermoelectric potentials. This point will of course depend upon the metal with which the iron is compared.

It must be borne in mind that there was no clear conception of heat at this time. The caloric theory was still accepted by all but the most enlightened. It was not until 1841 that James Joule (1818-89) recorded his measurements on the heating effect of a current and some nine years later that he published his accurate values for the mechanical equivalent of heat energy. It is therefore not surprising that when Jean Charles Peltier (1785-1845) noticed that a junction of two metals could be cooled by the passage of a current he did not appreciate that heat energy was being transferred (Peltier 1834). This effect (which was later named after him) was certainly made clearer in 1838 by the famous demonstration of E. Lenz (1804-1865) to the St Petersburg Academy showing that water could be frozen by passing a current through a submerged bismuth-antimony junction. It is ^{not} generally appreciated that the water had previously been cooled to '33 or 34 °F' (Clark 1876). Michael Faraday (1791-1867) had not heard of Peltier's experiments in 1836 but he showed his understanding of the thermoelectric effect by a sentence written in his laboratory note book on 28th July of that year:

'Surely the converse of thermoelectricity ought to be obtained experimentally - Pass current through a circuit of antimony and bismuth.' (Whittaker 1951).

The mathematical relationship between the Peltier and Seebeck effects was reported by Sir William Thomson (later Lord Kelvin) in 1851. Basically he established that the Peltier heat coefficient Π is the product of the Seebeck coefficient α and the absolute temperature T . (i.e. $\Pi = \alpha T$). He also defined a 'specific heat of electricity' s in the form:

$$s = T \frac{d}{dT} \left(\frac{\Pi}{T} \right) \quad \text{---(1.5)}$$

It was nearly twenty years later that P. G. Tait established that the specific heat of electricity was proportional to the absolute temperature, ($s \propto T$). The coefficient s later became known as the Thomson coefficient, τ .

1.2.2. Thermoelectric Generation before the second world war.

The possibility that the thermoelectric effect could be used for generating electricity had certainly crossed the minds of a number of scientists by the early eighteen-thirties. Professor Cumming himself had made a small thermopile (shown in the previous section) and had also obtained continuous rotation by pivoting a closed thermoelectric circuit about a permanent magnet in such a fashion that the rotation caused the ends of the circuit to pass alternately over a spirit lamp. The potential produced by a thermopile consisting of thermoelectric pairs acting over about two hundred degrees centigrade is only of the order of a hundred millivolts. Michael Faraday wrote in January 1833:

'..... the very conditions under which it (thermoelectricity) is excited are such as to give no ground for expecting that it can be raised like common electricity to any degree of tension'

During the eighteen-sixties Dove in England, Farmer in America and Marcus in Germany were experimenting with trial generators which generally consisted of series connected bismuth and antimony couples. Marcus is reported to have devised 'a powerful form of battery' in which the positive element consisted of 10 parts copper, 6 parts zinc and 6 parts nickel and the negative element consisted of 12 parts antimony, 5 parts zinc and 5 parts bismuth'. (Clark 1876). He was obviously endeavouring to optimise the properties of the thermoelectric materials even as we are a hundred years later. The use of semiconductor materials is not modern either, for in 1869 Monsieur Becquerel demonstrated a thermopile using couples of galena (or natural Pb S) and iron.

One of the best of the early thermoelectric generators was built by M.C. Clamond of Paris about 1870. He developed his generators into a saleable proposition and in 1875 set up the Thermoelectric Generator Company with offices in Paris and a London manufactory. The Clamond generators contained elements of a zinc antimony alloy on the negative side, ^{and} tinned iron on the positive side. Each element was about two inches long with a cross-sectional area of about one inch squared. Gas and coke generators were manufactured with outputs ranging up to 34 volts with 680 elements. They were mainly used by the great electroplating houses of the day and by 1876 some 250 generators were being used in Britain, 300 in France and many in other countries.

On 11th May of that year Mr. Latimer Clark demonstrated one to the Society of Telegraph Engineers and Electricians (later I.E.E.). M. Clamond received the grand medal of the Société d' Encouragement pour l' Industrie Internationale in recognition of his inventions. (Details of the generators are given by Clark (1876) and the following discussions. A rather well used specimen of a Clamond Generator survives in the Science Museum, London).

Development of the fundamental theory of thermoelectric generation rather lagged behind the ingenuity of the engineers. But Mr. Clark (in the previously cited reference) elegantly summarised the qualitative aspects of material selection:

'If we seek through the table (of thermoelectric potentials) for useful thermo-electric combinations we must remember that our elements ought to be very good conductors of electricity, and very poor conductors of heat: they should also be cheap'.

Around the turn of the century several attempts were made to evaluate the efficiency of a thermoelectric generator (Rayleigh 1892, Johansen 1910, Altenkirch 1909 and 1911 and others). Various forms of the efficiency formula continued to appear in the literature to the nineteen-forties (see Telkes 1947). Although the arrangement of material properties in the form of the product of the thermoelectric potential squared and the ratio of electrical and thermal conductivity ($\alpha^2 \sigma / k$) was very prominent in many of these formulae, it was not singled out as the basic material parameter for thermoelectric generation until the nineteen-fifties.

The experimental work from the end of the nineteenth century to the Second World War was orientated towards producing cheap generators for specific uses where efficiency was not of prime importance. Electroplating has been mentioned and for many years thermoelectric generators provided the cheapest method of obtaining the low voltage high current supply required for this purpose. Several attempts were made to generate power using solar heated thermopiles and the Sun Electric Generator Company was formed in America in 1910. Wall (1927), Milne (1939) and others produced generators for powering radio sets and charging batteries. Metallic thermoelements were generally used and the efficiencies were less than 1%.

1.2.3. Thermoelectric Generation in the Semiconductor Age.

During the nineteen-forties Maria Telkes at the Massachusetts Institute of Technology was working in a systematic way on the thermoelectric properties of certain semiconductors including Zn Sb, PbS, ZnO and Bi₂ Te₃. (The term 'thermoelectric properties' is often used as a general title to include the thermoelectric potential, and the electrical and thermal conductivities). In 1947 she reported on a thermoelectric couple of PbS and Zn Sb which had a theoretical thermal efficiency of 10% at a temperature difference between the junctions of 400 C. The actual observed efficiency was 7%, the difference being attributed mainly to contact resistance. It is interesting to note that in spite of the vast amount of theoretical and experimental work on semiconductors and thermoelectrics performed during the following twenty years only marginal advance was made in the theoretical generator efficiency.

At about the same time Ioffe and his co-workers in Russia were working on semiconductors as thermoelements for generation and refrigeration. They developed generators for use in the remote areas of Russia. The most famous of these was a paraffin lamp which besides giving light also produced a few milli-amps of electricity at about nine volts suitable for powering a radio set. They were the first to appreciate the full significance of the combination of the thermoelectric properties which arises in the generator (or refrigerator) efficiency formula (Ioffe 1957). This combination of the thermoelectric potential squared multiplied by the ratio of electrical to thermal conductivity became known as the figure of merit of a single material:

$$Z_m = \frac{\alpha^2 \sigma}{K} \quad \text{----- (1.6)}$$

They found that certain semiconductors of high molecular weight such as Pb Te and Pb Se when doped to give electron concentrations of about 10^{16} electrons / mm³ possessed an optimum figure of merit.

The search for better thermoelectric semiconductor materials then began in earnest in a number of countries. Fritts (1960), Heikes and Ure (1961) and others in the United States worked on materials such as lead, tin and germanium telluride, Goldsmid (1960) in Britain did much of the development work on bismuth telluride and Fleischmann et al. (1959) in Germany studied silver antimony telluride combinations. The present trend in material research is outlined in chapter 2 and some of the more recently constructed thermoelectric generators are mentioned in section 1.4.

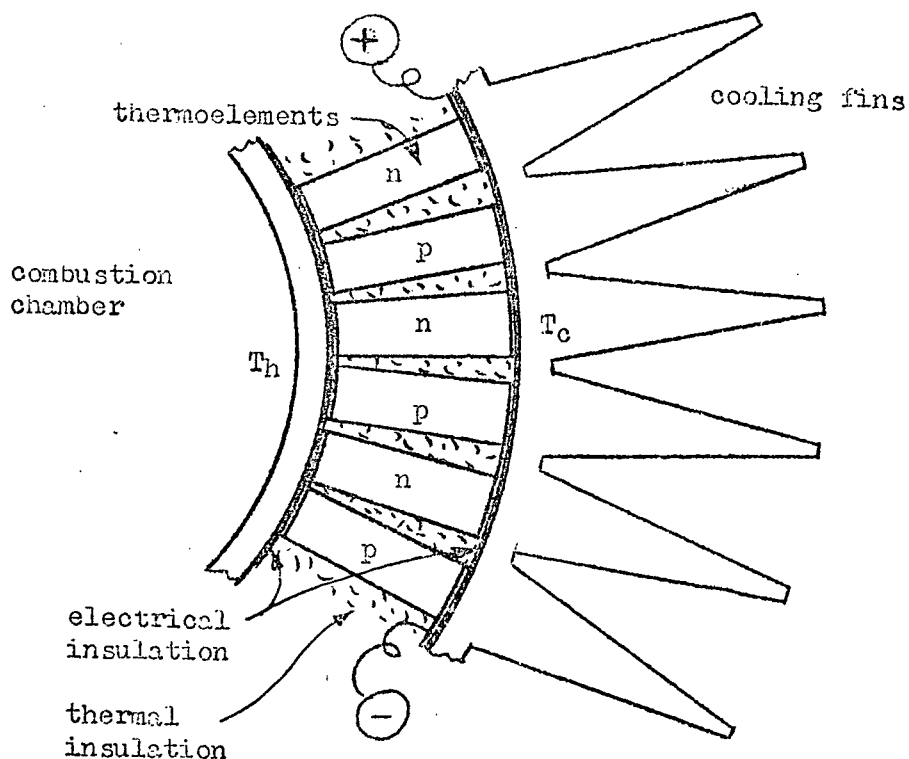
In summary it may be said that the thermoelectric effect was noticed in 1821 but for the next 130 years no hopes were entertained that it would ever be an efficient method of generating electricity. This is not to say that it was not used for generation during this period. For some purposes such as electroplating which required high direct currents and low voltages it was adequately suited. With the increase in understanding of semiconductor materials around 1950 speculations were made regarding the possibility of semiconductor thermoelectric materials yielding high conversion efficiencies and being used for major power generation. These hopes proved to be unfounded and in 1962 Spring and Swift-Hook showed that for major power generation materials were required having a figure of merit some two to four times higher than the best known at that time. Since then only marginally better materials have been developed but they have found applications in small, quiet and reliable generators for terrestrial and space uses. The quest for greater conversion efficiency has led to research on the possibility of increasing the temperature range over which the material may be used, (thus increasing the Carnot efficiency), and the feasibility of using materials other than solid semiconductors, such as liquid semiconductors and ionically conducting materials.

1.3. The engineering problems.

Details of the design of thermoelectric generators may be found in most books on thermoelectricity (such as Heikes and Ure 1961). This section has been included in order to highlight the main engineering problems involved in the design and construction of semiconductor thermoelectric generators.

1.3.1. Thermal and electrical energy transfer problems

In a thermoelectric engine heat has to be transferred to one side of a number of small thermoelements and transferred away from the other side. The high heat flux necessary on the hot side is usually supplied by specially designed burners in oil fired generators, by the decay of radioisotopes in nuclear power generators or by concentrating mirrors in solar generators. On the cool side, heat is conveniently transferred to the surroundings by natural convection using fins in the atmosphere or by radiation in outer space. Consideration of the following arrangement of a generator shows that heat energy may be lost to the system due to heat flow through the insulation between the matrix of thermoelements and the thermal resistance at the junctions.



A good insulation material has a thermal conductivity of about 0.0005 watts $\text{cm}^{-1}\text{K}^{-1}$ and typical semiconductor thermoelement materials such as Bi_2Te_3 and PbTe have thermal conductivities of 0.02 watts $\text{cm}^{-1}\text{K}^{-1}$. Even when the area of insulation material is not more than the total cross-sectional area of the thermoelements there is therefore a 2½% heat loss and in most generators the total insulation area is much greater.

The fins conducting heat away from the cool junctions are usually metallic and must therefore be electrically insulated from the thermoelements and the connecting links. Since electrical insulation materials are also good thermal insulators there would be a considerable temperature drop between the cool junctions and the fins. Fortunately nature is not entirely opposed to the designer in this case because the electrical resistance of an insulator is up to 10^{24} times greater than a metal whereas the thermal resistance is only 10^4 times greater. A very thin sheet of insulation such as mica may therefore be used as this will give almost complete electrical insulation with a minimum of thermal resistance.

The greater problem where electrical resistance is concerned occurs at the junctions between the thermoelements and the connecting links. The case of a lead telluride thermoelement may be taken as an example. The connecting material and any solder used must not react with the lead telluride or the doping material. Copper forms a eutectic with lead telluride and common solders leach out the dopants, thus altering the carrier concentration. It was eventually found that a bismuth-tin solder could be used at low temperatures but no successful hot junction solder has been developed. Iron is usually used for the hot junction connecting strip and it is held against the lead telluride by spring pressure. This pressure together with the high temperature causes the telluride to flow plastically and after a short period to become in intimate contact with the iron. Thermoelements with these junctions have operated for over five years with no detriment to the material. Nevertheless practical generators usually lose about 10% of the power generated to 'I² R losses' in the electrical contacts.

1.3.2. Material property problems.

The best semiconductor thermoelements are weak and rather brittle. Although careful mounting can result in fairly robust generators they

cannot withstand sudden shocks or vibration. Thermal expansion causes a problem which is at least partially overcome in the case of lead telluride by the spring loading of the thermoelements. The internal stresses set up in the material by thermal shock can cause the thermoelement to crack. This can be overcome by arranging for the generator to heat up slowly, but the lifetime (in total operating hours or years) of a cycled generator is invariably shorter than one which is run continuously.

The material itself must also be stable. Internally the structure must not change with time and the dopants must remain in the same concentration. Externally the surroundings must be compatible, and at high temperatures this generally involves the atmosphere being non-oxidising. It is not possible to use a vacuum as the sublimation rates are quite high, hence an inert gas is most suitable. Encapsulation of the thermoelements in inert gas surroundings together with all the other problems mentioned ensure that generator design is complicated and involves much precision engineering.

1.5.3. Design and economic problems.

There are still further problems to harass the thermoelectric generator designer. The generator should ideally be designed to suit a particular load and for either maximum efficiency or maximum power. This means that the length / area ratio of the thermoelements is confined to a particular value. When the heat source is a radioisotope or nuclear reactor the thermoelements must not be affected by nuclear bombardment and the generator must be adequately shielded. When the heat is obtained from a fossil-fueled burner the output will fluctuate depending on the ambient temperature (and if in the open the wind velocity and direction). If a steady supply voltage is required this will necessitate a control system or the generator output may be used to trickle charge a battery.

Finally there is the cost. If a thermoelectric generator is to be commercially successful it must either work under conditions or in places where no other generator may be used or it must be cheaper than other forms of generation. The former possibility has been widely explored during the last few years (as is shown in section 1.4), but the latter possibility has not been explored and the capital cost of generators is still very high.

1.4. Thermoelectric generation today.

In this section a few details of some modern generators are given to show the present stage of development. The future of thermoelectric generation is also discussed.

1.4.1. Fossil - fuel fired generators.

Generators with power outputs up to 100 watts have been produced commercially for some years. The range of generators manufactured by the Minnesota Mining and Manufacturing (3M) Co. Ltd. may be taken as an example. The general lay-out is shown in figure 1.1. These generators may be run on propane or natural gas and have power outputs in the range of 15 to 50 watts. The 50 watts generator consumes 0.136 kg propane/Wh giving an overall efficiency of $2\frac{1}{2}\%$. It can generate in remote locations for periods up to ten years requiring only an annual visit to replenish the fuel supply and check the operation. The reliability off-sets the capital cost (of several hundred pounds sterling for the 50 watts model) and makes the generator very competitive for certain applications. A solid-state DC/DC voltage converter and limiter is generally supplied with the generator to increase the voltage to 6, 12 or 24 volts and limit it at the specified value. These generators are now used to power remote weather and radio stations, operate beacons for marine and aviation purposes and to give cathodic protection on pipe lines. Substantially greater power outputs may be obtained for a few hours a day by using the generator to continuously trickle charge a battery.

An excellent example of a thermoelectric generator designed for a particular purpose is provided by Bergen (1963). This generator was built for the United States Coast Guard to operate a flashing navigational lamp on a buoy or shore location for a period of ten years. The general lay-out is shown in figure 1.2. The 102 thermoelements were of segmented lead telluride in the form of rods of 5 mm diameter and 20mm long. Each element was individually spring loaded to give good electric contact and to allow for thermal expansion. Although lead telluride may be used at temperatures over 600°C the hot junctions were kept in the range $500 - 550^{\circ}\text{C}$ to give a greater life expectancy. For initial tests the burner was replaced with an electrical heater. When the compartment containing the thermoelements was evacuated an initial thermal to

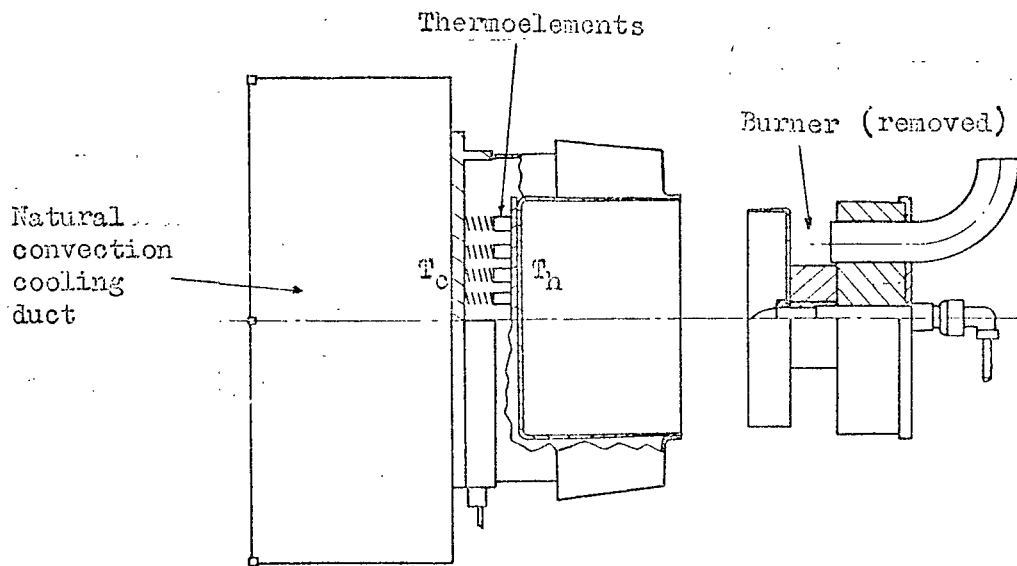


Figure 1.1. General arrangement of the 3M Co. generator.

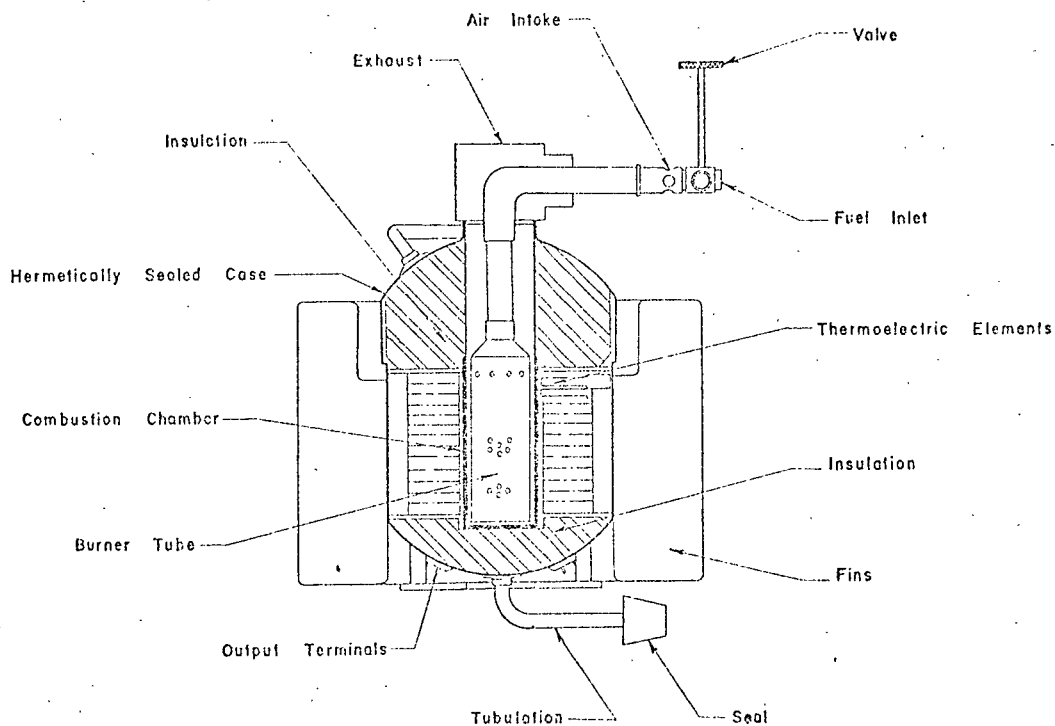


Figure 1.2 Sectional view of the Coast Guard generator.

(from Borgen 1963)

electrical efficiency of 8.5% was obtained at a power output of 15.1watts. After the compartment was filled with inert gas and hermetically sealed the efficiency was found to be 7.4%. When the specially designed propane burner was fitted the generator was found to yield 313 Wh/lb of fuel giving an overall efficiency of 5%.

Thermoelectric generation has been considered as a means of utilising the wasted heat of internal combustion exhaust gases. Pepper et al (1964) for example have considered the possibility of replacing the dynamo of a farm tractor with a thermoelectric generator situated on the exhaust piping. The exhaust temperature of the gasoline engine they used was about 600°C at 50% maximum engine power. They constructed a small model generator with ten lead telluride couples operating between 570 and 400°C. These were arranged radially around the exhaust pipe as shown in figure 1.5. The open circuit potential was 2.3 volts and the short circuit current was 6.25 amps. In a full scale generator designed to replace the dynamo about a 100 similar lead telluride couples would be required. After operation for ten hours on the tractor engine the generator was disassembled and four cold junctions were found to be disconnected. It was pointed out that considerably less brittle thermoelements were required and that the cost of these thermoelements would have to be lowered before such generators became competitive.

1.4.2. Isotope and reactor generators.

A review of thermoelectric generators using the decay of isotopes as a heat source is given by Poole (1967). Space and terrestrial applications are considered and particular regard is paid to the cost and availability of the fuel and the generator design. Some of these generators have now operated unattended for over five years and probably represent the most reliable generators obtainable. Isotope generators are being developed in Britain as the RIPPLE (Radio-Isotope Power Pulsed Lighting Equipment) programme, in the United States as part of the SNAP (Space Nuclear Auxiliary Power) programme and also in Russia.

The lay-out of a typical RIPPLE generator developed at the Atomic Engineering Research Establishment, Harwell is shown in figure 1.3. The fuel is strontium - 90 which is a β emitter with a half-life of 28 years and

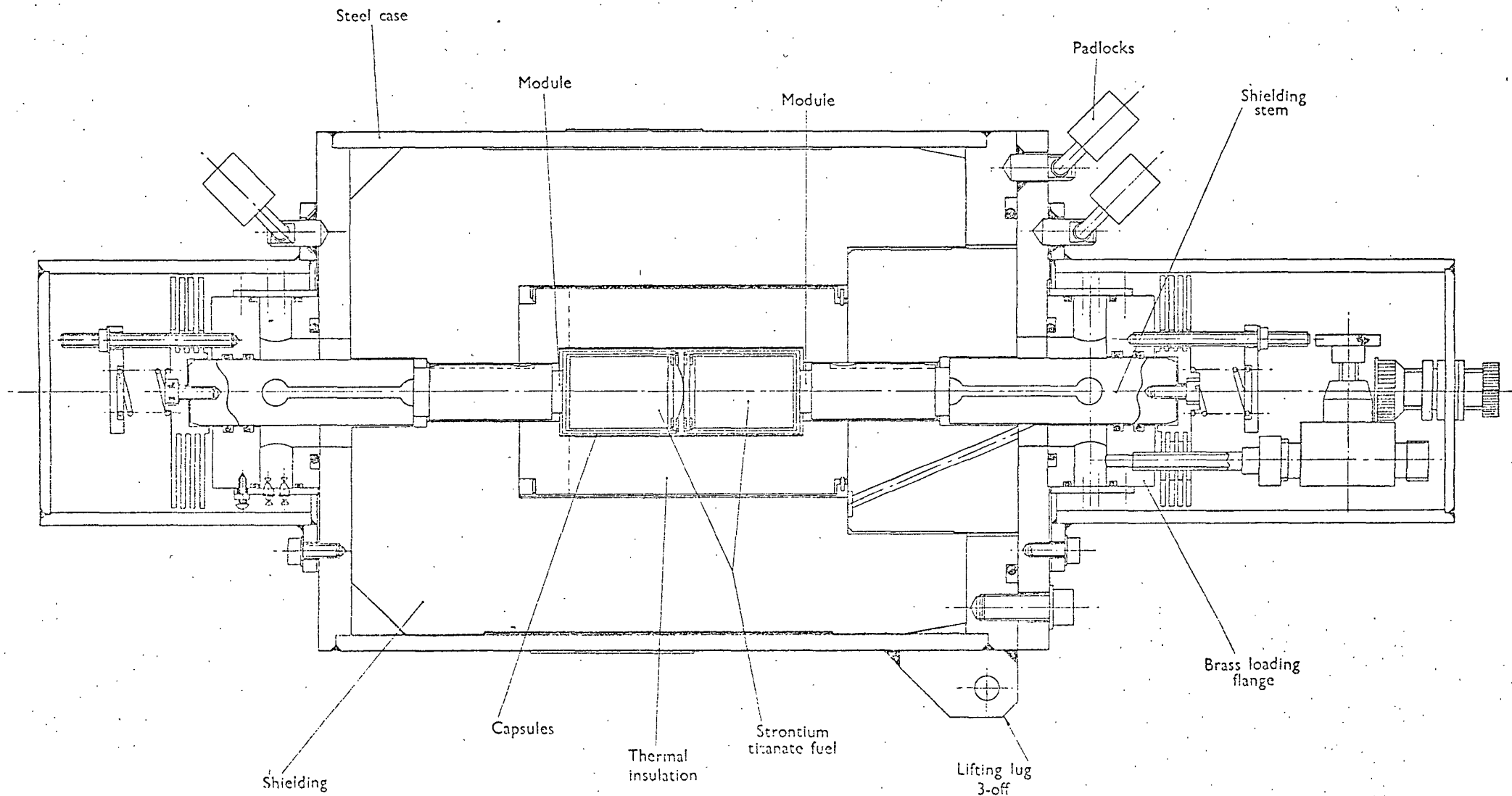


Fig. 1.3. Layout of 1W RIPPLE generator

from Poole (1967).

an initial output of about 1 watt/gm of isotope. Strontium - 90 is a fission product formed in large quantities as a by-product of nuclear power generation. The limitation on quantity is entirely caused by the extraction process from the spent fuel elements and one source supplying it in commercial quantities is the Oak Ridge National Laboratory, Tennessee. The thermal insulation is a microporous silica having an overall thermal conductivity which is less than the conductivity of the gas in which it is situated. The radiation shield is of concrete or depleted uranium. The power output depends on the number of bismuth and lead telluride thermoelectric modules and is generally of the order of a few watts. The thermal to electrical energy conversion may exceed 5% but is more typically in the range 1-3%.

The first isotope generator of the SNAP series was demonstrated to President Eisenhower in January 1959 and a similar unit was used as auxiliary power for a satellite in June 1961. Most of the incentive has come from the space programme although terrestrial generators have also been developed. In SNAP generators the lead telluride thermoelements are arranged radially around the radioactive source containing the isotope capsules. The power outputs range from 2.7 to 60 watts with efficiencies up to 5%. The specifications for the SNAP space and terrestrial generators are given by Morse (1966).

On the 3rd April, 1965 SNAP 10A, the first nuclear reactor power plant incorporated in a rocket, was blasted into space. The heat from the reactor was converted into 500 watts of electrical power using Si Ge thermoelectric modules. A liquid sodium - potassium alloy was used to transport the heat from the reactor to semicircular tubes to which the thermoelectric modules were attached as shown in Figure 1.4. The 2880 modules produced an output potential of 30 volts and a conversion efficiency of 1.6%. This low efficiency was due to the small temperature difference caused by the necessity of having the cool junction at a high enough temperature for radiation of the rejected heat into space. By increasing the temperature of the hot junction from its design value of 500°C to about 700°C (at which Si Ge modules function successfully) the output could be increased to over 1 kW and the efficiency also raised.

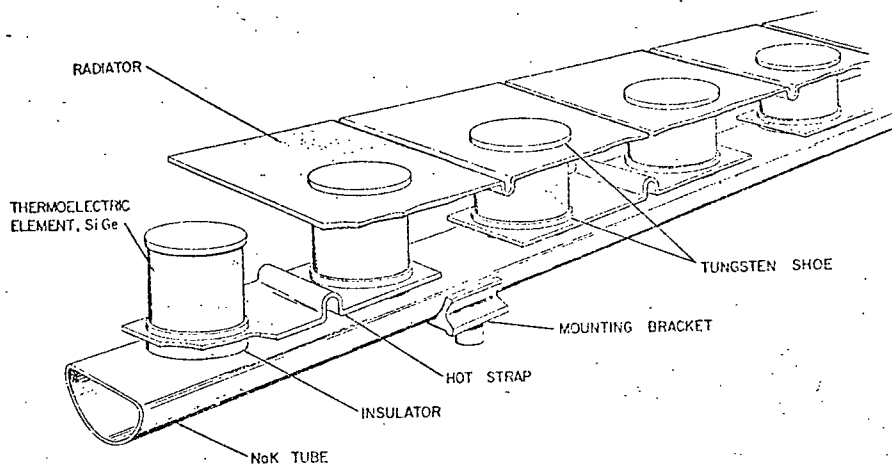


Figure 1.4. A sub-section of the thermoelectric generator used in the SNAP 10A system showing the arrangement of the Ge-Si alloy thermoelements. (from Dismukes and Rosi 1965.)

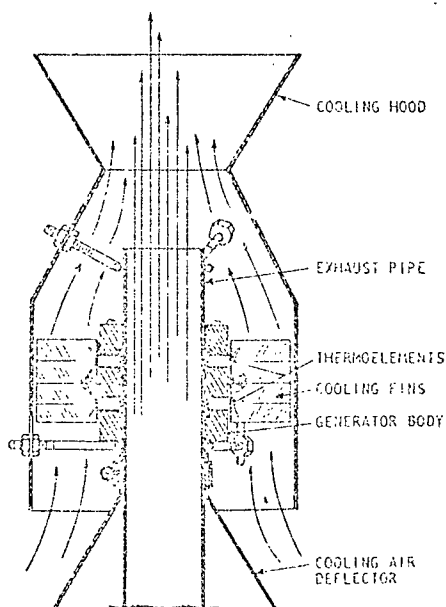


Figure 1.5. Sectional sketch of exhaust gas generator and cooling hood used for forced-air cooling.

(from Pepper et al 1964.)

1.4.3. The future of thermoelectric generators.

Dismales and Rosi (1965) report on the construction of a two stage generator; the first stage consisting of bismuth and antimony tellurides and selenides and the second stage with couples of germanium - silicon alloys. These represent the best materials available over the temperature range used and the theoretical maximum efficiency was 14.8% between 1040 and 25°C. The experimental conversion efficiency from heat to electricity was 13.5%. This discrepancy was due entirely to electrical contact resistance and radiation losses. Using these materials in a fossil - fuel fired generator and taking account of the burner efficiency and the thermal and electrical losses it should be possible to construct a generator with an overall efficiency of 8%. Since this represents the best that can be achieved after twenty years of intensive research on semiconductor materials it would seem unlikely that thermoelectric generation will be really efficient in the near future.

Although much of this research has been directed towards producing materials yielding higher conversion efficiencies it is most likely that that thermoelectric generation will survive in areas where reliability is more important than efficiency. This is the case with some of the generators discussed previously. They could also find application in areas where the capital cost is more important than the efficiency. Apart from replacing vehicle dynamos there are possible domestic uses such as silent petrol lawn mowers. Design for minimum material cost and generator engineering can lead to the use of cheap semiconductor materials such as Fe Si₂, cheap liquids such as molten salts or even certain metals as the thermoelement material.

Chapter 2.

Thermoelectric Materials

Contents:

- 2.1. Solid metals and semiconductors.
- 2.2. Electronically conducting liquids.
- 2.3. Ionically conducting liquids.

This chapter is mainly concerned with liquid thermoelectric generation materials as they are the topic of this thesis, and solid thermoelectric materials are more extensively reviewed elsewhere. A brief summary of the state of development of solid thermoelectric materials is given in the first section.

2.1. Solid metals and semiconductors.

It was mentioned in section 1.2. that metals and alloys were used as thermoelectric materials during the nineteenth century in the construction of generators to supply the power for electroplating. Although the efficiencies were low the generators were cheap to build and they had a long life expectancy.

In metals the electrical and thermal conductivities are determined by the motion of the electrons and are related by the Wiedemann - Franz Law. At room temperatures this yields a conductivity ratio of $\sigma/T = 0.13 \times 10^6 \text{ K watts}^{-1} \Omega^{-1}$. Since the thermoelectric potential α is typically about $10 \mu\text{V/K}$ the $Z_m T$ value ($= \alpha^2 \sigma T/K$) is 10^{-2} at $T = 1000^\circ\text{K}$. Substitution of this value in equation 1.2 (page 13) shows the conversion efficiency of a metallic couple operating over a few hundred degrees temperature difference to be about 0.1%. Certain metals such as antimony and bismuth have a maximum thermoelectric potential of over $50 \mu\text{V/K}$ and could yield an efficiency of about 1%.

Although it is possible to increase the figure of merit by alloying, the maximum efficiency obtainable using metallic couples is still only about 2%. Constantan (60% Cu, 40% Ni) for example has a thermoelectric potential of about $44 \mu\text{V/K}$ between 0 and 1000°C and a $Z_m T$ value of about 10^{-1} at $T = 1000^\circ\text{K}$. In addition to being used for temperature measurement metallic thermocouples have been designed for operating control devices. The automatic gas shut - off valve for the trial generator mentioned in section 10.2 was operated by a thermocouple with a hot junction situated in the burner flame.

Solid semiconductor materials have yielded the highest thermal to electrical energy conversion efficiencies to date and have been extensively studied for this application for the last fifteen years.

Rosi et al. (1961), Wright (1965), and Sutton (1966) give excellent reviews of these materials.

It is not proposed to repeat here the information on the theory and the details of particular semiconductors given in these reviews. Pb Te and Bi₂ Te₃ which were developed in the nineteen - fifties are still the most popular materials for practical thermoelectric generation. The only important materials which have been developed since 1960 are compounds of the type Ag Sb Te₂ studied by Fleischmann et al. (1961 and 1963) and Ge Si developed by Abeles et al. (1962). The former owing to its very low energy gap has a $Z_m T$ value of 1.3 at a temperature of 500°C. The latter has $Z_m T$ value of less than unity but may be used at temperatures up to 1000°C. Sintered silver selenide (Epstein 1961) and compounds of the type Ge Te - Tl Bi Te₂ (Lubell and Maselsky 1965) have also yielded reasonable figures of merit.

It is becoming increasingly evident that very complex compounds must be investigated if materials with higher figures of merit are to be developed. Unfortunately these compounds are generally unsuitable from an engineering viewpoint. Ware and Mc.Neil (1964) have considered the use of Fe Si₂ as a cheap thermoelectric material. This material may be doped as p or n type and gives a $Z_m T$ value of about 0.2 at 500°C. Taking heat losses into account this material would yield about 2% conversion efficiency in an actual generator. More expensive materials seldom yield more than about 3% in a practical thermoelectric generator.

Figures 2.1 and 2.2 show the $Z_m T$ values for various p type and n type materials and are taken from Poole (1967).

2.2. Electronically conducting liquids.

In a crystal there is an equilibrium state defined by a minimum of potential energy in which the molecules arrange themselves in a symmetrical geometrical pattern. When this equilibrium state cannot be obtained due to thermal motion or weak binding forces a liquid state occurs. The average interatomic distances in liquids are slightly greater than in solids owing to the occurrence of vacancies on melting.

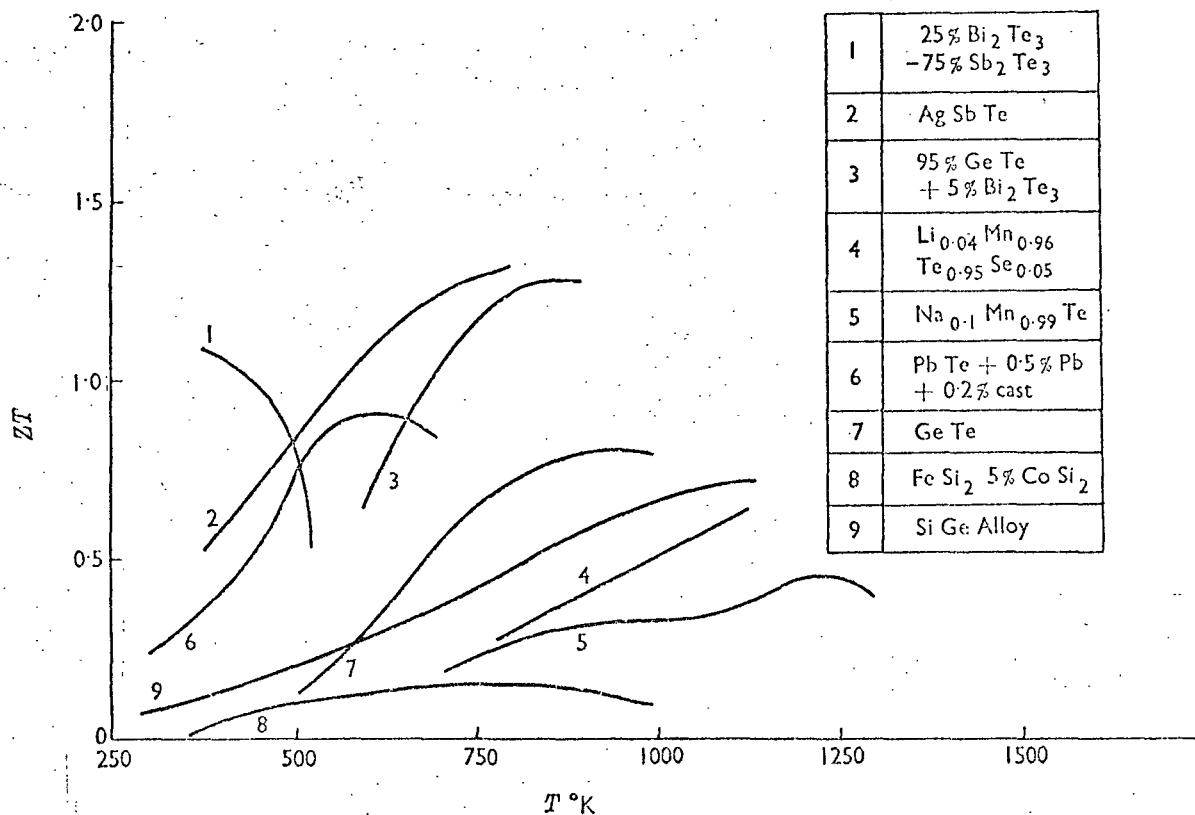


Fig 2.1 (ZT) vs T for p-type thermoelectric materials

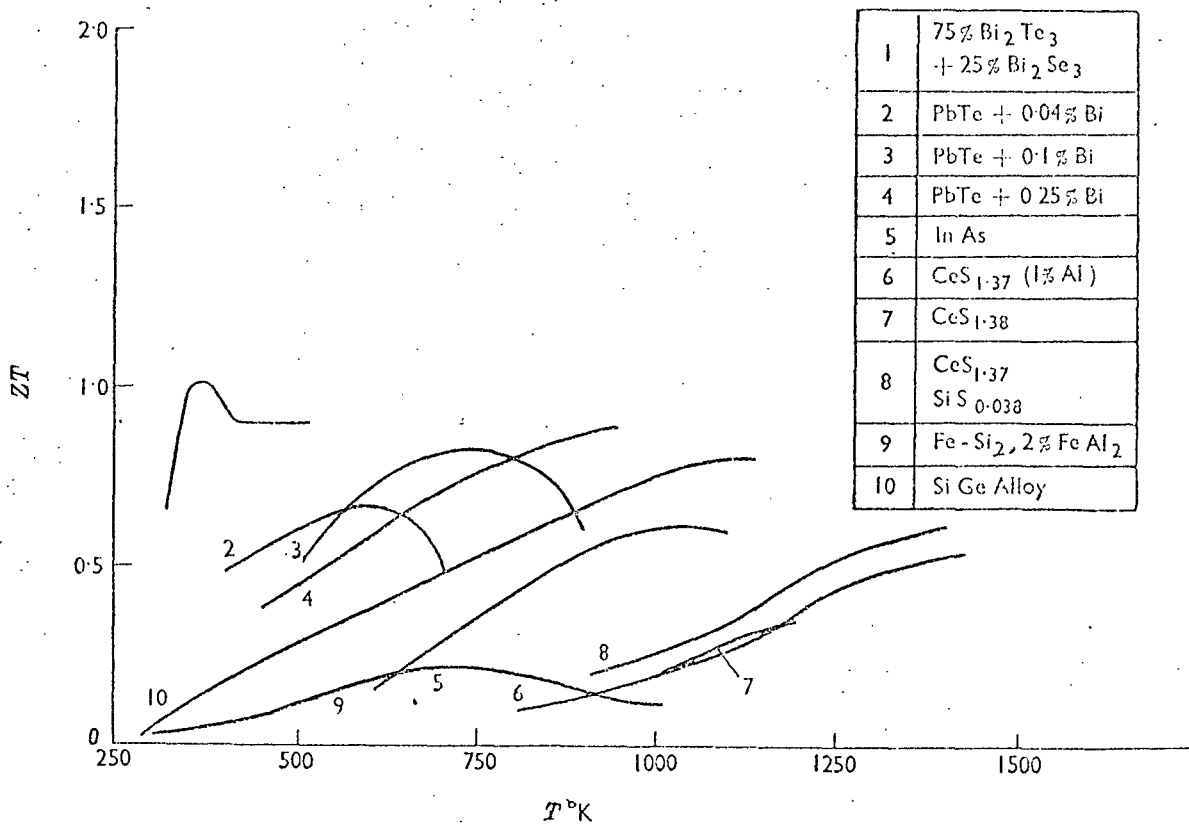


Fig 2.2 (ZT) vs T for n-type thermoelectric materials

from Poole (1967)

The formation of these vacancies requires energy to be supplied at the melting point and this energy when supplied at constant pressure is the enthalpy of fusion.

For a long time it was considered that there was no order in liquids but more recent evidence has shown that there is a degree of order and that even compressed gases do not have a completely random distribution. In the liquid state at the melting point liquid crystals consisting of clusters of ordered atoms or molecules exist. As these clusters are not orientated with respect to each other the liquid is said to exhibit short range order. A crystal exhibits long range order which is macroscopic and does not change with time. The short range order at the melting point gradually disappears as the temperature is raised due to the breakdown of the clusters.

Long range order is not a necessary condition for electrical semiconduction. Glazov et al. (1969) give a review of liquid semiconductors. Many substances which are semiconducting in the solid state become metallic in the liquid state (eg. Si, Ge, In Sb). Some substances retain their semiconducting properties immediately above the melting point but then gradually become metallic as the temperature is raised and the short range order decreases (eg. Pb Se). On the other hand a few semiconducting materials lose their electronic conduction on melting and may become ionic conductors (eg. Cu I). Finally some substances such as certain sulphides and tellurides remain as semiconductors in the liquid state for several hundred degrees above the melting point. It is these materials with which this section is particularly concerned.

Kelly (1962) and Johnson and Readal (1963) report on the thermoelectric properties of liquid $\text{Cu}_2\text{S} - \text{Cu}_2\text{Te}$ mixtures. The most promising composition is 25% Cu_2S , 75% Cu_2Te which melts at about 1000°C and has a $Z_m T$ value of 0.62 at 1100°C . As the temperature is raised the $Z_m T$ value drops owing to the decrease in the thermoelectric potential and the increase in the thermal conductivity.

An other semiconductor system studied in detail with a view to thermoelectric generation is the thallium-tellurium system by Cutler and Mallon (1965). The thermoelectric potential at the melting point varied from +180 to -170 $\mu\text{V}/\text{K}$ depending on the composition, but in all cases it gradually tended towards zero as the temperature was raised.

The eutectic mixture $Tl_{31}Te_{69}$ yielded a $Z_m T$ value of 0.85 at the melting point of approximately $200^\circ C$ but dropped to 0.2 by $400^\circ C$. Other mixtures showed a similar decrease of the $Z_m T$ value as the temperature was raised.

It would thus appear that as the temperature is raised above the melting point and the short range order gradually disappears the liquid becomes less useful for thermoelectric generation. Nevertheless there are many systems which have not been studied and could yield much higher $Z_m T$ values.

The thermoelectric potential and electrical conductivity (but not the thermal conductivity) of some other semiconductor systems are available in the literature and are given in the following table. The $\alpha^2 \sigma T$ value is also given as this must be high if the material is to have a reasonable $Z_m T$ value. ($Z_m T = \alpha^2 \sigma T / K$).

Liquid Semiconductor	T ($^\circ C$)	$ \alpha $ ($\mu V/K$)	σ ($\Omega^{-1} cm^{-1}$)	$\alpha^2 \sigma T$ ($watts \cdot cm^{-1} K^{-1}$) $\times 10^{+3}$	Reference
$Cu_2 Te$	1100	110	550	9.14	Dancy 1965
$Ag Te$	700	110	900	10.6	"
$Sn Te$	700	40	1500	2.34	"
$Ga_2 Te_3$	840	~100	150	1.67	Glasov et al 1969
$Pb S$	1200	~200	340	20.0	"
$Ag_2 S$	845- 945	90-170	-	-	Stoneburner 1959
$Cu_2 S$	1130- 1205	70-80	-	-	"
$Fe S$	1115- 1180	60-70	-	-	"
$Tl S$	460	582	1.1	0.27	Stoneburner 1965
$Tl Se$	465	306	4.2	0.29	"
$Tl_2 Se$	463	1537	5.4	9.38	"
$Cu O$	1231	250	2.0	0.19	Zuev 1960

Kelly (1962) discusses some of the problems of thermoelectric generation using electronically conducting liquids. Suitable containment materials must be found and the contacts must not corrode in the hot liquid. Design must be such that the heat transferred through the material due to natural convection and radiation is low. But these engineering problems are considerably less than those which have been solved for thermoelectric generators using solid semiconductors.

2.5. Ionically conducting liquids.

The thermoelectric effect in the previously mentioned materials is due to the flow of electrons in the material. There is also a thermoelectric effect due to the movement of ions in a substance. The fundamental difference is that the flow of ions always involves a net mass transfer. In the solid state the mobility of the ions in ionically (or polar) bonded crystals is dependent upon the lattice defects and is generally very low. (A notable exception is α - phase AgI which has a high conductivity). This means that the electrical conductivity, being dependent upon the density and mobility of the ions is also very low. Although the thermoelectric potential is high, and very often in the range 1-10 mV/K the thermoelectric figure of merit is too low to be suitable for generation.

On the other hand in the case of an ionic liquid the mobility is much higher and as the density of ions is about the same, the electrical conductivity is also higher and in the range 1-10 $\Omega^{-1} \text{ cm}^{-1}$. The thermoelectric potential is rather lower than in solid ionic materials and generally falls in the range up to 1 mV/K. Molten salts (as ^{pure} ionic liquids are usually termed) are very stable liquids often melting at about 500°C and remaining in the molten state at atmospheric pressure to well over 1000°C. The properties vary only slightly with temperature and this fact enables differentiation to be made between electronic and ionic conduction for materials with conductivities in the range 1-10 $\Omega^{-1} \text{ cm}^{-1}$. For example Stoneburner (1965) gives properties for molten $\text{Tl}_2 \text{Se}_3$ which may initially suggest an ionic compound. But the variation of the properties with temperature over an increment of 165°C (say) as compared to the variation of a typical molten salt over the same increment show correctly that $\text{Tl}_2 \text{Se}_3$ is an electronic conductor.

	T (°C)	$(\Omega^{-1} \text{ cm}^{-1})$	$ \alpha $ (mV/K)
$\text{Tl}_2 \text{Se}_3$	305	1.59	0.229
	470	5.90	0.355
Ag Cl	430	2.9	0.440
	595	3.2	0.440

In the later chapters it is shown that $Z_m T$ for some mixtures of molten salts is of a similar order to solid semiconductors and further development could yield considerably higher $Z_m T$ values. The power output per unit of thermoelectric element material is typically about five times less than that for the best semiconductor material.

A problem with the use of molten salts is the mass transfer associated with the flow of ions. If the connections to the molten salt are both of the cation metal a reversible cell of the form $M/T_h \text{ MX}/T_c M$ results and electrolysis occurs on the passage of current. This electrolysis would continue until the anode was completely eaten away and an equivalent amount of metal was deposited on the cathode. A method of returning the metal from the cathode back to the anode must therefore be found. The other main problem is that of corrosion. As mentioned earlier an important advantage of molten salts is the large temperature range over which they may be used. If this is to be fully utilised the cells must operate to temperatures around 1000°C . At this temperature the molten salt, electrode material and refractory container must not react with each other or oxidise if in contact with the atmosphere.

The idea of using molten salts for thermoelectric generation is not new. Clark (1876) knew that the thermoelectric effect existed in molten salts:

'There is another source of thermo-electric power - viz. that produced when two pieces of metal are heated to different temperatures and connected by a fused salt capable of conducting electricity.'

Sundheim (1960) was the first to consider their use for thermoelectric generation. As an example he measured the thermoelectric potential of Ag NO_3 and discussed the other relevant properties of molten salts. He concluded that these properties were rather unfavourable and saw no way of overcoming the mass transfer problem. In 1964 Wartenowicz published a theoretical analysis of a molten salt generator. No account was taken of the mass transfer between the electrodes although this is a consequence of high current density transfer by ions. This mass transfer provides another heat transfer mechanism which, together with radiation and natural convection, ensures that the heat energy transferred is greater than that transferred due to the conductivity of the salt. This analysis is therefore of limited practical significance.

Besides using metal electrodes it is also possible to operate a thermocell using gaseous electrodes such as $\text{Cl}_2/\text{Metal Cl}/\text{Cl}_2$. Meissner et al. (1965) has studied the possibility of using these cells for thermoelectric generation. The electrodes were made of an inert conductor such as porous graphite and the chlorine evolved at the anode as the result of the current flow was passed to the cathode - thus overcoming the mass transfer problem. They studied the thermoelectric potential and the effect of the chlorine pressure on this potential for cells containing molten AgCl , NaCl , KCl and LiCl . Anionic thermoelectric potentials in excess of 0.7 mV/K were measured at low chlorine pressures. The high melting temperatures of these salts ensured that the cold junction temperature of the cell was high. They estimated the conversion efficiency of a cell using AgCl as falling in the range of 2-4% and for a $\text{F}_2/\text{LiF}/\text{F}_2$ cell as about 10%.

This work is confined to thermocells with ionic liquid electrolytes and reversible metallic electrodes. Preliminary considerations of molten salts and their mixtures indicated that reasonable values of the figure of merit are obtainable and that the mass transfer problem is not insuperable. In addition the performance is not sensitive to impurities in the melt and the cells are simple to build. This is a definite advantage over semiconductor thermoelectric generators where the material must be doped to within fine limits and the construction of the generator requires much precision engineering.

Chapter 3

The Thermal and Electrical Conductivity of Molten Salts.

Contents

Introduction.

- 3.1 Correlation between the measurements and the theory on the thermal conductivity of molten salts.
 - 3.1.1. Theory to the thermal conductivity of molten salts.
 - 3.1.2. A review of thermal conductivity data on molten salts.
- 3.2. Experimental results using the transient hot wire method.
 - 3.2.1. Introduction.
 - 3.2.2. The bridge circuit.
 - 3.2.3. The cell.
 - 3.2.4. The switching circuit.
 - 3.2.5. The test procedure.
 - 3.2.6. Results.
 - 3.2.6.1. Results for common liquids.
 - 3.2.6.2. Results for salts.
 - 3.2.7. The cause of the initial anomaly in the V_p -log t curve for salts.
- 3.3 The electrical conductivity of molten salts.

Introduction

It was pointed out in chapter 2 that it is advantageous for a thermoelectric material to have a low thermal conductivity. Thermal conductivity is the most difficult thermoelectric property to measure experimentally. For this reason there are few thermal conductivity values reported in the literature, and it is often estimated. This is particularly so in the case of liquids where the prevention of natural convection currents adds to the experimental difficulties. This chapter is mainly concerned with the thermal conductivity of molten salts at high temperatures.

In section 3.1 the semi-empirical theories given in the literature are described and the author has shown that there exists an empirical correlation between the conductivity and the molecular weight of a pure molten salt. In section 3.2 the thermal conductivities of some molten salts are measured using the transient hot wire method. The criticism of the transient hot wire apparatus made by some authors is discussed and it is found that, although the accuracy initially claimed for the method was possibly too high, it provides a very useful way of obtaining thermal conductivity data for many applications.

In contrast, the electrical conductivity is easy to measure experimentally and it has been extensively studied and reported in the literature. The electrical conductivities of the molten salts encountered in this work are given in section 3.3.

3.1 Correlation between the measurements and the theory on the thermal conductivity of molten salts.

3.1.1 Theory to the thermal conductivity of molten salts.

Modern theories generally assume that the thermal conductivity of molten salts is predominantly due to two mechanisms: the vibration mechanism arising from short-range order of the molecules in the liquid state and the translational or diffusion mechanism due to the motion of the ions. It was originally postulated that ionic diffusion, (or the electrical conduction mechanism) made a substantial contribution (Gambill 1959, Sundheim and Rosentreich 1959). But the high ratio of thermal diffusivity to mass diffusivity and the high value of the Lorenz number indicate a low contribution from diffusion. Turnbull (1961b) has shown this to be the case and found the ratio of diffusion conduction to total conduction to be less than 5%. Any theory which is to lead to useful results must therefore be based on the vibrational mechanism. It is for this reason that molten salts have thermal conductivity values of a similar order to solid dielectrics.

In 1949 Bridgeman adapted his equation for the thermal conductivity of insulators to liquids. Basically he assumed that liquid molecules were arranged in a cubic lattice with a spacing d and an energy of $3kT$ per particle flowing from row to row at the speed of sound U . This led to:-

$$K = \frac{3kU}{d^2} \dots\dots\dots(3.1)$$

Rao (1941) also assumed a liquid to be composed of a cubic arrangement of particles vibrating at a certain frequency. By analysing the heat flow mechanism and using the Lindemann theory relating the frequency to the melting point he predicted the thermal conductivity at the melting point to be given by the following equation:

$$K = \text{constant} \times \left[\frac{T_m}{M V_{at}^{4/3}} \right]^{1/2} \dots\dots\dots(3.2)$$

where T_m is the melting point (K), M is the molecular weight and V_{at} is the atomic volume.

Turnbull (1961b) applied both of these formulae to molten salts. Bridgeman's expression could only be applied to three of the salts he studied owing to lack of data on the velocity of sound. The predicted thermal conductivity values were certainly of the correct order of magnitude but deviated by up to 30% from the measured values. Rao's expression was applied to ten salts and gave correlation within 22% for eight of them. But data reported since the publication of this paper show large deviations from this expression. White and Davis (1967) attempted to apply a law of corresponding states for the transport coefficients to alkali-nitrates by correlating the density, viscosity and thermal conductivity changes with temperature. Only a limited degree of correlation was established.

It would therefore appear that there is no satisfactory method for predicting the thermal conductivity of molten salts. The experimental results (given in detail in the following sub-section, 3.1.2) were then studied in order to determine whether there was any empirical relationship between the thermal conductivity and an other property. The author found that some correlation existed between the thermal conductivity of a pure salt and its molecular weight with the thermal conductivity decreasing as the molecular weight increased. Re-examination of the theory in the light of this discovery then showed that this relationship is implied (indirectly) by Rao's expression, equation 3.2. If the substitution $V_{at} = M/\rho$ is made, (where ρ is the density), equation 3.2 becomes:

$$K = \text{constant} \times \frac{T_m^{1/2} \rho^{2/3}}{M^{7/6}} \dots\dots\dots(3.3)$$

The square root of the melting temperature (in°K) does not vary greatly from salt to salt and the density is to some extent dependent upon the molecular weight. This formula therefore implies that the conductivity at the melting point is largely dependent upon the molecular weight and decreases as the molecular weight increases. It also implies that, to a first approximation, the relationship between the conductivity and the molecular weight is of the exponential form $K = \text{constant} \times M^n$ where n is a negative power index.

Experimental data on the thermal conductivity of sixteen pure molten salts is reported in the literature and summarised in table 3.1. A graph of the thermal conductivity values given in table 3.1 as a function of molecular weight is plotted in figure 3.1. The correlation between these two properties is very evident and the equation to the curve drawn in figure 3.1. is given by:

$$K = 0.134 M^{-0.727} \quad \text{---(3.4)}$$

This simple relationship yields a better correlation with the reported experimental data than any other more complex expression, and is therefore the best method of estimating the thermal conductivity of a pure molten salt (at the melting point) at the present time.

3.1.2. A review of thermal conductivity data on molten salts.

The thermal conductivity values of molten salts available in the literature up to 1959 were all obtained using apparatus based on a steady heat flow through a plane or cylindrical liquid film. Turnbull (1961a) critically reviewed the data up to this date. The useful results included measurements of the thermal conductivity of NaOH by Lucks and Deem (1956), NaNO_3 and KNO_3 by Bloom (1959) and heat transfer salt ($\text{KNO}_3 + \text{NaNO}_2 + \text{NaNO}_3$ ratio 44 : 49 : 7) by Vargaftik (1952). The other results generally had an estimated possible error of 25% or more and are not included in this survey.

The experimental results of Turnbull (1961a and b) were obtained using a transient hot wire method (described in section 4.2). He estimated the accuracy of his results as $\pm 3\%$. In 1962 Ewing et al. reported measurements on the thermal conductivity of B_2O_3 and 'Flinak' ($\text{NaF} + \text{KF} + \text{LiF}$; ratio 11.5 : 42 : 46.5). He also ascertained experimentally the effect of radiation in steady radial and axial heat flow rigs and found it to be considerable. Bloom et al. (1965) measured the conductivity of some nitrates and nitrate mixtures using a radial steady heat flow apparatus and estimated their accuracy as $\pm 5\%$. The results of White and Davis (1967) on solid^{and} liquid alkali nitrates were also obtained using a radial steady heat flow apparatus. They estimated their accuracy as 3 - 5% and in the cases of NaNO_3 and KNO_3 gave reasons

Salt	Molecular Weight	T (°C)	$K \times 10^3$ (watts $\text{cm}^{-1} \text{K}^{-1}$) $\pm 5\%$	Reference
LiNO_3	68.95	252	5.82	White & Davis 1967
NaNO_3	84.99	307	5.66	White & Davis 1967
	-	329	5.52	Bloom et al. 1965
KNO_3	101.1	334	4.31	White & Davis 1967
	-	343	4.98	Bloom et al. 1965
	-	343	4.28	Turnbull 1961b
RbNO_3	147.5	311	3.77	White & Davis 1967
CsNO_3	194.9	314	2.85	White & Davis 1967
AgNO_3	169.9	210	3.7 extrap.	Bloom et al 1965
	-	210	3.77	Turnbull 1961b
Ag Br	187.8	460	2.77 ($\pm 10\%$)	See Section 4.2
(Na Cl)	58.44	801	8.8 ($\pm 25\%$)	Turnbull 1961b
Zn Cl_2	136.3	320	3.05	Turnbull 1961b
KHSO_4	136.2	206	3.39	Turnbull 1961b
NaHSO_4	120.1	179	4.60	Turnbull 1961b
$\text{NH}_4 \text{HSO}_4$	115.1	145	3.94	Turnbull 1961b
NaNO_2	69.00	209	6.0 extrap.	Bloom et al. 1965
KCNS	97.18	175	2.72	Turnbull 1961b
Na OH	40.00	319	9.2 ($\pm 10\%$)	Lucks & Deem 1956
($\text{B}_2 \text{O}_3$)	69.62	500	5.4	Ewing et al. 1962

TABLE 3. showing the thermal conductivity of molten salts near the melting point.

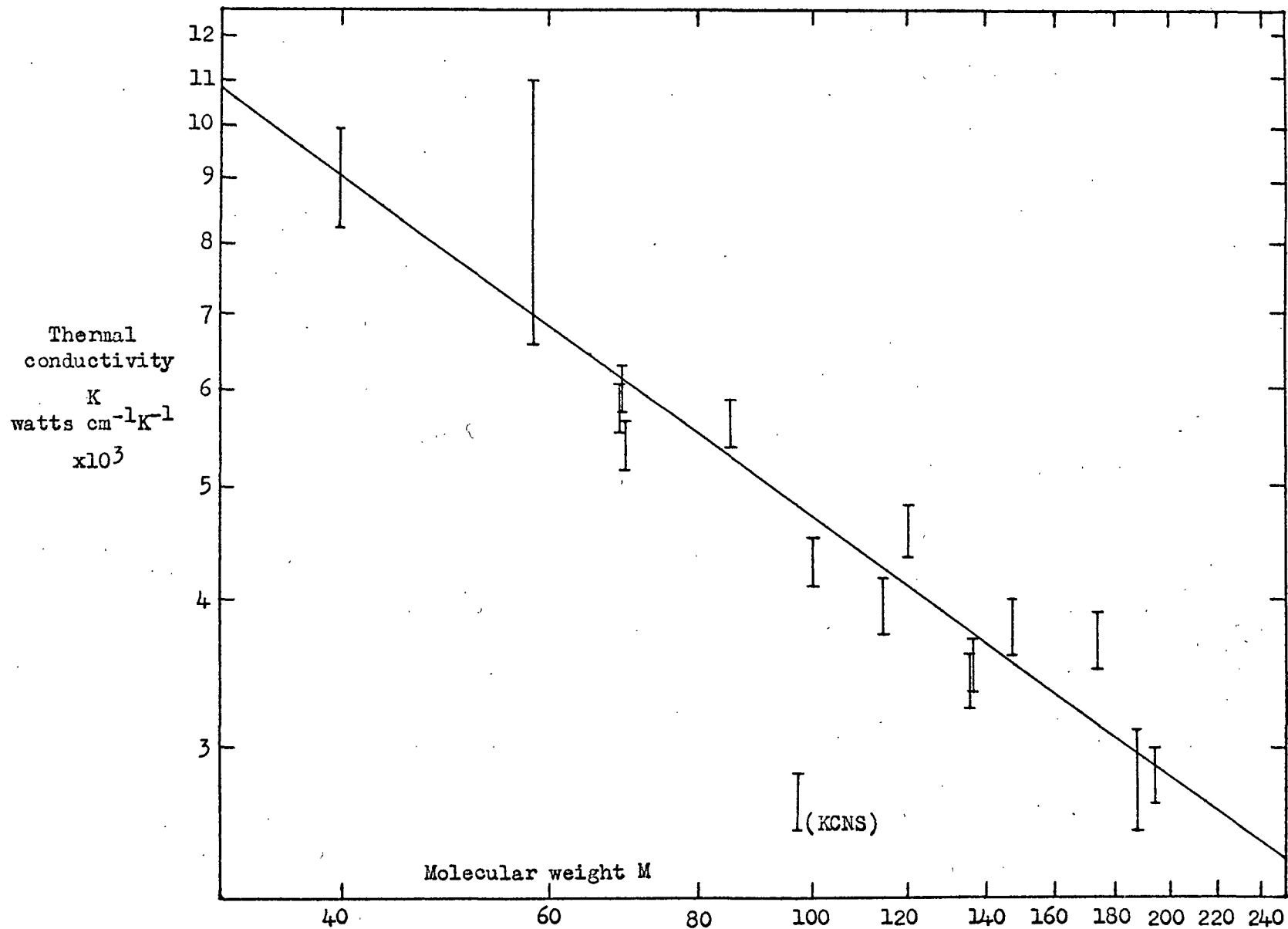


Figure 3.1
The thermal conductivity
of pure molten salts.

for the deviations of previous investigators. The foregoing data together with the thermal conductivity value for AgBr measured by the author (section 3.2.) are summarised in table 3.1. A graph of the thermal conductivity of molten salts at the melting point against the molecular weight has been mentioned previously and is shown in figure 3.1. In cases where more than one conductivity value was available in the literature for a particular molten salt the most recent measurement was used.

Mixtures of molten salts have a thermal conductivity which is less than the proportional mean of the constituent salts. This is to be expected owing to the general increase in the disorder of the short-range quasi-crystalline lattice of the molten salt on the addition of another salt. This in turn increases the resistance of the salt to the lattice vibration modes which are transferring heat energy. Experimental thermal conductivity values for salt mixtures are given in table 3.2. and the correlation with the proportional mean molecular weight is shown in figure 3.2. The curve shown in figure 3.1 for pure salts has been repeated in figure 3.2, to illustrate the general negative deviation for salt mixtures.

It should be pointed out that most of the pure salt thermal conductivity values available are for uni-valent compounds at temperatures less than 500°C. As data on a wider range of salts becomes available it is possible that the correlation with molecular weight will become less pronounced. Fortunately most of the salts studied in this thesis fall within this category and the curve shown in figure 3.1. has been used for approximate prediction of thermal conductivity where experimental data is not available. Prediction in the case of mixtures is more difficult. Generally a value equal to that given by the curve for pure molten salts, (at the mean molecular weight of the mixture), less about 25% has been used in accordance with the trend towards negative deviation shown in figure 3.2. This estimation method is obviously only very approximate but it is the best available at the present time.

The temperature coefficient of the thermal conductivity is usually small and positive, with conductivity values increasing at the rate of 0.2 - 0.4 watts $\text{cm}^{-1}\text{K}^{-1}$ per 100°C. Exceptions are NH_4HSO_4 and ZnCl_2 which have negative temperature coefficients.

<u>Salt Mixture</u>	<u>Mean Molecular Weight</u>	<u>T (°C)</u>	<u>K x 10³ (watts cm⁻¹ K⁻¹) ± 5%</u>	<u>Reference</u>
AgNO ₃ + Na NO ₃ (49,51)	126.7	278	3.73	Bloom et al.1965
AgNO ₃ + KNO ₃ (54,46)	138.2	150	3.6 extrap.	Bloom et al.1965
KNO ₃ + NaNO ₃ (71,29)	96.3	330	3.60	Bloom et al.1965
KNO ₃ + NaNO ₃ (40,60)	91.4	333	3.80	Bloom et al.1965
	-	140	5.28	Turnbull 1961a
NaHSO ₄ + KHSO ₄ (53.5, 46.5)	130.8	125	4.27	Turnbull 1961a
Ag Cl + Ag I (47,53)	192.1	300	1.82 (± 10%)	Section 4.2
Na Cl + Fe Cl ₂ (46,54)	95.5	158	2.60	Turnbull 1961a
Na Cl + Zn Cl ₂ (42,58)	103.6	270	3.68	Turnbull 1961a
LiCl + K Cl (59,41)	55.7	353	6.90	Turnbull 1961a
* KNO ₃ + NaNO ₂ + NaNO ₃ (44, 49, 7)	84.4	142	4.98	Turnbull 1961a
	-	142	5.6 (± 10%)	Lane et al.1958
	-	142	4.6 (± 10%)	Vargaftik 1952
+ NaF + KF + LiF (51.5, 42, 6.5)	58.1	500	6.0	Ewing et al.1962

* heat transfer salt; + 'Flinak'

TABLE 3.2 showing the thermal conductivity of molten salt mixtures near the melting point.

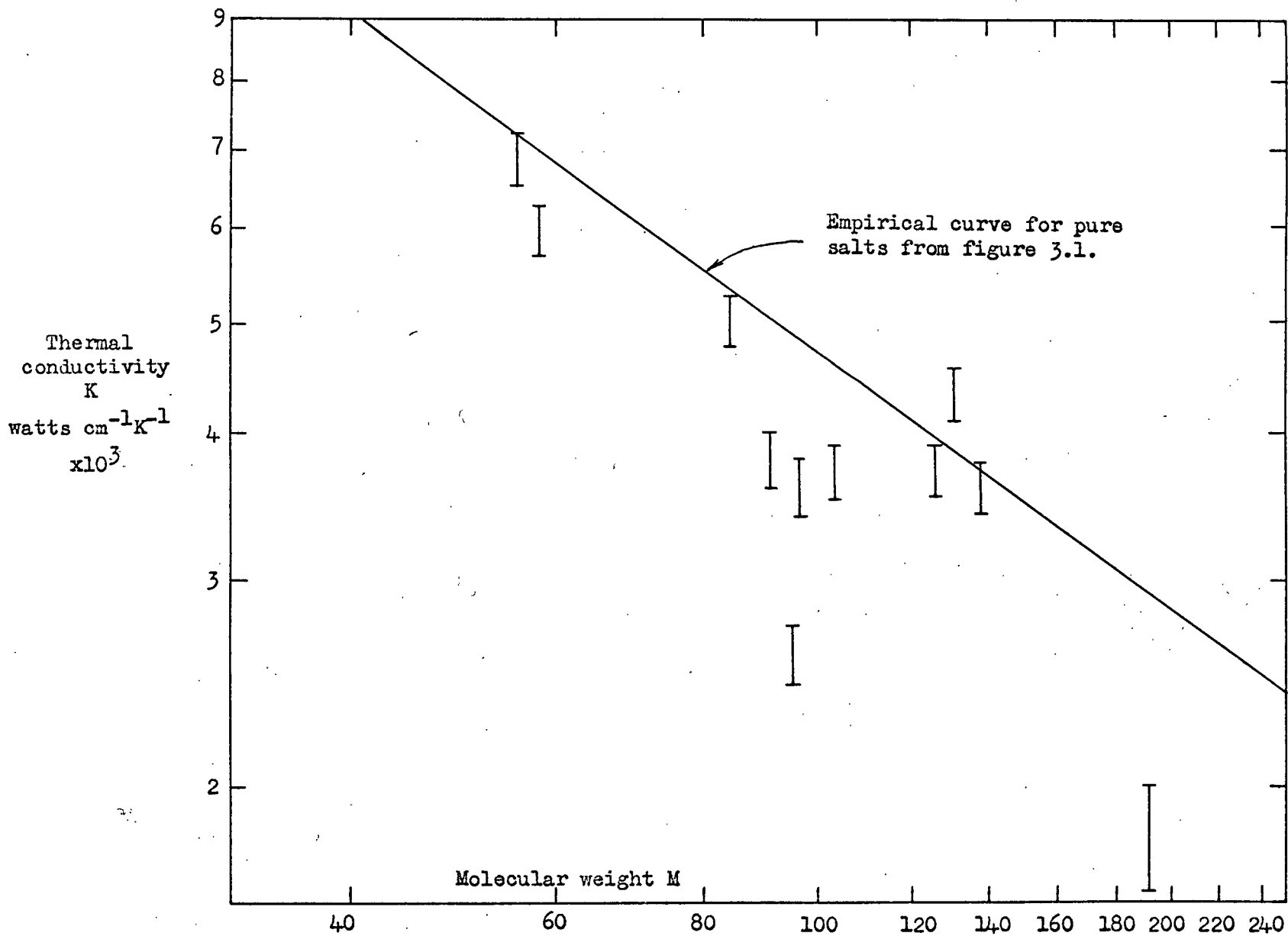


Figure 3.2.
The thermal conductivity of molten salt mixtures.

3.2 Experimental results using the transient hot wire method.

3.2.1 Introduction.

There has been much discussion in the literature during recent years regarding the advantages and disadvantages of the classical steady state methods of measuring thermal conductivity and the transient hot wire method. This controversy has spread into the realm of molten salts. Until 1960 all the experimental thermal conductivity data on molten salts had been obtained using steady state apparatuses. Often there were problems of containment and some of the values were over 50% high owing to radiation. The basic advantages of the transient hot wire method are that under suitable conditions the effects due to radiation and natural convection are negligible and it is not necessary to know the thermal conductivity of the containing material.

In this section it is not proposed to discuss the various methods of measuring liquid conductivities as this has been done many times before (for example by Tait and Hills 1964); nor to include a rigorous theoretical analysis of the transient hot wire method and the errors involved as this also has been studied (and the pertinent results summarised by Turnbull 1961a). But rather to describe some experiments using a transient hot wire rig with some modifications of previous methods made in an attempt to adapt this technique to measurements on molten salts. The precise cause of any inconsistencies in the results have been ascertained and (not incidentally) a few thermal conductivity values of use in this project have been measured.

Basically the transient hot wire method involves passing a current through a fine wire submerged in the liquid to be measured and measuring the rate at which heat is dissipated from the wire. This rate of heat dissipation determines the rate of increase of the mean temperature of the wire which in turn is related to the rate at which the resistance of the wire increases. In its most primitive form therefore the rig consists of a Wheatstone Bridge circuit with one of the arms as a wire immersed in the liquid to be measured. If the bridge is accurately balanced the rate of deflection of the galvanometer after full current is switched on may be directly related to the thermal conductivity of the liquid. Refinements used by Turnbull (1961a)

included the use of a potential probe, stabilising resistance and a fast recorder or oscilloscope in place of the galvanometer. Further refinements used in this project include the introduction of another potential probe and the use of a relay switching circuit to enable tests to be conducted within a period of a few seconds, thus ensuring that the effects of natural convection and general fluid movement are negligible.

The complete circuit is shown in figure 3.3. It is analysed in three parts which constitute the following three sections; the bridge circuit, the cell and the switching circuit.

3.2.2 The Bridge Circuit

A number of authors (including Turnbull 1961a) have shown that for the ideal case where a wire (of length l) is considered as a line source in a liquid of infinite extent:

$$K = \frac{\dot{q}}{4\pi l} \frac{d \ln t}{dT_t} \quad \dots\dots(3.5)$$

where K = thermal conductivity of the liquid

\dot{q} = rate of heat dissipation from the wire

t = time after $t = 0$ when the current was switched on.

T_t = temperature (above T_0) at time t .

The relevant part of the bridge circuit shown in figure 3.3 may be redrawn in the form shown in figure 3.4. It is then evident that at the balance point when the potentiometer voltage $V_p (= V_{bd})$

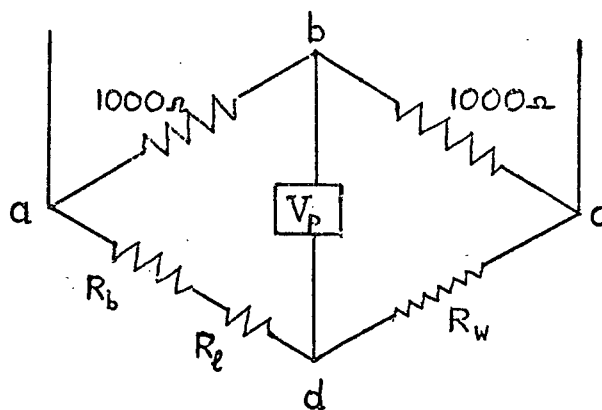


figure 3.4.

is zero :

$$V_{cd} = V_{da} = \frac{1}{2} V_{ac}$$

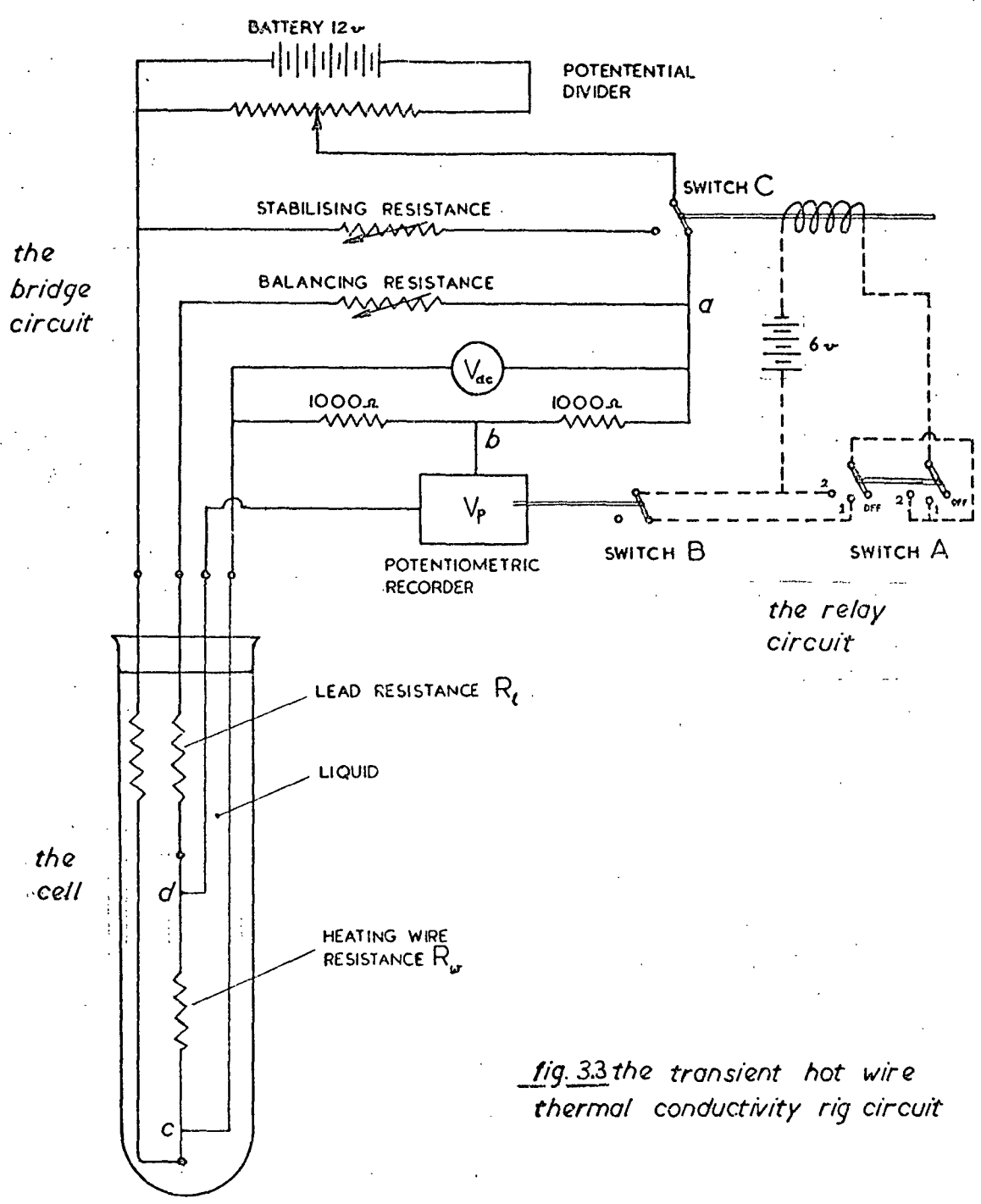


fig.33 the transient hot wire thermal conductivity rig circuit

$$\text{Hence } \dot{q} = \frac{V_{cd}^2}{R_w} = \frac{V_{ac}^2}{4R_w} \dots\dots(3.6)$$

where V_{ac} = voltage across the bridge
 R_w = is the initial resistance of the wire at the temperature at which the test is being conducted.

The term $d \ln t / dT_t$ may be subdivided into a number of measurable quantities:

$$\frac{d \ln t}{dT_t} = \frac{d \ln t}{dV_p} \frac{dV_p}{dR_w} \frac{dR_w}{dT_t} \dots\dots(3.7)$$

$\frac{d \ln t}{dV_p}$ is the rate of change of the balance voltage of the bridge and may be measured using a fast potentiometric recorder or oscilloscope.

$\frac{dV_p}{dR_w}$ is the bridge sensitivity. At the balance point an analysis of the circuit shows that this is equal to $V_{ac} / 4R_w$.

$\frac{dR_w}{dT_t}$ is the product of the temperature coefficient of resistance of the wire α and the resistance of the wire R_w .

Hence from equation 3.7 :

$$\frac{d \ln t}{dT_t} = \frac{\alpha V_{ac}}{4} \frac{d \ln t}{dV_p} \dots\dots(3.8)$$

Substitution of equations 3.6 and 3.8 into equation 3.5 shows that

$$K = \frac{V_{ac}^3 \alpha}{64 \pi l R_w} \frac{d \ln t}{dV_p}$$

For experimental purposes the change in length of the wire with temperature change may be neglected and K may be expressed in the following form :

$$K = \frac{C V_{ac}^3 \alpha}{R_w} \frac{\log_{10} t}{V_p} \dots\dots(3.9)$$

where the constant C may be found by calibrating the apparatus with liquids of known conductivity.

An experimental check of this equation is shown by figures 3.5 and 3.6. The former shows the lineality of the $V_p - \log t$ curve during the first few seconds after switching on the current. The latter shows that for a particular liquid at one temperature (when α , R_w and K are constant) the following proportionality holds:

$$\frac{1}{V_{ac}^3} \propto \frac{\log t}{V_p}$$

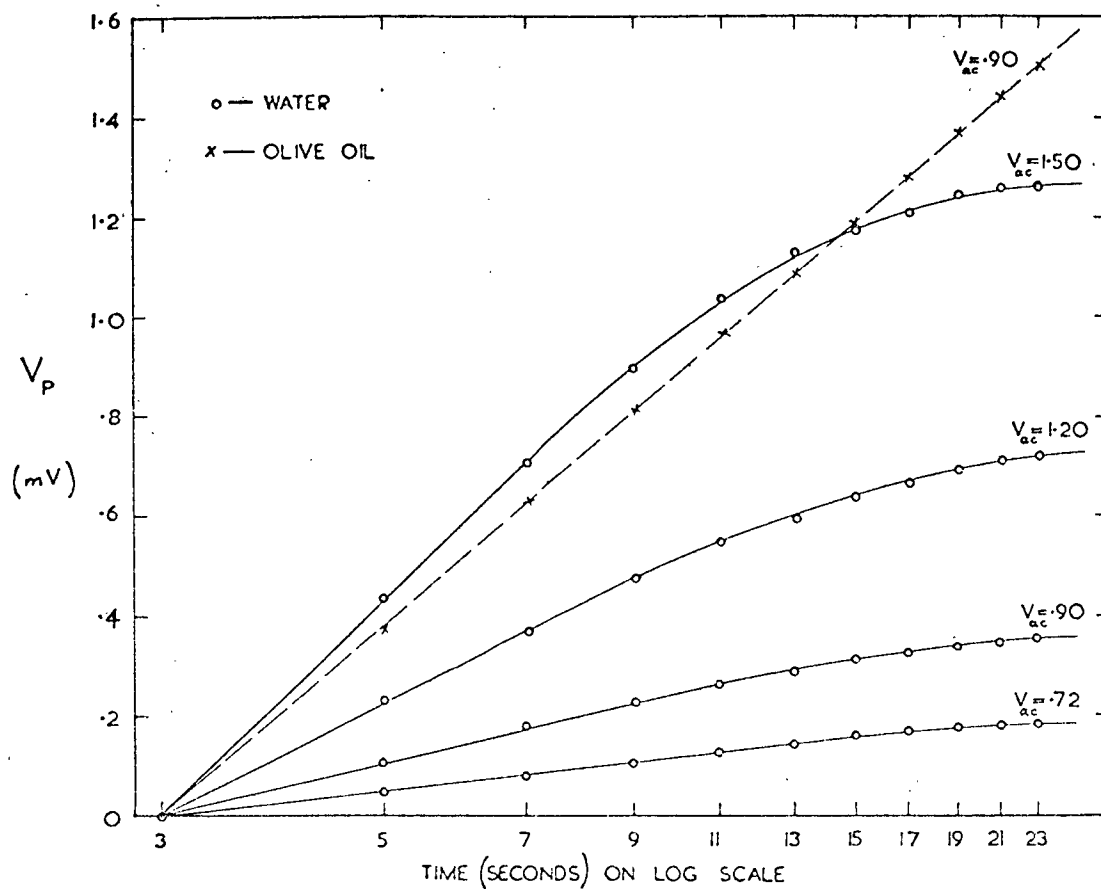


figure 3.5 graph of potentiometer voltage (V_p) against log time (t)

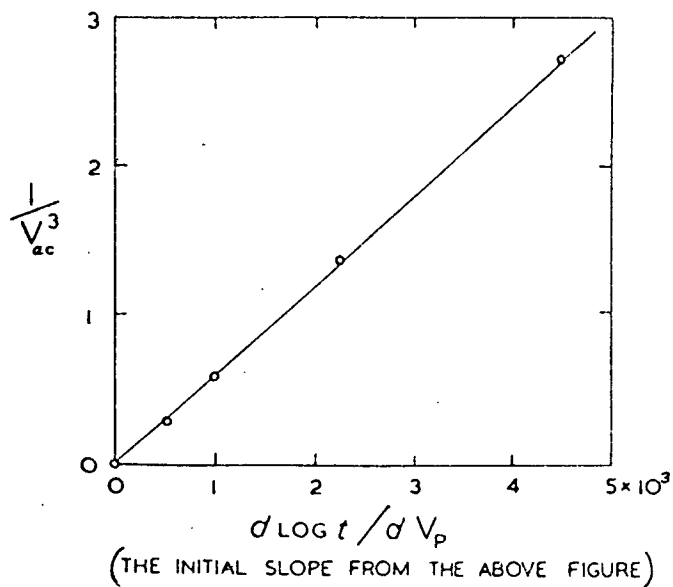


figure 3.6

a plot of the slopes of the above curves for water showing that:

$$V_{ac}^3 \frac{d \log t}{d V_p} = \text{constant}$$

as derived in equation 3.9.

3.2.3 The cell.

The furnace, cell and probe arrangement in its final form is shown in figures 3.7 to 3.10 and with the accompanying notes are largely self explanatory. This rig was in fact the third to be built and the following are some of constructional problems that were encountered.

The platinum heating wire itself must be fine enough to have a resistance of at least two orders of magnitude greater than the copper wire circuitry and yet be strong enough (at the operating temperature) to withstand reasonable tension. In addition the resistance of this wire must at no time be sufficient at a particular current flow to produce a potential difference across the ends which is in excess of the decomposition potential of the salt. Theory and experimental investigations showed that for this particular cell an optimum wire size was 36 S.W.G. Other current carrying wires in the cell were of 22 S.W.G. platinum and the potential probe wires were of 36 S.W.G. platinum. Effects due to change of resistance with temperature change of the current carrying wires in the cell were small and tended to cancel when the cell was calibrated with liquids of known conductivity.

Initially no steel liner was used in the furnace and a temperature difference of up to 10°C was found between the top and bottom of the cell. This difference was reduced to about 3°C at 300°C and 5°C at 500°C upon the introduction of the liner and the addition of more windings at the top of the furnace. This was sufficiently accurate as the temperature coefficient of the conductivity of the liquids measured was very low. The mean temperature of the cell was conveniently measured using the platinum heating wire itself by effectively treating it as a platinum resistance thermometer. The Chromel-Alumel thermocouple was used to check this result.

In the final development a small loop was included in the upper current carrying conductor as shown in figures 3.7 and 3.8. (This modification was suggested by Mr. D.T. Jamieson of the National Engineering Laboratory who kindly inspected the apparatus). This loop increased the length of the submerged section of the conductor thus decreasing the temperature difference between the top current conductor and the liquid.

(to face page 57)

- a. Nitrogen inlet tube.
- b. Platinum leads to current carrying wires.
- c. Loop in upper lead to ensure the temperature is the same as the surrounding liquid.
- d. 36 S.W.G. platinum current carrying wire.
- e. Liquid under test.
- f. Wire tensioning device.
- g. Rubber band.
- h. Stainless - steel sheathed Chromel-Alumel thermocouple wires.
- i. Potential tapping wires.
- j. 'Caposil HT' 25 mm thick insulation board used for furnace construction.
- k. 'Triton' ceramic fibre insulation.
- l. Nickel - chrome wire wound heater.
- m. Aluminous porcelain tube.
- n. Thick steel tube.
- o. 'Vitreosil' fused silica test tube.

Notes on figure 3.7.

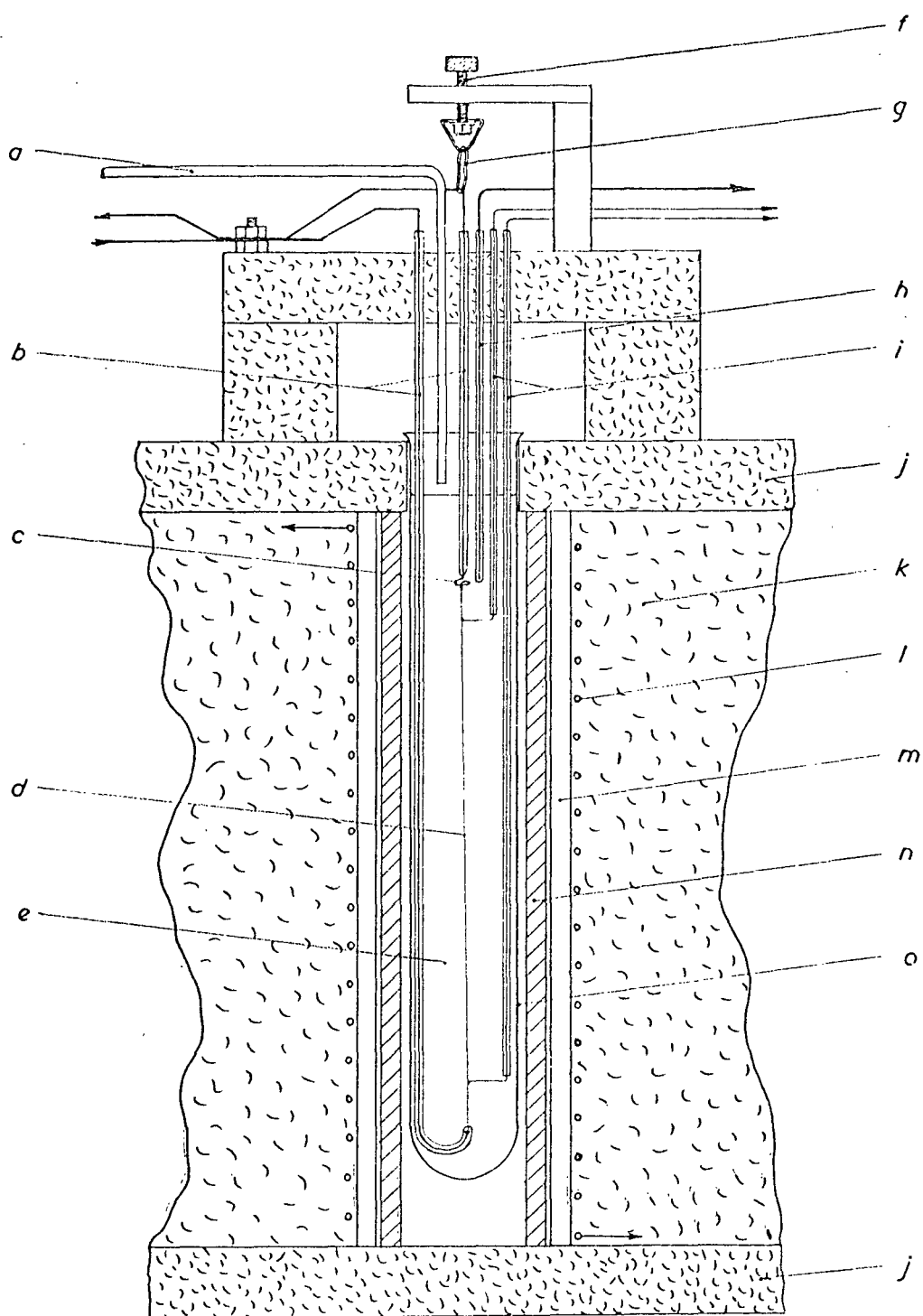


figure 3.7 the transient hot wire thermal conductivity apparatus

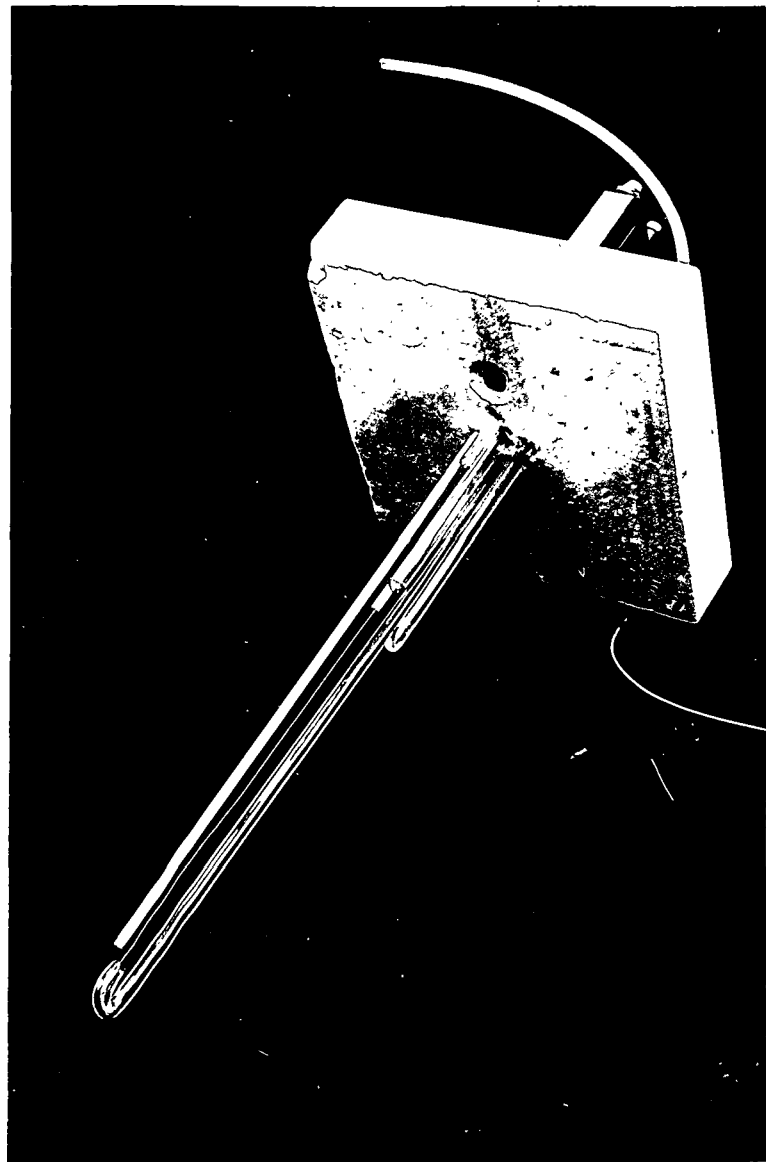


Figure 3.8

Showing the probes before
insertion in cell.

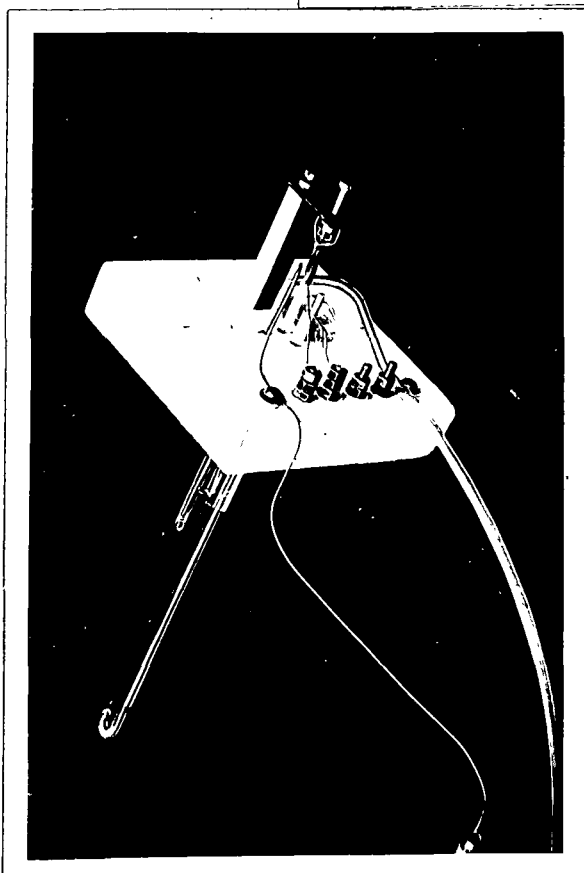


Figure 3.9 Showing the probe
assembly. Connections left to
right:

- stainless-steel sheathed
thermocouple wires
- upper current carrying wire
with tensioning device
- lower current carrying wire
- upper potential tapping wire
- lower potential tapping wire
- nitrogen inlet tube

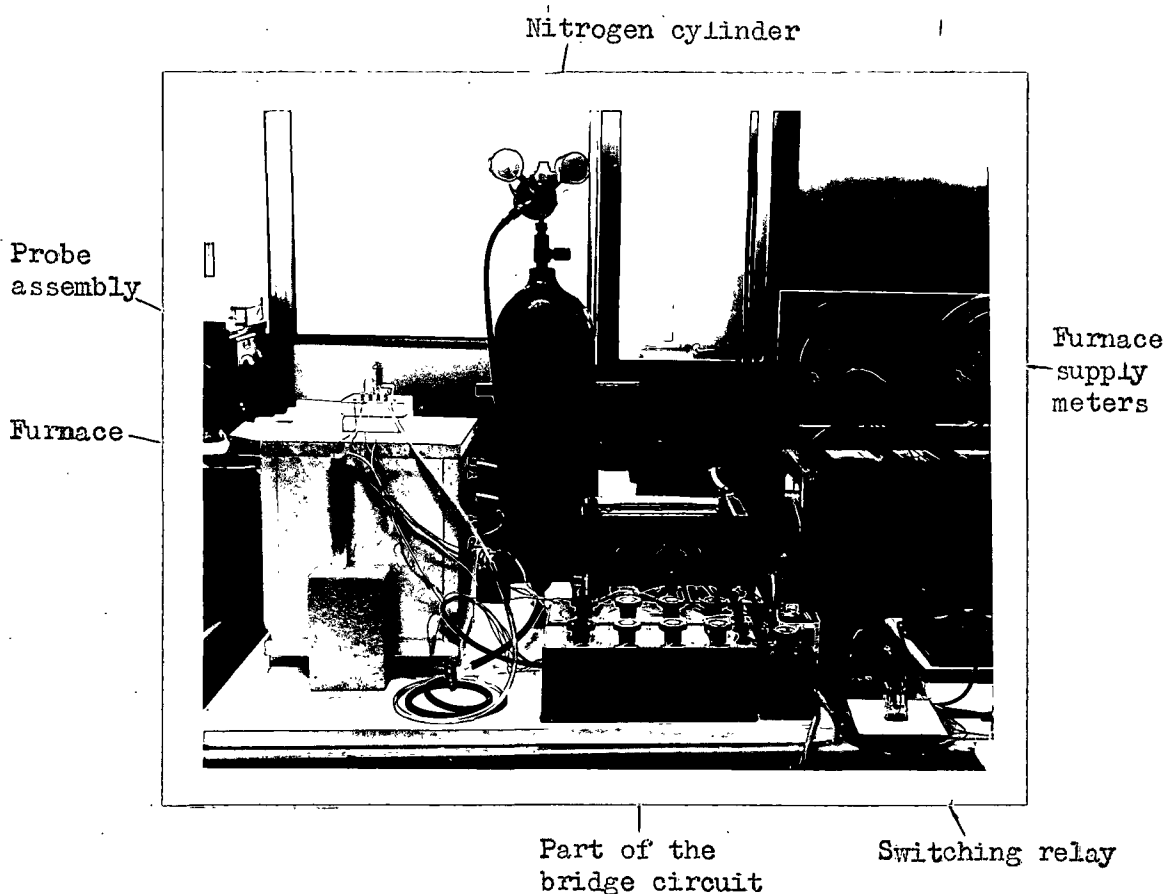


Figure 3.10. The furnace and probe assembly ready for use.

3.2.4 The switching circuit

The onset of free convection in the cell is very clearly shown on a plot of V_p versus $\log t$ as a departure from lineality. Figure 3.5 shows that in the case of a viscous liquid such as olive oil there is no indication of convective currents for over 20 seconds. But a less viscous and more thermally conductive liquid such as water can exhibit non-lineality after less than 10 seconds. Since molten salts often fall into the latter category the possibility of measuring the conductivity of liquids within a few seconds was investigated. This was eventually achieved by selecting two particular points on the time scale and measuring the change in millivolts across the potentiometer during this period. This has the additional advantage that $\log t$ becomes a constant and equation 3.9 is thus simplified.

The precise point at which the circuit was closed then became rather critical and the relay switching circuit shown in figure 3.3 was incorporated. The Philips PR3210 12-point automatic

potentiometric recorder was set to record the balance voltage V_p every two seconds; hence a recorder channel cycle took 24 seconds. The switch B was fitted to a shaft in the recorder and arranged to close the external relay circuit every time it reached channel position '12'. The procedure for commencing a V_p - time plot then consisted of the following steps:

1. Switch A (with two poles and three positions as shown in figure 3.3) was moved from the OFF position to position 1 at any time on the recorder channel cycle.
2. At channel position 12 switch B was closed by the recorder mechanism. This completed the relay circuit which in turn closed switch C and thus closed the bridge circuit.
3. After switch C was seen or heard to have closed switch B was manually changed from position 1 to position 2. This closed the relay via another circuit and thus ensured that as the recorder moved from position 12 the relay was not reopened.

The potential V_p was taken as the millivolt difference on the chart between points 1 and 2 (at 2 and 4 seconds after closure of the bridge circuit) and $\log t$ is a constant.

Before being connected to the bridge circuit the 12 volt battery was allowed to pass current through a stabilising resistance which was set equal to that of the bridge circuit. As its name would suggest this stabilised the output from the battery. Careful adjustment of the switches enabled results to be obtained with good consistency.

3.2.5 The test procedure.

In the case of tests on common liquids at room temperature there were no problems regarding the setting up of the cell. The cell and probes were cleaned and dried, the liquid to be measured was added to the cell and the probes were placed in position. A period of an hour or two was allowed before tests were commenced to enable liquid motion to reach a minimum level. About four runs each were made on Olive Oil, Toluene, Carbon tetrachloride and distilled water. The switching circuit described previously was used for the tests although sometimes

the plotting was allowed to continue until there were obvious signs of convection. The results were used to check the functioning of the apparatus and for calibration to find the constant C of equation 3.9.

Tests at high temperature on salts were more difficult. The cell was heated to about the desired temperature and the molten salt in powdered form was dried in an oven at 150°C and poured in the cell. The probes were then inserted and nitrogen was allowed to flow slowly into the volume above the salt, finding its exit in the crevices between the insulation board joints. On two occasions some component of the probe assembly broke at this stage, presumably owing to thermal shock, although it was inserted very slowly. A period of about six hours was required for the furnace and cell to settle at the desired temperature. An anomaly occurred in some of the $V_p - \log t$ curves and this is discussed later. Nevertheless some meaningful results were obtained although inevitably the accuracy suffered.

Hot wire methods are seldom applied to solids owing to the difficulty of getting the fine wire into the solid. Some solids such as salts may of course be melted and allowed to solidify around the wire as was done in this case with ZnCl_2 and the $\text{AgCl} - \text{AgI}$ eutectic mixture. The conductivity of the eutectic was measured at four temperatures between the melting point and room temperature. This test was arranged to be the last performed on the rig as reheating after solidification caused the solid salt mixture to expand and shatter the cell and probes.

3.2.6 Results.

3.2.6.1 Results for common liquids at room temperature.

The thermal conductivity of four common liquids whose conductivities are known accurately from the literature were measured at a temperature of $20^{\circ}\text{C} \pm 0.1^{\circ}\text{C}$ in order to calibrate and check the apparatus. The results are shown in table 3.3. V_{2-4} ($=V_p$) represents the millivolt difference between the recorded points at 2 and 4 seconds. Differentiation of the equation giving the variation of the resistance of a platinum wire with temperature over the required range (Turnbull

Liquid	V_{2-4} (millivolts)	Vac (volts)	$C \frac{(\text{Vac}^3 \alpha)(\log t)}{R_w V_p}$	K (ref.) (watts cm ⁻¹ K ⁻¹)	Error (%)	
Olive Oil	0.350) 0.346) 0.346) 0.342)	0.346	0.665	1.67×10^{-3}	1.68×10^{-3}	- 0.6
Toluene	0.440) 0.448) 0.445) 0.443) 0.448) 0.445)	0.445	0.666	1.305×10^{-3}	1.35×10^{-3}	- 3.3
C Cl ₄	0.545) 0.555) 0.567) 0.559)	0.557	0.664	1.02×10^{-3}	1.035×10^{-3}	- 1.5
Water (distilled)	0.0963) 0.0943) 0.0963)	0.0956	0.663	5.99×10^{-3}	6.00×10^{-3}	- 0.2
	0.338) 0.338) 0.338) 0.338)	0.338	1.018	6.09×10^{-3}	6.00×10^{-3}	+ 1.5

TABLE 3.3 showing results for common liquids at 20°C.

1961a) yields $\alpha = 3.959 \times 10^{-3} \text{ K}^{-1}$ at 20°C . The wire resistance between the probes was measured as 0.450Ω and the potential across the bridge V_{ac} was ascertained for each set of curves. The values of conductivity used for calibration have been taken from the review by Jamieson and Tudhope (1964).

Substitution of this information into equation 3.9 enabled the constant C to be calculated. A graphical representation (using the zero intersection as an additional point and ignoring Toluene) yielded the best value of C as 0.742×10^{-3} in S.I. units. The right hand three columns of table 3.3 show the value of conductivity obtained using this constant in equation 3.9, the conductivity from the reference quoted and the percentage error assuming the reference value to be correct. Toluene was ignored because it persistently yielded a value about 3% low. It is necessary for the calibration at room temperature to be as accurate as possible if a reasonable accuracy at higher temperatures is to be obtained. The other liquids are seen to deviate from the reference value by no more than 1.5%

3.2.6.2 Results for salts

The thermal conductivity of ZnCl_2 was measured at 300°C which is about 18°C below its melting point. (This was found not to break the cell and probe assembly on remelting). The conductivity of the $\text{AgCl} - \text{Ag I}$ eutectic mixture (m.p. 259°C) was measured at 300°C and pure Ag Br (m.p. 430°C) was measured at 460°C . Initially the results were obtained by measuring V_p over the period from 2 to 4 seconds as in the previous section. The results for ZnCl_2 were reasonable but those for the molten eutectic were rather inconsistent and those for Ag Br were virtually meaningless. Some plots were therefore made showing the variation of V_p with $\log t$ over a period of about 12 seconds and a typical curve is shown in figure 3.11. It can be seen that after an initial

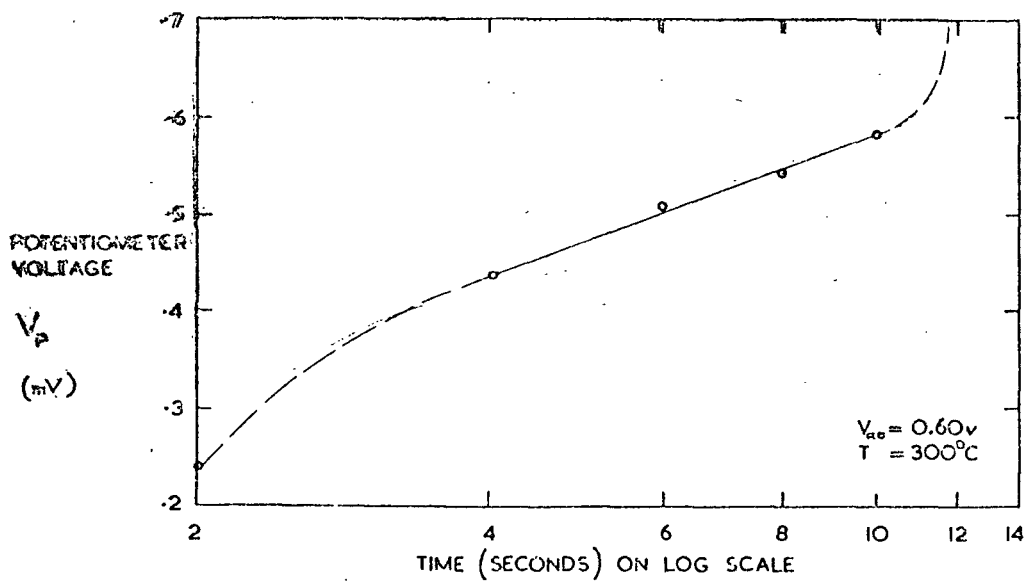


figure 3.11 typical curve for AgCl/AgI at 300 °C.

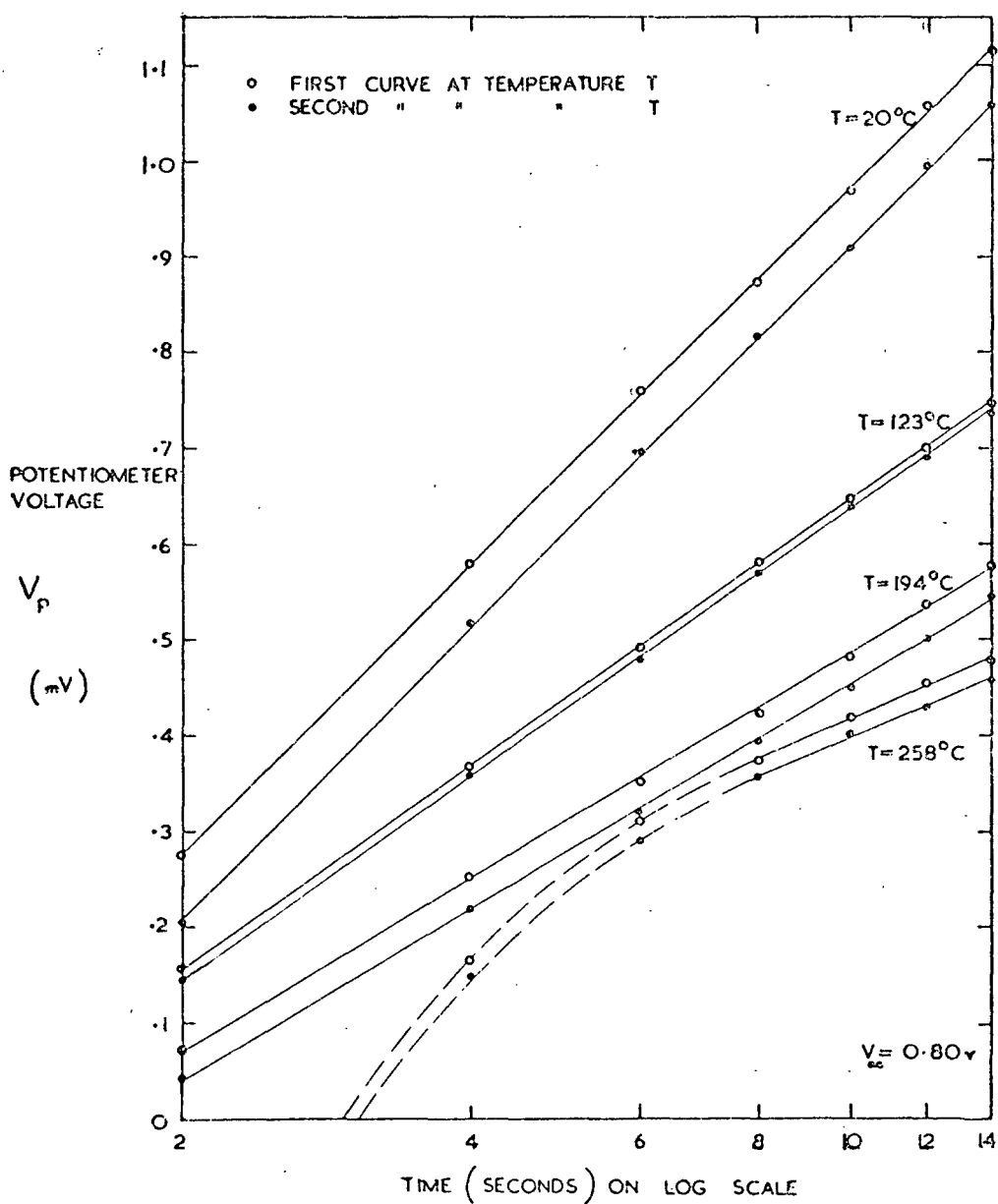


figure 3.12 curves for the solid AgCl/AgI eutectic.

anomaly the curve has a short linear section before convection sets in at about 10 seconds. Sometimes this linear section commenced at the 2 second point. The results shown in table 3.4 for the molten salts are based on the linear portion of each curve. Tests were conducted at several values of V_{ac} in an attempt to increase this linear part. Only two curves were obtained for Ag Br and no meaningful curves could be obtained for the eutectic mixture at 460°C .

The standard deviation of the results for Zn Cl_2 and the AgCl - AgI eutectic mixture are about 5% but the accumulation of errors in measurement and calibration could lead to a further inaccuracy of 4%. The absolute values of thermal conductivity for these salts could therefore be in error by about 10%.

Although only two results were obtained for Ag Br they were at least consistent and the maximum possible error may rather arbitrarily also be given as about 10%.

The $V_p - \log t$ curves for the solid AgCl - AgI eutectic are shown in figure 3.12. The curves at temperatures of 20, 123 and 194°C exhibit excellent linearity as is to be expected when there are no convection currents and the electrical conductivity of the salt is low. But the curves at 258°C show an initial anomaly which is rather similar to that shown by the liquid AgCl - AgI eutectic mixture. The results for the solid eutectic are also tabulated in table 3.4.

3.2.6.3 Summary of results.

A graphical summary of these results together with the measurements of Turnbull (1961b) on two salts are shown in figure 3.13. The decrease in thermal conductivity on melting would appear to be greater in the case of the eutectic than in the case of a pure salt (such as Ag NO_3). Turnbull's value for Zn Cl_2 at 300°C is about 12% lower than that obtained in this work.

Salt	T ($^{\circ}\text{C}$)	$\frac{\log t}{V_p} \times 10^{-3}$	V_{ac}	$\frac{C\alpha}{R_w} \times 10^{-6}$	$K \times 10^3$ (watts $\text{cm}^{-1} \text{K}^{-1}$)
Zn Cl_2 (solid)	300 (± 2)	5.68	0.60	2.922	3.58)
		5.20	0.60		3.29)
		2.37	0.80		3.55)
		2.47	0.80		3.70)
		2.23	0.80		3.34)
		2.40	0.80		3.59)
					3.51
Ag Cl-Ag I eutectic (solid)	20	0.994	0.80	6.39	3.25)
		1.015	0.80		3.32)
	123	1.43	0.80	4.48	3.28)
		1.43	0.80		3.28)
	194	1.70	0.80	3.74	3.26)
		1.71	0.80		3.28)
	258	2.21	0.80	3.18	3.60)
		2.31	0.80		3.77)
					3.29
					3.28
					3.27
					3.68
Ag Cl-Ag I eutectic (liquid)	300 (± 2)	4.96	0.50	2.922	1.81)
		4.71	0.50		1.72)
		2.79	0.60		1.76)
		1.28	0.80		1.96)
		0.684	1.00		2.00)
		0.338	1.20		1.71)
					1.82
Ag Br (liquid)	460 (± 3)	1.72	0.90	2.20	2.76)
		0.73	1.20		2.78)
					2.77

TABLE 3.4 showing results for molten and solid salts.

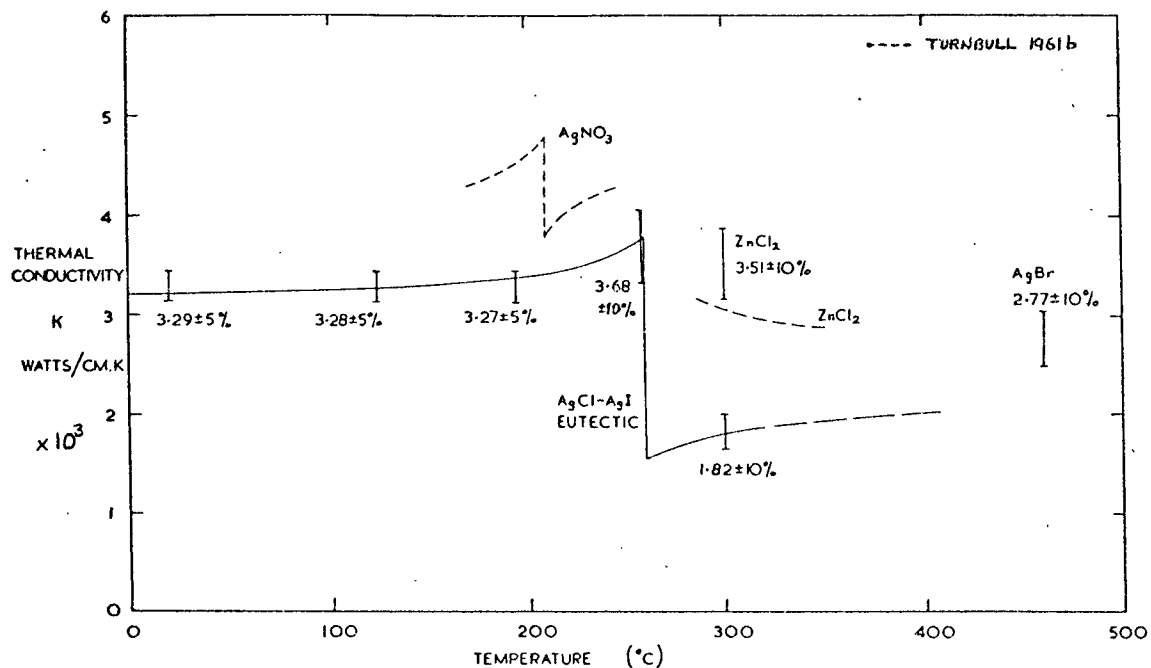


figure 3.13 summary of thermal conductivity results on salts

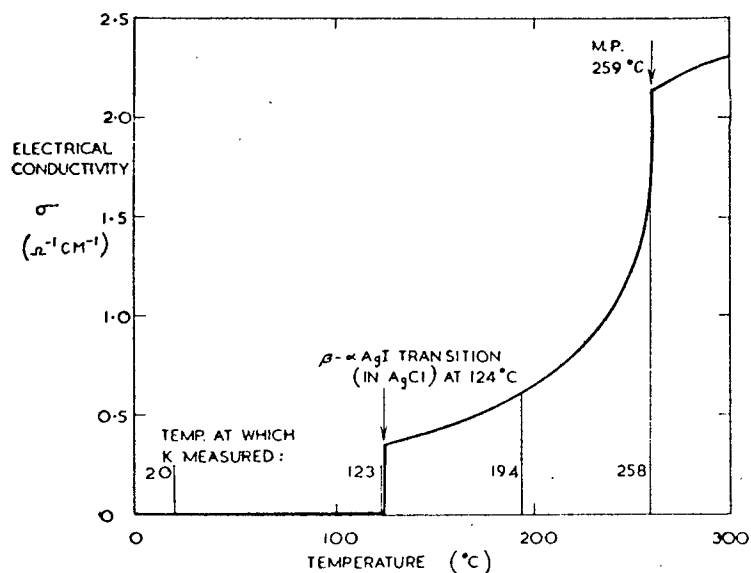


figure 3.14 electrical conductivity-temperature curve for the AgCl-AgI eutectic

(interpolated from the data of Tubandt & Lorenz 1914b)

3.2.7. The cause of the initial anomaly in the $V_p - \log t$ curve for salts.

White and Davis (1967) have criticised the transient hot wire method of measuring thermal conductivity. The main point of their criticism was that in electrically conducting liquids a sizeable current flows through the liquid itself rather than the wire. Turnbull (1961a) was aware of this but claimed that polarization of the salt around the wire rendered the proportion of current flowing through the liquid as negligible. Examination of the equipment used in this project showed that in the absence of any polarization about one fifth of the current could flow through the salt in the case of the molten $\text{AgCl} - \text{AgI}$ eutectic for example. It is therefore pertinent to examine the results with this in mind.

The $V_p - \log t$ curves for common liquids of low electrical conductivity at room temperature show excellent linearity up to the point where convection commences. The same curve for molten salt at 300°C shows an initial non-linearity. This could have been caused by an initial surge of current through the salt before chemical polarization or overpotential was established. Once established the proportion of current flowing through the salt would be negligible and the curve would tend to become linear until convection occurred.

In the case of the solid $\text{AgCl} - \text{AgI}$ eutectic, as mentioned earlier, the $V_p - \log t$ curves at temperatures of 20, 123 and 194°C show no initial anomaly whereas the curve at 258°C shows a millivolt build up similar to that of the liquid eutectic. Examination of the variation of electrical conductivity with temperature for this eutectic shown in figure 3.14 shows that the conductivity at 258°C is almost as high as it is in the liquid state while at the other temperatures it is considerably lower. It is also apparent that the overpotential build up takes longer in the case of the solid than in the liquid.

The evidence therefore suggests that under certain conditions a sizeable proportion of the current can flow through the salt during the first few seconds after switching on the bridge circuit. Nevertheless careful analysis of the part of the curve which is linear can yield reasonable results although the accuracy is reduced. This accuracy for the molten salts measured cannot reasonably be given as better than $\pm 10\%$. Turnbull used a less refined apparatus and it is felt that his quoted tolerance of $\pm 3\%$ is rather optimistic.

3.3 The electrical conductivity of molten salts.

At high temperatures the electrical conductivity of solid ionic materials depends upon the number and mobility of the lattice defects. In the molten state the density of the lattice defects and the mobile ions is at its maximum. Hence conductivity in molten salts is predominantly dependent on the mobility of the cations and anions. The mobility varies exponentially with temperature leading to the following expression for electrical conductivity :

$$\sigma = A_1 \exp (-C_1/RT) + A_2 \exp (-C_2/RT)$$

It is generally found that C_1 and C_2 the activation energies of the cation and anion respectively are either approximately equal or that one is negligible compared to the other (Bloom and Heymann 1947). In either case the above equation may be simplified to the form :

$$\sigma = A \exp (-C/RT) \quad \text{---(3.10)}$$

Data is available on the electrical conductivity of most pure ionic molten salts and it is often presented as the value of constants in the above expression (Janz 1967). The variation of conductivity with temperature of some salts of interest in this investigation is shown in figure 3.15. The conductivity of mixtures of molten salts generally exhibit a slight negative deviation from lineality (Klemm 1964).

Most molten salts have a conductivity in the range 0.5 to $5 \Omega^{-1} \text{ cm}^{-1}$. Salts which have a partially molecular 'structure' in the melt (such as ZnCl_2 just above the melting point) have a conductivity about two orders of magnitude below this range and electronic conduction in the melt (as in Ag_2S and Cu_2Te) usually leads to conductivities about two orders of magnitude higher.

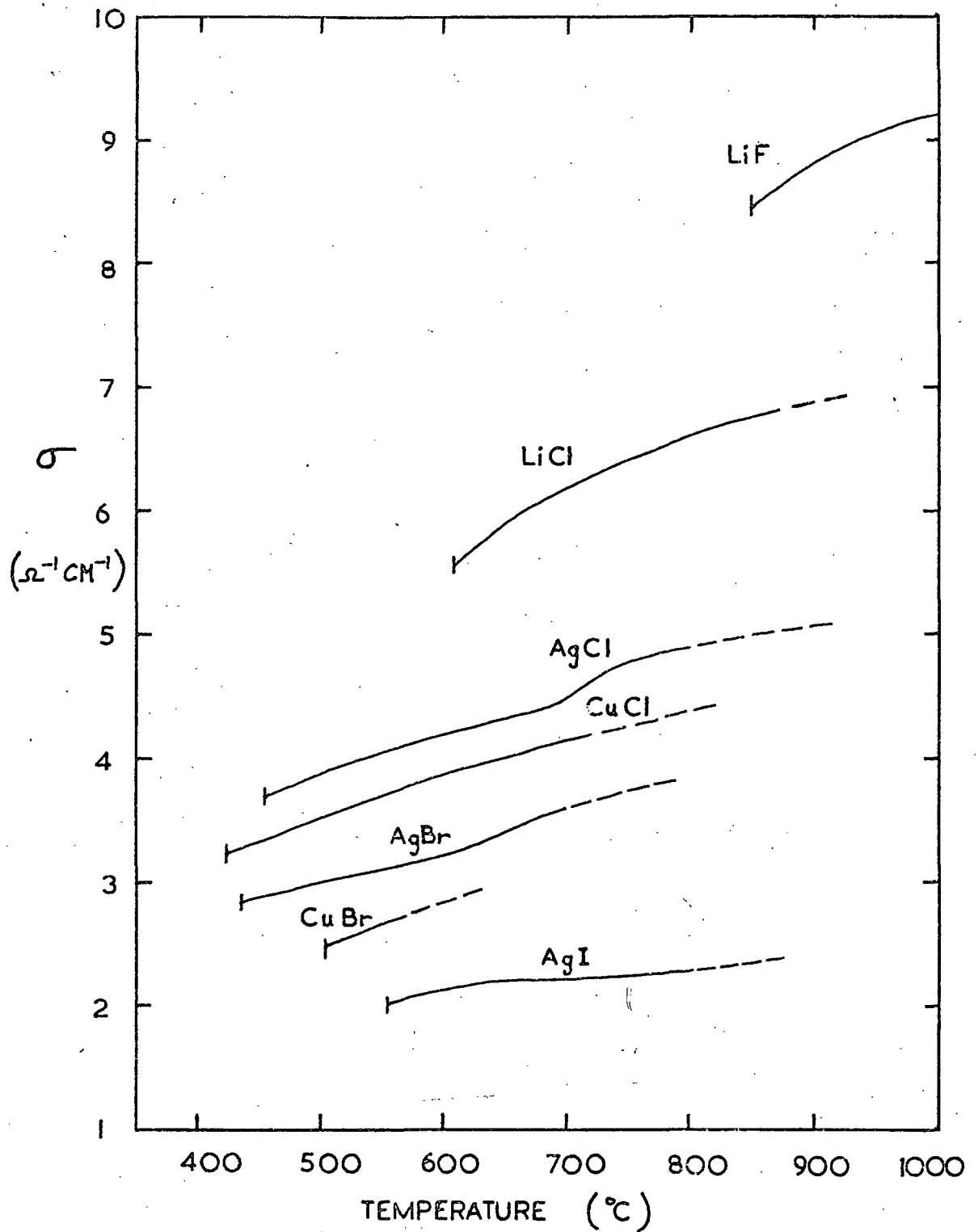


FIGURE 3.15 VARIATION OF ELECTRICAL CONDUCTIVITY σ WITH TEMPERATURE

Chapter 4.

The Thermoelectric Potential of Pure
Molten Salts.

Contents

- 4.1. Theory to the thermoelectric potential of pure molten salts.
- 4.2. Literature review of cationic thermoelectric potential measurements.
- 4.3. Methods of measuring the cationic thermoelectric potential.
- 4.4. Methods of estimating the cationic thermoelectric potential.

* * * * *

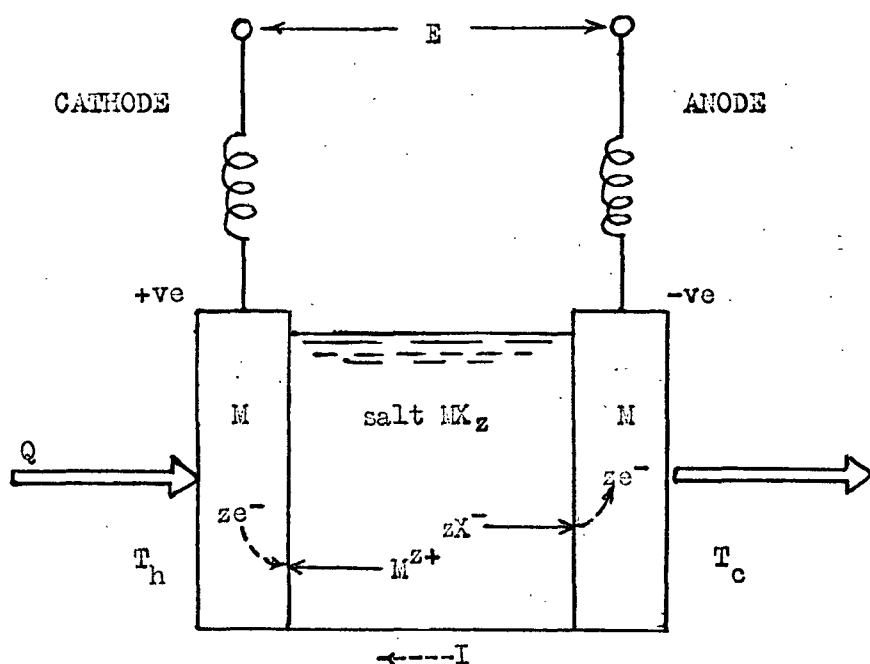


Figure 4.1 A pure salt thermocell (arranged for +ve α).

an electrolysis in which metal is transferred from the anode to the cathode. (Early workers in the field assumed that when the electrolyte was a pure salt all the current was carried by the metal ions and the anion took no part in the transfer. It may easily be shown that the anion can transfer current between the electrodes while still maintaining the stoichiometry of the pure salt).

The following thermodynamic expressions may be applied to the cell:

$$\Delta G = -zEF$$

$$\Delta S = - \left(\frac{\partial \Delta G}{\partial T} \right)_p$$

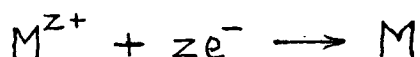
where ΔG is the molal Gibbs free energy change for the process, z is the charge on the ion, E is the open circuit electrical potential difference between the electrodes and ΔS is the molal entropy change of the process.

These may be combined to give:

$$z F \alpha = \Delta S \quad \text{---(4.1)}$$

where α is the thermoelectric potential dE/dT of the cell at constant pressure.

Now consider the process occurring at the hot electrode as electrons flow from the electrode to the electrolyte. The positively charged metal ions in the electrolyte adjacent to the electrode combine with the negatively charged electrons in the metal to give metal atoms at the electrode surface. The equation for this process may be written:



and the entropy change may be written:

$$S_M - \bar{S}_{M^{z+}} - z \bar{S}_e$$

where S_M is the molal entropy of the metal, $\bar{S}_{M^{z+}}$ is the partial molal entropy of the metal ion in the salt and \bar{S}_e is the partial molal entropy of the electron in the metal*. The thermoelectric potential due to this entropy change is termed the heterogeneous part by many authors (for example Mazur 1954, and Kvist 1967). Hence:

$$z F \alpha_{\text{het}} = S_M - \bar{S}_{M^{z+}} - z \bar{S}_e \quad \text{---(4.2)}$$

There is also an entropy change at the junction due to the energy contained by the ions in the salt and the electrons in the metal as they transfer to or from the junction through the surrounding temperature gradient. This energy or 'heat of transfer' is usually denoted Q^* and is taken as positive for energy flow down a temperature gradient. The net heat of transfer is therefore given by:

$$\Delta Q^* = \sum_{\text{ion}} \frac{t_{\text{ion}}}{z_{\text{ion}}} Q_{\text{ion}}^* - Q_e^*$$

* see comment on notation page 7 .

where t is the transference number (the proportion of total current carried by the particular ion). The entropy of transfer S^* ($= Q^*/T$) associated with this heat of transfer leads to a thermoelectric potential which is termed the homogeneous part by the authors mentioned previously. Thus:

$$F\alpha_{\text{hom}} = \sum_{\text{ion}} \frac{t_{\text{ion}}}{z_{\text{ion}}} S_{\text{ion}}^* - S_e^* \quad \text{---(4.3)}$$

The total thermoelectric potential is:

$$\alpha = \alpha_{\text{het}} + \alpha_{\text{hom}} \quad \text{---(4.4)}$$

From equations 4.2, 4.3 & 4.4 the total cationic thermoelectric power of a metal halide salt of the form MX_z as shown in figure 4.1 is :

$$F\alpha = \frac{S_M}{z} - \frac{\bar{S}_{\text{M}^{z+}}}{z} - \bar{S}_e - \frac{t_{\text{M}^{z+}} S_{\text{M}^{z+}}^*}{z} + t_{\text{X}^-} S_{\text{X}^-}^* - S_e^*$$

Now $Q_{\text{M}^{z+}}^* - zQ_{\text{X}^-}^* = Q_{\text{MX}_z}^*$ and $Q_{\text{MX}_z}^*$ refers to the gross transfer of the salt which is obviously zero in a pure salt. Hence $S_{\text{M}^{z+}}^* - zS_{\text{X}^-}^* = 0$.

In addition $t_{\text{M}^{z+}} + t_{\text{X}^-} = 1$ hence:

$$F\alpha = \frac{S_M}{z} - \left(\frac{\bar{S}_{\text{M}^{z+}} + S_{\text{M}^{z+}}^*}{z} \right) - (\bar{S}_e + S_e^*)$$

This may be further simplified by noting that the total transported molal entropy of a species is defined as the sum of the partial molal entropy and the molal entropy transfer of that species:

$$\bar{\bar{S}}_k = \bar{S}_k + S_k^*$$

This yields:

$$zF\alpha = S_M - \bar{S}_{M^{z+}} - z\bar{S}_e \quad \text{---(4.5)}$$

which is essentially the expression derived by Holtan (1953), Lazur (1954), Kvist (1967) and others. In this work the equation will generally be used in the form:

$$zF\alpha = S_M - \bar{S}_{M^{z+}} - S_{M^{z+}}^* - z\bar{S}_e \quad \text{---(4.6)}$$

The total molal transported entropy of the electron in the metal has been shown by Temkin and Khoroshin (1952) and others to be at least two orders of magnitude less than the other terms.

In most molten salt thermocells the hot electrode is found to be the negative electrode (or anode in a galvanic cell) and the thermoelectric potential is therefore generally negative. This means that metal is transferred from the hot to the cool electrode when the external circuit is closed. All purely ionic molten salts appear to have a practically zero temperature coefficient of thermoelectric potential indicating that S_M and $\bar{S}_{M^{z+}}$ increase with temperature at about the same rate.

4.2. Literature review of cationic thermoelectric potential measurements.

Table 4.1 shows the available data on the thermoelectric potentials of thermocells of the type $M/MX_z/M$ where M is a metal and MX_z is a molten salt. The thermoelectric potentials measured in the following section are also included. The temperature coefficient of the thermoelectric potential is practically zero except for $Zn Cl_2$ and possibly $AgNO_3$. Where more than one value is available for a particular molten salt the first measurement listed is considered to be the most accurate and this value is used throughout the subsequent work.

It is apparent that the thermoelectric potentials of cuprous, argentous, plumbous and cadmium halides decrease in the order chlorine, bromine, iodine. Kvist et al. (1966) have shown that this implies that the entropy of transfer of the metal ion, S_{Mz+}^* increases with the ratio of radius of the anion to the radius of the cation.

Although it is not theoretically impossible for the thermoelectric potential of an ionic molten salt to be positive all the measured potentials are in fact negative. This means that in the $M/MX_z/M$ thermocell the metal ions flow to the cool electrode which therefore becomes the cathode. Below a temperature of about $500^\circ C$ $Zn Cl_2$ is not a purely ionic salt as the liquid has a largely molecular 'lattice' (Bockris et al. 1960). But the proportion of ions in the melt increases rapidly with temperature until the salt is largely ionic and the thermoelectric potential is then negative.

<u>Molten Salt</u>	<u>Thermoelectric Potential (mV/K)</u>	<u>Accuracy</u>	<u>Temperature (°C)</u>	<u>Reference</u>
Cu Cl	-0.436	std.dev. .006	462-588	Nichols & Langford 1960
	-0.42	from graph	500	Mogilevski & Usmanov 1967
Cu Br	-0.462	std.dev. .013	482-657	see section 4.3
	-0.470	'rough value'	625	Kvist et al. 1966
	-0.480	from graph	500	Mogilevski & Usmanov 1967
Cu I	-0.5074	±0.0064	610-710	Kvist et al. 1966
	-0.52	from graph	610	Mogilevski & Usmanov 1967
	-0.53	±0.02	620-810	see section 4.3.
Ag F	-0.36	from graph	500	Mogilevski & Usmanov 1967
Ag Cl	-0.375	std.dev. .010	500-900	Senderoff & Bretz 1962
	-0.40	from graph	460-650	Holten 1953
	-0.42	not given	487-590	Markov 1956
	-0.41	from graph	500	Mogilevski & Usmanov 1967
	-0.53	from graph	460-550	Reinhold 1928
Ag Br	-0.440	±0.01	474-599	Ruch & Dupuy 1965
	-0.456	not given	448-549	Markov 1956
	-0.46	from graph	500	Mogilevski & Usmanov 1967
	-0.52	from graph	430-500	Reinhold 1928
Ag I	-0.4898	±0.0028	560-650	Kvist et al. 1966
	-0.505	not given	504(?) - 624	Markov 1956
	-0.50	from graph	600	Mogilevski & Usmanov 1967
	-0.51	from graph	560-600	Reinhold 1928
Pb Cl ₂	-0.006	error 4-8%	565	Detig & Archer 1963
	-0.009	±0.003	500-625	see section 4.3
Pb Br ₂	-0.038	error 4-8%	500	Detig & Archer 1963
Pb I ₂	-0.049	±0.003	400-525	see section 4.3.
Cd Cl ₂	-0.146	not given	584-730	Markov & Kuzyakin 1967
Cd Br ₂	-0.135	not given	580-720	Markov & Kuzyakin 1968b
Cd I ₂	-0.118	not given	400-600	Markov & Kuzyakin 1968b
Sn Cl ₂	-0.031	not given	263	Markov & Kuzyakin 1967
	-0.028	approximate	about 350	Poincaré 1890

Table 4.1 showing the thermoelectric potentials of Metal/Molten Salt/
Metal Thermocells.

continued.....

continued.....

<u>Molten Salt</u>	<u>Thermoelectric Potential (mV/K)</u>	<u>Accuracy</u>	<u>Temperature (°C)</u>	<u>Reference</u>
Zn Cl ₂	varies from +0.06 to -0.04		346-600	Markov & Kuzyakin 1968a
	+0.13	approximate	about 350	Poincaré 1890
Ag NO ₃	-0.323	±0.002	250	Sinistri 1965
	-0.306	std.dev. .005	222-281	Dupuy 1964
	-0.34	error 4-8%	250	Detig & Archer 1963
	-0.319	95%conf: ±.007	310	Schneebaum & Sundheim 1961
	-0.27	approximate	about 250	Poincaré 1890
Ag SO ₄	-0.31	±0.01	657-750	Kvist & Rendsalu 1966

4.3. Methods of measuring the cationic thermoelectric potential.

Measurement of the thermoelectric potential of a molten salt in a cell of the type $M/MX_2/M$ involves simultaneously measuring the electrical and thermal gradients between the two metal electrodes. Most molten salts have no measurable variation of the thermoelectric potential with temperature hence the temperature difference between the electrodes is not important. The proportional error of both the electrical and thermal measurements is obviously reduced by using a fairly ^{large} temperature difference (say 100°C) and some authors have done this. Four basic arrangements for measuring the thermoelectric potential are shown in figure 4.2. Arrangements a, b and c were tried during the initial stages of this project and are discussed in the following paragraphs.

Arrangement a is perhaps the crudest method, but if certain precautions are taken it can yield reasonable results. Kvist (1967) mentions the use of this arrangement to measure the system $\text{Pt}/\text{LiSO}_4/\text{Pt}$. The quartz glass test tube used in this work was 150 mm long and of 10 mm bore. The furnace consisted of a container filled with mineral wool in which the test tube could be inserted. A 'Thermocoax' stainless steel sheathed nickel-chrome resistance wire was wound around the test tube near the top of the furnace. The bottom of the test tube protruded from the raised base of the furnace by about 10 mm and was thus cooled by natural convection and radiation to the surroundings. The electrodes were of pure copper wire situated in closed-end quartz glass tubes. The temperatures were measured using 'Thermocoax' stainless steel sheathed Chromel-Alumel thermocouples fitted in the glass probes. The hot and cold junction temperatures were not very sensitive to the exact position of the probes. This cell was used to make approximate measurements of the thermoelectric potentials of cuprous halides. The thermoelectric potential of Cu Cl was found to be -0.44 mV/K at about 600°C in accordance with the literature value.

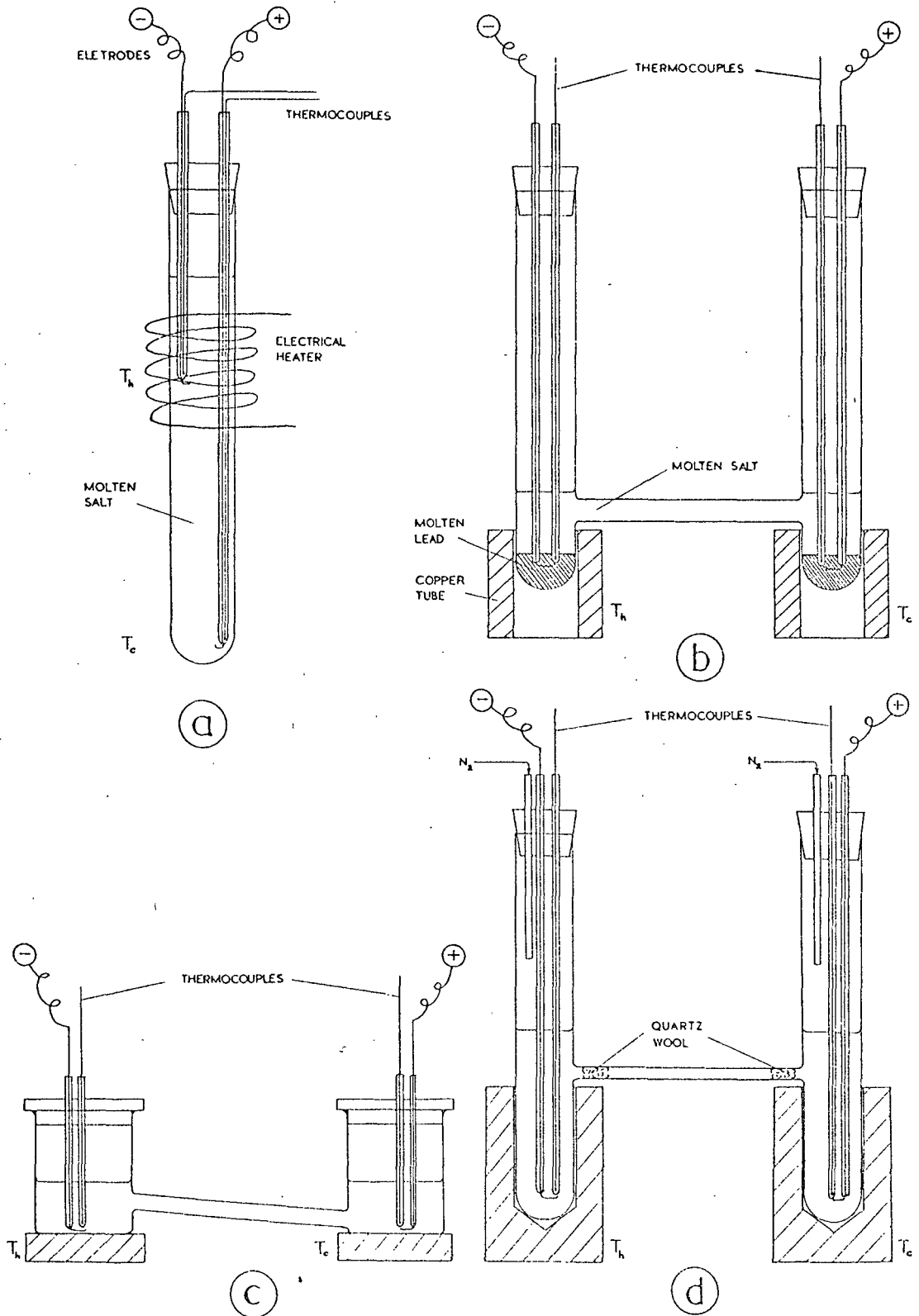
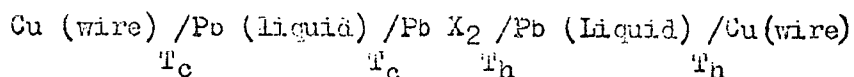


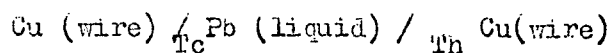
FIGURE 4.2 CELL ARRANGEMENTS FOR THERMOELECTRIC POTENTIAL MEASUREMENTS

No literature values were known to the author at the time of these experiments for the thermoelectric potentials of Cu Br and Cu I and these were measured approximately using this method as -0.46 and -0.53 mV/K between 600 and 800°C. The chemicals used in these tests and also in the following work were general purpose reagent grade (from British Drug Houses or Hopkins and Williams) and they were dried before use.

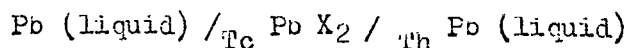
The most common arrangement for measuring molten salt thermoelectric potentials is an 'H' cell or 'U' cell in which a temperature difference exists between the legs (as used by Markov 1956 and Senderoff and Bretz 1962 for example). The arrangement shown in figure 2b is a rather special case as the electrode metal is molten. (A cell of this type would be ideal for thermoelectric generation as the mass transfer between the electrodes could go no further than filling up one of the pockets to the level of the connecting arm). Thermoelectric potential data are available on Pb Cl₂ and Pb Br₂ but not on Pb I₂. This cell was used to measure the system:



where X₂ was Cl₂ or I₂. The cell:



was also measured by filling the cell to the arm with molten lead. Hence on subtraction the cationic thermoelectric potential of the cell:



as defined earlier was found and the results were as follows:

	T_c ($^{\circ}\text{C}$)	T_h ($^{\circ}\text{C}$)	ΔT (K)	V (mV)	α (mV/K)	
Pb Cl_2	500	590	90	-0.9	-0.010	} -0.009
	502	620	118	-1.0	-0.0084	
	502	625	123	-1.0	-0.0081	
Pb I_2	402	505	103	-5.0	-0.0485	} -0.048
	402	510	108	-5.0	-0.0462	
	404	525	121	-5.5	-0.0455	
	410	507	97	-4.9	-0.0506	

For these tests the legs of the 'H' cell were fitted with thick copper tubes which were heated by Bunsen burners. The error was estimated as ± 0.003 mV/K.

Arrangement c consisted of two small quartz glass beakers connected by a small bore tube. The cell was placed in a muffle furnace in which the insulation at one end had been removed so that a temperature gradient existed along the length of the furnace. Nichols and Langford (1960) have used a similar arrangement to make precision measurements of the thermoelectric potential of Cu Cl. Mr. B. Howes used this method to measure the thermoelectric potential of Cu Br in an undergraduate project supervised by the author. The beakers of the cell were of 25 mm internal diameter and were about 100 mm apart. The electrodes were pure copper wire and the temperatures were measured using 'Thermocoax' stainless steel sheathed Chromel - Alumel thermocouples which had been previously paired to give exactly the same potential at the same temperature difference. No inert gas atmosphere was used but the beakers were covered throughout. (It was found that small quantities of impurities made negligible difference to the thermoelectric potential of molten salts). The results obtained were as follows:

	<u>T_c (°C)</u>	<u>T_h (°C)</u>	<u>ΔT (K)</u>	<u>V(mV)</u>	<u>(mV/K)</u>	
CuBr	482	598	116	-55.8	-0.481	} -0.462
	508	609	101	-47.9	-0.474	
	522	620	98	-46.2	-0.471	
	530	628	98	-44.8	-0.457	
	539	638	99	-44.2	-0.446	
	557	653	96	-42.7	-0.444	
	566	657	91	-42.2	-0.463	

The potential between the ends of the copper electrode wires was measured (as it was in all these tests) using a Philips PR 3210 potentiometric recorder. The standard deviation of the set is 0.013 mV/K.

For completeness arrangement d is included in figure 4.2. This was similar to arrangement b but the connecting arm was of smaller bore and wire electrodes were used. Arrangements c and d were used for measuring the thermoelectric potentials of salt mixtures and quartz wool was usually inserted in the connecting arm to reduce thermal diffusion effects.

4.4 Methods of estimating the cationic thermoelectric potential.

In section 4.1. the following expression was derived for the cationic thermoelectric potential α_c , (equation 4.6):

$$zF\alpha_c = S_M - \bar{S}_{M^{z+}} - S_{M^{z+}}^* - z\bar{\bar{S}}_e$$

It was mentioned earlier that the total transported partial molal entropy of the electron $\bar{\bar{S}}_e$ was two orders of magnitude less than the other terms. The molal entropy of the metal S_M is generally available directly from the literature or it may be calculated from specific heat data. The partial molal entropy of the ion $\bar{S}_{M^{z+}}$ in a uni-valent salt is approximately half the molal entropy of the salt. (A more exact expression is given by Pitzer 1961). There is no method of calculating the molal entropy of transfer of the ion $S_{M^{z+}}^*$ and values of this quantity are found to be of a similar order to $(S_M - \bar{S}_{M^{z+}})$. It is therefore not possible to estimate α_c from this expression.

Estimation is possible however when the thermoelectric potential of the anionic and isothermal cells (as defined earlier) are known. Calculation of the anionic thermoelectric potential of the molten halide MX_z along similar lines to that of the cationic thermoelectric potential leads to :

$$zF\alpha_a = -z\left(\frac{1}{2}S_{X_2} - \bar{S}_{X^-} - S_{X^-}^*\right) - z\bar{\bar{S}}_e \quad \text{--- (4.7)}$$

The two partial molal transported entropies of the electron are not strictly equal since one applies to the cathode metal and the other to the anode gas, but they are both very much less than the ionic entropies. The isothermal cell is a formation cell for the salt and the thermoelectric potential is given by:

$$zF\alpha_{iso} = S_{MX_z} - S_M - z\frac{1}{2}S_{X_2} \quad \text{--- (4.8)}$$

From these equations by neglecting the entropy of the electrons:

$$\alpha_c = \alpha_a - \alpha_{iso} \quad \text{--- (4.9)}$$

α_{iso} may be found from the variation of potential of the formation cell with temperature or indirectly from entropy values. Unfortunately there are few data in ^{the} literature on the anionic thermoelectric potential. The following table shows some values of α_c estimated from this expression. α_{iso} values have been calculated from the variation of the potentials of formation cells listed by Hamer et al. (1956). All thermoelectric values are in units of mV/K.

<u>Salt</u>	<u>α_a</u>	<u>T(°C)</u>	<u>Reference for α_a</u>	<u>α_{iso}</u>	<u>α_c</u>	<u>α_c from table 4.1.</u>
Ag Cl	-0.667	500	Fisher 1966	-0.26	-0.41	-0.38
	-0.664	500	Senderoff & Bretz 1962			
Pb Cl ₂	-0.587	550	Fisher 1966	-0.56	-0.03	-0.01
Li Cl	-0.534	750	"	-0.52	-0.01	
Na Cl	-0.483	850	"	-1.10	+0.62	
	-0.45	860	Detig & Archer 1963			
K Cl	-0.504	800	Fisher 1966	-1.43	+0.93	
	-0.40	830	Detig & Archer 1963			
Rb Cl	-0.544	750	Fisher 1966	-1.57	+1.03	
Cs Cl	-0.533	700	"	-1.42	+0.89	

The indications are that some alkali-halides have high positive cationic thermoelectric potentials. However these salts are not suitable for thermoelectric generation owing to the considerable solubility of the metal electrode in the salt and the high vapour pressure of the metal.

It is possible to calculate α_a from known data on α_c and α_{iso} and it is generally found that values fall in the range -0.4 to -0.7 mV/K (as is the case for the chlorides in the above table). This implies that the total transported partial molal entropy of the halide ion \bar{S}_x^- does not vary greatly from salt to salt. It is possible to predict that certain salts will not have a particularly high cationic thermoelectric potential using this information. For example Mg Cl₂ has an α_{iso} value of -0.577 mV/K at 800°C (Hamer et al. 1956). If a value of -0.55 ± 0.2 mV/K is taken for α_a this leads to a value of α_c in the range -0.18 to +0.22 mV/K which is at least a factor of two less than α_c for silver salts.

Chapter 5

The Conversion Efficiency and Engineering Problems of Thermocell Generation

- 5.1. The conversion efficiency of a thermocell and the figure of merit of the salt.
- 5.2. The $Z_s T$ values of some pure molten salts.
- 5.3. Configurational and Electrochemical problems of thermocell generation.
 - 5.3.1. Cells with solid electrodes.
 - 5.3.2. Cells with liquid electrodes.

5.1. The conversion efficiency of a thermocell and the figure of merit of the salt

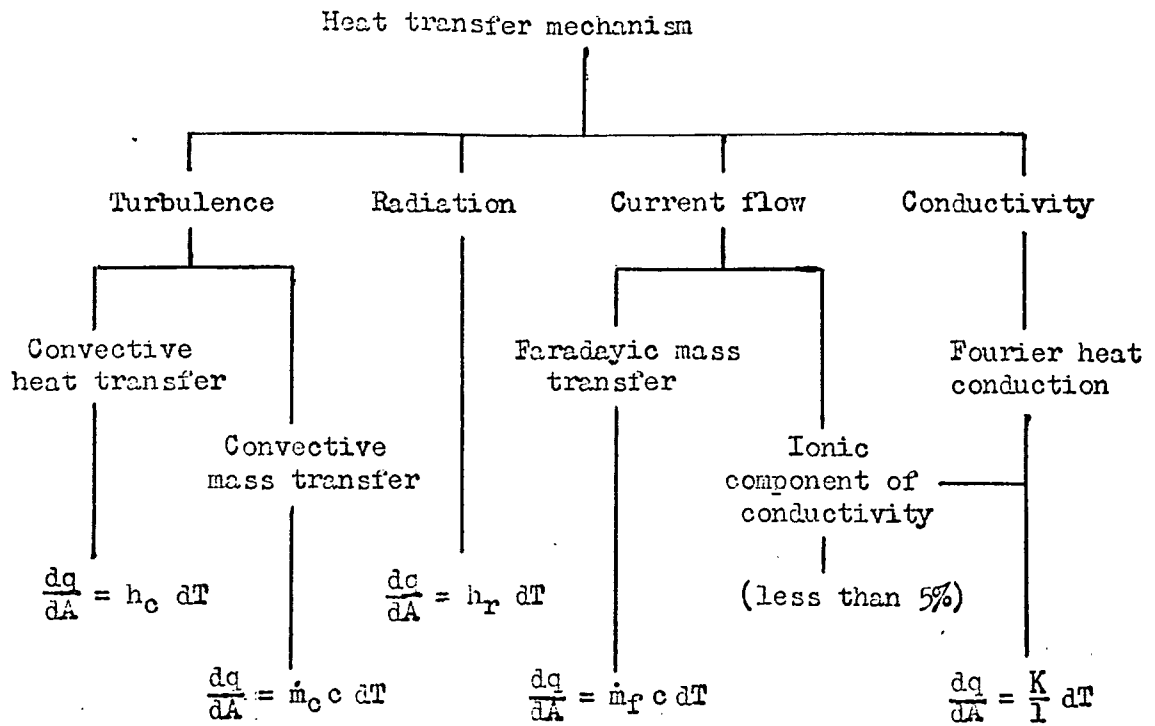
The conversion efficiency of a molten salt — metal couple cannot be analysed theoretically in a simple manner. The dependence of the thermoelectric potential on the electrodes as well as the salt has already been pointed out. The heat transfer between the electrodes is not only dependent upon the electrode temperatures and the thermal conductivity of the salt but also on the natural convection currents set up in the cell and the electrical current flowing. Natural convection besides contributing to the heat transfer is also found to cause convective mass transfer between the electrodes (especially when these are molten metals) and this mass transfer itself has an associated heat transfer. The electrical current flowing through the salt causes a mass transfer due to the Faraday electrolysis effect and again this mass transfer has an associated heat transfer. In addition the thermal conductivity itself has a small ionic component (as was mentioned in section 3.1.1.) which may be affected by the current direction and flow. Thus, even in the case of a pure molten salt thermocell where there can be no concentration gradient, a number of inter-related heat transfer mechanisms are found and these are shown diagrammatically in figure 5.1. The coefficients of the equations are not independent constants as they vary with temperature and also with each other. The electrical energy transfer is less complicated and when there are no polarization effects it is given by:

$$\frac{dI}{dA} = \frac{\sigma}{l} dV$$

where dI/dA is the electrical flux, σ is the electrical conductivity, l is the length between the electrodes and V is the voltage.

The optimum efficiency of a thermoelectric device incorporating semiconductor thermoelements is given by equation 1.2 (page 13). This efficiency is seen to depend upon a figure of merit Z_c defined as:

$$Z_c = \frac{(\alpha_a - \alpha_b)^2}{\left[\left(\frac{K}{\sigma} \right)_a^{1/2} + \left(\frac{K}{\sigma} \right)_b^{1/2} \right]^2} \quad \text{---(5.1)}$$



where $\frac{dq}{dA}$ = heat transfer flux
 h_c = heat transfer coefficient for all convective effects
 \dot{m}_c = mass transfer rate due to convection per unit area
 c = specific heat of electrode material
 h_r = radiation heat transfer coefficient (proportional to T^4)
 \dot{m}_f = mass transfer rate due to the Faraday effect per unit area
 K = thermal conductivity of molten salt
 l = length between electrodes

Figure 5.1 Heat transfer mechanisms in a pure molten salt thermocell.

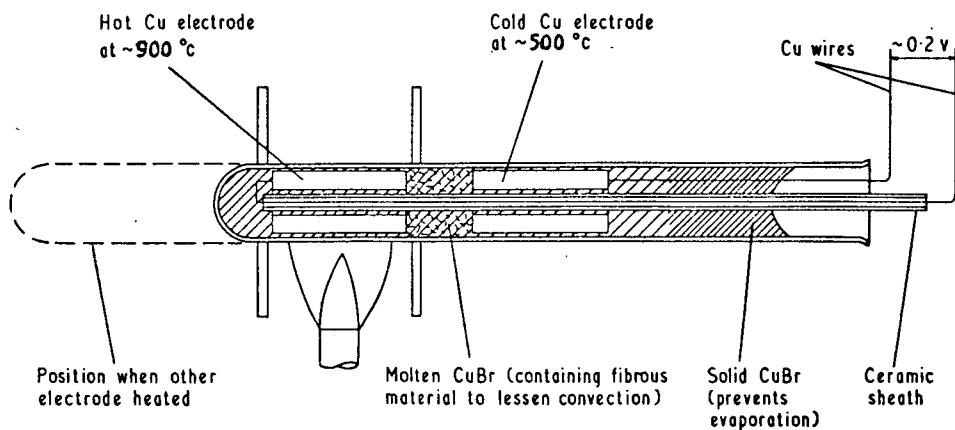
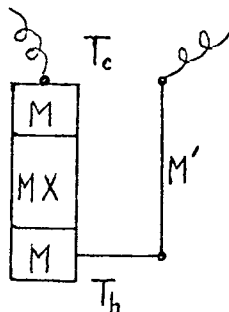


Figure 5.2 Generation thermocell arrangement with solid electrodes.

Under optimum conditions the thermoelectric potential of the couple arms α_a and α_b are equal and of opposite sign and the term K/σ is the same for each arm. The figure of merit then simplifies to $Z_c = \alpha^2 \sigma / K$ and this ratio of properties is given as the figure of merit for a single material.

For a couple consisting of a molten salt thermocell as one arm and a metal as the other arm as shown below the figure of merit cannot be simplified in this way.



The thermoelectric potential of the metal is at least an order of magnitude less than ^{the} salt. In addition the heat transferred through the salt must be considered as depending upon the thermal conductivity together with a number of other mechanisms as discussed previously. Some degree of simplification is possible however if the combined heat transferred by these other mechanisms (per unit area and time) is represented by U . The total heat transferred may then be represented by the following equation:

$$\ell \left(\frac{dq}{dA} \right)_{total} = [K + U] dT$$

Combination of the formulae given in figure 5.1 yields :

$$\ell \left(\frac{dq}{dA} \right)_{total} = [K + \ell(\dot{m}c + h)] dT$$

where \dot{m} is the total mass transfer rate between the electrodes, c is the mean specific heat of the electrode metal and h is the combined heat transfer coefficient. U may therefore be estimated from:

$$U = \ell(\dot{m}c + h) \quad \text{————— (5.2)}$$

For a metal the Wiedemann - Franz Law yields $K/\sigma = LT$ where L denotes the Lorenz number. Thus the figure of merit (at a temperature T) for a thermocell-metal couple becomes from equation 5.1 :

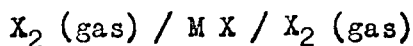
$$Z_c = \frac{(\alpha_s - \alpha_m)^2}{\left[\left(\frac{K+U}{\sigma} \right)_s^{1/2} + (LT)_m^{1/2} \right]^2} \quad \text{--- (5.3)}$$

where suffix s denotes the molten salt and m the metal electrode.

The term $|\alpha_m|$ is usually about fifty times less than $|\alpha_s|$; $(LT)_m^{1/2}$ is about ten times less than $\left[(K+U)/\sigma \right]_s^{1/2}$; and in a suitably designed thermocell U is less than K . Under these conditions the figure of merit of the molten salt-metal couple is predominantly determined by the ratio $\alpha_s^2 \sigma_s / K_s$ which is by definition the figure of merit of a single material, (in this case the molten salt). Thus:

$$Z_s = \left(\frac{\alpha_s^2 \sigma_s}{K} \right)_s \approx Z_c \quad \text{--- (5.4)}$$

The ratio Z_s should more precisely be named the 'cationic figure of merit of the salt'. But since this work is not directly concerned with cells of the form:



the term 'figure of merit of the salt' will suffice, and it will be assumed to refer to the cationic thermoelectric potential as defined in section 4.1.

5.2. The Z_sT values of some pure molten salts.

The Z_sT value ($Z_sT = \alpha^2 \sigma^{-1} T / K$) may now be evaluated using the thermal and electrical data of chapter 3 and the thermoelectric potentials given in chapter 4. Only in the case of AgBr and AgNO₃ have the relevant properties been measured experimentally. Estimation of K is however possible using the curve in figure 3.1 and this enables the figure of merit of a number of other salts to be predicted. Silver and cuprous salts have the highest Z_sT values of the salts studied and some values are given in table 5.1. The Z_sT value at the high temperature is liable to be over-estimated as the thermal conductivity increases slightly with temperature increase.

Some idea of the conversion efficiency obtained using a pure molten salt thermocell-metal couple may be gained by considering the case of AgBr operating between 460 and 960°C. Substitution of reasonable values for the unknown quantities shows that Z_c is of the order of 0.8 Z_s and, making use of the Z_sT values for AgBr given in table 5.1, this yields Z_cT (mean) = 0.2. The conversion efficiency (that is the proportion of heat energy flowing through the salt and the metal which is converted into electrical energy) is found to be 2 $\frac{1}{4}$ %.

In following chapters these salts are taken as the basic constituents in the search for molten salt mixtures capable of efficient conversion of heat energy into electrical energy. In the semiconductor field suitable alloying has led to materials having a figure of merit many orders of magnitude higher than the pure constituents of the alloy.

Molten salt	T (°C)	α (mV/K)	σ ($\Omega^{-1} \text{cm}^{-1}$)	$\frac{K}{\text{watts cm}^{-1} \text{K}^{-1}}$	$\frac{Z_s}{(\text{K}^{-1})} \times 10^3$	$Z_s T$
Ag F	500	-0.36	4.10	4.0 est.	0.13	0.11
	900	"	7.2 extrap.	"	0.23	0.27
Ag Cl	500	-0.375	3.90	3.6 est.	0.15	0.12
	900	"	5.2 extrap.	"	0.20	0.23
Ag Br	460	-0.44	2.93	2.8	0.20	0.16
	900	"	4.0 extrap.	"	0.28	0.33
Ag I	600	-0.49	2.17	2.6 est.	0.20	0.19
	900	"	2.4 extrap.	"	0.22	0.26
Ag NO ₃	250	-0.323	0.85	4.1	0.02	0.01
Cu Cl	450	-0.436	3.32	4.7 est.	0.14	0.10
	900	"	4.4 estrap.	"	0.18	0.21
Cu Br	500	-0.462	2.52	3.6 est.	0.15	0.12
	900	"	3.5 estrap.	"	0.21	0.25

Table 5.1 The figure of merit and the $Z_s T$ value of pure molten argentous and cuprous salts.

No such drastic increase is expected by mixing ionically conducting liquids as the properties are relatively insensitive to mixing proportions. Nevertheless pure molten salts, with their figures of merit in excess of $0.2 \times 10^{-3} \text{ K}^{-1}$, have a reasonably advantageous starting point and an increase of a few times in their efficiency would elevate them to the ranks of good thermoelectric materials.

It was envisaged that the optimum conversion efficiency of a thermoelectric device as given by equation 1.2 (page 13) would often have to be calculated in the subsequent work. The Enfield College 'Honeywell 2000' computer was therefore programmed using Fortran IV to evaluate this efficiency and to represent the results graphically. Some 60 curves were drawn by the automatic plotter to show the variation of the efficiency, Z , T_h and T_c over the ranges of interest. These curves were used for estimating the optimum efficiency throughout the rest of this project. At this stage it was decided to construct some thermocells and observe their operation in order to highlight the major problems to be solved.

5.3. Configurational and electrochemical problems of thermocell generation

5.3.1. Cells with solid electrodes.

It has already been mentioned that the passage of current in a cell of the type $M/T_h \quad MX/T_c \quad M$ causes electrode metal to be eaten away at the anode and deposited at the cathode. In most thermocells the cooler electrode is the cathode. This mass transfer problem must be overcome if a molten salt thermocell is to continuously generate electrical energy from heat energy. In the initial stages of the project three methods of attacking this problem were foreseen. The electrodes could be periodically interchanged, the heat source and sink could be periodically interchanged or the cell could be disposable after limited operation.

To ascertain the feasibility of these methods some cells of the type shown in figure 5.2 were made. These consisted essentially of a 'Vitreosil' test tube of 10 mm internal diameter containing copper electrodes immersed in cuprous bromide. In some cells a small quantity of 'Triton' mineral wool was inserted between the electrodes in an attempt to lessen natural convection. These cells were assembled by placing the test tube in the vertical position, heating to about 500°C and partially

filling with cuprous bromide. The complete electrode assembly was then inserted and the surface of the molten salt was allowed to cool and solidify thus sealing the contents. The test tube was turned into the horizontal position and arranged as shown in figure 5.2 so that either electrode could be heated by positioning it above the gas and forced air flame.

Initially the cell operated successfully and generated about 0.2 volts on open circuit. But after about five minutes this voltage began to drop and within forty minutes it had decreased to zero and the cell was found to have short-circuited. On subsequent withdrawal of the electrode assembly it was seen that a spongy mass of copper had grown between the electrodes and also on the outer ends of the electrodes as shown in figure 5.3. This spongy mass formed irrespective of whether or not a current was flowing in the cell.

When the cells were allowed to cool and then reheated the test tubes broke owing to the thermal expansion of the copper electrodes and the solid salt entrapped between the electrodes and the glass. This was overcome by forming the electrodes of coiled copper wire. The cell shown in figure 5.4 was operated on closed circuit until it short circuited when the electrode was withdrawn. The major part of the growth can be seen to be on the cool electrode due to the electrochemical mass transfer from the hot anode to the cool cathode. The smaller growth on the hot electrode shows the presence of some other mass transfer mechanism acting in opposition to the electrolysis. The mass transfer problem is studied in greater detail in chapter 8 but these tests are sufficient to show that there is little possibility of basing a continuously generating thermocell on this configuration.

5.3.2. Cells with liquid electrodes.

It was mentioned in section 4.3. that one method of overcoming the mass transfer problem would be to arrange an 'H' cell so that the legs contained liquid electrodes. The passage of current would then result in one of the legs being filled until the metal overflowed back into the other leg. Unfortunately the metals of salts with high thermoelectric potentials such as silver do not melt at low temperatures. Nevertheless it is possible to alloy silver with a low melting point metal in such a way that it still acts as a silver electrode (This is equivalent to a metal amalgam electrode in aqueous electrochemical cells). The cell is

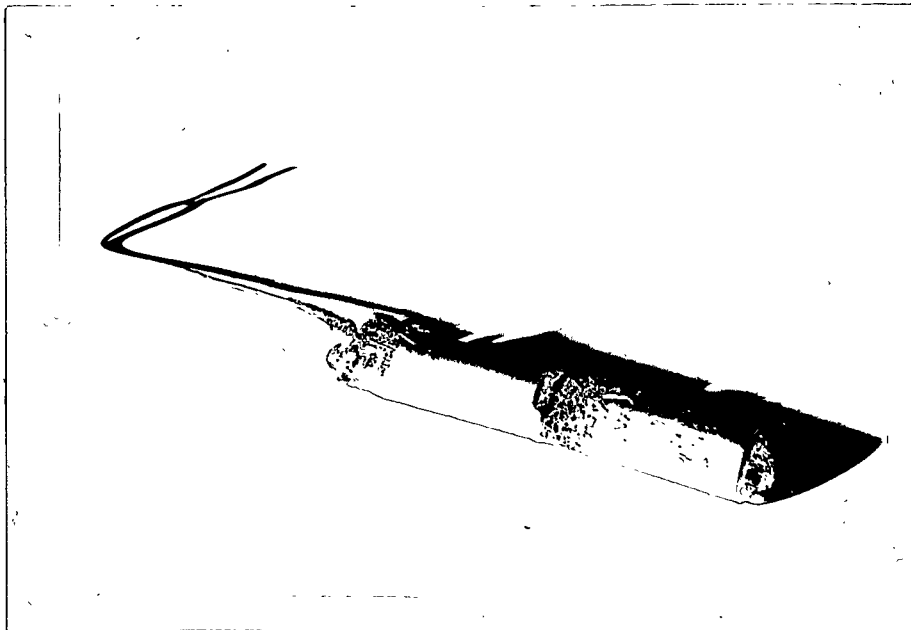


Figure 5.3

The electrode assembly of the cell shown in figure 5.2 after operation.

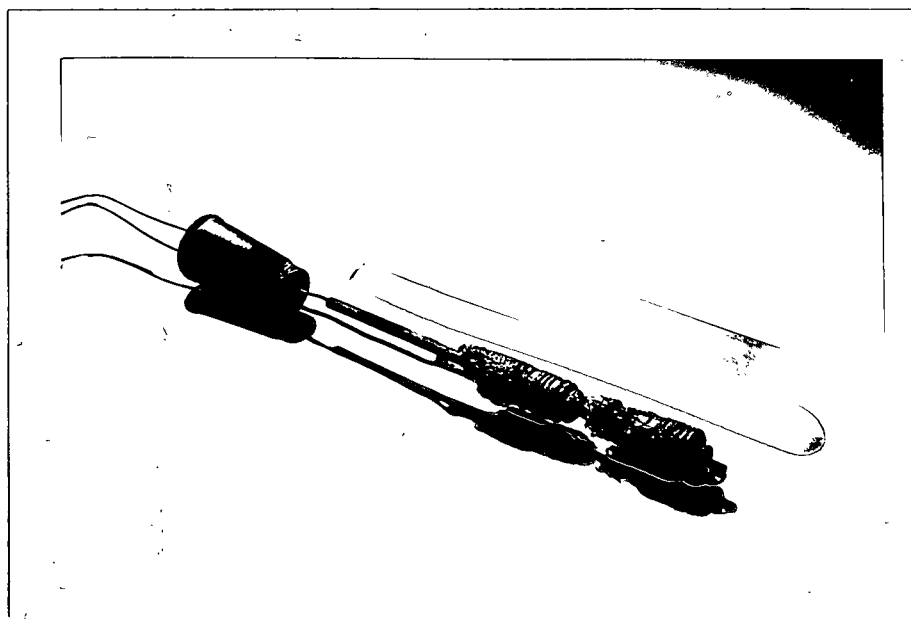
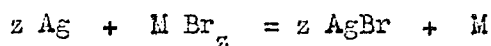


Figure 5.4

Thermocell with coiled copper electrodes after operation.
(Left hand electrode heated).

then of the form $\text{Ag (M)} /_{T_h} \text{Ag halide} /_{T_c} \text{Ag (M)}$ where M is the low melting point metal. This metal must be selected so that the above cell is in thermal equilibrium.

If a closed system contains a metal alloy (of Ag and M) and a silver salt (such as AgBr) a thermal equilibrium of the following type is approached:



Application of the mass action law yields the equilibrium constant K_c in terms of the molal concentrations (denoted by brackets):

$$K_c = \frac{[\text{AgBr}]^z [\text{M}]}{[\text{Ag}]^z [\text{M Br}_z]} \quad \text{-----(5.5)}$$

If the cell is to be maintained with a high proportion of Ag Br in the salt phase the equilibrium must lie to the right hand side and K_c must therefore be greater than unity.

One method of estimating K_c is by using the relationship:

$$E^{\circ} = \frac{RT}{zF} \ln K_a \quad \text{-----(5.6)}$$

where E° is the standard potential of the electrochemical cell $\text{Ag/AgBr// M Br}_z/\text{M}$ and K_a , the equilibrium constant based on activities, is assumed equal to K_c . E may be considered as the difference of the potentials of two formation cells:

$$E^{\circ} = E_1^{\circ} - E_2^{\circ} \quad \text{-----(5.7)}$$

where

E_1° is the potential of the cell $\text{M/M Br}_z/\text{Br}_2$
 E_2° is the potential of the cell Ag/AgBr/Br_2

Consideration of equations 5.6 & 5.7 show that if K is greater than unity E_1° is greater than E_2° and M is more noble than silver. Potentials of metals in their fused chlorides at various temperatures are given by Delimarskii and Markov (1961) and Hamer et al. (1965).

The only suitable low melting point alloy which is more noble than silver is bismuth; and for this reason bismuth was used as the metal M.

From the standard electrode potentials the equilibrium constant was estimated as approximately 30 at 450°C. Equation 5.5 then shows that an equimolar alloy of silver and bismuth is in thermal equilibrium with a salt mixture of about 90 mole % AgBr and 10 mole % BiBr₃.

A convenient method of approximately checking the composition of the salt mixture is to measure the electrical conductivity. It was mentioned in section 3.3. that the specific conductivity of molten salt mixtures is approximately linear. In the case of AgBr and BiBr₃ the conductivities are very different and the composition of the mixture may therefore be estimated from the following relationship:

$$x_{\text{AgBr}} \approx \frac{\sigma_{\text{mix}} - \sigma_{\text{BiBr}_3}}{\sigma_{\text{AgBr}} - \sigma_{\text{BiBr}_3}}$$

where x is the molar concentration. The variation of the conductivity of the equilibrium salt mixture with the composition of the silver - bismuth alloy was measured at 450°C using the cell shown in figure 5.5. (It is allowable to use direct current for conductivity measurement in this cell as it is shown in chapter 8 that there is no polarization. One result was checked using a 3000 Hz supply and no discrepancy was found). The results are shown graphically in figure 5.6. This method can be seen to indicate that an equimolar silver - bismuth alloy is in thermal equilibrium with a salt mixture containing about 15 mole % BiBr₃. The discrepancy between this value and the previous estimation of about 10 mole % BiBr₃ may be due to the presence of bismuth bromide (BiBr) which has been identified in some fused salt systems and metallic bismuth which is soluble to a certain extent in BiBr₃. It can be shown that as the temperature is raised above 450°C the proportion of bismuth salt in the mixture may be expected to increase slightly.

It has been ascertained then that the thermocell $\text{Ag}(\text{Bi}) / \text{T}_h \text{AgBr} / \text{T}_c \text{Ag}(\text{Bi})$ can be arranged so that when thermal equilibrium is attained the salt is still predominantly silver bromide. If a cell of this type is to be used for generation it will be necessary to measure the effect of the bismuth on the thermoelectric potential and also to study the electrochemical equilibrium. In the meantime however it was decided to construct and test a thermocell with liquid alloy electrodes (as shown in figure 5.7) to determine the general feasibility of this arrangement.

A silver chloride - silver iodide mixture rather than pure silver bromide was used in this cell. It is shown in the following chapter that this mixture has superior thermoelectric properties and a much lower

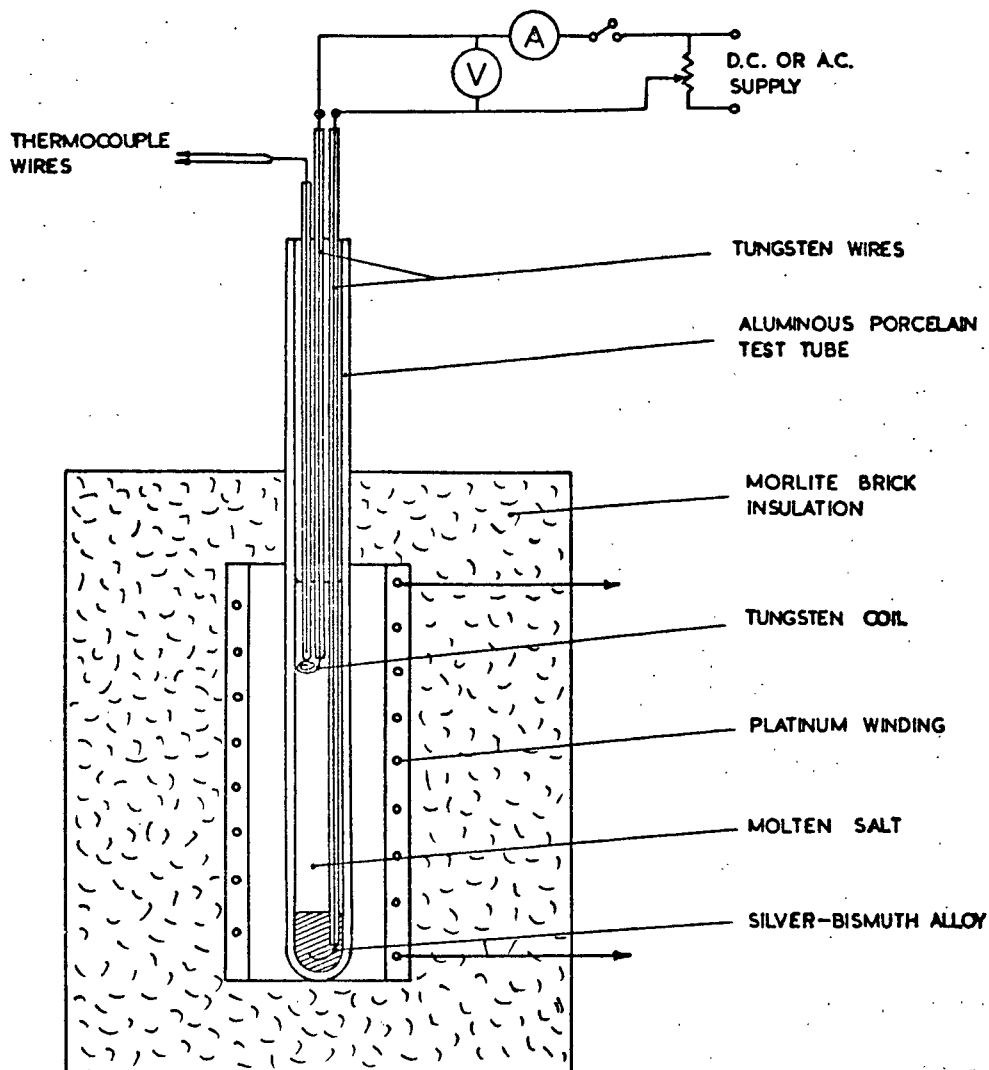


figure 5.5 rig for determining the conductivity of a salt phase in equilibrium with an alloy.

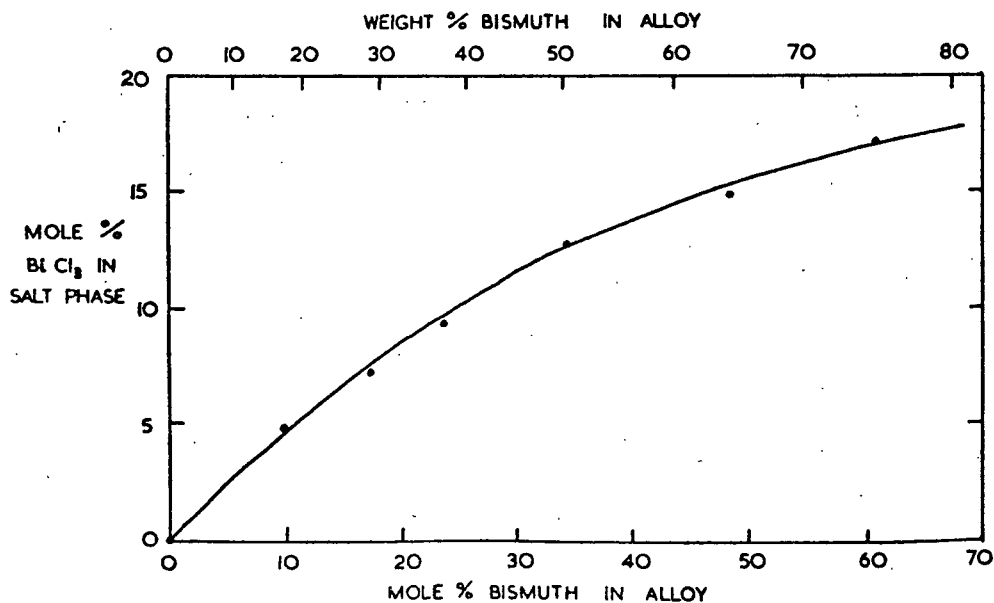


figure 5.6 composition of the salt phase in thermal equilibrium with the Ag-Bi alloy from electrical conductivity measurements.

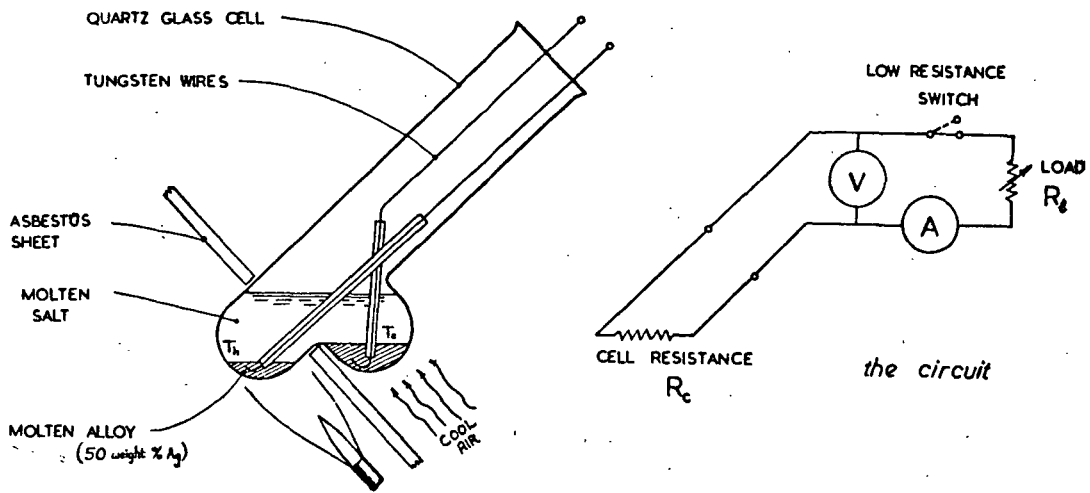


figure 5.7 generation thermocell with liquid electrodes.

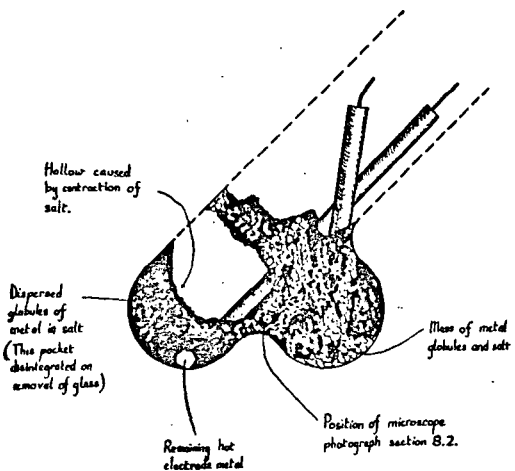


figure 5.8 section through the above cell after 2 1/4 hours operation on load. Photograph shows cell, and right hand pocket after sectioning.



melting point than the pure constituents. The open circuit potential, V_{oc} , was measured as 0.25 volts. The cell was allowed to operate on a load of $1\ \Omega$ for $2\frac{1}{2}$ hours and during this period the closed - circuit potential across the cell, V_{cc} , dropped from 0.125 to 0.06 volts. Analysis of the circuit shown in figure 5.7 shows that the resistance of the cell (plus leads) may be calculated from V_{oc} and V_{cc} :

$$R_c = R_l \left(\frac{V_{oc}}{V_{cc}} - 1 \right)$$

where R_c is the cell resistance and R_l is the load resistance. The resistance of the cell was found to increase from 1.0 to $1.6\ \Omega$ during the test. The cell was finally quenched, the glass was broken away and the solid contents were sectioned as shown in figure 5.8.

The increase in cell resistance was due to the decrease in the quantity of liquid metal in the hot left-hand pocket of the cell and the consequent decrease in surface area. This ionic transfer of material from the hot pocket did not result in the cool pocket being filled as expected. It can be seen that the metal was dispersed partly as globules within the molten salt and partly as a growth adhering to the cooler surfaces of the cell. This test was repeated with similar results and it was evident that sustained operation of more than a few hours was not possible using this configuration.

It thus appeared at this stage that, although the answer to the mass transfer problem lay in the use of liquid alloy electrodes, there were many development problems to be overcome before a continuously generating cell could be produced. In the following two chapters the AgCl - Ag I salt mixture and the effect of alloy electrodes on the thermoelectric potential are studied in greater detail and in chapter 8 the attack on the mass transfer problem is resumed.

Chapter 6

Common - Cation Salt Mixtures -- the AgCl - AgI System

- 6.1. The equilibrium diagram.
- 6.2. The thermoelectric potential of the AgCl - AgI eutectic mixture to high temperatures.
- 6.3. The $Z_s T$ Value of the AgCl - AgI eutectic mixture.

If reasonable conversion efficiencies of heat energy to electrical energy are to be obtained using ionic liquids the possibility of using salt mixtures must be considered. There are three advantageous effects of mixing pure salts. Firstly most pure salts melt at a high temperature and mixing can greatly reduce the melting point. Secondly it has already been shown that the thermal conductivity of salt mixtures is less than the pure constituents and finally there is the possibility that the thermoelectric potential of the mixture may be greater than the pure constituents. After an initial consideration of a number of common-cation fused salt systems silver chloride - silver iodide was selected for more detailed study as the electrical conductivity had already been measured, (Tubandt and Lorenz 1914b), and data on most of the properties of the pure constituents were available.

6.1. The equilibrium diagram.

Pure molten silver iodide freezes at 556°C into an α -form structure consisting essentially of a body-centred cubic lattice of iodine ions with randomly-placed silver ions. At 146°C there is a solid-solid transition to a β -form hexagonal structure. Mixing of silver chloride with silver iodide was found to form a eutectic system with considerable solid solubility of the silver chloride in the α -form silver iodide, and some solid solubility of the α -form silver iodide in the silver chloride.

The equilibrium diagram shown in figure 6.1 was obtained independently by Dr. R. W. Dyson using a Perkin - Elmer DCS 1b differential scanning calorimeter and the author using cooling curves. The silver chloride and silver iodide were not less than 99% and 98% pure respectively. Our results matched very well, but disagreed with those of previous workers. Mönkemeyer (1906) recorded a eutectic temperature of 211°C while Rosstkowski (1929) measured a eutectic temperature of 264°C but found very limited mutual solid solubility of the salts. The discontinuities in the variation of electrical conductivity with temperature at various compositions recorded by Tubandt and Lorenz (1914b) may be successfully accounted for using our diagram. (It is worthy of note their results also fit the completely different diagram of Mönkemeyer (1906). This would suggest that they assumed Mönkemeyer's diagram was correct, and disregarded any of their results which were not consistent with his diagram).

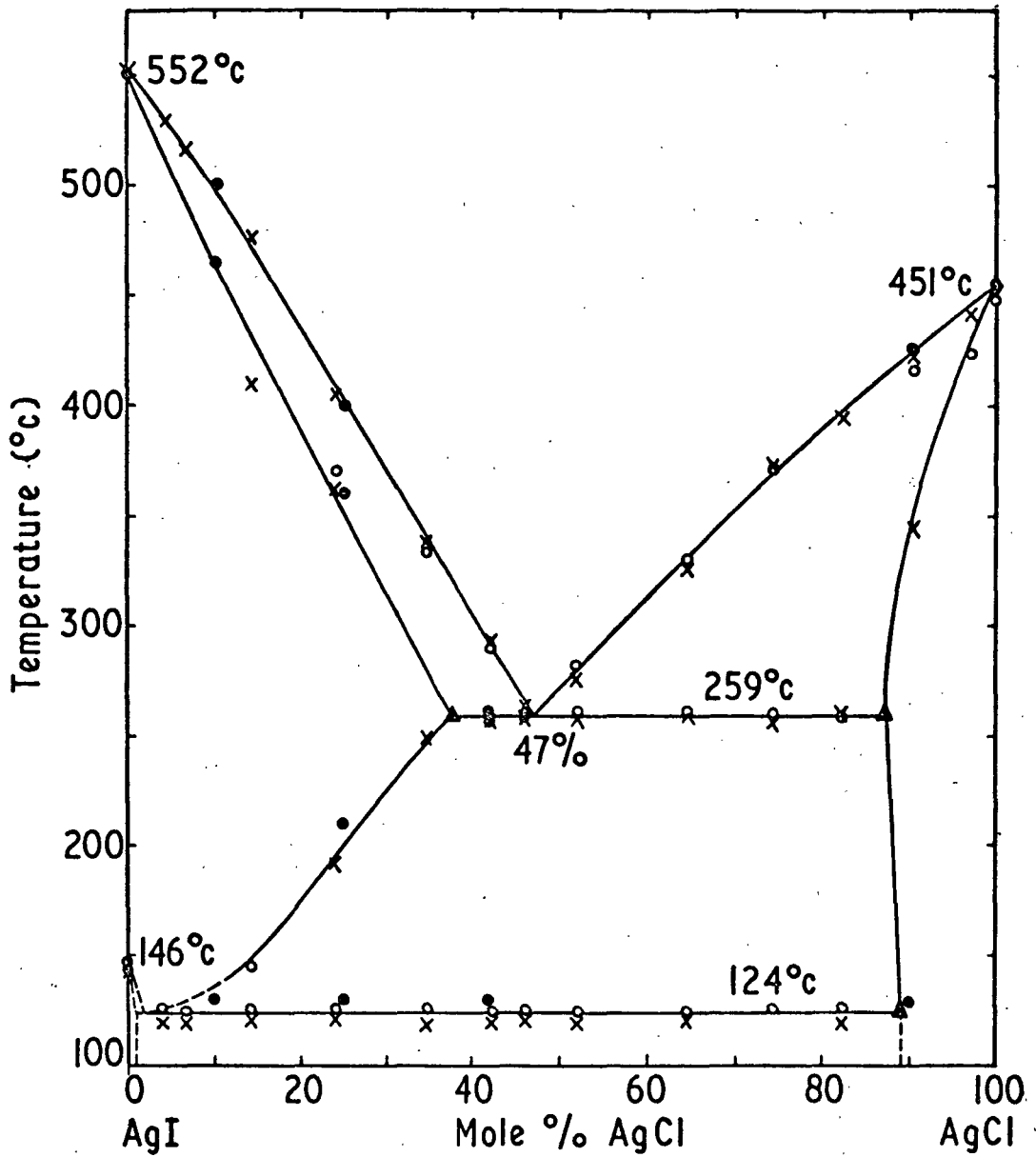


figure 6.1 the equilibrium diagram for the AgCl-AgI system.

- x* points obtained from cooling curves.
- o* points obtained using the differential scanning calorimeter.
- ▲ points calculated from phase change enthalpies.
- points from discontinuities in the electrical conductivity curves of Tubandt and Lorenz (1914b).

6.2. The thermoelectric potential of the Ag Cl - Ag I eutectic mixture to high temperatures.

Initial measurements by the author of the steady - state thermoelectric potential of the Ag Cl - Ag I eutectic salt mixture between 260 and 956°C yielded a mean value of -0.498 mV/K. In the following experiment this value was checked and the temperature range was increased to about 1200°C.

The experimental rig was arranged as shown in figure 6.2. The upper electrode consisted of a fine bore quartz tube terminating in a U bend in which the silver metal was situated. This arrangement enabled the electrode to be used above the melting point of silver at 961°C. Connections to both electrodes were of tungsten and a correction to the thermoelectric potential (in the order of a few microvolts) was made for these wires. The thermocouples, which consisted of 'Thermocoax' stainless-steel sheathed Chromel-Alumel wires, were connected back to back so that the temperature difference was measured, and the cool electrode was maintained at $300 \pm 3^{\circ}\text{C}$ throughout the test. The hot electrode was heated to 1200°C and the power to the furnace was reduced in a series of steps during which the temperature was allowed to stabilise and the readings were taken. The Potential measurements were made using a Phillips PR3210 automatic measuring bridge.

The results are shown graphically in figure 6.3. The estimated maximum possible error is about 2% up to about 1000°C and rather more above this temperature where Chromel-Alumel thermocouples are less reliable. Up to a temperature of 850°C the thermoelectric potential ($\alpha = dE/dT$) is constant at -0.50 mV/K but above this temperature α rises rapidly and undergoes a change of sign at 1100°C. This result was entirely unexpected and warrants a further look at the theory to the thermoelectric potential.

In section 4.1. the following expression was derived (equation 4.5):

$$zF\alpha = S_M - \bar{S}_{M^{z+}} - z\bar{S}_e$$

where S_M and $\bar{S}_{M^{z+}}$ denote the molal entropy of the metal and the total transported molal entropy of the metal ion in the salt respectively and \bar{S}_e is the total transported entropy of the electron in the external

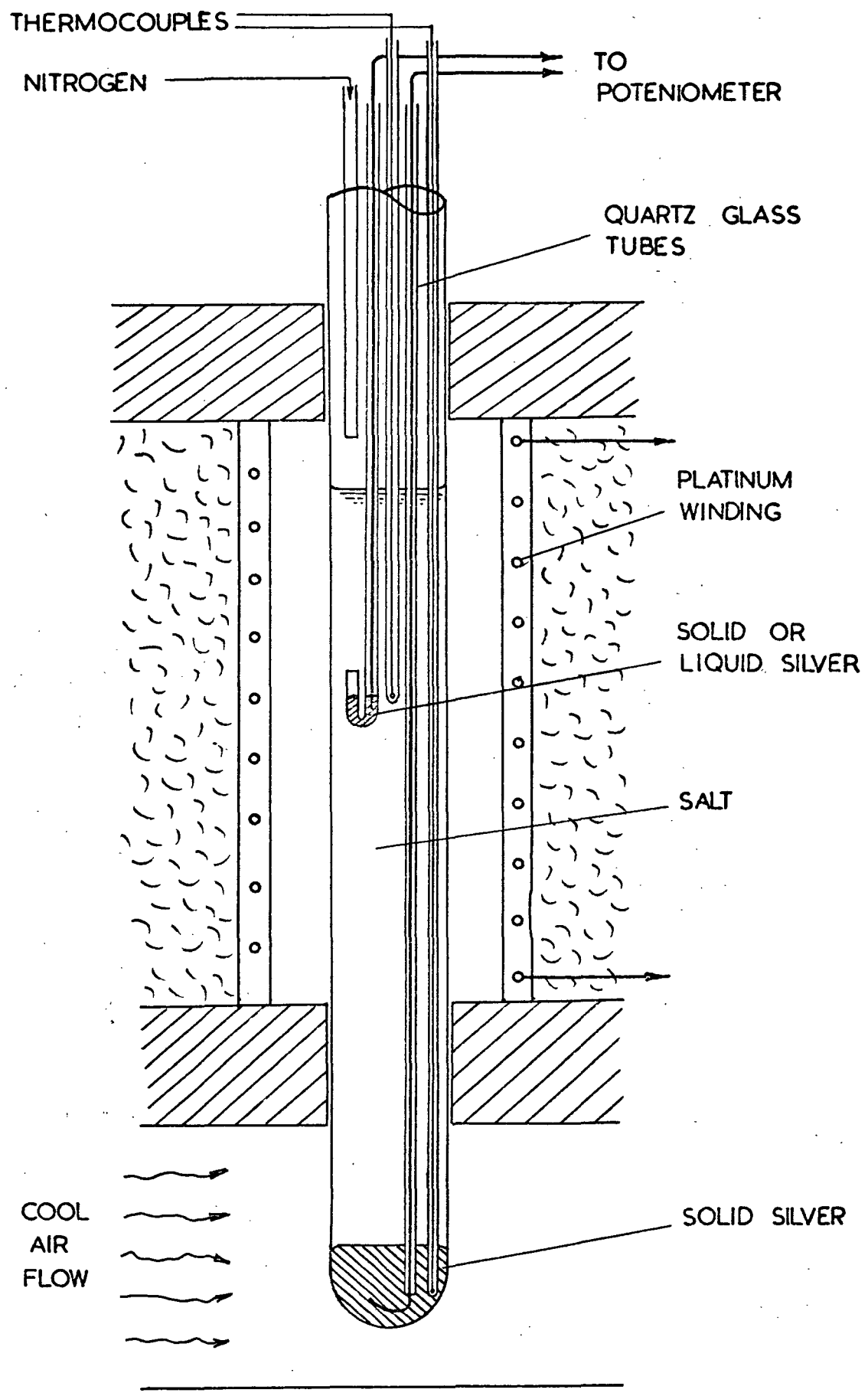


figure 6.2 rig for measuring the thermoelectric potential of silver salts to high temperatures.

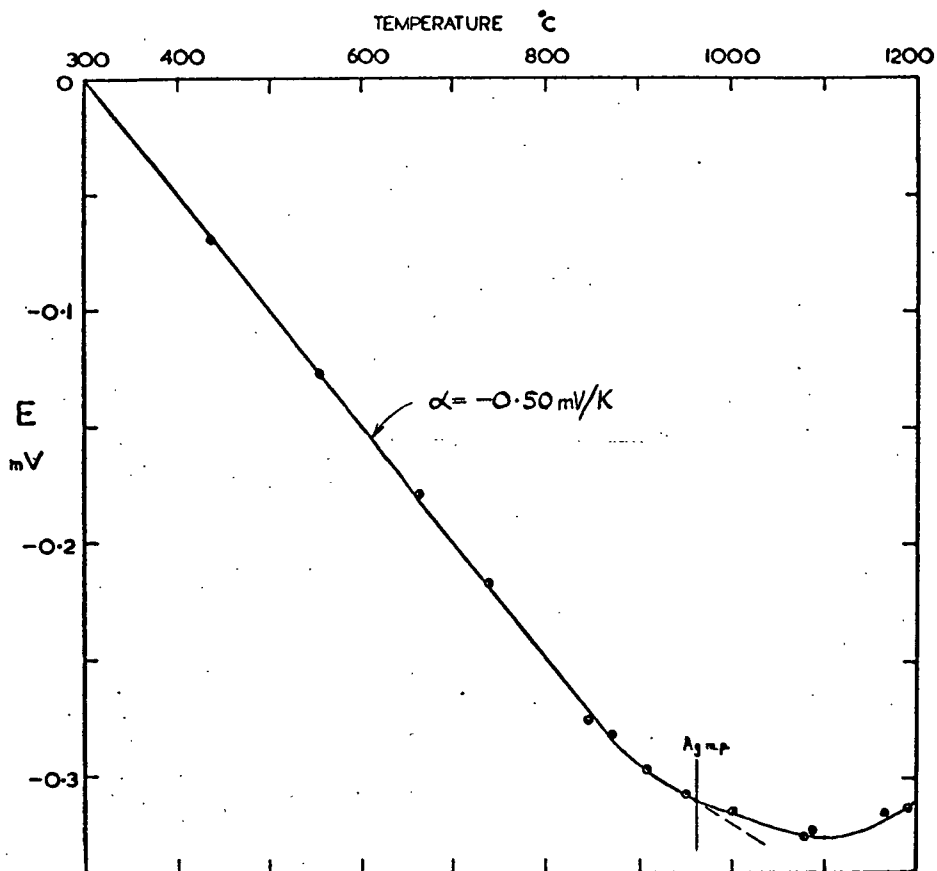


figure 6.3 showing the variation of potential of the cell Ag/AgCl-AgI/Ag with temperature.

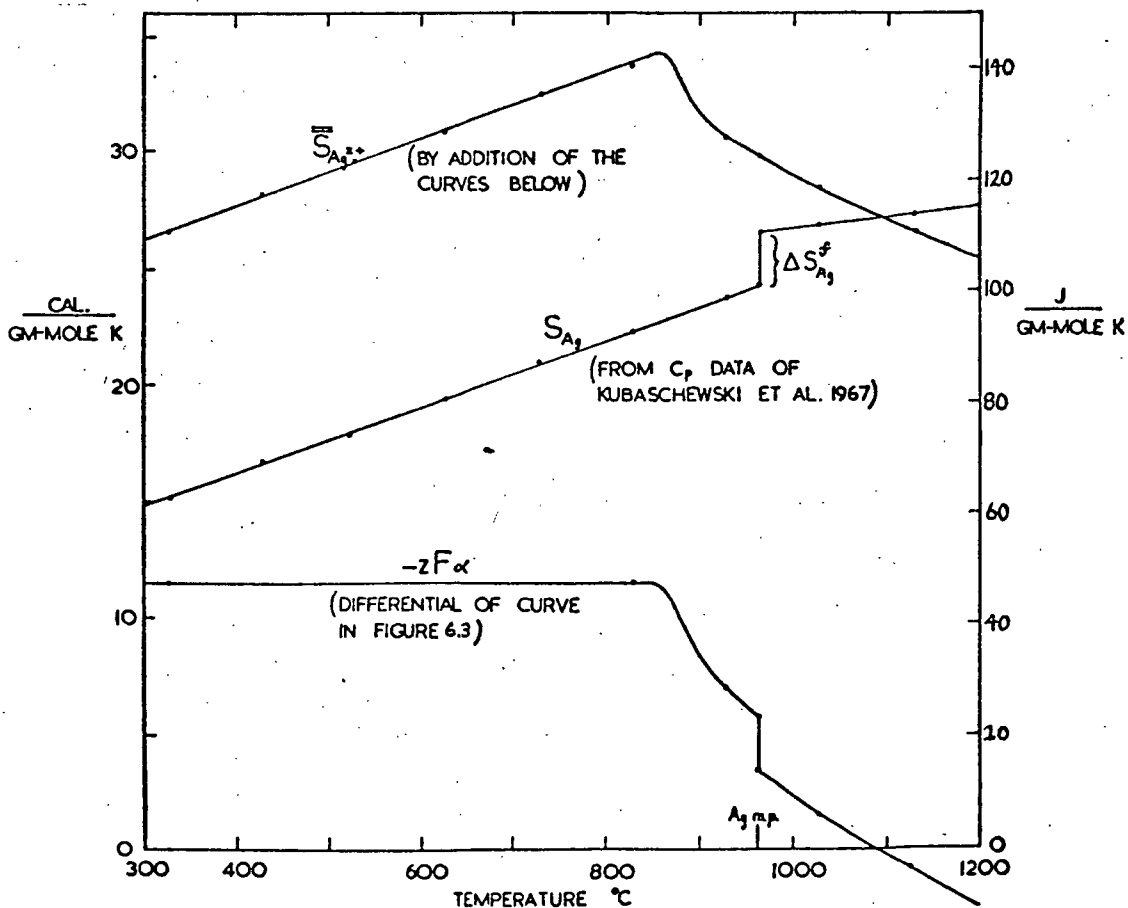


figure 6.4 showing the variation of the terms of equation: $zF\alpha = S_M - \bar{S}_{M^{z+}}$ with temperature.

circuit (which is negligible compared to the other terms). The variation of S_M with temperature may be calculated from the specific heat data of Kubaschewski et al. (1967). Just above the melting point of the metal T_2 the thermoelectric potential is given by:

$$zF(\alpha)_{T>T_2} = S_{M(solid)} + \Delta S_M^f - \bar{S}_{M^{z+}} - z\bar{S}_e \quad (6.1)$$

where ΔS_M^f is the molal entropy of fusion of the metal. Thus at the metal melting point there is a change in the thermoelectric potential $\Delta\alpha$ of:

$$\left(\Delta\alpha\right)_{T_2} = \Delta S_M^f / zF \quad (6.2)$$

In the case of silver ΔS_M^f is $9.7 \text{ Jmole}^{-1}\text{K}^{-1}$ and $(\Delta\alpha)_{T_2}$ is therefore 0.100 mV/K . In figure 6.3 there is an increase in the slope of the curve of about this magnitude at the melting point of silver, but unfortunately this change is masked to a certain extent by the overall increase in the slope at temperatures above 850°C . This overall increase cannot be explained theoretically and is due to a decrease in the value of $\bar{S}_{M^{z+}}$ at high temperatures. The variation of terms $zF\alpha$, S_M and $\bar{S}_{M^{z+}}$ with temperature are shown in figure 6.4. No measurements of the thermoelectric potential of purely ionic molten salts at temperatures around the electrode melting point are recorded in the literature, but some values for the cell $\text{Zn (solid-liquid)} / \text{T}_2 \text{ Zn Cl}_2 / \text{T}_1 \text{ Zn (solid liquid)}$ are given by Markov and Kuzyakin (1963 a). Although $\text{Zn}^{\text{C}} \text{Cl}_2$ was partly covalent in the temperature range studied the α -temperature characteristic was of a similar form to that obtained for the eutectic in this work, with a sharp inflection equivalent to $\Delta S_M^f / zF$ at the melting point of zinc.

It is possible that the thermoelectric potential (and also the electrical and thermal conductivity) are affected by thermal diffusivity in the silver salt mixture. Attempts to measure any thermal diffusion effect by stirring the salt mixture and allowing it to stabilise over a period of hours did not yield any consistent quantitative results but did show that the thermal diffusion potential was only a few microvolts per degree.

In summary then it would appear that the $\text{Ag Cl} - \text{Ag I}$ eutectic salt mixture is of limited use at temperatures above the melting point

of silver owing to the change in the thermoelectric potential. This change is due to a decrease in the transported molal entropy of the silver ion in the salt at high temperatures and the molal entropy of fusion of the silver metal.

6.3. The Z_sT Value of the AgCl - AgI eutectic mixture.

The Z_sT value ($Z_sT = \alpha^2 \sigma T / K$) may now be calculated for the AgCl - AgI eutectic mixture. The thermoelectric potential was measured in the previous section and the thermal conductivity was given in section 3.2.6.2 as 1.82×10^{-3} watts $\text{cm}^{-1} \text{K}^{-1}$ at 300°C . The electrical conductivity has been studied by Tubandt and Lorenz (1914 a and b) and values for the eutectic at 47 mole % silver chloride were interpolated using these data up to 600°C . Above this temperature values were extrapolated using a plot of $\log \sigma$ against the reciprocal temperature as suggested by Delimarskii and Markov (1961). The variation of the Z_sT value with temperature (assuming a constant thermal conductivity) is shown in figure 6.5 together with the estimated Z_sT value of the constituents taken from table 5.1.

Some idea of the conversion efficiency between 260 and 850°C may be obtained if Z_c is taken as $0.8Z_s$ (as in section 5.2 on pure salts). Z_cT (mean) between these two temperatures is approximately 0.26 and the overall efficiency from equation 1.3 is then $4\frac{1}{2}\%$. The increase in the Z_sT value and the expanded temperature range of the molten phase demonstrate the advantageous effect of mixing argentous halides for use in generation thermocells. Other common-anion salt systems such as the CuCl - CuI mixture exhibit similar eutectics and are expected to have considerably higher Z_sT values.

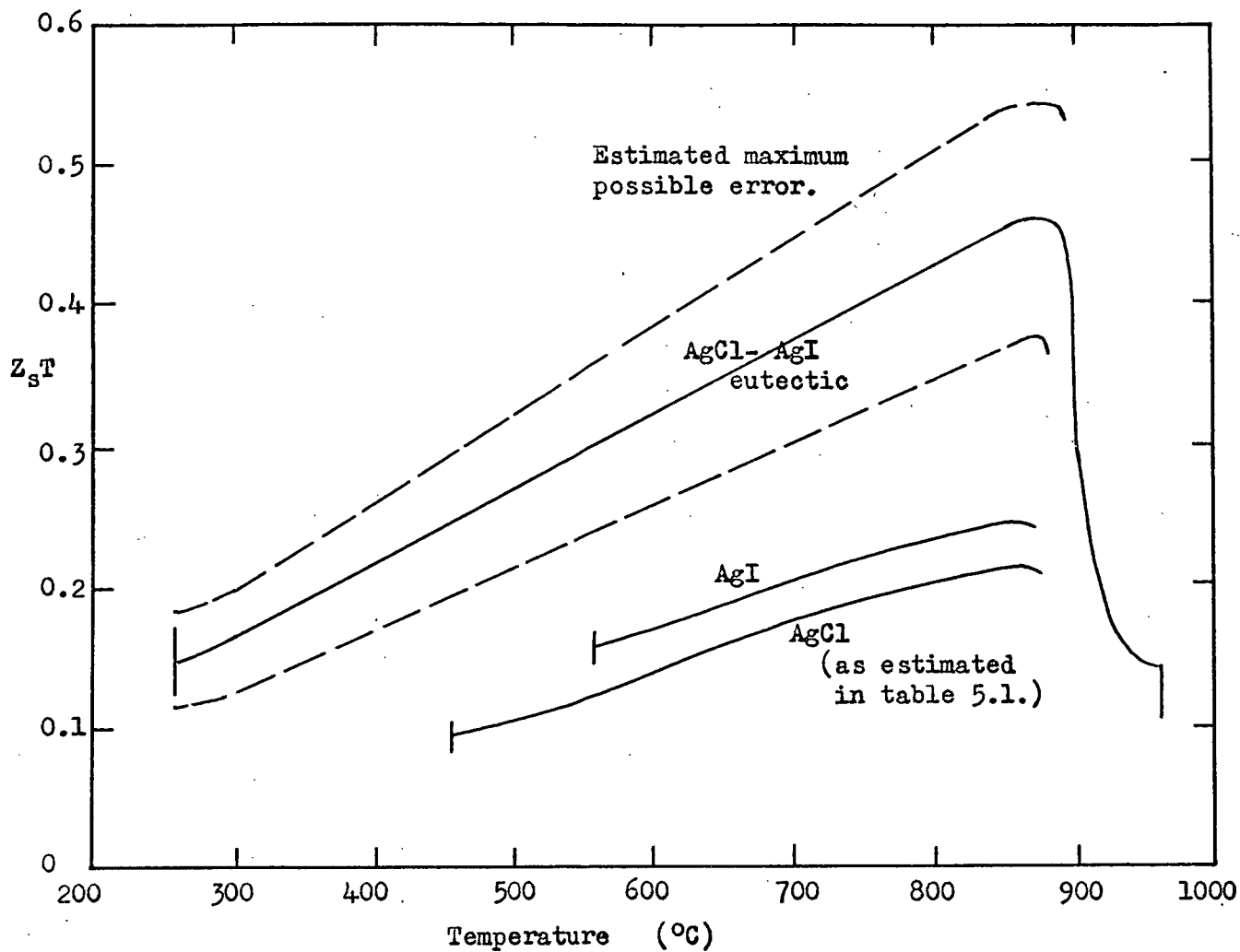


Figure 6.5. The $Z_s T$ value of the AgCl-AgI eutectic mixture.
 (The estimated maximum possible error is about 20% owing to the accumulation of errors in the property measurements).

Chapter 7.

The Thermoelectric Potential of Cells with Alloy Electrodes -

the Ag (Bi) /_{T_n} AgCl - AgI /_{T_c} Ag (Bi) system

Contents :

- 7.1. Theory to the thermoelectric potential.
- 7.2. Experimental results and discussion.
- 7.3. Trial of the 'H' cell configuration for thermoelectric generation.

7.1. Theory to the thermoelectric potential.

The thermoelectric potential of a silver halide thermocell in which both electrodes are identical alloys of silver with another metal is affected by the increase in molal entropy of the silver due to the alloying. In particular the term S_{Ag} in the equations of the previous chapter must be replaced by $S_{Ag(Bi)}$. Classical thermodynamics yields an expression for the molal entropy of a component in an ideal mixture :

$$S_{Ag(Bi)} = S_{Ag} - R \ln a_{Ag} \quad \text{---(7.1)}$$

where a_{Ag} is the activity of the silver in the alloy.

The silver - bismuth equilibrium diagram given by Hansen (1958) is shown in figure 7.1. At temperatures just above the liquidus of the alloy, T_L , all the silver present is liquid. Hence:

$$\left(S_{Ag(Bi)} \right)_{T > T_L} = S_{Ag(solid)} + \Delta S_{Ag}^f - R \ln a_{Ag}$$

where ΔS_{Ag}^f is the molal entropy change due to fusion of the silver. Account of the fact that the alloy is not an ideal mixture may be made by rewriting the equation in the following form:

$$\left(S_{Ag(Bi)} \right)_{T > T_L} = S_{Ag(solid)} + \Delta S_{Ag}^f - R \ln x_{Ag} + S_{Ag}^E \quad \text{---(7.2)}$$

where x_{Ag} is the molal concentration of silver in the alloy. The molal excess entropy S_{Ag}^E is effectively a correction factor between the ideal entropy change due to alloying of the silver ($-R \ln a_{Ag}$) and the entropy change indicated by the concentration ($-R \ln x_{Ag}$). In the silver - bismuth system it is small compared to the other entropy terms. At temperatures below the liquidus (and to the silver side of the eutectic composition) there are two phases in the alloy - a liquid phase, and a solid phase consisting of almost pure silver:

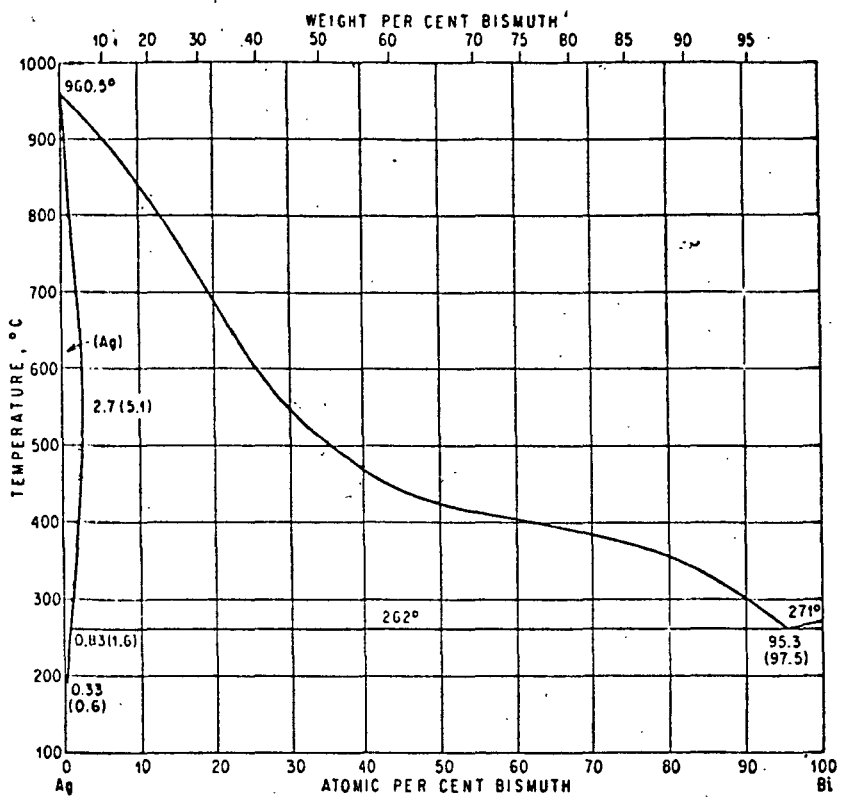
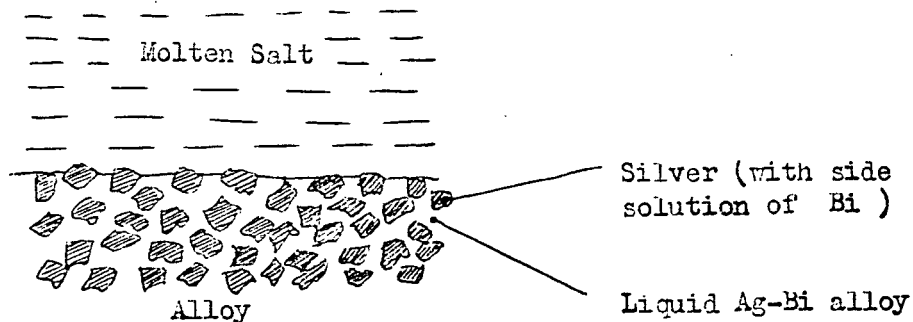


Figure 7.1 The Ag-Bi equilibrium diagram (Hansen 1958).



In this situation the activity of silver in the alloy as a whole is determined by the activity of silver in the solid phase (see for example Wagner (1952), chapter 1). Hence:

$$\left(S_{\text{Ag}(\text{Bi})} \right)_{T < T_l} \approx S_{\text{Ag}(\text{solid})} \quad \text{---(7.3)}$$

In summary then it would appear that the thermoelectric potential up to the liquidus at any particular composition is approximately the same as that obtained using pure silver electrodes. Thus from equation 4.5 page 78, (with \bar{S}_e negligible) :

$$(\alpha)_{T < T_l} \approx \frac{1}{F} \left(S_{\text{Ag}(\text{solid})} - \bar{S}_{\text{Ag}^+} \right)$$

At temperatures just above the liquidus the term S_{Ag} is modified to take account of the bismuth as in equation 7.2 :

$$(\alpha)_{T > T_l} = \frac{1}{F} \left(S_{\text{Ag}(\text{solid})} + \Delta S_{\text{Ag}}^f - R \ln x_{\text{Ag}} + S_{\text{Ag}}^E - \bar{S}_{\text{Ag}^+} \right) \quad \text{(7.4)}$$

Thus at the liquidus there is a change in the thermoelectric potential $(\Delta \alpha)_{T_l}$ given by:

$$\begin{aligned} (\Delta \alpha)_{T_l} &= (\alpha)_{T > T_l} - (\alpha)_{T < T_l} \\ &= \frac{1}{F} \left(\Delta S_{\text{Ag}}^f - R \ln x_{\text{Ag}} + S_{\text{Ag}}^E \right) \quad \text{---(7.5)} \end{aligned}$$

7.2. Experimental results and discussion.

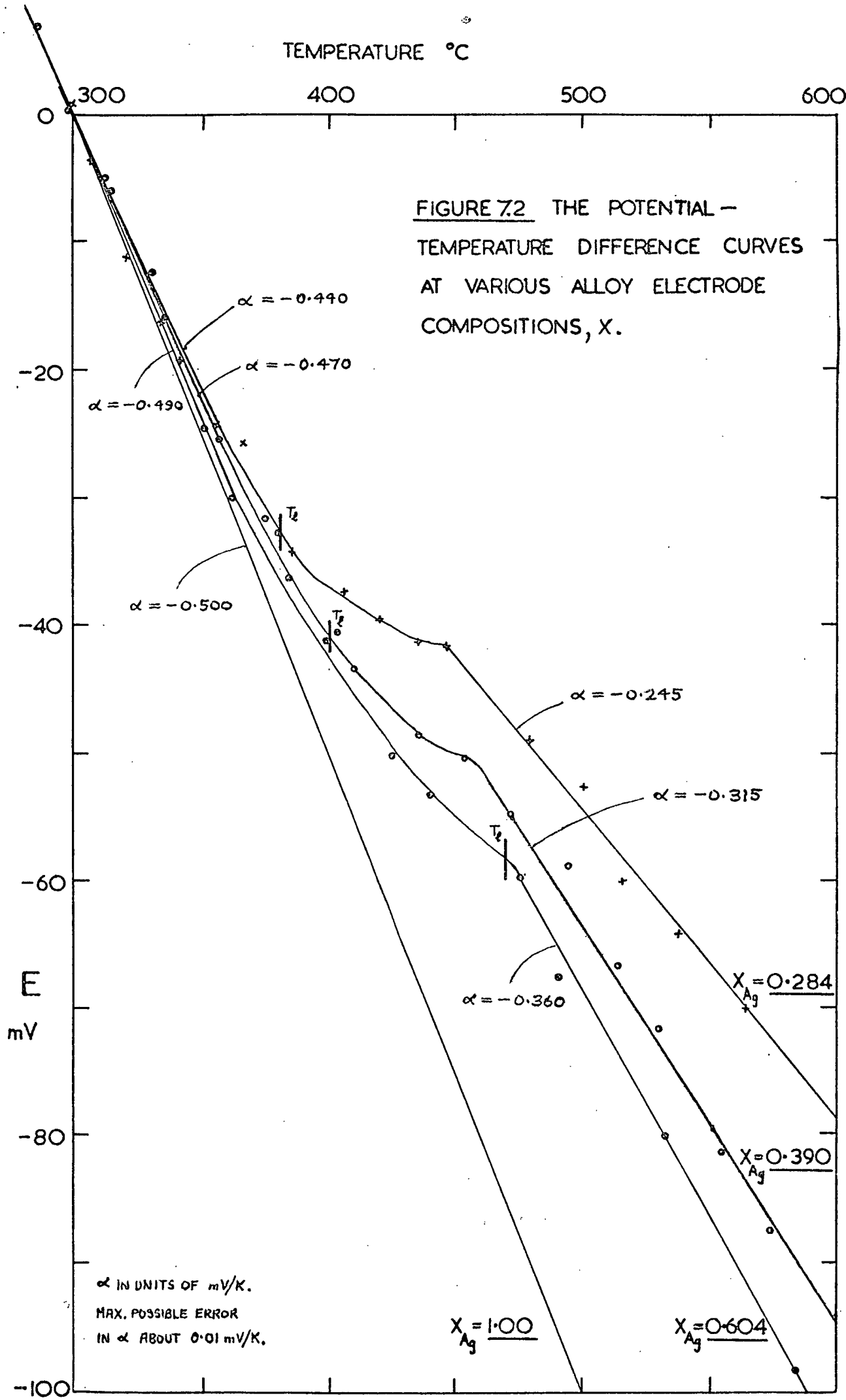
An experiment was set up to measure the thermoelectric potential of the cell $\text{Ag}(\text{Bi})/_{T_h} \text{AgCl} - \text{Ag I}/_{T_c} \text{Ag}(\text{Bi})$ at various alloy concentrations. The cell was similar to that shown in figure 4.2 and consisted of two quartz glass beakers of 24 mm diameter connected by a quartz glass tube of 5 mm bore. The Ag - Bi alloy was situated at the base of each beaker and electrical connection was made using tungsten wires enclosed in small bore quartz glass tubes. Temperatures were measured using Chromel - Alumel thermocouples situated in probes within the alloy of each beaker. The electrical potential was measured using a Philips FR 3210 automatic measuring bridge and correction was made to the thermoelectric potential of the salt for the small effect of the tungsten wires. The beakers were thermally insulated and situated on copper blocks which were heated externally by Bunsen burners. One beaker was maintained at $300^\circ\text{C} \pm 3^\circ\text{C}$ and the other was varied from 280 to over 600°C . Any effect due to thermal diffusion was minimised by periodically inclining the cell so that most of the salt flowed to one end.

The potential - temperature difference characteristics at alloy compositions of 28.4, 39.0 and 60.4 mole % silver are shown in figure 7.2, (after correction for any small zero temperature difference errors). The (steady - state) potential - temperature difference curve for pure silver electrodes taken from the previous chapter is also included for comparison. It is noticeable that at temperatures around the liquidus for each composition there is a range where the potential does not increase steadily, but above and below this range the curve is linear within experimental error, (slope = $\frac{\Delta E}{\Delta T} = \alpha = \text{constant}$). Initially it is proposed to consider the two linear sections and compare their thermoelectric potentials with those predicted by the theory of the previous section.

Reference to figure 7.2 shows that the thermoelectric potential at temperatures well below the liquidus is similar for each composition and is also similar to that obtained using pure silver electrodes. This is consistent with equation 7.3 to a first degree of approximation. It is also apparent that as the proportion of silver in the alloy x_{Ag} decreases so the deviation of the thermoelectric potential from that obtained with pure silver electrodes increases. Initially it may be considered that

TEMPERATURE °C

FIGURE 7.2 THE POTENTIAL - TEMPERATURE DIFFERENCE CURVES AT VARIOUS ALLOY ELECTRODE COMPOSITIONS, X.



this is due to the solid solubility of bismuth in the silver of the solid phase and the consequent lowering of the silver activity. Reference to figure 7.1 shows that the maximum solid solubility of the bismuth is 2.7 mole % and the change in thermoelectric potential due to this (calculated from $R \ln x_{Ag}^s / F$ where x_{Ag}^s is the proportion of silver in the solid phase), is only of the order of a few microvolts per degree. The major part of this deviation is therefore due to some other cause and this is probably the proportion of bismuth salt in the salt phase according to a thermal equilibrium of the type discussed in section 5.3.2. As the concentration of bismuth in the alloy is increased so the concentration of bismuth salt in the salt phase is increased. This is consistent with the observed increase in deviation of the thermoelectric potential from that obtained with pure silver electrodes as the concentration of bismuth in the alloy is increased. In this case the deviation is towards more positive values of α (i.e. less negative values). In chapter 9 it is shown that the mixing of salts with different cations may lead to an increase or decrease in the thermoelectric potential depending on the value of the ionic entropy terms in the mixture.

The thermoelectric potential well above the liquidus temperature is seen from figure 7.2 to be considerably less (in numerical value) than it is before the liquidus temperature at the same composition. The difference between these two slopes, $(\Delta\alpha)_{T_l}$ is given in the following table, (in units of mV/K):

x_{Ag} (mole %)	$\alpha_{T > T_l}$	$\alpha_{T < T_l}$	$(\Delta\alpha)_{T_l}$ (experimental)
23.4	-0.245	-0.440	0.195
39.0	-0.315	-0.470	0.155
60.4	-0.360	-0.490	0.130
100	~ -0.15	~ -0.25	~ 0.100 (from section 6.2.)

The value of $(\Delta\alpha)_{T_l}$ predicted by the theory of the previous section may be calculated by rearranging equation 7.5 :

$$(\Delta\alpha)_{T_l} = \frac{\Delta S_{Ag}^s}{F} - \frac{R \ln x_{Ag}}{F} + \frac{S_{Ag}^E}{F}$$

The first term on the right hand side has already been shown in section 6.2. to be 0.100 mV/K and the second term may be calculated from the concentration of the alloy. Fortunately the excess entropy of silver in a silver - bismuth alloy may be calculated at the liquidus temperature from data available in a report by Gregorczyk (1960). The theoretical values of $(\Delta\alpha)_{T_2}$ at the same concentrations as the experimental results are calculated in the following table, (in units of mV/K):

x_{Ag} (mole %)	$R \ln x_{Ag} / F$	S_{Ag}^E / F	$\Delta S_{Ag}^f / F$	$(\Delta\alpha)_{T_2}$ (theoretical)
28.4	-0.109	-0.004	0.100	0.205
39.0	-0.081	-0.007	"	0.174
60.4	-0.044	-0.008	"	0.136
100	0	0	"	0.100

The agreement between the experimental and theoretical values of $(\Delta\alpha)_{T_2}$ is good when it is considered that the experimental value is determined by the difference of two slopes each with an accompanying possible error of about 0.01 mV/K, (i.e. a few %).

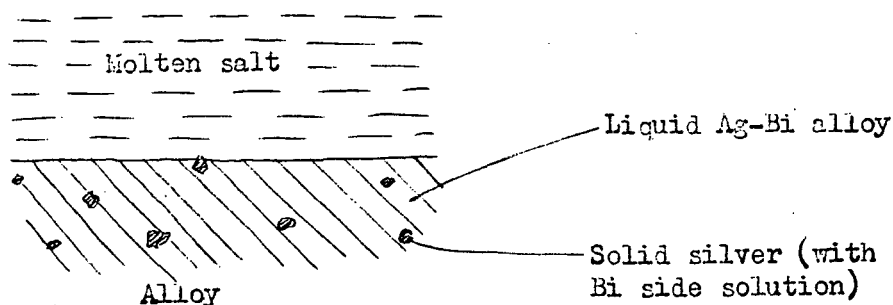
Consideration must now be given to the unsteady part of the potential - temperature difference curve around the liquidus temperature. To a certain extent this can be explained theoretically. One aspect of the cell under study which has not been mentioned is the isothermal potential difference between the electrodes owing to the different activities of silver in each electrode. Thus in addition to thermoelectric effects an isothermal cell of the following form is established:



The potential of the cell is given by $E_{iso} = -RT \ln a_{Ag} / F$ (where a_{Ag} is the activity of the silver in the alloy) and it has been measured experimentally by Gregorczyk (1960). Below the liquidus temperature both electrodes are effectively pure silver as discussed earlier and the isothermal potential difference is practically zero. But as one electrode is raised above the liquidus temperature while the cool electrode is still below it, a cell of the above form is set up and there is theoretically a sharp positive change in potential at the liquidus.

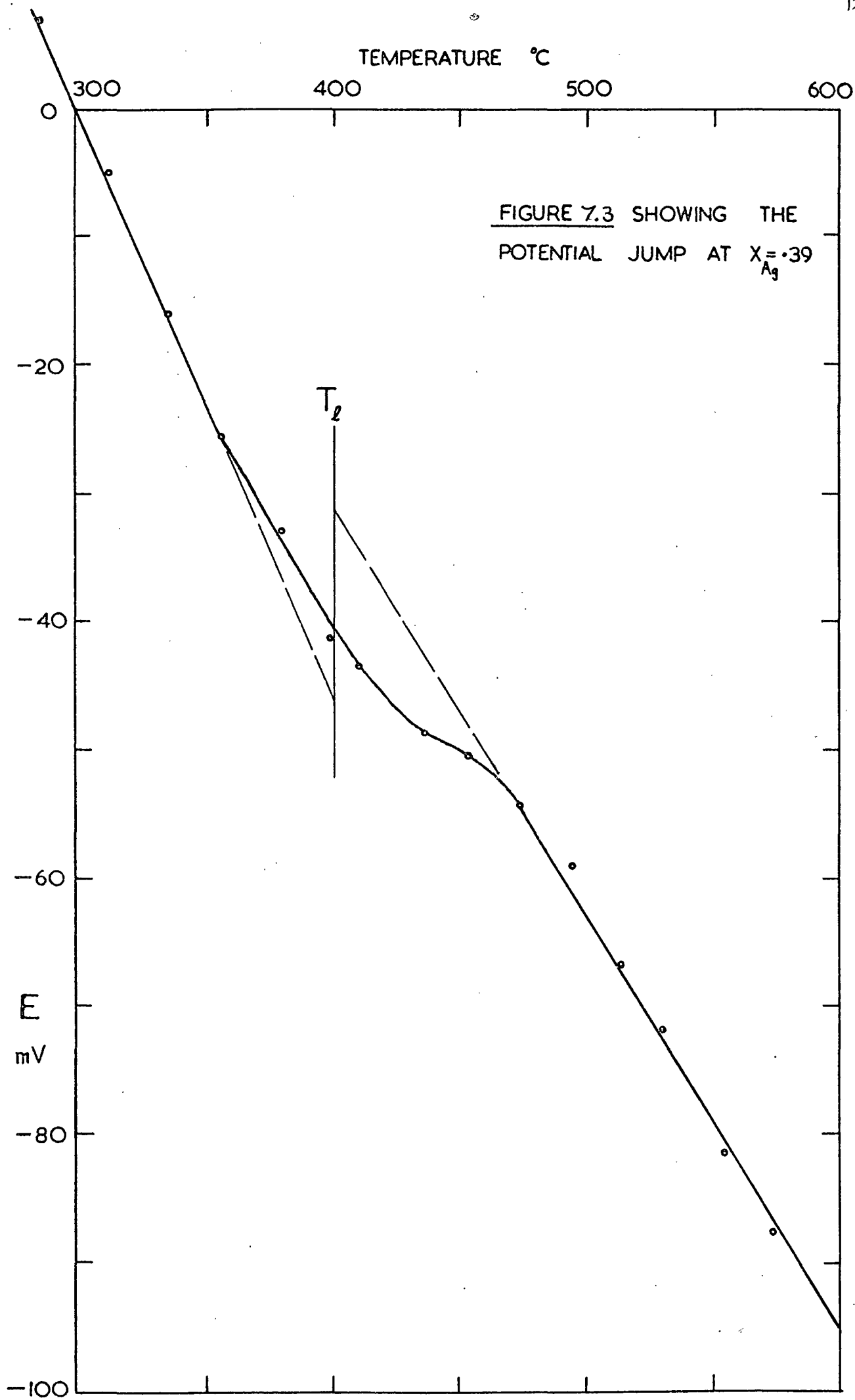
Let us now search for experimental evidence of this in, (for example), the potential - temperature difference characteristic of the cell with 39 mole % silver in the alloy. The characteristic is redrawn in figure 7.3 and it can be seen that continuation of the linear portions to the liquidus temperature indicates a change in potential of 15 mV. Theoretically $E_{iso} = -R \times 673 \times \ln 0.39 / F = 55 \text{ mV}$. The inaccuracy in the liquidus temperature and that caused by extrapolation of the linear sections of the curves cannot account for a difference of this order and the isothermal potential drop cannot therefore be completely determined by the potential of the isothermal cell $\text{Ag}(\text{Bi}) / \text{Molten Salt} / \text{Ag}$.

In addition the experimental curve in figure 7.3 is seen to change gradually from one slope to the other. This may be partially explained by considering a point just below the liquidus temperature. At this point the proportion of the solid silver phase in the liquid alloy is very low and the potential of the cell may fluctuate depending on the exact composition of the surface:



Fluctuations due to this cause should cease as soon as the temperature rises above the liquidus. The unsteadiness in the experimental curve above the liquidus would suggest that either the liquidus temperature is not 400°C or that there is some other completely different cause of this effect. Precise measurements of the thermoelectric potential at temperatures around the liquidus on a number of different systems would be required to ascertain in detail the reason for the anomalous changes in this region. Unfortunately no study of a similar system has been found in the literature and the theory and postulations of this section must therefore, to a certain degree, remain tentative.

In summary it may be said that at temperatures well below the liquidus the thermoelectric potential of the cell $\text{Ag}(\text{Bi}) / T_h \text{ Ag Halide} / T_c \text{ Ag}(\text{Bi})$ is similar to that of a cell with pure silver electrodes (with the deviation between the two decreasing as the quantity of bismuth in the



alloy decreases). Around the liquidus temperature there is a positive potential step of the order of 20 mV and the thermoelectric potential is unsteady. Above this range it is constant at a value considerably lower than that below the liquidus temperature. The difference in these two thermoelectric potentials is dependent on the fusion process and the activity of the silver in the electrodes. Figure 7.4 has been included in order that the potential of a thermocell with silver - bismuth alloy electrodes of any particular composition may be calculated. (The broken line at high percentages of silver indicates the change in α as the liquidus temperature rises above that temperature at which the thermoelectric potential of the cell with pure silver electrodes begins to change, as shown in figure 6.3).

7.3. Trial of the 'H' cell configuration for thermoelectric generation.

From the forgoing work it would appear that an 'H' cell with silver - bismuth alloy electrodes would be suitable for thermoelectric generation. The alloy has a eutectic temperature of 262°C which is conveniently near the eutectic of the $\text{AgCl} - \text{AgI}$ system at 259°C . At a hot electrode temperature of 850°C with an alloy composition of 80 mole % figure 7.4 shows that a potential of about 0.26 volts is generated (allowing for a decrease of 20 mV due to the potential step).

Tests on a cell with two pockets containing the alloy electrodes have already been described in section 5.3. The 'H' cell shown in figure 7.5 was designed to overcome the convective mass transfer problem encountered in this cell. It was milled out of a small block of 'Alsil' pyrophyllite. (This material is a hydrous aluminium silicate $(\text{Al}_2\text{Si}_4\text{O}_{10}(\text{OH})_2)$ occurring in certain crystalline schists. It is easy to machine but on firing at 1000°C for a few hours it changes colour from grey to pink and becomes brittle and reputedly non-porous). The cell was charged with the alloy, salt and quartz fibre and was set up in a temperature gradient as shown.

Once the contents had melted the cell generated 0.2 volts on open circuit for ten minutes and then practically short-circuited. It was suspected that the metal was distributed along the base of the cell

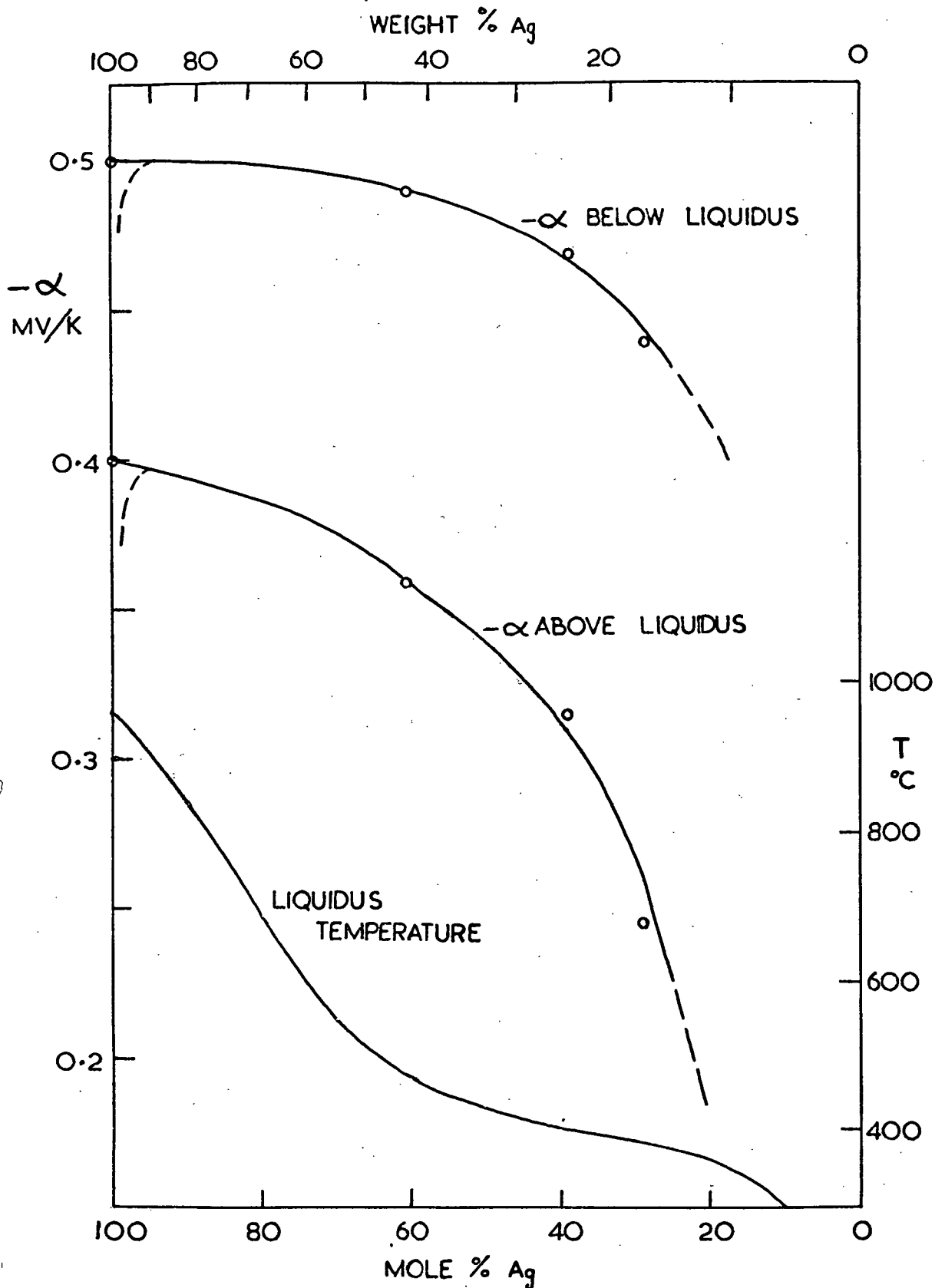


figure 7.4 showing the thermoelectric potential of the cell $\text{Ag}(\text{Bi})_{T_h} | \text{salt} | \text{Ag}(\text{Bi})_{T_c}$ above and below the liquidus temperature.

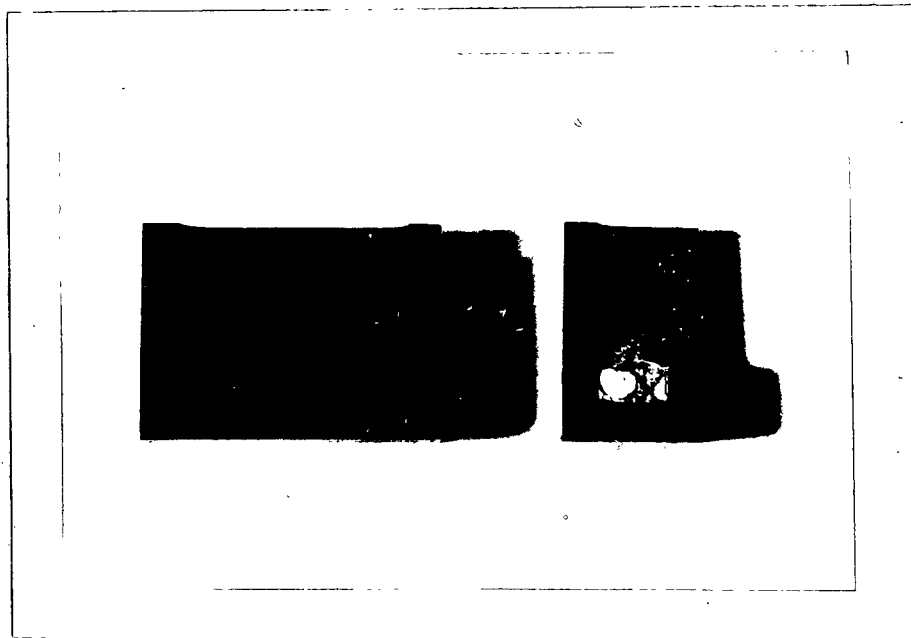
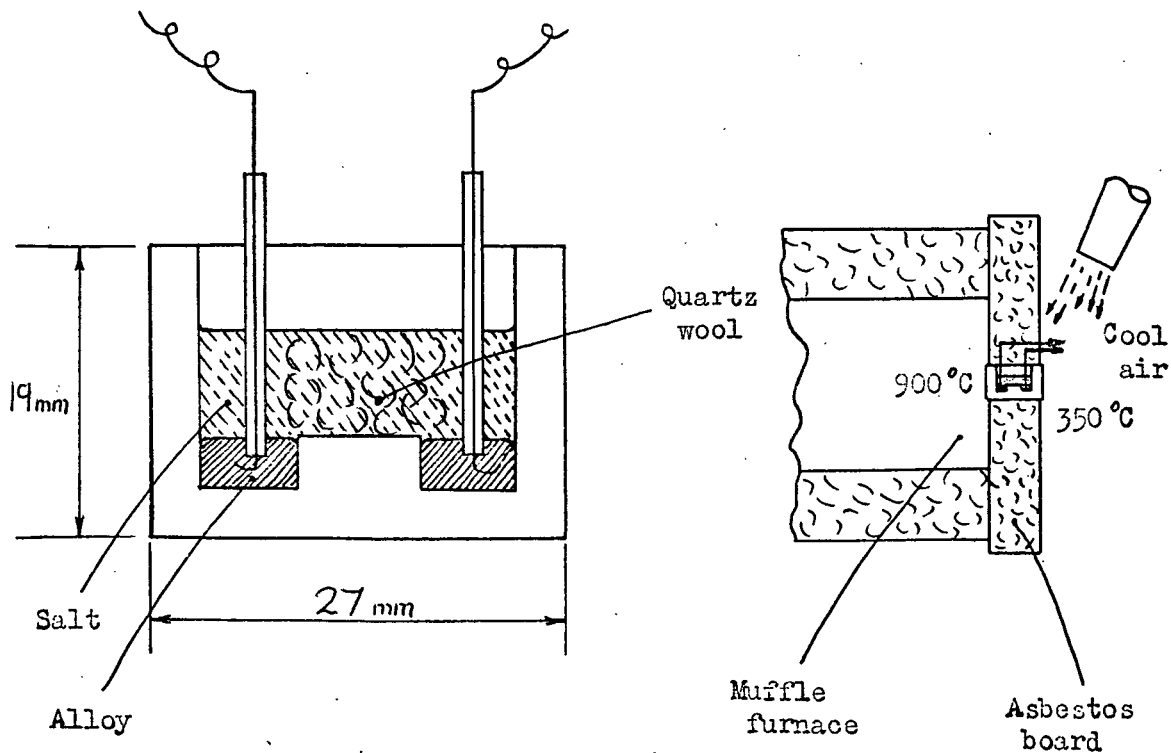


Figure 7.5 The pyrophyllite 'E' cell. The photograph shows a section through the cell, and a section of one of the pockets after operation.

rather than in the pockets, thus shorting the electrodes. Quenching and sectioning of the cell showed that this was the case, and that the pockets contained a mass of salt and alloy rather than a homogeneous layer of alloy. Other tests on similar cells with minor modifications yielded similar results and further attempts to use the 'H' cell configuration were abandoned.

Following the failure in this and earlier tests to operate a thermocell continuously for long periods it was decided to study the problem of mass transfer in thermocells in greater detail.

Chapter 8

The Mass Transfer Problem in Generation Thermocells.

- 8.1. Electrochemical Mass Transfer.
 - 8.1.1. The decomposition potential.
 - 8.1.2. The voltage - current characteristic during electrolysis.
 - 8.1.3. The Faradayic mass transfer.
- 8.2. Convective Mass Transfer.
- 8.3. Trials of various Vertical Tube configurations for Thermocell Generation.
 - 8.3.1. Trials of thermocells with the lower electrode heated.
 - 8.3.1.1. The cell operation.
 - 8.3.1.2. Pyrophyllite cells.
 - 8.3.1.3. Crucible cells.
 - 8.3.1.4. Low resistance cells.
 - 8.3.2. Trials of thermocells with the upper electrode heated.
 - 8.3.2.1. The cell operation.
 - 8.3.2.2. Trials of various arrangements of the upper electrode.
 - 8.3.3. Conclusion.

8.1. Electrochemical Mass Transfer.

8.1.1. The decomposition potential.

When the closed - circuit potential across the electrodes of a pure molten salt thermocell exceeds the decomposition potential, the salt will decompose yielding the metal at the cathode and bubbles of gas at the anode. Thus in a thermocell suitable for electrical generation it must be insured that the closed - circuit potential across the electrodes is less than the decomposition potential of the salt. In addition information on the decomposition potential and its variation with temperature can yield thermodynamic and thermoelectric data.

The voltage - current characteristic at selected temperatures was measured using the cell and circuit shown in figure 8.1 and the results are shown in figure 8.2. The decomposition potential decreases as the temperature increases and extrapolation yields a value of about 0.47 volts at 900°C. Since a thermocell containing AgCl - AgI eutectic salt mixture operating over a temperature difference of 600°C with a thermoelectric potential of 0.5 mV/K has an open - circuit potential of 0.3 volts, the salt is not in danger of decomposition. This may not be the case with certain other salt systems.

The theoretical decomposition potential, E_d , of a pure salt may be calculated from $\Delta G = -zFE_d$ or simply equated to the formation potential. In the case of AgCl E_d is 0.90 volts at 500°C and for AgI E_d is 0.57 volts at the melting point of 552°C, (Hamer et al. 1965). The decomposition potential of the mixture at 500°C is 0.59 volts (from figure 8.2) and it would appear to be reasonable that the decomposition potential of a simple mixture should be about the same as the lowest decomposition potential of the constituents. (Literature values (Delimarskii and Markov, 1961) show that this is not always the case and it may depend upon the particular 'structure' of the melt).

The variation of the theoretical decomposition potential with temperature, dE_d/dT , is equivalent to the isothermal thermoelectric potential of the cell Ag/salt/Cl₂, which is the term α_{iso} defined in in section 4.4. From the data of Hamer et al. (1956 and 1965) the value

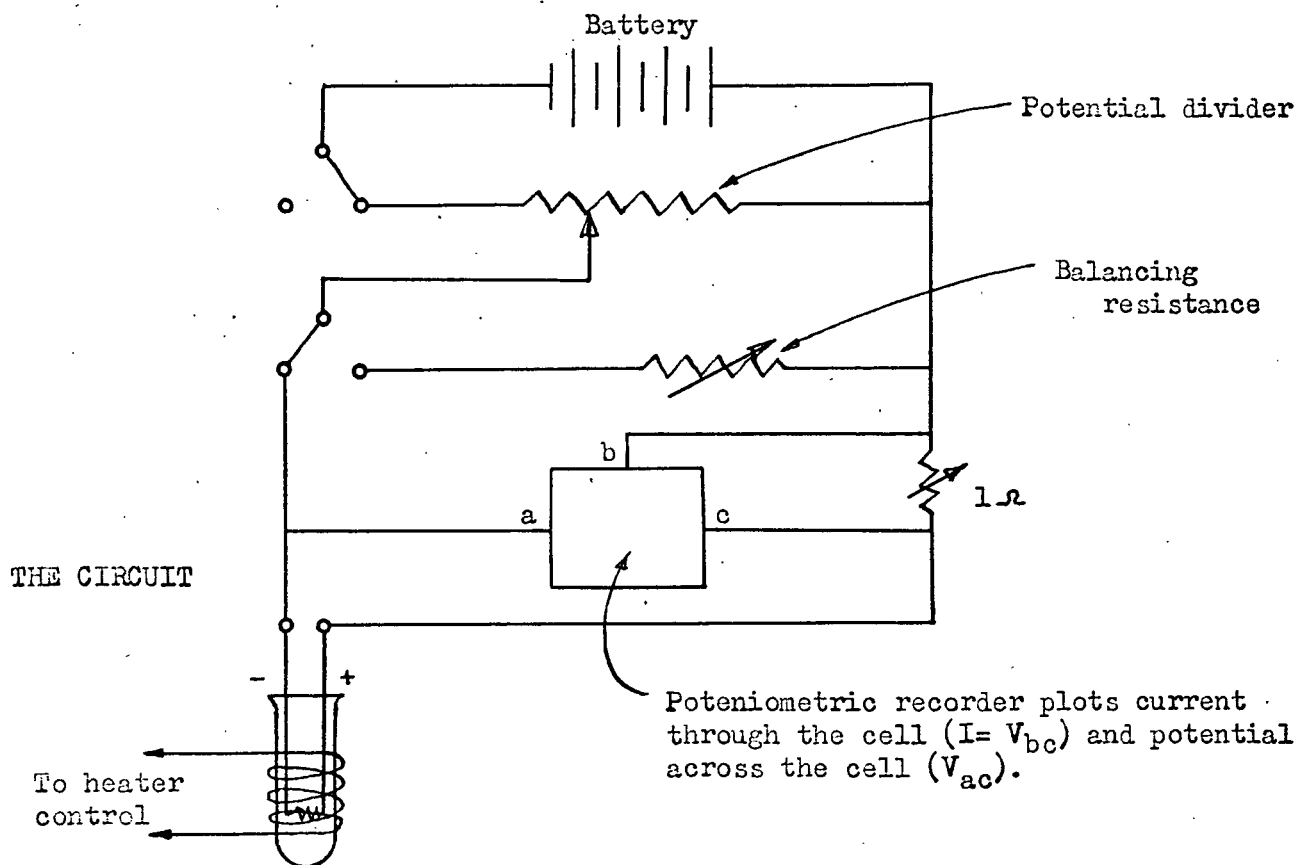
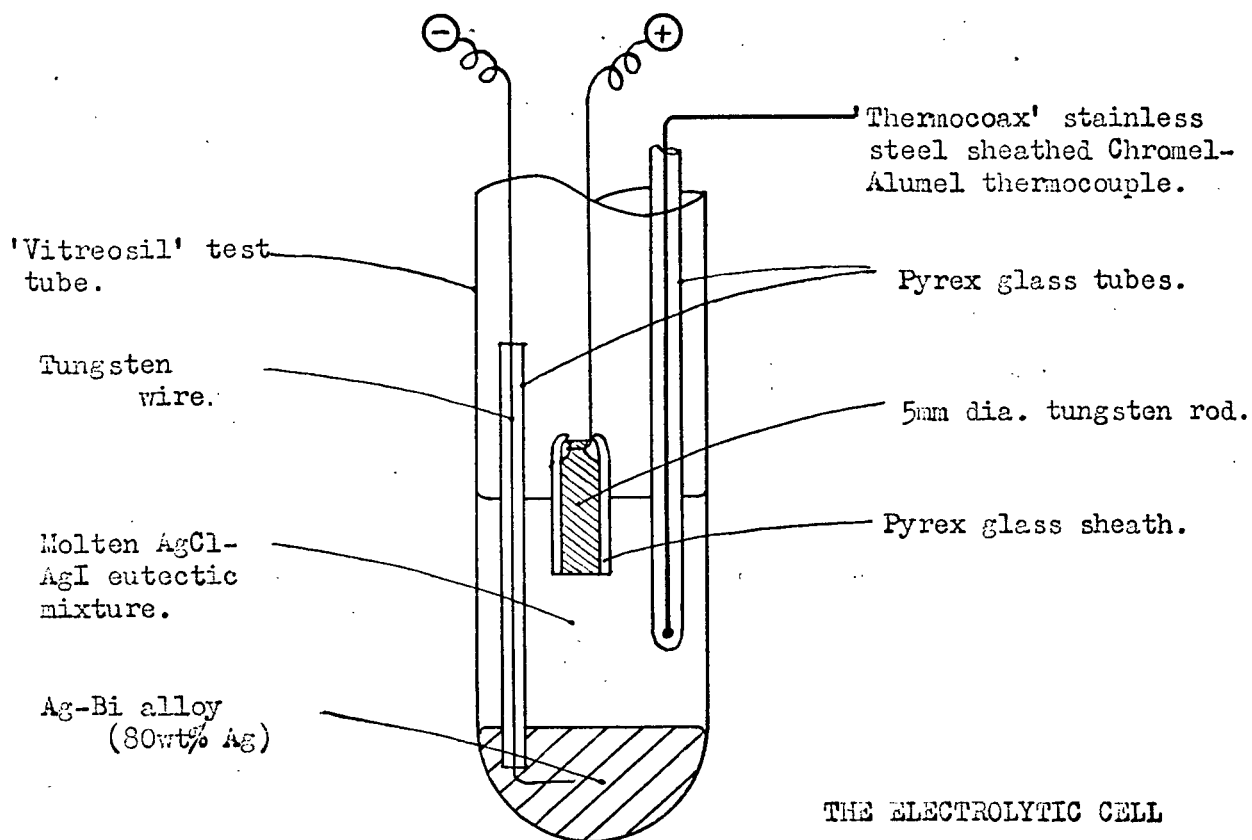


Figure 8.1 The cell and circuit used for determination of the V-I characteristic.

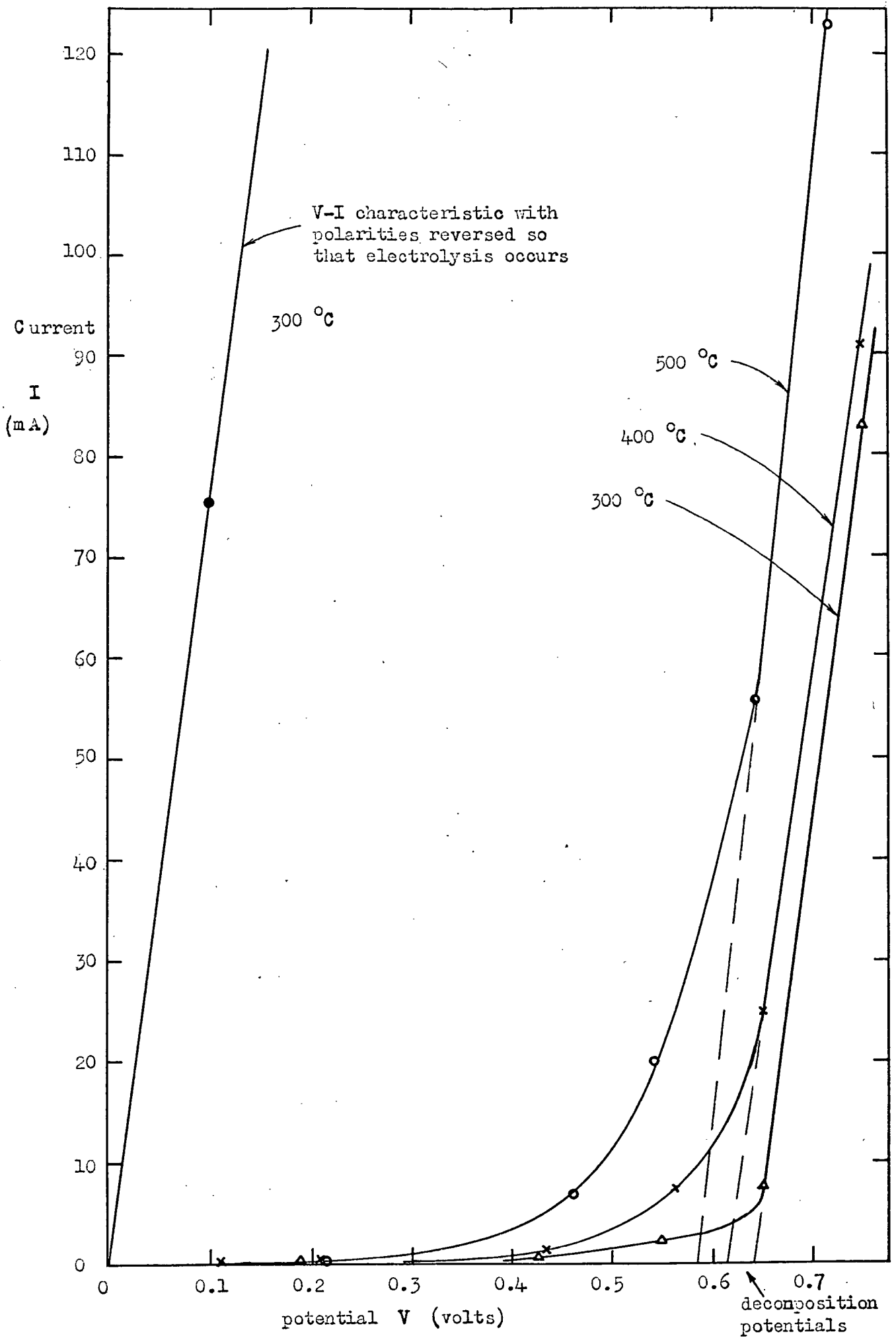


Figure 8.2 The V-I characteristic at various temperatures.

of $\alpha_{i_{50}}$ for AgCl at 500°C was calculated as - 0.26 mV/K and for AgI at the melting point of 552°C as - 0.19 mV/K. It is not possible to give a precise value for dE_d/dT from figure 8.2 as considerable error is inevitable in the extrapolation of the curves to the zero current axis. Nevertheless it can be seen that the variation of E_d with temperature for the mixture is of a similar order to $\alpha_{i_{50}}$ for the mixture, (assuming this is similar to $\alpha_{i_{50}}$ for the constituents).

If the decomposition curves had been obtained under ideal conditions with perfectly pure salt constituents and electrodes, and with no dissolution of impurities from the container or the gas above the salt surface, no current would have flowed until the decomposition potential was reached. In practice these conditions are never attained and a small current flows at voltages below the decomposition potential owing to the impurities supporting ionic or electronic conduction mechanisms. From figure 8.2 it is evident that the effect of these impurities on electrical conduction increases as the temperature increases.

When the polarities of the electrodes of the cell shown in figure 8.1 are interchanged a simple electrolysis occurs on the passage of a current, with silver leaving the lower electrode and depositing on the upper tungsten electrode. This is the process which occurs in a generation thermocell and in the following two sub-sections the V - I characteristic during electrolysis and the details of the electrolysis itself are examined.

8.1.2. The voltage - current characteristic during electrolysis.

In the initial stages of this work a simple experiment was conducted. A cell similar to that shown in figure 8.1, (but with the polarities interchanged), was set up and the voltage - direct current characteristic was measured. This characteristic was linear and showed that the d. c. resistance of the cell was constant. The resistance was also measured using a 3000 Hz a.c. supply and found to be the same as the d. c. resistance. This showed that under these conditions there was no polarization or overpotential of any form at the electrodes and a literature search confirmed this conclusion. (Murgulescu et al. (1963) measured the activation overpotential at silver electrodes immersed in molten silver halides and found it to be virtually zero).

The electrochemical information yielded by this type of experiment is rather limited as it does not indicate whether the current transfer is purely ionic or due partly to other effects. In molten salts these other effects include electronic conduction and conduction due to the breakdown of salt molecules or the formation of complexes in the melt. If it is known that the salt under test is purely ionic there is still the possibility that the deposited metal is dissolved back into the salt at a high rate so that no more than a micro-layer of the deposited metal is present on the cathode at any particular time.

8.1.3. The Faradayic mass transfer.

Faraday's laws yield an expression for the mass of electrode metal deposited during electrolysis, m :

$$m = \frac{I t A}{z F} \quad \text{---(8.1)}$$

where z is the number of charges on the ion, F is the Faraday, A is the atomic weight of the metal and t is the time of electrolysis. In practice cells with aqueous electrolytes are generally found to follow this law but cells containing molten salt often have a mass transfer which is considerably less than that predicted by this expression owing to the effects mentioned in the previous section, (8.1.2).

Initially a cell similar to that shown in figure 8.1, (but with the polarities interchanged), was assembled and a known current was passed for a specified time. The tungsten electrode^{was} removed and a silver growth was found on it. (A dendritic growth rather than an even coat is usually formed when silver is deposited from a molten halide, as discussed by Reddy, 1966). Visual inspection showed that the quantity of silver on the tungsten was much less than that predicted by Faraday's laws. On the assumption that some of the loosely attached silver dendrites may have fallen off during electrolysis a small Pyrex glass cup was fitted below the tungsten electrode. After electrolysis a very small quantity of silver was found at the bottom of the cup in addition to that on the tungsten, but visual inspection showed that the total quantity of silver was still less than that transferred according to Faraday's laws. This indicated that some of the silver deposited was dissolved in the melt or that some proportion of the current was transferred by another mechanism. It thus appeared that if an experimental rig is to be suitable for quantitatively measuring the ionic

mass transfer during electrolysis in this salt mixture, it must be designed to prevent dendrites of silver leaving the electrode and dissolution of the silver in the salt. Attempts to measure the increase in weight of a tungsten electrode suspended in the melt during electrolysis were unsuccessful and were abandoned when the following method occurred to the writer.

Besides being applicable to the cathode equation 8.1 is also applicable to the anode, when m is the decrease in weight of the electrode. With this in mind the cell shown in figure 8.3 was set up with a known quantity of silver, m , situated at the anode on the tungsten wire screen. When a voltage was applied across the cell current flowed until no silver remained at the anode at which point the voltage dropped to a small residual value. The current during electrolysis was not constant, as the effective area of the anode decreased during electrolysis, but the current was measured using an automatic potentiometric recorder in such a way that the area under the recording represented the product It . The results of five runs with various quantities of silver are shown graphically in figure 8.4 together with the characteristic yielded by equation 8.1. To a first approximation it can be seen that the silver transferred from the anode is correctly given by equation 8.1 and that the current flow through the salt is therefore entirely ionic. The scatter of the experimental results shown in figure 8.4 is probably due to a limited amount of dissolution of silver in the salt during electrolysis and the presence of impurities in the salt which supported current flow mechanisms other than that of the univalent ion transfer.

Having ascertained that the current transfer in the $\text{AgCl} - \text{AgI}$ mixture is basically ionic and the mass transfers are therefore given by Faraday's laws, consideration must now be given to the apparent deviation from these laws when the cathode is an unenclosed tungsten electrode. The cell was again set up as in figure 8.1 and a current was passed through the cell for a known time (of 2 or 5 minutes) and then suddenly reversed so that any silver deposited on the tungsten was transferred back to the lower electrode. When all the silver had been transferred from the tungsten electrode the current dropped to a very low value, thus indicating the electrolysis time t . (Ideally when the current efficiency is 100% the It product for the flow in each direction should be the same; but when some of the silver dissolves back into the salt or is transferred by any other

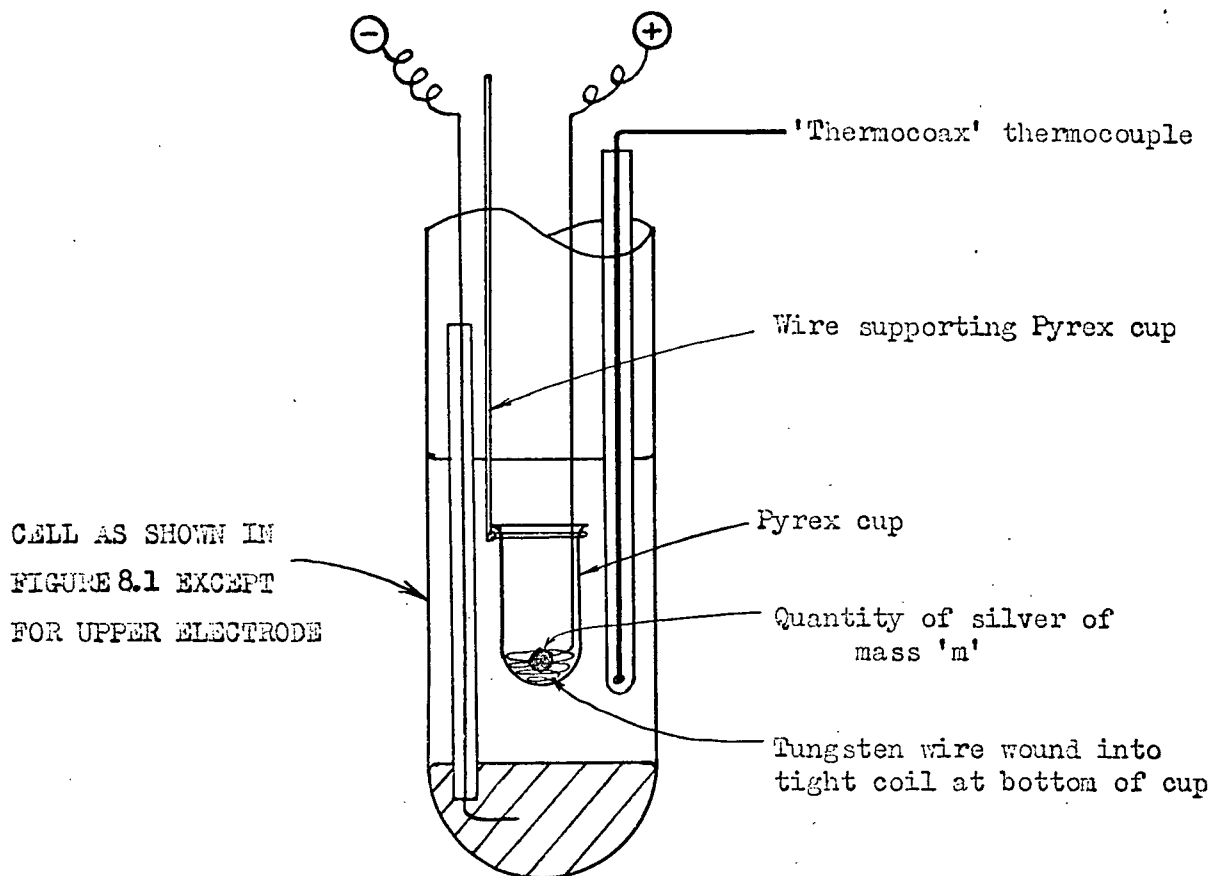


Figure 8.3 The cell arranged to measure the mass transferred during electrolysis.

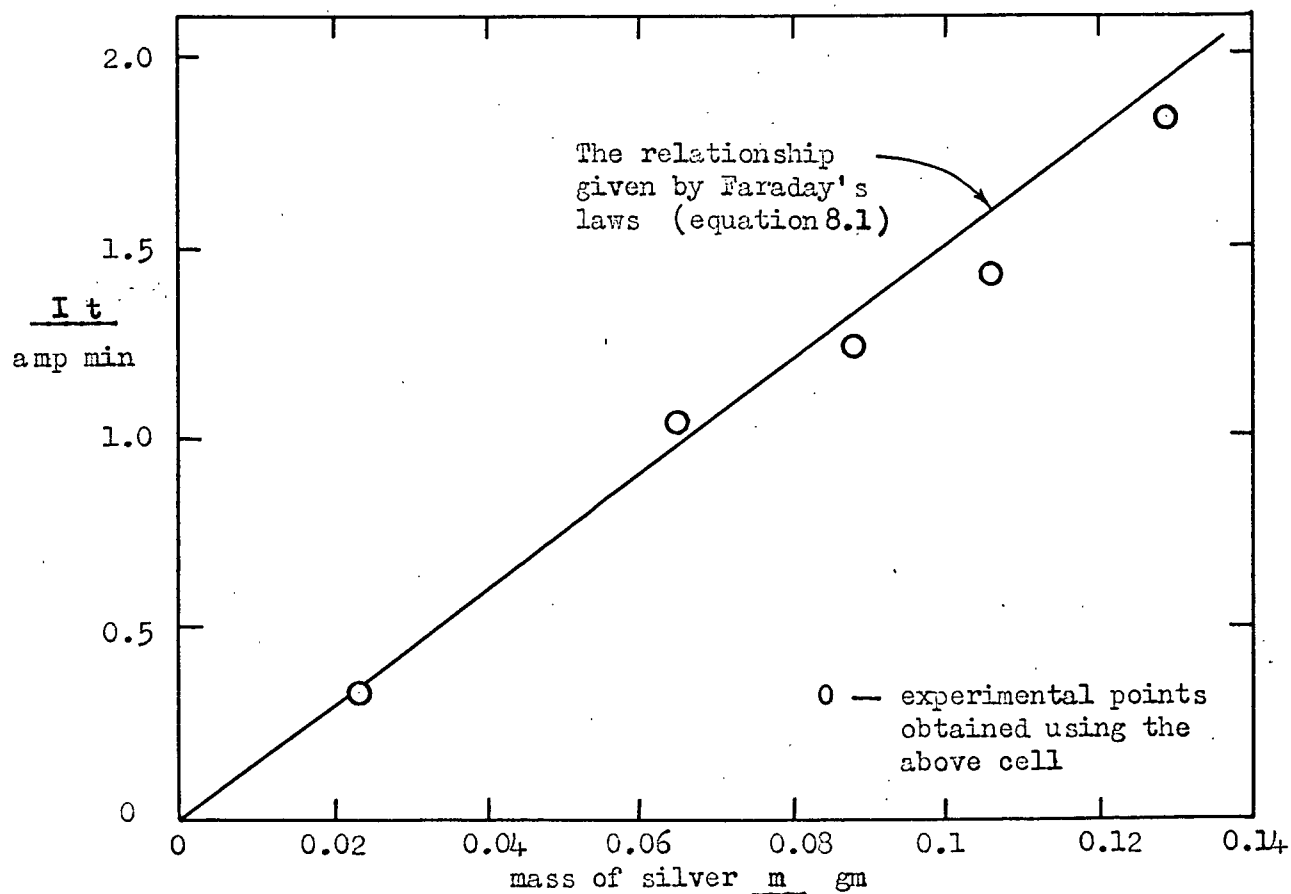


Figure 8.4 The current efficiency of the AgCl-AgI eutectic mixture.

mechanism the 'It' product for the material removed from the tungsten will be considerably less than that for the material deposited). Experiments of this type were conducted using an unenclosed tungsten electrode and also for the case when a quantity of quartz wool was submerged in the salt to lessen convection currents, and the results are shown in the following table:

	<u>Deposition</u> <u>time t</u>	<u>Deposition</u> <u>It product</u>	<u>Removal</u> <u>It product</u>	<u>Removal It</u> <u>Deposition It</u>
Tungsten electrode in pure salt mixture	2 min.	0.220 amp min.	0.046amp min.	21%
	5 "	0.475 "	0.054 "	11%
Tungsten electrode in salt mixture containing quartz fibre to lessen convection.	2 "	0.164 "	0.080 "	49%
	5 "	0.450 "	0.258 "	57%

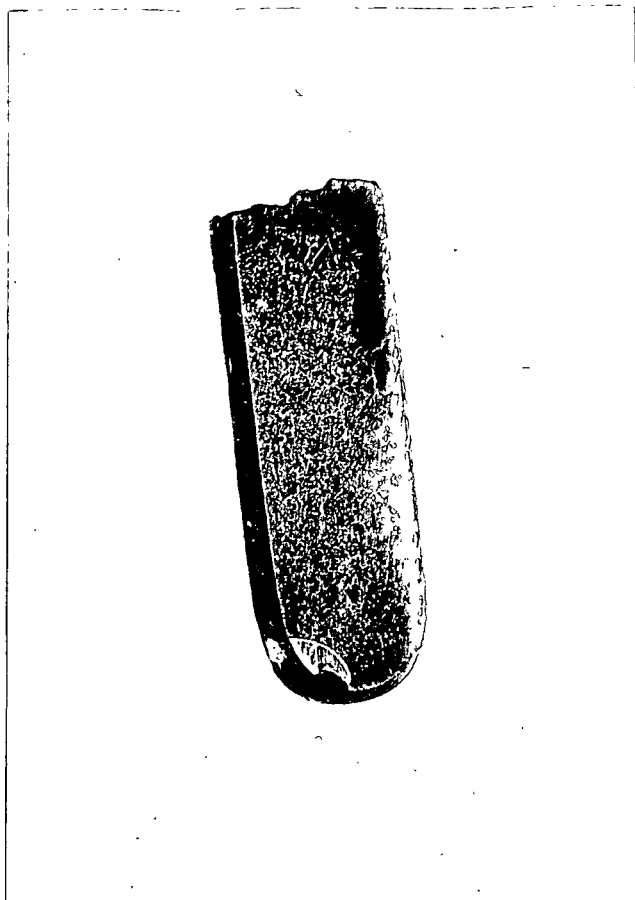
Diffusion of the silver in the salt melt and any other mechanism transferring silver to or from the tungsten electrode other than electrolysis may be classed under the general heading of convective mass transfer. It is apparent from the table that for the simple case of a tungsten electrode in the eutectic AgCl - AgI melt, silver is removed from the electrode almost as quickly as it is deposited by electrolysis. When convection in the cell is reduced by introducing a fibrous material the convective mass transfer of silver from the electrode is also reduced.

8.2. Convective Mass Transfer.

The mass transfer due to convection in a thermocell containing molten salt and molten metal may be considered as being caused by two mechanisms. One of these is described by Cubicciotti (1964) in an article on the corrosion of metals in fused salts. It involves the molten salt at a high temperature dissolving the metal and then flowing to a cool region where the solubility of the metal in the salt is less and the metal is precipitated out. This effect causes a net transfer of metal from the hot to the cool region. The second mechanism is due to the thermal convection currents causing a stirring action in the salt which encourages globules of liquid metal to leave the surface and float about within the salt.

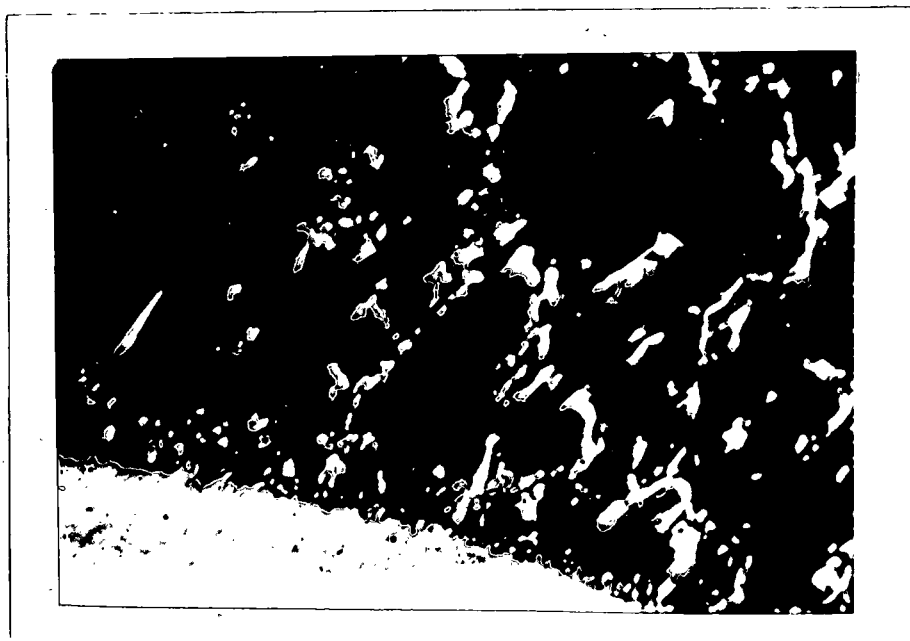
The solubility of silver in molten silver halides is very low. Corbett and Winbush (1955) measured the solubility of silver in silver chloride at 490°C as 0.03 mole % and at 700°C as < 0.06 mole %. Although the solubility of silver in a mixture of silver halides (such as the AgCl - AgI eutectic), may be considerably higher than in the pure halides it is nevertheless unlikely that the silver transferred by the first mechanism will be very great. The silver transferred by the physical action of the convection currents was experimentally demonstrated by heating a quantity of silver immersed in the AgCl - AgI eutectic salt mixture (in a transparent quartz glass test tube) to above the melting point of the silver. Small flecks of silver were clearly visible floating about in the salt. On quenching one of these test tubes in water, removing the broken glass and sectioning the solid salt, the silver was found to have frozen in the salt as shown in figure 8.5. Microscopic examination of the interface between the metal and the salt showed the general turbulence in this area prior to quenching, (figure 8.6).

It has been shown that there are advantages to using a silver-bismuth alloy as the electrode metal. The above test was therefore repeated with the silver replaced by an alloy of 30 weight % silver and 70 weight % bismuth. In this case considerably less metal was noticed in the salt melt and, on quenching and sectioning, it was found that this metal was in the form of small globules rather than flecks (figure 8.7). No explanation of this can be offered except that the addition of bismuth to the silver affected the surface tension between the metal and the salt.



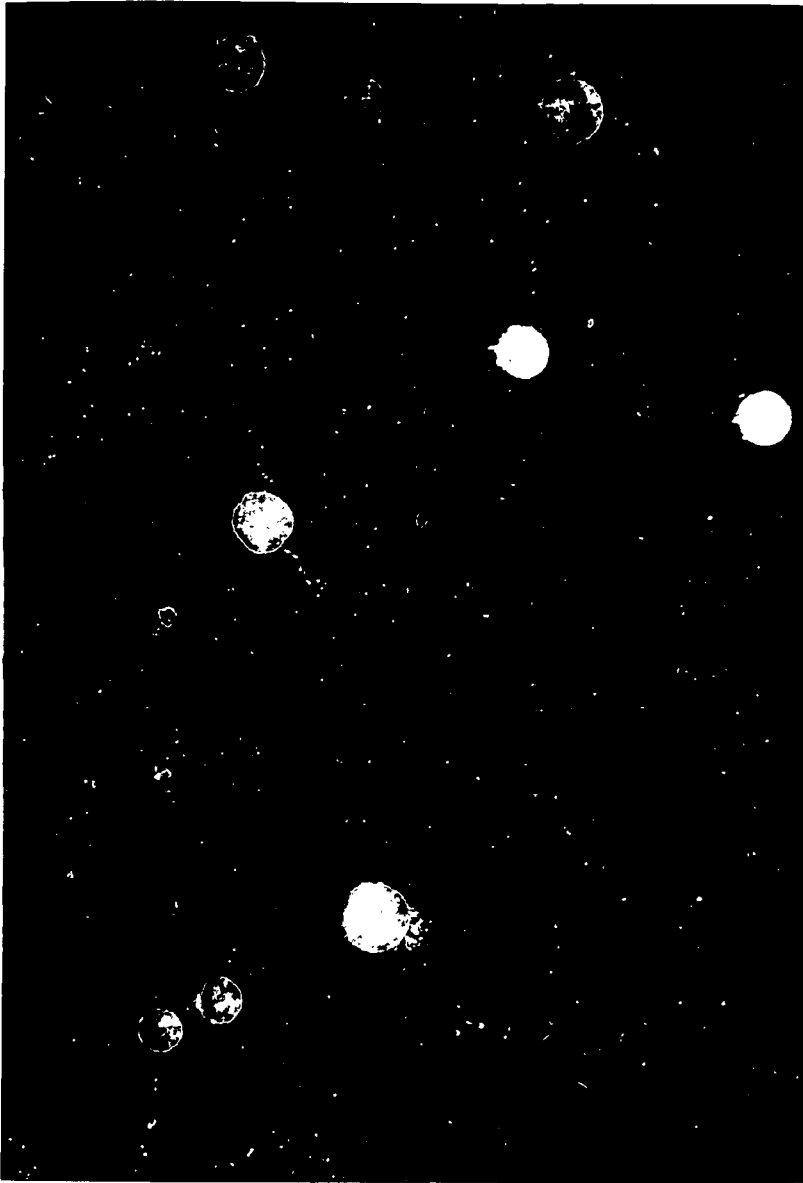
x2

Figure 8.5 Silver flecks in silver halide salt mixture (quenched from $\sim 1000^{\circ}\text{C}$).



x50

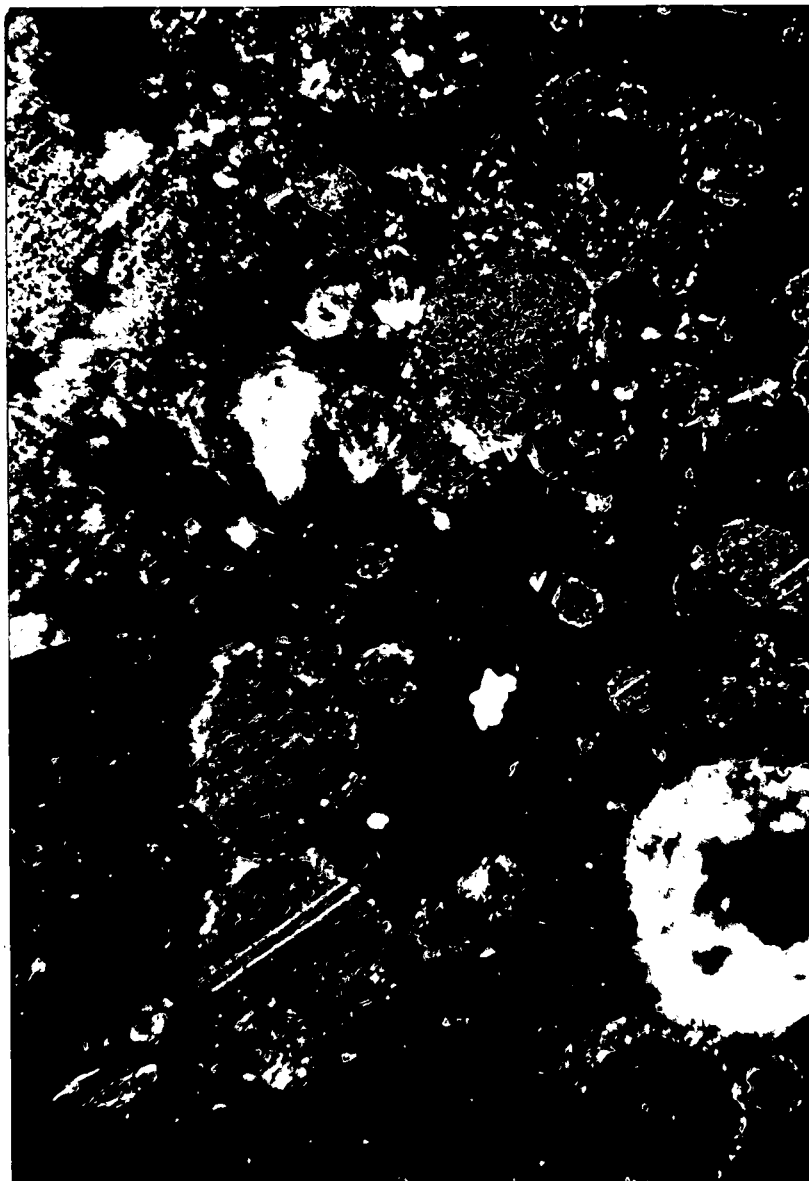
Figure 8.6 The metal-salt interface from the above section.



x60

Figure 8.7 Globules of alloy in the salt mixture
(quenched from 1000°C).

Referring back to the generation thermocell discussed in section 5.3.2 it was noticed that a mass of salt and metal was present in the cool pocket. This was probably caused by a mass transfer mechanism similar to that just described. A part of a section through the cell (shown encircled in figure 5.8) was examined under the microscope. The photograph shown in figure 8.8 shows crowded globules of the alloy in the molten salt (and also an air hole on the right hand side with the centre out of focus owing to the depth, caused by the contraction on solidification).



x 60

Figure 8.8 Magnification of part of the cell shown in figure 5.8.

8.3. Trials of various vertical tube configurations for thermocell generation.

This section is confined to descriptions of practical trials of thermocells arranged with one electrode vertically above the other. The lower electrode in each case was a molten alloy of silver and bismuth as discussed in chapter 7. The thermocells are divided into two subsections according to whether the lower or the upper electrode is heated.

8.3.1. Trials of thermocells with the lower electrode heated.

8.3.1.1. The cell operation.

Consider the cell shown in figure 8.9. When the external circuit is closed through a resistance the current which flows causes electrolysis within the cell, with silver passing from the hot lower electrode to the cool upper tungsten electrode. In addition there is convective mass transfer within the cell which also transfers alloy between the electrodes. From the tests described in sections 8.1 and 8.2 it may be predicted that some of this metal will remain at the tungsten electrode but the majority will fall back into the surrounding salt and eventually to the lower electrode reservoir. After an initial period a steady state will be reached with continuous mass circulation of the metal.

A number of trials of this cell were conducted with the lower alloy electrode heated to about 900°C and the upper electrode cooled to about 300°C . The open circuit voltage (using the AgCl - AgI eutectic salt mixture) was typically 0.27 volts and the cell resistance was between 1 and $2\ \Omega$. During one of these trials the tungsten wire electrode was withdrawn after the cell had been generating for one hour and some alloy was found on the tungsten wire as shown in figure 8.10.

8.3.1.2 Pyrophyllite Cells.

The use of pyrophyllite, as a ceramic material which may be machined and subsequently hardened, has already been mentioned in section 7.3. A small generator designed to have an open circuit potential of about two volts was constructed by arranging seven cells in a single block of pyrophyllite as shown in figures 8.11 and 8.12. The bases of the cells were heated by resting the block on a platinum furnace winding, and the

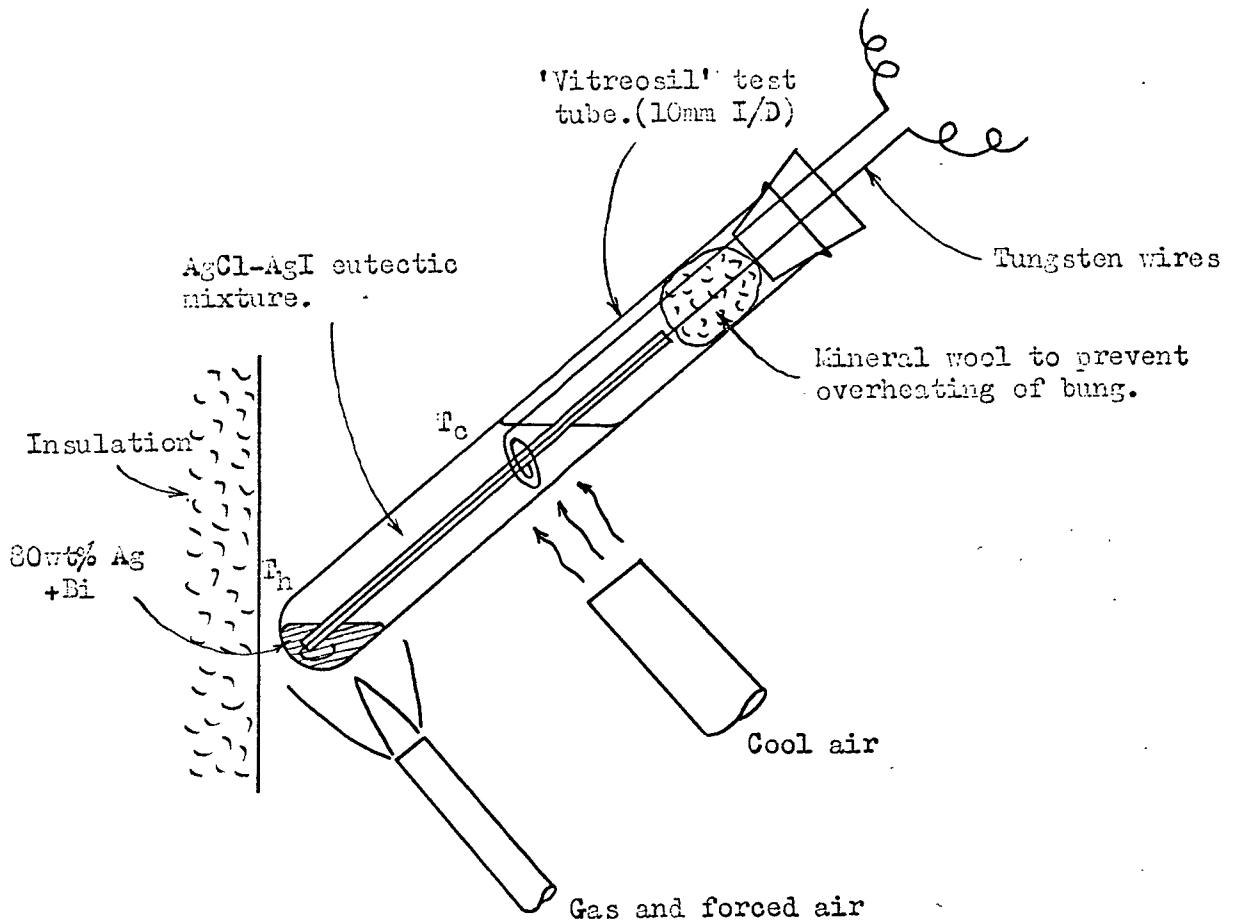


Figure 8.9 Generation thermocell.



Figure 8.10 The upper electrode of the above cell after operation.

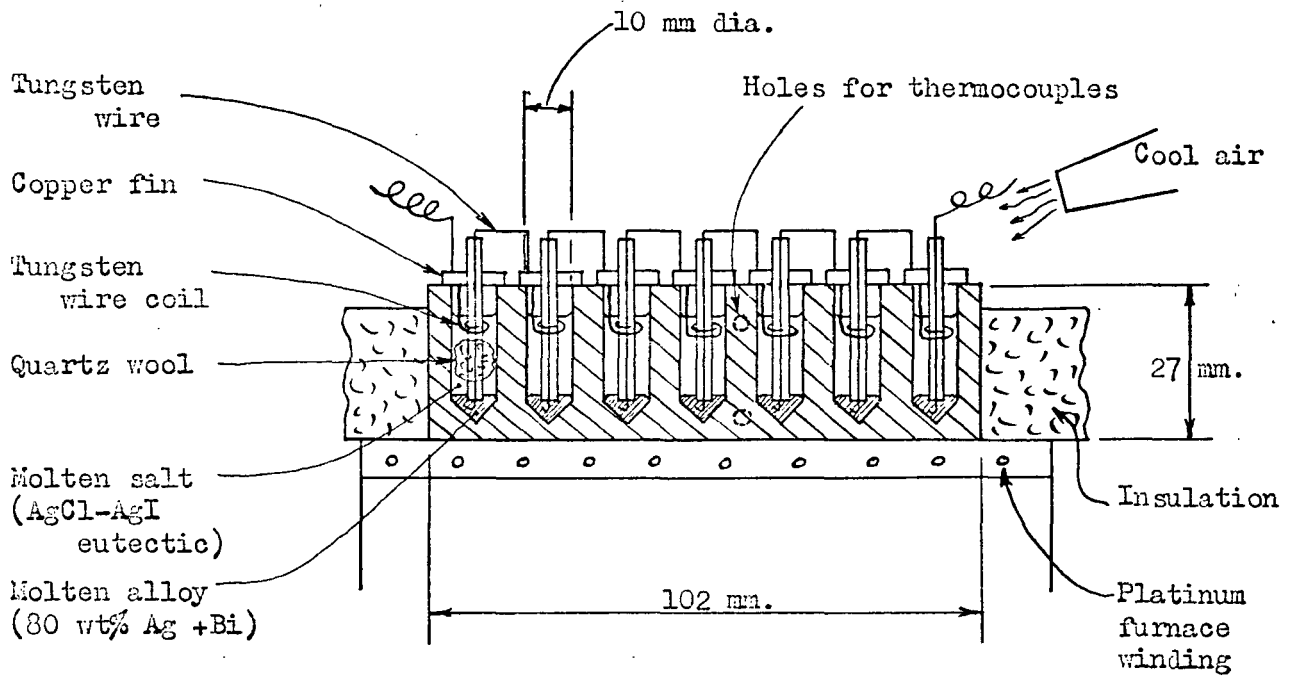


Figure 8.11A molten salt-metal thermopile.

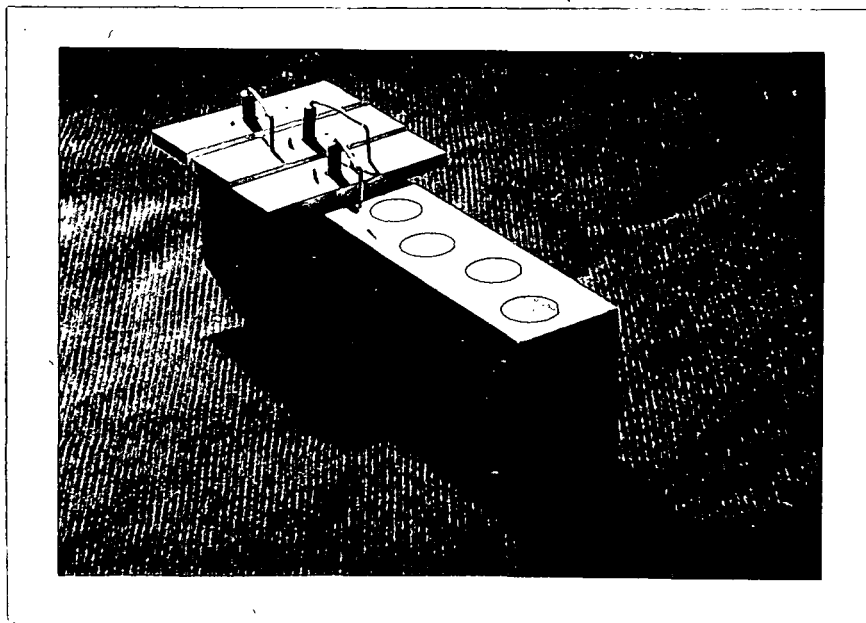


Figure 8.12 The thermocell partially assembled.

upper electrodes were cooled by an air blast from a blower directed onto the copper fins. The upper and the maximum lower temperatures were about 300°C and 850°C respectively.

The generator was assembled by placing the pyrophyllite block in position on the hot platinum winding and filling the seven holes with the pre-weighed amounts of alloy and salt. When the contents had melted the tungsten wire electrode and fin assemblies were fitted as shown in figures 8.11 and 8.12. The initial open circuit voltage was 1.6 volts and this was maintained for five minutes. The voltage then dropped to below 1 volt and gradually decreased to practically zero during the next hour after which the test was terminated. Some salt had evaporated from the tops of the cells and condensed on the cooler portion of the block and on the copper fins as shown in figure 8.13. Three of the tungsten wire electrodes and fin assemblies were withdrawn before the salt solidified, and alloy was found surrounding the tungsten wire as expected (figure 8.14). As no obvious reason for the voltage drop was apparent, one of the holes (complete with solid salt and alloy) was sectioned, and it was found that the pyrophyllite was porous to the salt at high temperature. Figure 8.15 shows the infiltration of the salt into the pyrophyllite in the lower part of the cell. It was this that shorted out the cells and eventually caused the voltage to drop to practically zero.

This porosity at high temperatures virtually ruled out the possibility of using pyrophyllite for thermocells, unless some form of lining for the cells could be found. In order to ascertain the feasibility of this general arrangement of thermocell for generation, a single cell as shown in figure 8.16 was tested. The open circuit potential was 0.23 volts, the cell resistance was $0.65\ \Omega$ and the short circuit current was 0.35 amps. The cell generated on a load of $1\ \Omega$ for five hours and then failed owing to salt seeping through the pyrophyllite, and evaporating from the top of the cell. On being allowed to cool the cell cracked demonstrating that when containing this particular salt mixture it would be unsuitable for thermal recycling. The following cell arrangement was studied in an attempt to reduce the internal resistance and allow thermal recycling without cracking the container.

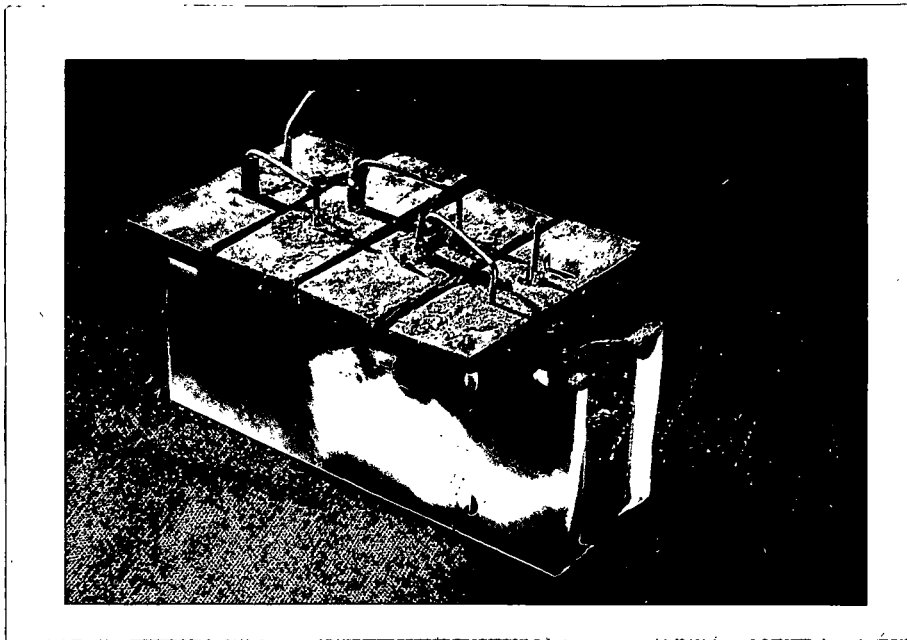


Figure 8.13 Part of the pyrophyllite block assembly after use.

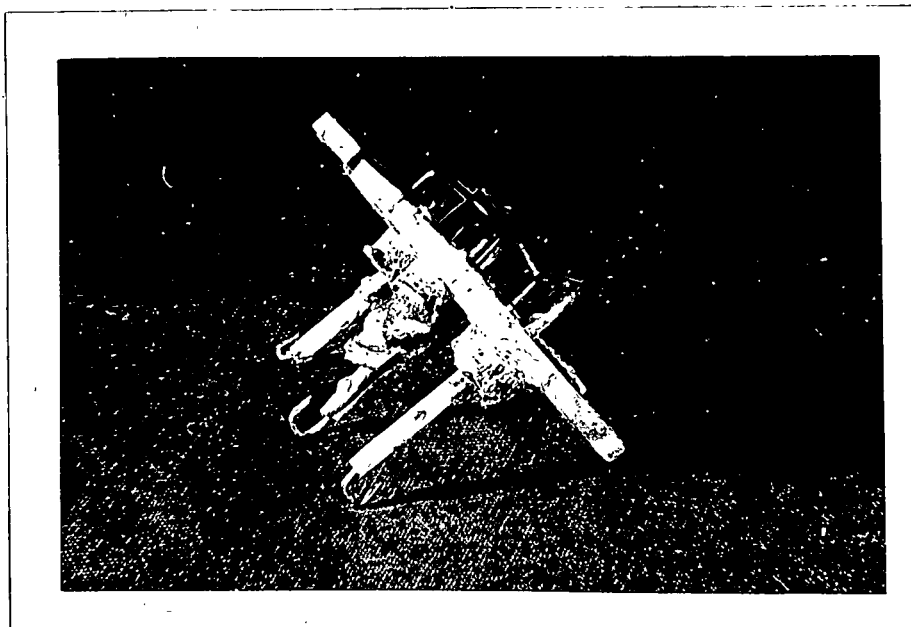
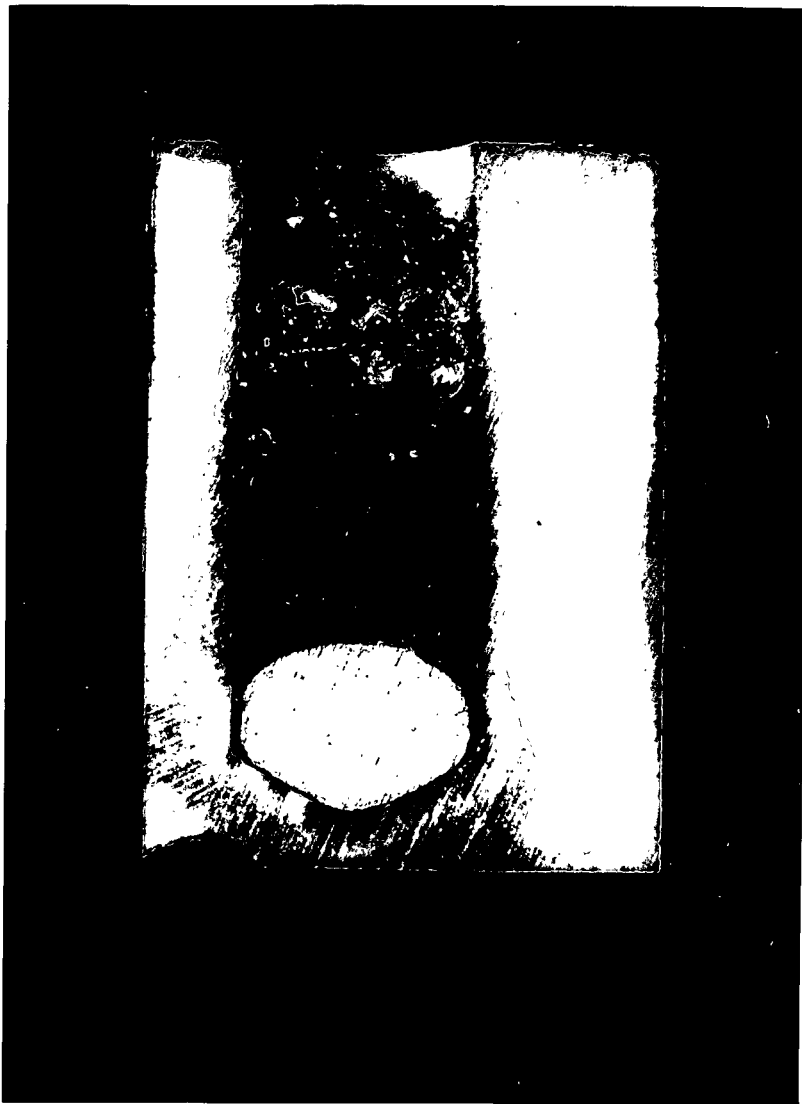


Figure 8.14 Part of the cool electrode and fin assembly after use.



x $\frac{3}{2}$

Figure 8.15 Section through a cell showing the infiltration of salt into the pyrophyllite.

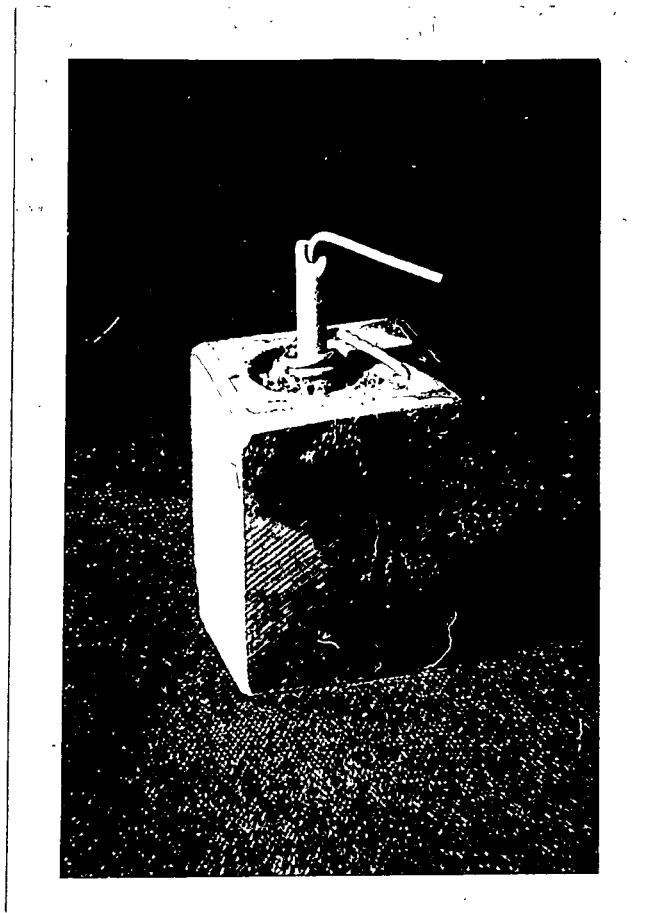


Figure 8.16 The single pyrophyllite cell after use.

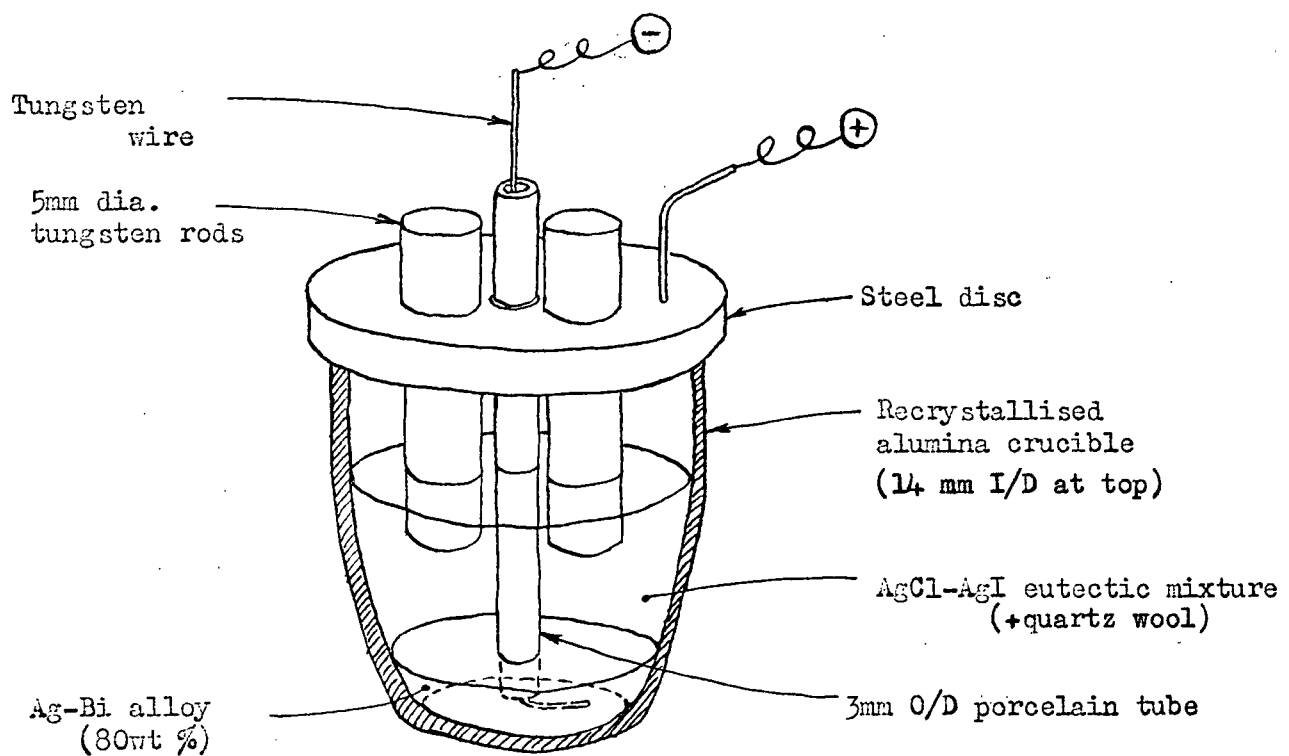


Figure 8.17 The crucible cell.

8.3.1.3. Crucible cells.

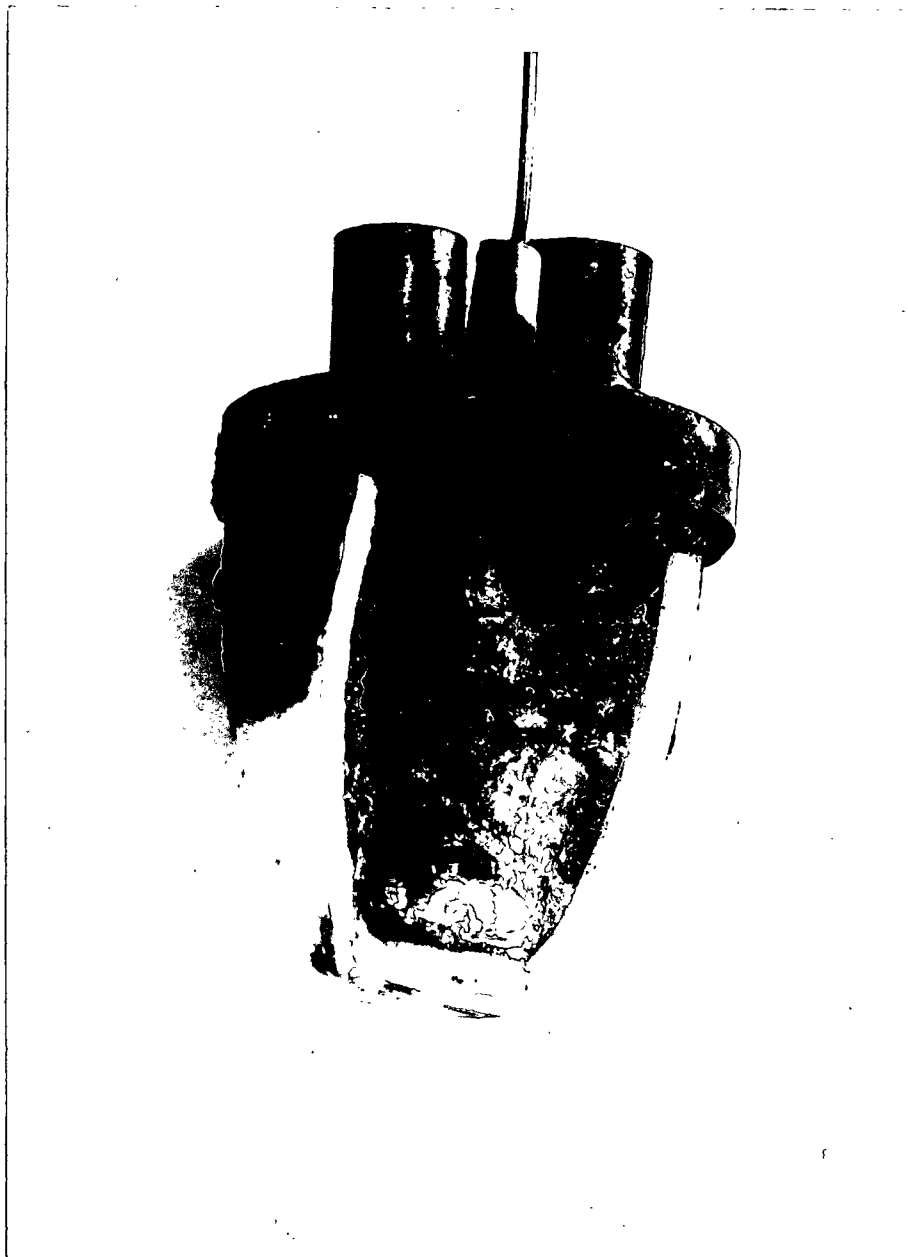
The cell shown in figure 8.17 was constructed using a commercial 'Thermal Syndicate' recrystallised alumina crucible. The mild steel cap was fitted flush with the top of the crucible thus enclosing the contents while allowing for differential thermal expansion. The upper electrode consisted of two 5 mm diameter tungsten rods dipping into the molten salt. For feasibility trials the crucible base was heated by a gas and air burner and the top assembly was cooled by forced air flow. No temperatures were measured.

Initially the open circuit potential was measured as 0.26 volts, the cell resistance as 0.30Ω and the short circuit current as 0.87 amps; but during the next hour the voltage gradually dropped to a low value. Subsequent examination showed that a mass of alloy had formed around the tungsten rods as expected, but had also extended practically down to the hot electrode, thus reducing the temperature difference and electrical potential between the electrodes. Five cells of this type were tested and each yielded a similar result.

It was found that the cells could not be thermally recycled between the operating temperature and room temperature more than two or three times without cracking the crucible. (Figure 8.18 shows one of these cells after cracking open and exposing the contents). Closer examination showed that the cells fractured while cooling in the range between 200°C and 100°C . The equilibrium diagram of the AgCl - AgI mixture, (figure 6.1, page 106), shows that there is a solid - solid transition at a temperature of 124°C . It was probably the volume decrease at this transition which caused the cells to fracture. The crucibles were filled with other salts and mixtures and, (except in the case of AgI), the container did not fracture on thermal recycling. This effect must therefore be considered as a disadvantage of using the AgCl - AgI salt mixture.

8.3.1.4. Low resistance cells.

If a thermocell is to generate large currents the electrode area must be large and the distance between the electrodes must be a minimum. The logical extension of this concept is a thermocell in the form of a sandwich with a hot lower electrode, a molten salt containing a fibrous material and a cool upper electrode. The current flowing once steady conditions are attained will be directly proportional to the electrode



x 5

Figure 8.18 The crucible cell after use.

area but will not be directly proportional to the electrode spacing owing to the convective mass transfer. The object of the following experiment was to determine the effect of electrode spacing on cell performance.

Figures 8.19 and 8.20 show the experimental rig. The upper electrode and cooling fin assembly was suspended from pulleys in order that the height could be easily adjusted and the assembly could be quickly withdrawn from the cell for visual examination of the upper electrode. After some experimentation it was found that the tungsten could be brazed to the copper stem once the surface of the tungsten had been thoroughly roughened by grinding grooves in it. The temperature of the tungsten block was estimated from the measured temperatures at two positions along the copper stem.

At an electrode spacing, L , of more than 10 mm the cell was found to operate on load successfully for the period of the test (a few hours). The following table shows the open circuit potential V_{oc} , cell resistance R_c and short circuit current I_{sc} after steady conditions had been attained:

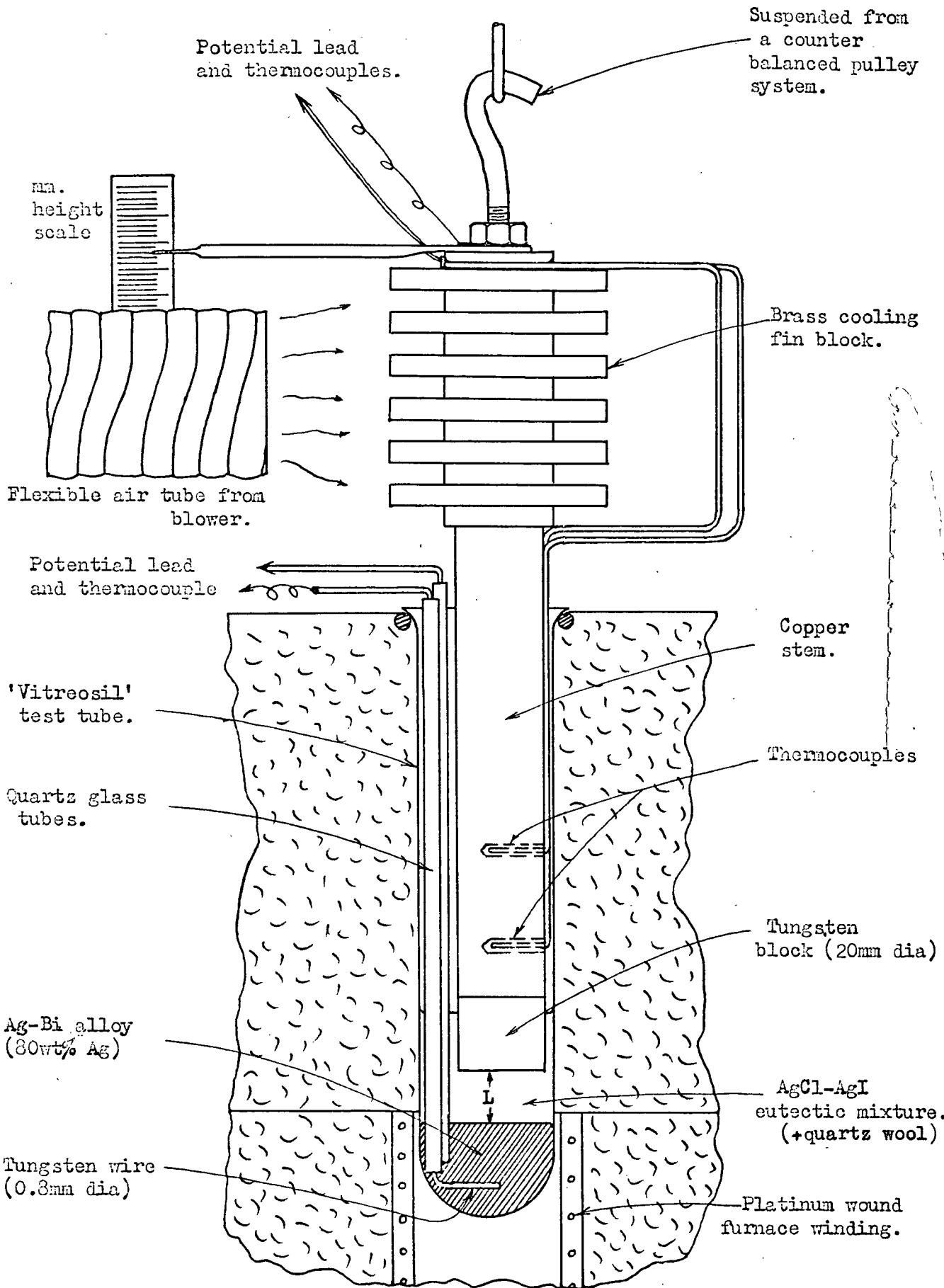
<u>L</u> (mm)	<u>T_h</u> (°C)	<u>T_c</u> (°C)	<u>V_{oc}</u> (volts)	<u>R_c</u> (Ω)	<u>I_{sc} (= V_{oc} / R_c)</u> (amps)
21	810	270	0.255	0.5	0.51
16	800	275	0.250	0.39	0.64
10	815	280	0.250(max.)	0.31 (min.)	0.81(fluctuating)

It would therefore appear that there is a lower limit to the electrode spacing which can be tolerated in a cell of this type owing to the quantity of metal adhering to the upper electrode. As far as thermo-cell generation is concerned this is rather disappointing, and emphasises the necessity of using a molten salt with a high electrical conductivity if a low cell resistance per unit electrode area is to be obtained.

8.3.2. Trials of cells with the upper electrode heated.

8.3.2.1. The cell operation.

On first consideration it appeared improbable that a cell of the type shown in figure 8.9 would operate at all when the upper tungsten



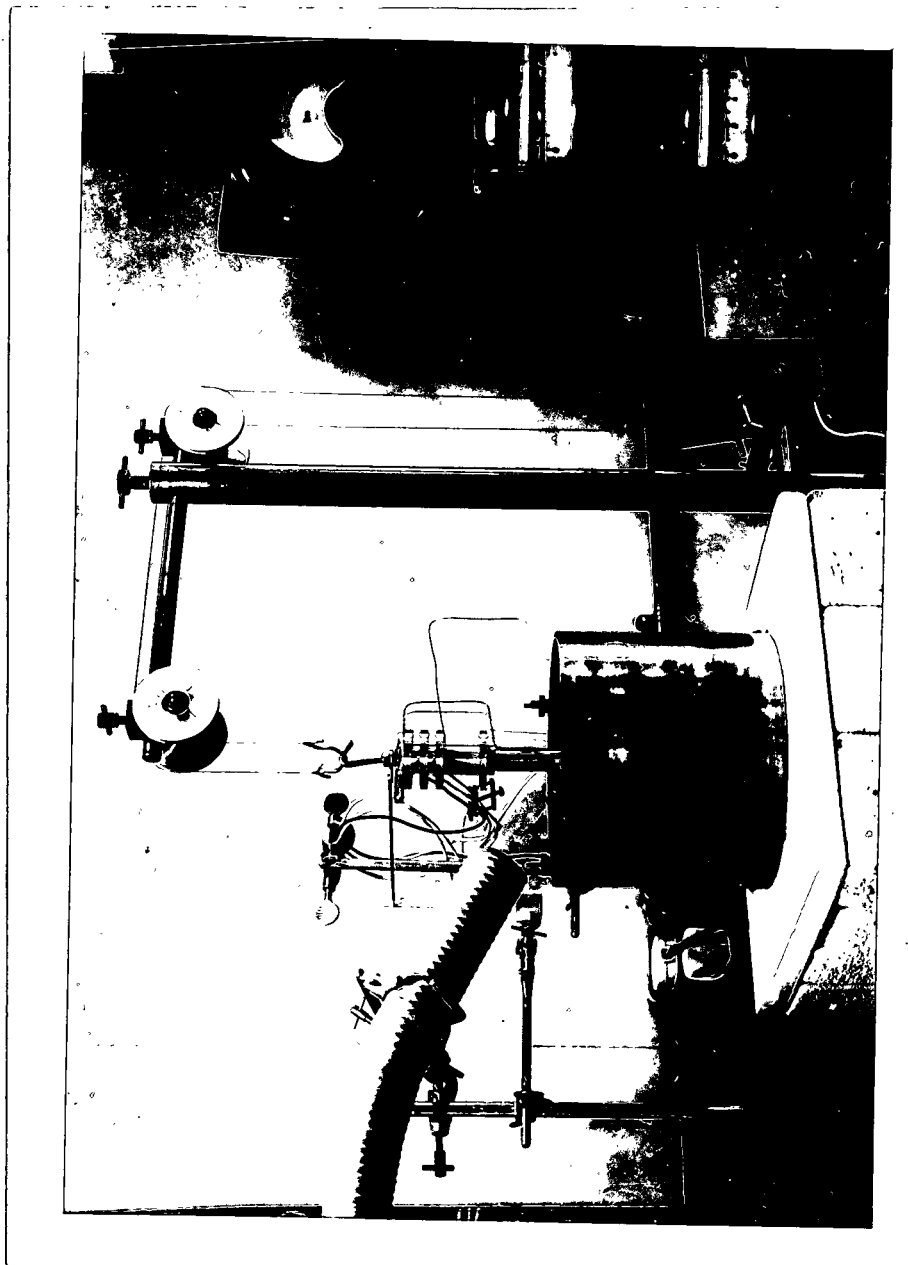


Figure 8.20 General view of experimental rig for testing the low resistance cell.

electrode (rather than the lower alloy electrode) was heated. Electrolysis which would occur on closing the circuit would cause silver ions to flow towards the lower electrode and a cell of the type Ag/Ag halide/Ag would not be established. The voltage - current characteristic of the cell Inert Metal/Ag halide/Ag has been examined in section 8.1.1. and it was established that only a small residual current flowed at voltages below the decomposition potential.

By accident it was found that, in practice, a sizeable current could flow when the upper electrode was heated. Investigation showed that small globules of the molten lower electrode metal floating about in the salt due to the convective mass transfer, (as shown in section 8.2), could adhere to the upper electrode, thus causing it to act as a silver electrode. Under suitable conditions it was found that an upper silver electrode could be maintained by this mechanism. In figure 8.21 an ordinary mild steel wood screw is shown after it has been used as the hot upper electrode in a silver halide thermocell. The (originally molten) mass of alloy can be seen together with some corrosion of the steel by the molten silver salt as is to be expected. Heating of the upper (rather than the lower) electrode reduces the heat transfer between the electrodes as the natural convection currents are reduced, but at the same time there must be sufficient convection to maintain the transfer of metal to the upper electrode.

8.3.2.2. Trials using various arrangements of the upper electrode

An experimental rig was constructed as shown in figures 8.22 and 8.23. The top assembly was hinged so that it could be turned back to enable the ceramic test tube to be inserted and filled. The upper electrode could be maintained continuously at a temperature of 850°C and at higher temperatures for short periods. The heater element consisted of nickel - chrome wire in an insulated stainless steel sheath and the power input was controlled by a variable transformer. Cooling at the lower electrode metal reservoir was by forced air from a variable blower and the molten alloy was maintained at about 300°C. Temperatures within the cell were measured by a 'Thermocoax' stainless steel sheathed Chromel - Alumel thermocouple fitted in a quartz glass tube so that its height could be adjusted. The salt used was either the AgCl - AgI eutectic mixture or an equal - weight mixture of AgCl and CuCl. The latter mixture of salts is studied in the following chapter, (9).

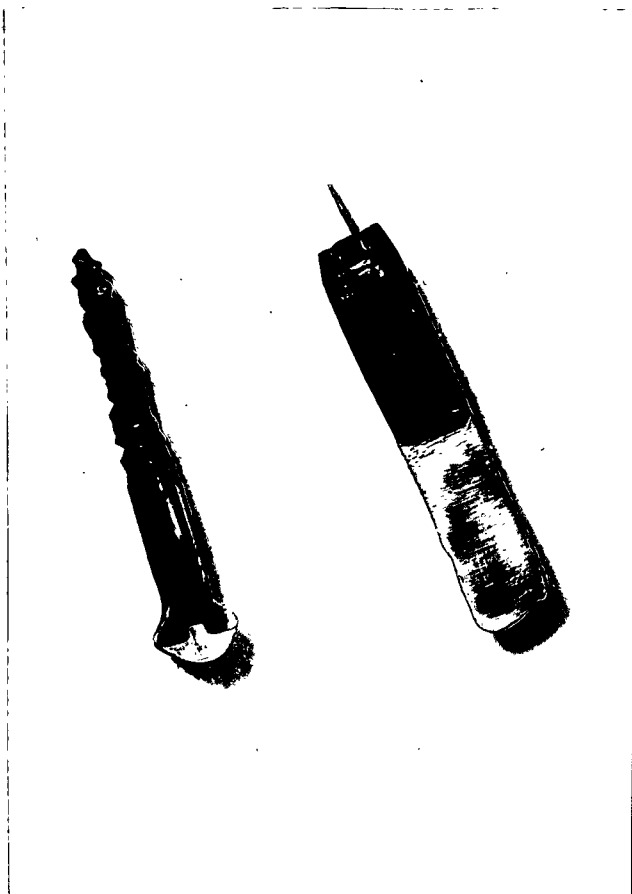


Figure 8.21 Steel upper electrodes after use and sectioning.

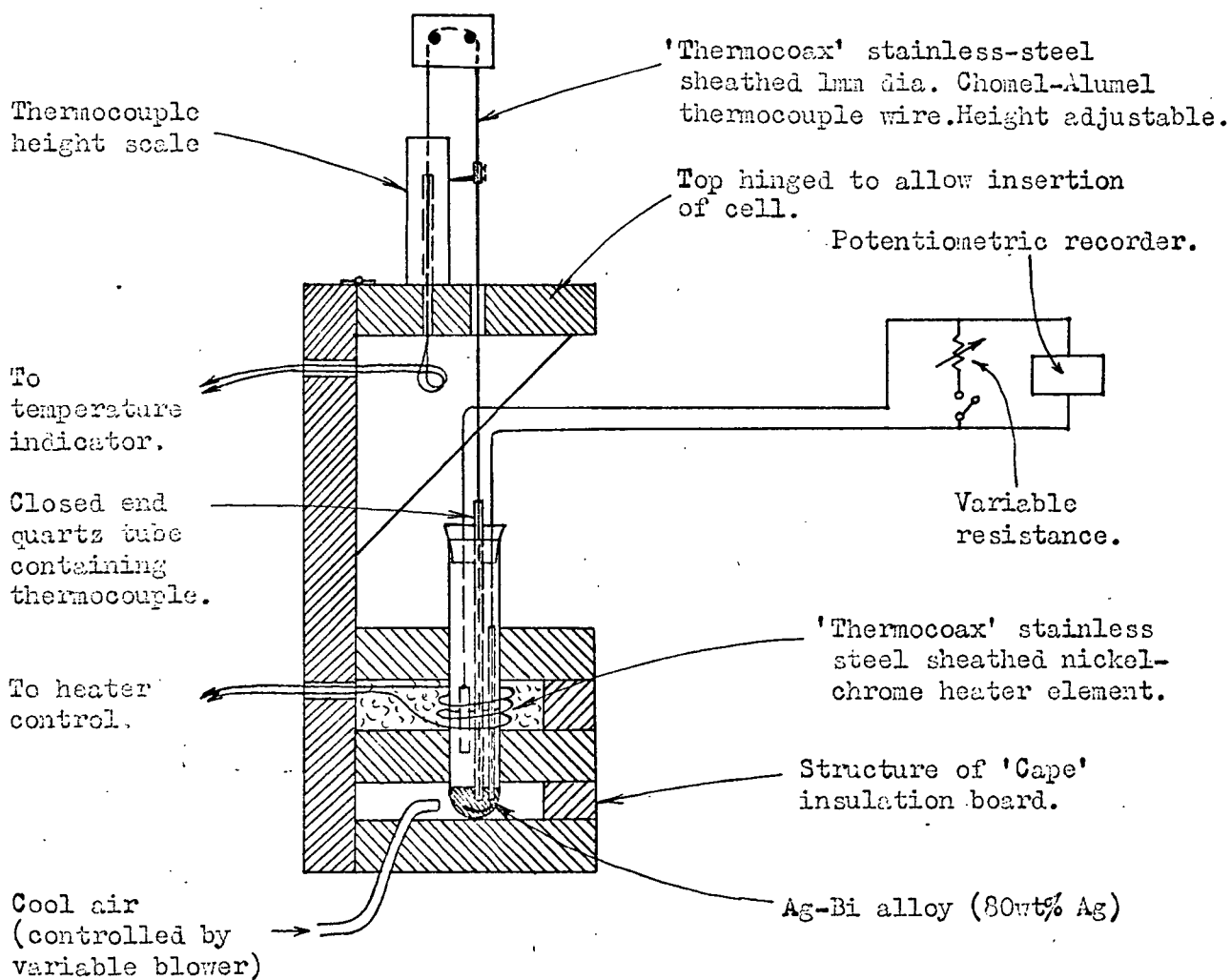


Figure 8.22 Section through rig for testing thermocells. (See also Fig. 8.23).



Figure 8.23 General view of therocell testing rig.
(May be arranged for upper or lower electrode heating).

Generation trials of this cell using tungsten wire as the upper electrode were unsuccessful. If the cell was stirred and a tungsten wire electrode was inserted, metal would adhere to it and a silver electrode would be established. Unfortunately this situation would only be maintained for about 15 minutes owing to the violent convection currents subsiding so that the quantity of metal floating in the salt around the tungsten wire decreased. The drawings of figure 8.24 illustrate four other electrode arrangements, with larger upper electrode areas, which were tried. The first consisted of a steel rod (and later a nickel rod) fitted in a quartz glass tube (with sufficient tolerance to prevent fracture of the glass on expansion of the steel). This glass tube prevented corrosion of the sides of the rod in the molten salt, and the bottom of the rod ideally had a layer of molten alloy adhering to it after an initial period of operation. (Silver and iron do not form an alloy in the temperature range used). The second was modified by introducing a quartz wool insert at the base of the electrode to reduce the loss of silver (by convective mass transfer) from the electrode. An unenclosed carbon (graphite) rod was used in the third case, and in the final arrangement this carbon was powdered and allowed to float on the salt.

The results of the tests using these electrode arrangements are given in table 8.1. In general, as the conditions steadied, convective mass transfer (upon which the operation of the cells relied) eventually decreased to a point where the rate of removal of silver from the upper electrode exceeded the rate of transfer of metal to that electrode. The operation of a cell similar to that described in figure 8.24 (part 1) and table 8.1 (cell 1a) is shown in the left hand chart of figure 8.25. The upper electrode temperature was maintained in the range 900°C to 1000°C in this case and the open circuit potential is seen to reach 0.35 volts at one point. After $2\frac{3}{4}$ hours from the commencement of the test, (at point 6 on the chart). the cell circuit was closed through a load of $\frac{1}{2}\Omega$ and the potential fell to 0.12 volts from which the cell resistance can be calculated as approximately 1Ω . After $6\frac{1}{4}$ hours the upper electrode was withdrawn, the glass was broken away and the electrode was sectioned as shown on the right hand side of figure 8.21. Some alloy was found on the base and some corrosion of the sides of the rod was evident notwithstanding the presence of the glass sheath. The recording (of the closed circuit potential) of the trial using the carbon rod (test 3, table 8.1) is also shown in figure 8.25.

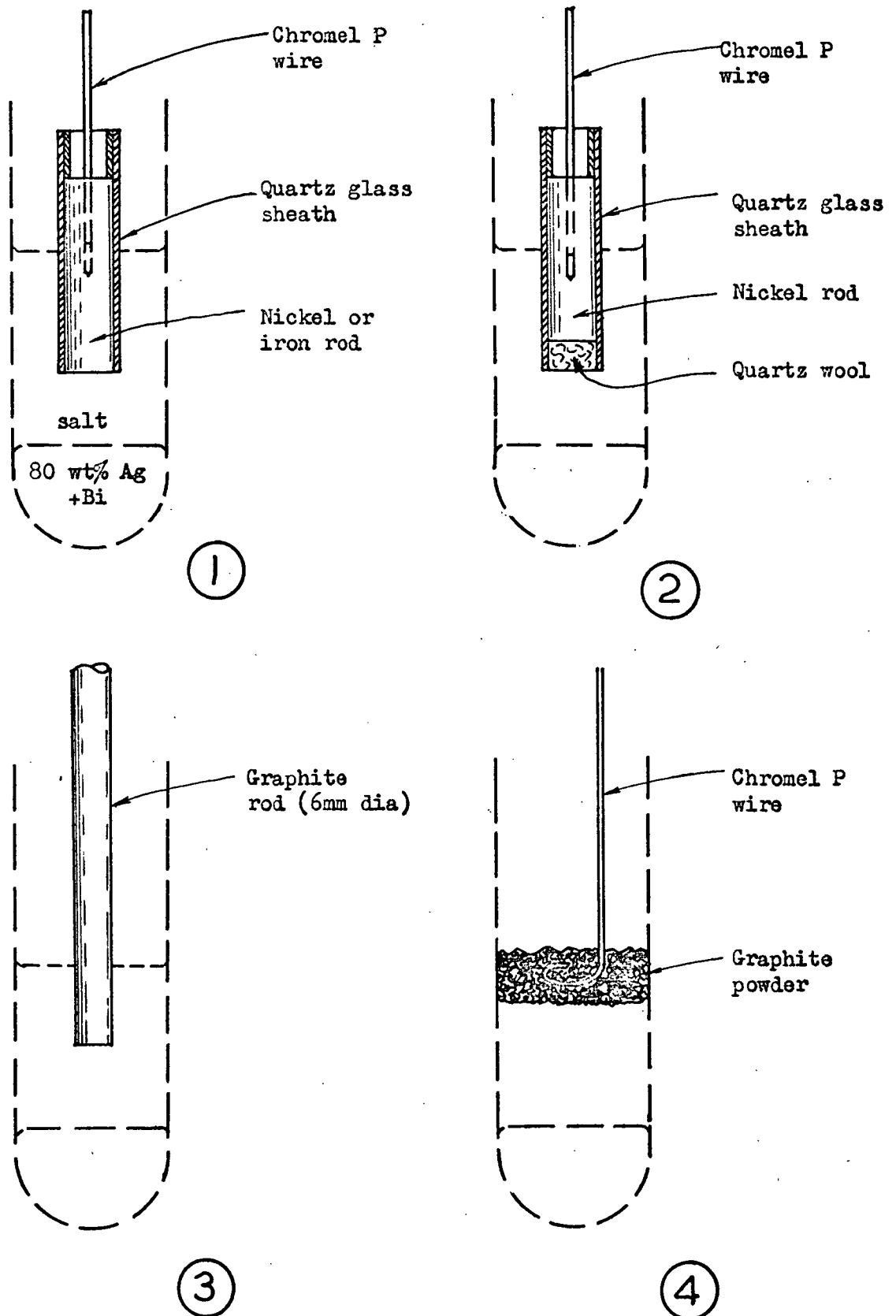


Figure 8.24 Hot upper electrode arrangements.

Upper electrode (Salt mixture)	$V_{oc}(\text{max.})$ (volts)	Load (Ω)	V_{cc} (volts)	t_0 (hours)	Reason for failure
1a Steel in sheath (AgCl + CuCl)	0.28	0.5	0.145	8	No silver on upper electrode. Corrosion of steel
1b Nickel in sheath (AgCl + AgI)	0.25	0.5	0.135	9	No silver on upper electrode. Corrosion of nickel.
2 Nickel in sheath with wool insert (AgCl + AgI)	0.265	1.0	0.140	~1	Corrosion of nickel and contamination of salt around upper electrode.
3 Carbon rod (AgCl AgI)	0.22	1.0	0.105	3.5	No silver on upper electrode.
4 Powdered carbon (AgCl - CuCl)	0.32	2.0	0.210	3.5	No silver around carbon layer.

Table 8.1 Results of tests on thermocells with the upper electrode heated.

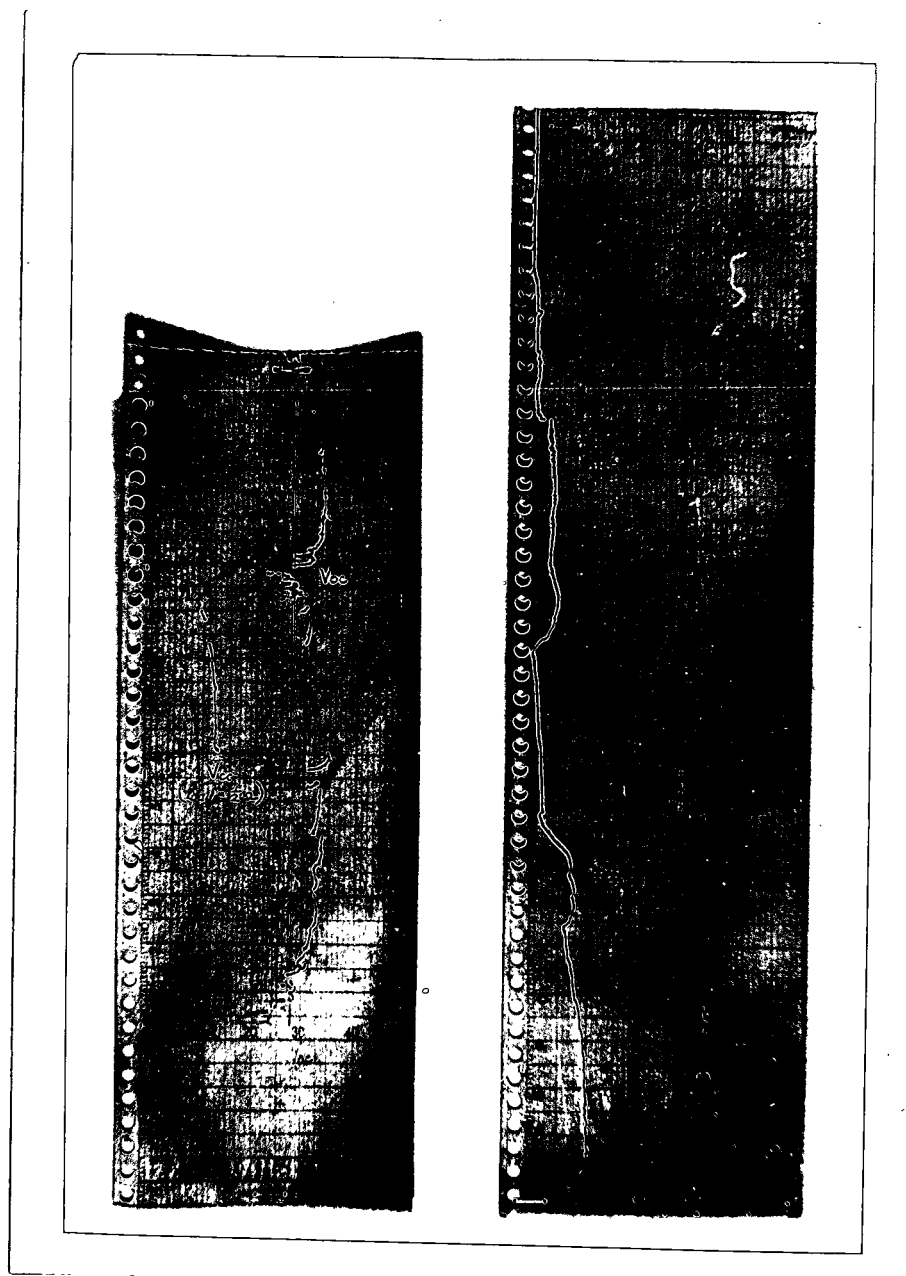
Notes:

electrode numbers refer to figure 8.24.

V_{oc} - open circuit potential.

V_{cc} - potential across cell when connected to the given load.

t_0 - time for V_{cc} to drop to $\frac{1}{2} V_{cc}$ when operating continuously on the given load.



1
Steel in glass sheath
upper electrode.

2
Graphite rod upper
electrode.

Figure 8.25 Terminal voltage recordings of cell tests.
(On 'Goertz Multiscript' recorder)

In general it may be said that heating of the upper electrode in this type of thermocell arrangement can result in generation of electricity but the operation is extremely sensitive to the electrode design and the convective mass transfer within the cell. For continuous generation of electricity this cell is therefore inherently unreliable. (As a laboratory demonstration of thermocell generation of electrical energy from heat energy this cell is excellent. It can be easily constructed from common laboratory equipment, (a silver wire may be used as the upper electrode for the purposes of the demonstration), and the output is sufficient to run a small electric motor. A similar demonstration is illustrated in figure 8.26).

8.3.3. Conclusion.

Looking back over the thermocell configurations studied in this and in previous chapters it appears that a vertical cell arrangement with a hot lower electrode of silver alloy and a cool upper electrode of an inert metal gives the most reliable arrangement for generation of electricity, under certain conditions. These conditions involve chemical stability within the cell and a limiting clearance between the molten metal electrode surface and the upper electrode. In chapter 10 tests of a longer duration are conducted on this type of cell. Meanwhile in the following chapter common anion salt mixtures are studied and found to open the possibility of producing salt mixtures with greater figures of merit than those studied to date.

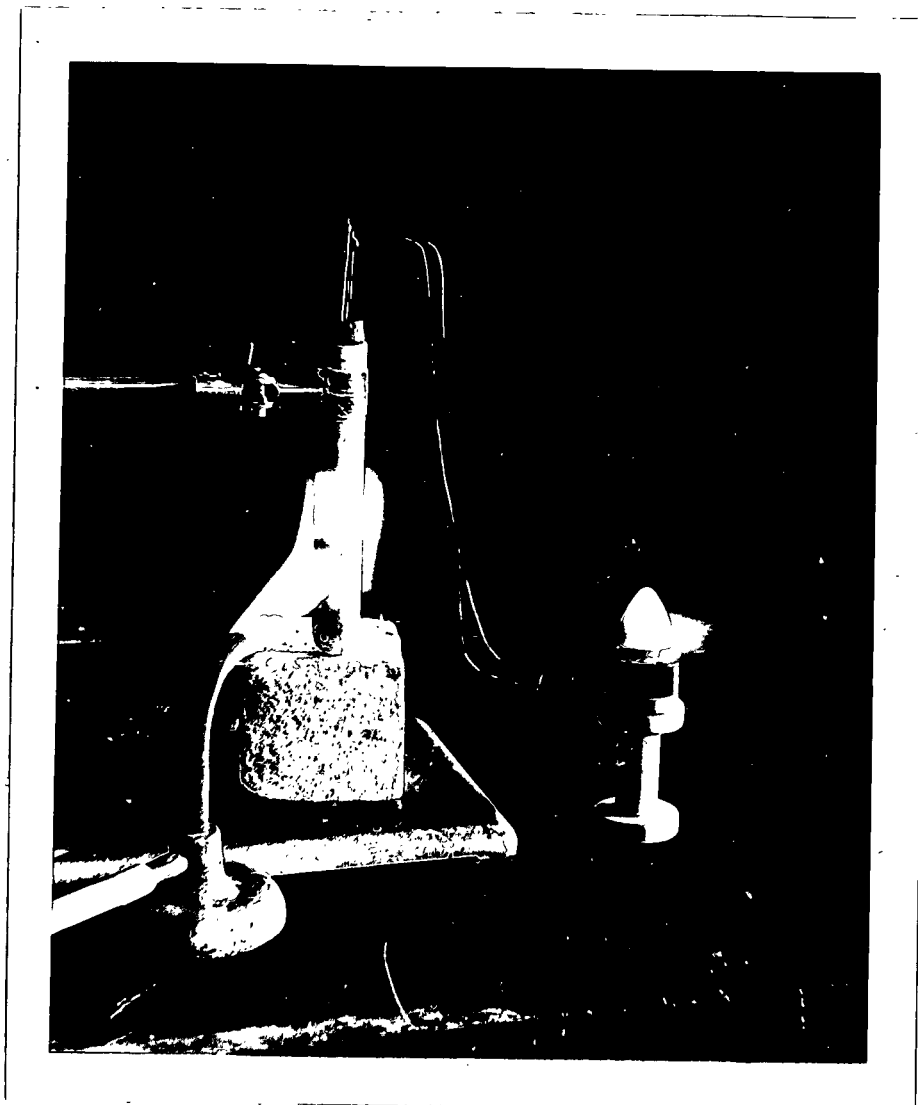


Figure 8.26 Thermocell demonstration.

Chapter 9

Common Anion Salt Mixtures - the
AgCl, CuCl, LiCl system

Contents.

- 9.1. Introduction.
- 9.2. The theoretical thermoelectric potential.
- 9.3. The experimental results.
- 9.4. The Z_3T values.

9.1. Introduction

Common cation salt mixtures were studied in chapter 6 with the object of determining whether the figure of merit of the pure constituents could be increased. The AgCl - AgI eutectic was found to have a figure of merit which was approximately double that of the pure constituents owing mainly to the decrease in thermal conductivity. The thermoelectric potential was about the same magnitude as that of the constituents and this is to be expected in common cation mixtures because it is predominantly the cation which determines the cationic thermoelectric potential. Kvist (1967) has reported thermoelectric data on the AgI - AgBr system and Sinistri and Pezzati (1967) have studied mixtures of silver halides with silver nitrate. In each case the thermoelectric values for the mixtures were found to fall between the values for the pure constituents of the mixture. If higher thermoelectric potentials are to be achieved it is therefore evident that mixtures with different cations must be examined and this chapter is devoted to mixtures with a common anion.

The univalent metal chloride system AgCl + CuCl + LiCl was selected for study as equilibrium diagrams are available in the literature for each pair of constituents and LiCl has a high electrical conductivity. In addition ionic entropy values are available for pure AgCl and CuCl and the theory to the thermoelectric potential developed by the author can be tested for this system. The equilibrium diagrams given in figure 9.1 are reproduced from the work of Sandonnini (1914).

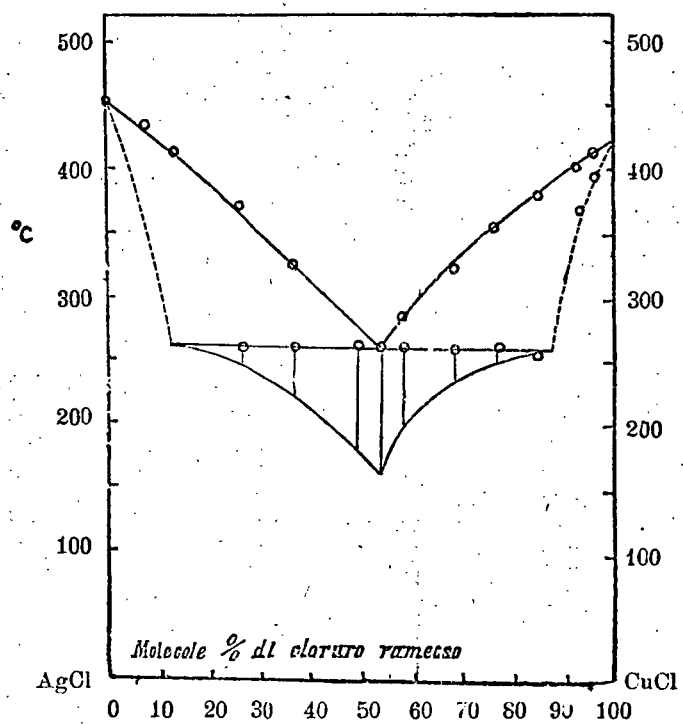
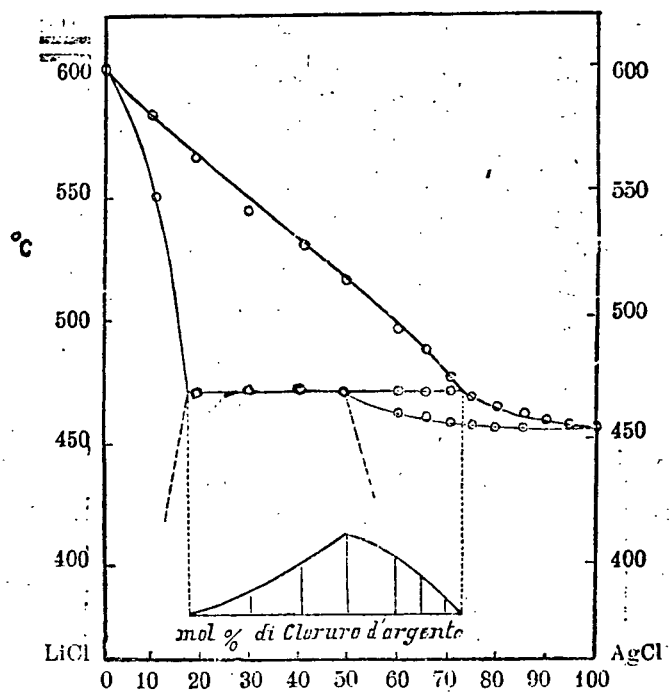


Figure 9.1 Equilibrium diagrams for the LiCl-AgCl and AgCl-CuCl systems from Sandonnini (1914).

9.2. The theoretical thermoelectric potential

In section 4.1. it was shown that the initial thermoelectric potential of a thermocell was composed of a heterogeneous and a homogeneous part; the former arising due to the energy transfer between the electrode and the salt, the latter from the heats of transfer of the ions as they move through the salt:

$$z F \alpha_{\text{het}} = S_M - \bar{S}_{M^{z+}} - z \bar{S}_e$$

$$F \alpha_{\text{hom}} = \sum_{\text{ion}} \frac{t_{\text{ion}}}{z_{\text{ion}}} S_{\text{ion}}^* - S_e^*$$

$$\alpha = \alpha_{\text{het}} + \alpha_{\text{hom}}$$

For a thermocell of the type $M/MCl + NCl/M$ where M and N are univalent metals these expressions lead to the following equation for the initial thermoelectric potential:

$$F \alpha = S_M - \bar{S}_{M^+} + \sum_{\text{ion}} t_{\text{ion}} S_{\text{ion}}^* - \bar{S}_e \quad \text{---(9.1)}$$

The partial molal entropy of an ion in a mixture is given by, (c.f. equation 7.1):

$$\bar{S}_{M^+} = {}^\circ \bar{S}_{M^+} - R \ln x_{M^+} + S_{M^+}^E$$

where ${}^\circ \bar{S}_{M^+}$ is the partial molal entropy of the ion in the pure salt (MCl), x_{M^+} is the molal concentration of the ion of metal M in the melt (note $x_{M^+} = x_{MCl}$) and $S_{M^+}^E$ is the molal excess entropy of the ion of M in the melt. By substituting this expression into equation 9.1 and expanding the summation (remembering that entropies of transfer are positive when transferred down a temperature gradient) the following equation is obtained:

$$F \alpha = S_M - {}^\circ \bar{S}_{M^+} + R \ln x_{M^+} - S_{M^+}^E - t_{N^+} S_{N^+}^* - t_{M^+} S_{M^+}^* + t_{Cl^-} S_{Cl^-}^* - \bar{S}_e \quad \text{---(9.2)}$$

In the case of a pure molten salt thermocell $M/\frac{M}{T_h} \text{MCl}/\frac{M}{T_c}$ the following simplifications may be made:

$$\begin{aligned} x_{M^+} &= x_{MCl} = 1 \\ t_{N^+} &= 0 \\ S_{M^+}^E &= 0 \end{aligned}$$

In addition it was shown in section 4.1. that for the pure salt

$$S_{M^+}^* + S_{Cl^-}^* = S_{MCl}^* = 0 \text{ and } t_{M^+} + t_{Cl^-} = 1 \text{ from which:}$$

$$t_{M^+} S_{M^+}^* - t_{Cl^-} S_{Cl^-}^* = S_{M^+}^* \quad \text{---(9.3)}$$

Thus for a pure salt (denoted by 'o' preceding the function) equation 9.2 becomes :

$$F\alpha = S_M - \bar{S}_{M^+} - S_{M^+}^* - \bar{S}_e \quad \text{---(9.4)}$$

This is effectively the same expression as that derived in equation 4.6, (page 78).

The change in the thermoelectric potential of the thermocell as MCl is added to the MCl may be evaluated by subtracting equation 9.4 from equation 9.2:

$$F(\alpha - \alpha_o) = R \ln x_{M^+} - S_{M^+}^E + S_{M^+}^* - t_{M^+} S_{M^+}^* - t_{N^+} S_{N^+}^* + t_{Cl^-} S_{Cl^-}^* \quad \text{---(9.5)}$$

Algebraic rearrangement of the entropy terms of this equation (using $t_{M^+} + t_{N^+} + t_{Cl^-} = 1$, say) does not lead to any helpful simplification. The term $(\alpha - \alpha_o)$ is seen to depend on the concentration of MCl in the mixture and a number of entropy terms. At low concentrations of MCl , $(\alpha - \alpha_o)$ depends predominantly on $R \ln x_{M^+}$ and this leads to a numerical value of the thermoelectric potential which is considerably higher than that of the pure salt (as is shown experimentally in the following section).

Some simplification of equation 9.5 is possible for the special case when the concentration of MCl in the salt mixture is low, that is when $x_{\text{M}^+} \rightarrow 0$. Under those conditions the salt is almost pure MCl and the following apply:

$$t_{\text{M}^+} \rightarrow 0$$

$$t_{\text{N}^+} \rightarrow {}^{\circ}t_{\text{N}^+} = \text{transference number of } \text{N}^+ \text{ in pure } \text{MCl}$$

$$t_{\text{Cl}^-} \rightarrow {}^{\circ}t_{\text{Cl}^-} = \text{transference number of } \text{Cl}^- \text{ in pure } \text{MCl}$$

$$S_{\text{N}^+}^* \rightarrow {}^{\circ}S_{\text{N}^+}^* = \text{molal entropy of transfer of } \text{N}^+ \text{ in pure } \text{MCl}$$

$$S_{\text{Cl}^-}^* \rightarrow {}^{\circ}S_{\text{Cl}^-}^* = \text{molal entropy of transfer of } \text{Cl}^- \text{ in pure } \text{MCl}$$

For pure MCl a similar expression to that given in equation 9.3 may be derived:

$${}^{\circ}t_{\text{N}^+} S_{\text{N}^+}^* - {}^{\circ}t_{\text{Cl}^-} S_{\text{Cl}^-}^* = {}^{\circ}S_{\text{N}^+}^*$$

Substitution into equation 9.5 then yields:

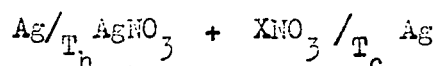
$$F(\alpha - {}^{\circ}\alpha)_{x_{\text{MCl}} \rightarrow 0} = R \ln x_{\text{M}^+} - S_{\text{M}^+}^{\text{E}} + {}^{\circ}S_{\text{M}^+}^* - {}^{\circ}S_{\text{N}^+}^* \quad (9.6)$$

If a graph is constructed of the term $F(\alpha - {}^{\circ}\alpha) - R \ln x_{\text{M}^+}$ against concentration, extrapolation can yield a value at $x_{\text{MCl}} = 0$ which is

is equivalent to $-S_{\text{M}^+}^{\text{E}} + {}^{\circ}S_{\text{M}^+}^* - {}^{\circ}S_{\text{N}^+}^*$. The molal excess entropy

term is usually small in simple halide salt mixtures and therefore, if the molal heat of transfer of the metal ion in its pure salt is known for one of the constituents, it is possible to estimate the same for the other constituent.

Some theoretical and experimental work on the thermoelectric potential of molten nitrate mixtures has been reported by Sinistri (1966) for cells of the type:



His theoretical expressions are derived using transference numbers of the metal ion relative to the nitrate ion rather than to the electrode or container. This may be satisfactory for the case of molten nitrates where most of the current is carried by the metal ions but in other systems a large proportion of the current is carried by the anion and this proportion may depend upon the composition. In the general case it is therefore necessary to take into account the transfer of current by the anion. But equation 9.6 is independent of transference numbers and a similar equation is derived by Sinistri, (but in a slightly different form). Markov (1956) and Kvist (1967) report experimental values on the thermoelectric potential of molten salt mixtures and their results are included in figure 9.5.

Finally a rather interesting situation occurs when the thermoelectric potential of a certain mixture of MCl and NCl is measured, firstly between electrodes of metal M and then between electrodes of metal N. The increase in thermoelectric potential of the mixture above that of MCl when measured between electrodes of M is given by equation 9.5. Analogously the increase in thermoelectric potential of the same mixture above that of NCl when measured between electrodes of N is:

$$F(\alpha-\alpha)_N = R \ln x_{N^+} - S_{N^+}^E + {}^\circ S_{N^+}^* - t_{N^+} S_{N^+}^* - t_{M^+} S_{M^+}^* + t_{\alpha^-} S_{\alpha^-}^* \quad (9.7)$$

Subtraction of equation 9.7 from equation 9.5, bearing in mind that

$$x_{N^+} = 1 - x_{M^+} \quad , \text{ yields:}$$

$$F(\alpha-\alpha)_M - F(\alpha-\alpha)_N = R \ln \left(\frac{x_{M^+}}{1 - x_{M^+}} \right) + ({}^\circ S_{M^+}^* - {}^\circ S_{N^+}^*) - (S_{M^+}^E - S_{N^+}^E) \quad (9.8)$$

Since the excess entropy terms are generally small for simple mixtures and the other terms are experimentally measurable the term $({}^\circ S_{M^+}^* - {}^\circ S_{N^+}^*)$ may be estimated. This method of estimating the entropy of transfer term is preferable to the previous method as it only requires measurements at one salt mixture composition and does not need a graphical extrapolation to zero concentration for one of the constituents.

9.3. The experimental results.

A pyrex glass cell was set up as arranged in figure 4.2d (page 83). As in the previous cells the temperatures were measured using 'Thermocoax' stainless steel sheathed Chromel-Alumel thermocouples and voltages were recorded using a Philips PR 3210 automatic potentiometric recorder. Figure 9.2 shows the cell and heater partially assembled.

A typical experiment involved heating up the cell as early as possible in the morning and adding (evenly to each side) the dried and preweighed quantities of constituents. Once the salt had melted the voltage and temperature probes were added and the nitrogen flow (to prevent oxidation at the salt surface) was started. A suitable temperature was then selected for one of the legs of the cell and it was maintained at approximately this temperature throughout the test. The temperature of the other leg was varied both above and below this temperature and readings of the temperatures and the terminal voltage were taken during the heating and cooling process. A typical graph of voltage versus the temperature difference is shown in figure 9.3. The curve was always linear but did not generally pass accurately through the origin owing to errors in temperature measurement and small composition differences between the mixtures in the cell legs. As this section is only concerned with the slope of the characteristic, (i.e. dE/dT), this error at the origin was ignored unless it exceeded a few millivolts, when the test was repeated.

The results for metal halide mixtures are represented graphically in figures 9.4 and 9.5 and the data of Markov (1956) and Kvist (1967) are also shown in figure 9.5. Each point represents the slope of a potential — temperature difference curve (similar to that shown in figure 9.3) in the temperature range of 300°C to 600°C. The tolerance limits were determined by the maximum and minimum slope which could reasonably be drawn through the points on the potential — temperature difference curve.

The results may be compared qualitatively with equation 9.5. It was suggested that, at low concentrations of MCl in the mixture (i.e. $x_{M^+} \rightarrow 0$), the term $R \ln x_{M^+}$ was predominant. As this term has a negative value the expression $F(\alpha - \alpha')$ must also be negative and in particular (at low concentrations of MCl) the thermoelectric power of the mixture, α , may be expected to decrease as the concentration of MCl decreases. This was confirmed experimentally in the case of the AgCl - CuCl mixture between

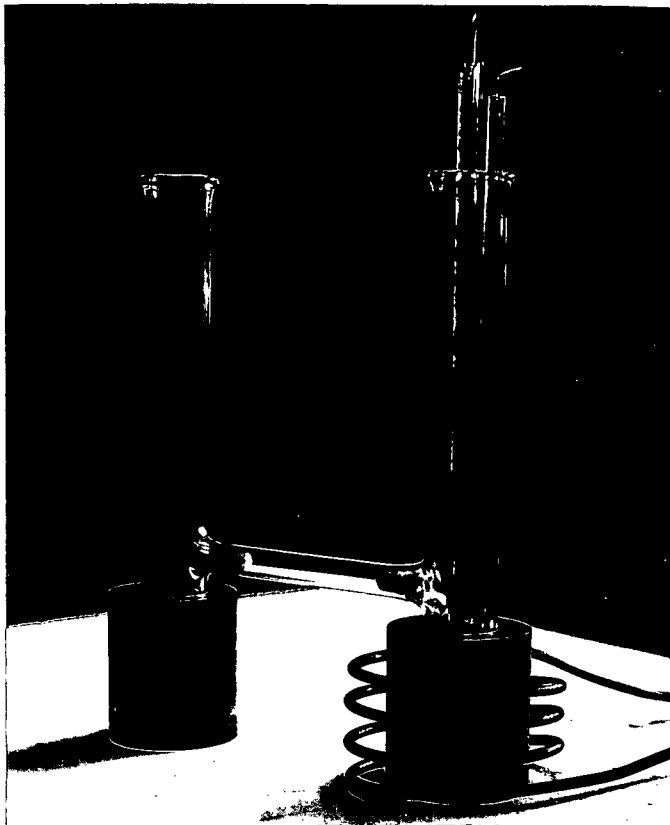


Figure 9.2 The H-cell and heater during assembly.

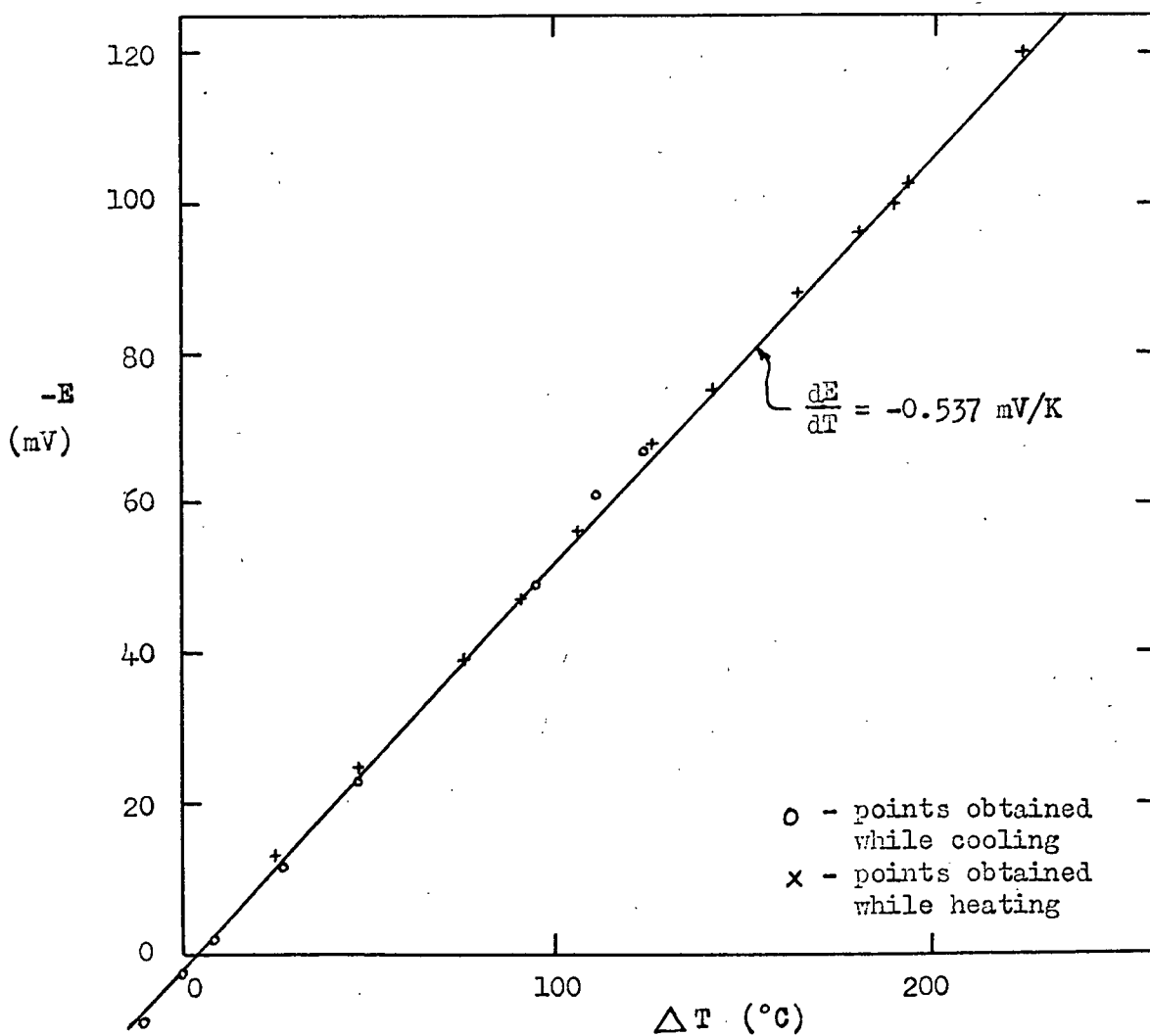


Figure 9.3 The $E - \Delta T$ plot for the mixture of 40mole % AgCl-60mole % CuCl.

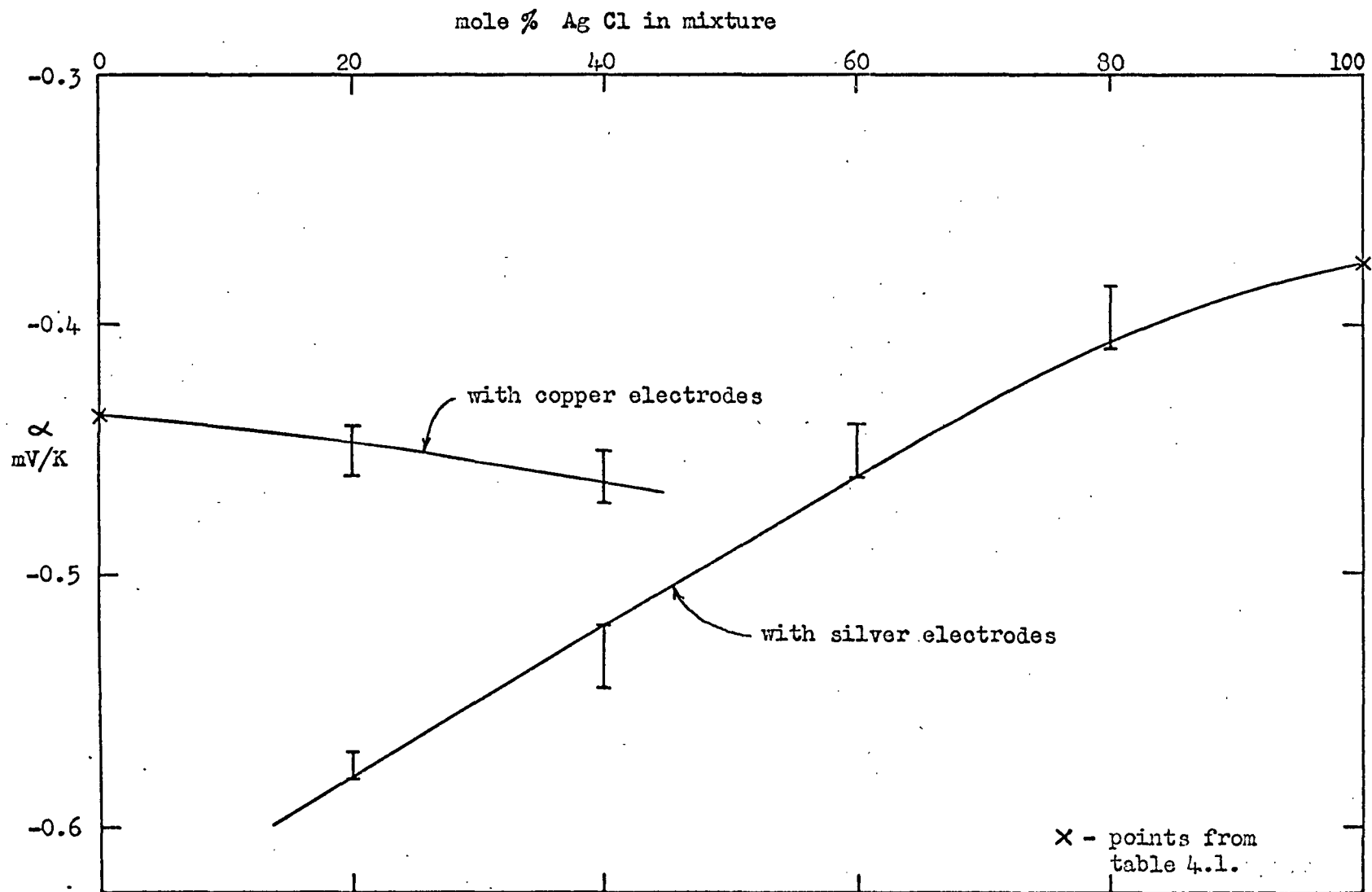


Figure 94 The thermoelectric potential of the AgCl - CuCl molten salt mixture.

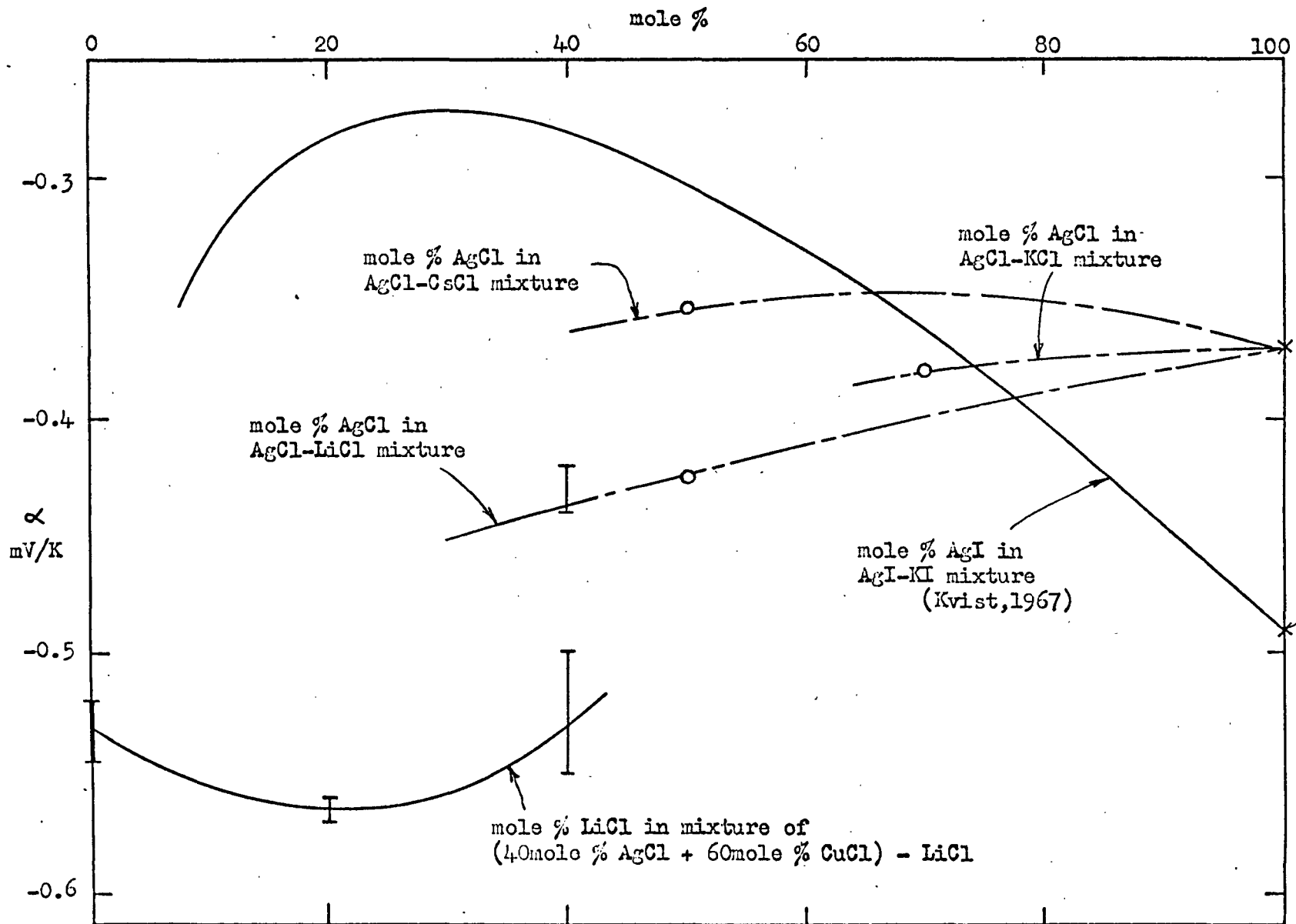


Figure 9.5 The thermoelectric potential of various halide salt mixtures between silver electrodes

x - points from table 4.1

o - data from Markov (1956)

silver electrodes (figure 9.4) and was also found to be the case for the AgI - KI mixture between silver electrodes (figure 9.5). At higher concentrations of MCl in the mixture the term $R \ln x_M$ is of a similar order to the entropy terms (of equation 9.5) and α may increase or decrease depending on the exact value of these terms.

This is a very favourable situation as far as the application of these salt mixtures to thermocell generation is concerned. The numerical value of the thermoelectric potential of the cell $Ag/\frac{1}{2}AgCl/\frac{1}{2}Ag$ for example is increased by 53% when 80 mole % (73.4 weight %) of cuprous chloride is added to the silver chloride. Since the figure of merit of the salt mixture is dependent upon the square of the thermoelectric potential this gives an effective increase in the figure of merit of 134%. This of course does not take into account the changes in the electrical conductivity, the thermal conductivity and the temperature range over which the mixture can be used. A more detailed study of this aspect is given in the next section, (9.4).

Returning to the thermoelectric potential theory of these mixtures, two methods of estimating the term $(^{\circ}S_{M^+}^* - ^{\circ}S_{N^+}^*)$ from experimental data were outlined in section 9.2, and the latter method using equation 9.8 was shown to be preferable. From figure 9.4 it can be seen that for mixtures of 20 mole % AgCl with 80 mole % CuCl, and 40 mole % AgCl with 60 mole % CuCl, the thermoelectric potential has been measured between both silver and copper electrodes. Hence at these compositions equation 9.8 may be applied in the following form (neglecting the small excess entropy terms):

$$F(\alpha - \alpha)_{Ag} - F(\alpha - \alpha)_{Cu} = R \ln \left(\frac{x_{Ag^+}}{1 - x_{Ag^+}} \right) + (^{\circ}S_{Ag^+}^* - ^{\circ}S_{Cu^+}^*) \quad (9.9)$$

The term α for silver is the cationic thermoelectric potential of pure AgCl (-0.375 mV/K), α for copper is the cationic thermoelectric potential of CuCl (-0.456 mV/K), and x_{Ag^+} is equal to the molal concentration of AgCl in the melt. The experimental values of the terms of equation 9.9 in units of $J \text{ g-mole}^{-1} \text{ K}^{-1}$ are given in the following table:

x_{AgCl} (mole %)	$F(\alpha - \alpha)_{Ag}$ (a)	$F(\alpha - \alpha)_{Cu}$ (b)	$R \ln\left(\frac{x_{Ag^+}}{1 - x_{Ag^+}}\right)$ (c)	$(^{\circ}S_{Ag^+}^* - ^{\circ}S_{Cu^+}^*)$ (from a-b-c)
20	-19.3 ± 0.5	-1.4 ± 1.0	-11.50	-6.4 ± 1.5
40	-15.2 ± 1.3	-2.6 ± 1.0	-3.37	-9.2 ± 2.3

This method can only yield differences in values of the entropy of transfer of ions in their pure salts. In order to find the absolute values at least one salt must be studied using a different method and an absolute value determined for that salt. This is not possible experimentally but Pitzer(1961) has studied the structure and the entropies of vibration and free rotation and has estimated the value of $^{\circ}S_{Ag^+}^*$ as about $17 \text{ J gm-mole}^{-1} \text{ K}^{-1}$ at 800°K in pure silver chloride. By subtraction $^{\circ}S_{Cu^+}^*$ is therefore about $24 \text{ J gm-mole}^{-1} \text{ K}^{-1}$ assuming the excess entropy terms are small. It was shown in section 4.1. that the cationic thermoelectric potential of a pure salt is given by the following expression (neglecting the electron entropy term):

$$zF\alpha = S_M - \bar{S}_{M^+} - S_{M^+}^*$$

For the case of CuCl at 500°C for example α is given in table 4.1, S_M may be calculated from thermodynamic data for copper and, now that the value of the entropy of transfer is known, \bar{S}_{M^+} may be approximately determined:

For CuCl :

$$zF\alpha = -4.2 \text{ J gm-mole}^{-1} \text{ K}^{-1}$$

$$S_M = 58 \quad "$$

$$S_{M^+}^* = 24 \quad "$$

$$\bar{S}_{M^+} = 76 \quad "$$

No more satisfactory method of finding these ionic entropy terms for molten salts is recorded in the literature.

9.4 The $Z_s T$ values.

Although the thermoelectric potential is the most important property determining the figure of merit, the effect of mixing on the other properties must be taken into account. The thermal conductivity may be expected to be rather less than the proportional mean of the constituents (as was discussed in section 3.1.2.) and the electrical conductivity (at 1000°K) will to a first approximation be the same as the proportional mean of the constituents, (at the same temperature). In the following table the thermoelectric properties and the $Z_s T$ values are estimated for the salt mixtures studied in the previous section. Some indication of the temperature range over which these salt mixtures could be used is shown by giving the melting point or liquidus temperature of the salt mixture T_1 and the lowest boiling point T_g of the constituents.

Salt (Ag electrodes)	$-\alpha$ (mV/K)	K (watts cm ⁻¹ K ⁻¹)	σ (Ω^{-1} cm ⁻¹)	$Z_s T (= \frac{\alpha^2 \sigma T}{K})$ (at 1000°K)	T_1 (°C)	T_g (°C)
Pure AgCl	0.375	3.6	4.6	0.18	455	1557
40 mole% AgCl } 60 mole% LiCl }	0.430	4.1	5.6	0.25	530	1382
40 mole% Ag Cl } 60 mole% CuCl }	0.533	3.4	4.3	0.36	290	1367
32 mole% AgCl } 48 mole% CuCl } 20 mole% LiCl }	0.565	3.6	4.7	0.42	~ 300	1367

Examination of the theory to the thermoelectric potential of common anion salt mixtures shows that the salt mixtures studied in this chapter are not the most suitable for thermocell generation. It would be more profitable in the first place to select a solvent salt mixture of low thermal conductivity and high electrical conductivity and to add to this a few mole % of a solute consisting of a salt of the metal of the electrode. For example a mixture of 71 mole % LiCl and 29 mole % LiF melts

at 485°C (Janz 1967) and values of σ and k for this mixture may be estimated as $7 \Omega^{-1} \text{ cm}^{-1}$ (at 1000°K) and $6.4 \text{ watts cm}^{-1} \text{ K}^{-1}$ respectively. When the mixture contains a few mole % of CuCl the thermoelectric potential between copper electrodes may be estimated from the theory given in this chapter as 0.75 mV/K. These values yield a $Z_s T$ value (at 1000°K) of 0.62, and for operation between the salt melting point and the melting point of copper, (with $Z_c = 0.8Z_s$), a conversion efficiency of 7% is obtained. While this is still low compared to dynamic methods of converting heat energy to electrical energy it compares favourably with solid - state thermoelectric materials. The maximum power output per unit area (of this particular salt) would be 3 kW/m^2 (0.3 watts/cm²).

Chapter 10

Trials of a Continuously Operating Thermocell and Conclusions on the Future Prospects for Thermocell Generation

Contents:

- 10.1. Tests on a continuously operating vertical tube thermocell.
- 10.2. Test of a small generator.
- 10.3. The prospects for thermocell generation.
 - 10.3.1. The possibilities.
 - 10.3.2. Proposals for future work.
 - 10.3.3. Applications.
- 10.4. Conclusion.

10.1. Tests on a continuously operating vertical tube thermocell.

In the conclusion to chapter 8 it was pointed out that a vertical tube thermocell configuration with the lower electrode heated gave the most satisfactory arrangement for generation of electricity at the present stage of development. In order to determine the reliability of this arrangement a cell was set up as shown in figure 10.1 (in an experimental rig similar to that illustrated in figures 8.22 and 8.23, pages 154 & 155, but with the heating coil and forced air flow interchanged).

The alloy reservoir consisted of 8gm of silver and 4gm of bismuth, (~ 80 mole % Ag), and the salt was the AgCl - AgI eutectic mixture containing a quantity of quartz wool to limit natural convection. It was obviously advantageous to select metals for the wires to the electrodes with thermoelectric potentials which would increase the cell voltage. Chromel P (10% Cr + Ni) wire was used between room temperature and the upper electrode at about 300°C and pure nickel was initially used between room temperature and the lower electrode at about 850°C . Nickel wire was found to dissolve in the silver - bismuth alloy at this temperature and so tungsten wire was used to connect the nickel to the alloy as shown in figure 10.1. The gain in the open circuit potential of the cell owing to the use of these metal wires at the quoted electrode temperatures was 0.01 volts.

When steady conditions had been attained the thermocell was found to have an open circuit potential of 0.24 volts which dropped to 0.16 volts when a load of $2\ \Omega$ was connected across the terminals. It was allowed to generate on this load overnight and the voltage remained constant for $22\frac{1}{2}$ hours after which it dropped to a low value. Investigation showed that during the early hours of the morning the ambient temperature, (and hence the cooling air flow), had dropped sufficiently for the salt to become solid around the upper electrode. The test was repeated with higher upper and lower electrode temperatures and the cell operated successfully on a load of $1\ \Omega$ and a closed circuit potential of 0.13 to 0.16 volts for 2 days. The cell was then open circuited and the heating of the lower electrode was gradually increased in an attempt to increase the cell voltage. After 56 hours (from the commencement of the test) the heater wire broke and the trial was terminated. At a period during this test the upper cool electrode temperature was intentionally decreased and

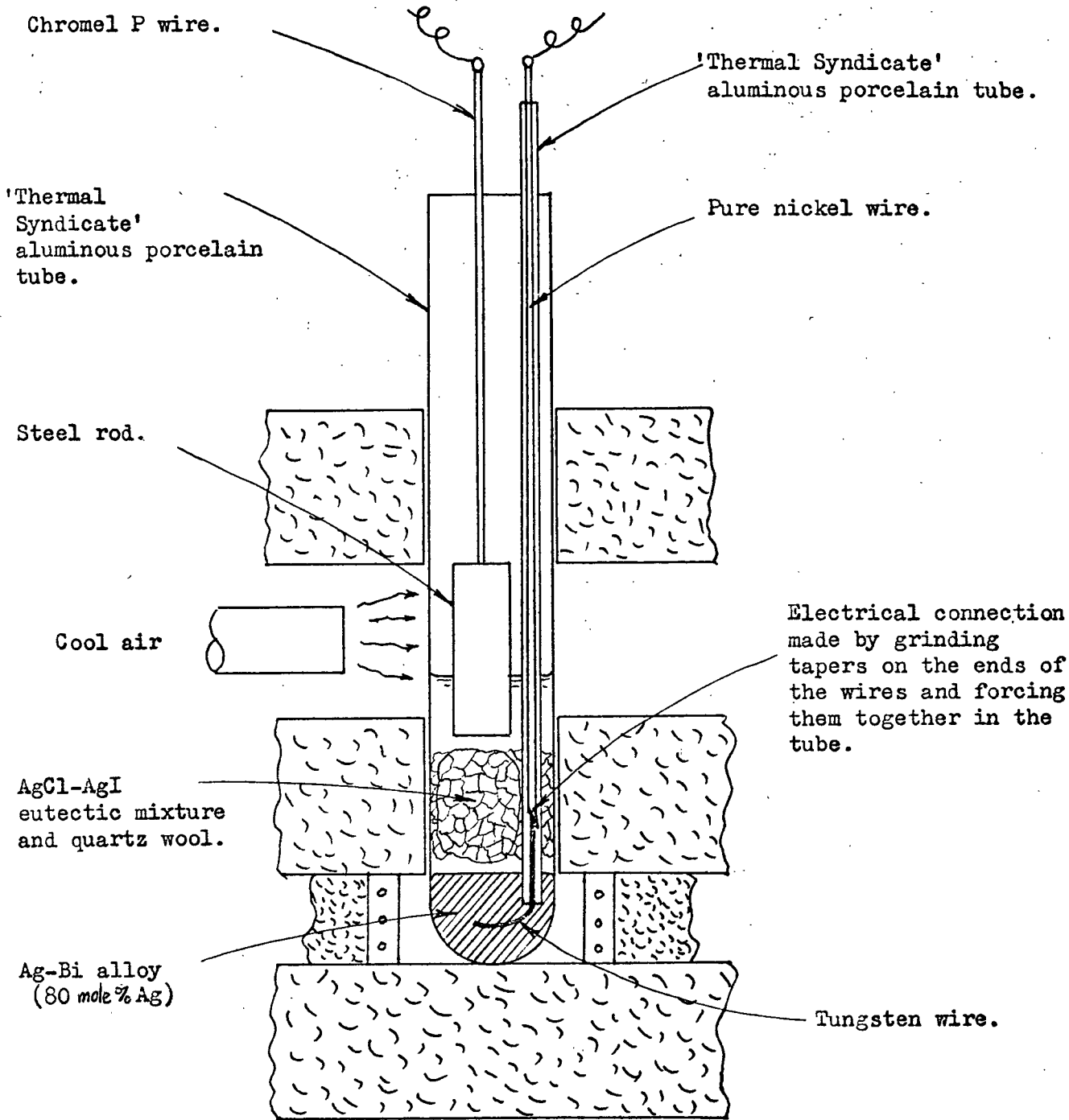


Figure 10.1 Generation thermocell.

it was found that the terminal voltage on load fluctuated between the previous steady value and a low value as shown on the chart in figure 10.2. This effect may have been due to solid salt, (with a much lower electrical conductivity than the molten salt), forming and later remelting on the upper electrode. The fluctuation ceased completely when the upper electrode temperature was slightly increased.

After this test the cell was broken open and the majority of alloy was found to have collected around the upper electrode in an unhomogeneous mass of metal and salt. (A similar cell, with a Chromel P wire upper electrode, is shown after operation in figure 10.2). A piece of the silver - bismuth alloy at the upper electrode was analysed by melting it down in a small crucible, obtaining a cooling curve and determining its composition from the liquidus temperature. The alloy was found to contain 78 mole % Ag and a similar procedure conducted on a piece of alloy from the lower electrode yielded 92% of silver. (This difference in alloy composition may be explained by noting that, at the upper electrode temperature, the alloy consisted of two phases; a liquid silver - bismuth eutectic and a silver rich solid. The effect of gravity and convective mass transfer may be expected to transfer the solid phase to the lower part of the cell more easily than the liquid phase).

10.2. Test of a small generator.

In order to conclude this stage in the development of thermocell generation of electricity a small generator consisting of a number of cells was manufactured. Basically the generator consisted of a matrix of vertical tube thermocells connected electrically in series and thermally in parallel. The bottoms of the tubes were heated by gas and forced air combustion and the upper electrode was cooled by forced air. No attempt was made to design for maximum conversion efficiency and only a fraction of the total combustion heat actually passed through the cells. In addition the current, (and hence the power output), produced was low as the electrode areas were small. The object was rather to produce a maximum voltage per cell and to show that a laboratory thermocell generator may be cheaply and easily made from commonly available components. The details of the generator design and the test arrangement are shown in figures 10.3 to 10.6.

Chart direction



Chart speed
20 mm/hour

Scale :
0 - 0.5 volts

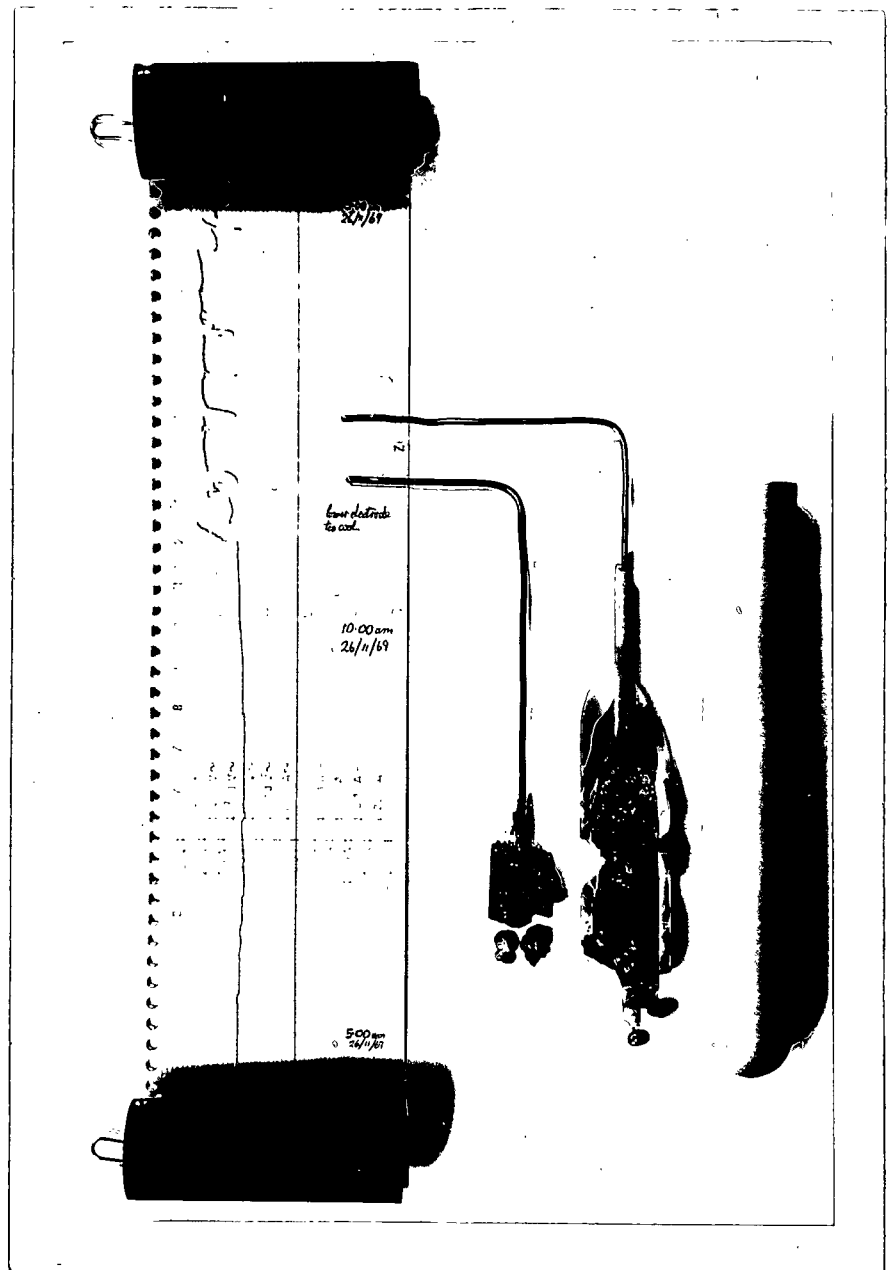


Figure 10.2 Part of the recording of the closed circuit voltage across the cell during the 56 hour test, and the contents of a similar cell after operation.

62 cells arranged in a matrix of
8 x 8 (with two vacancies for test
cells containing thermocouples).

WIDTH of generator 0.356m overall.

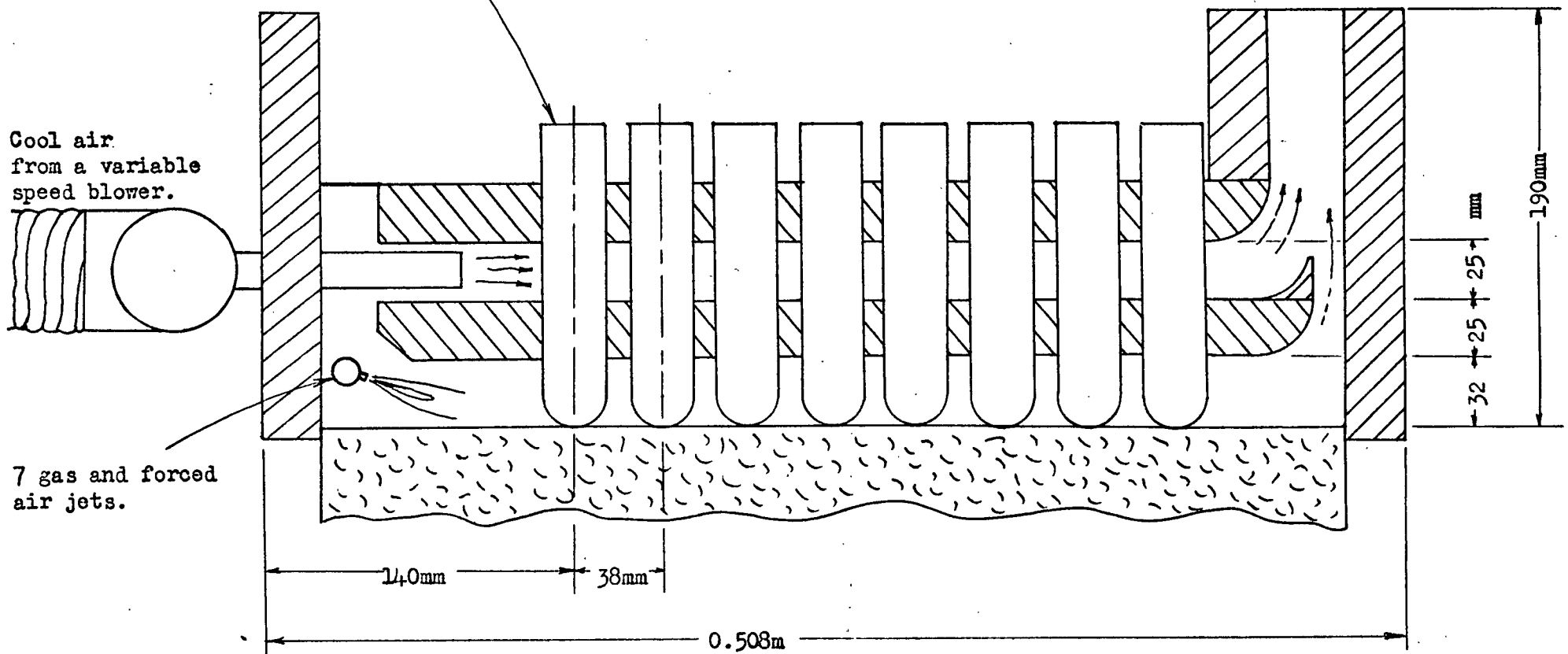


Figure 10.3 Section through the multi-cell generator.

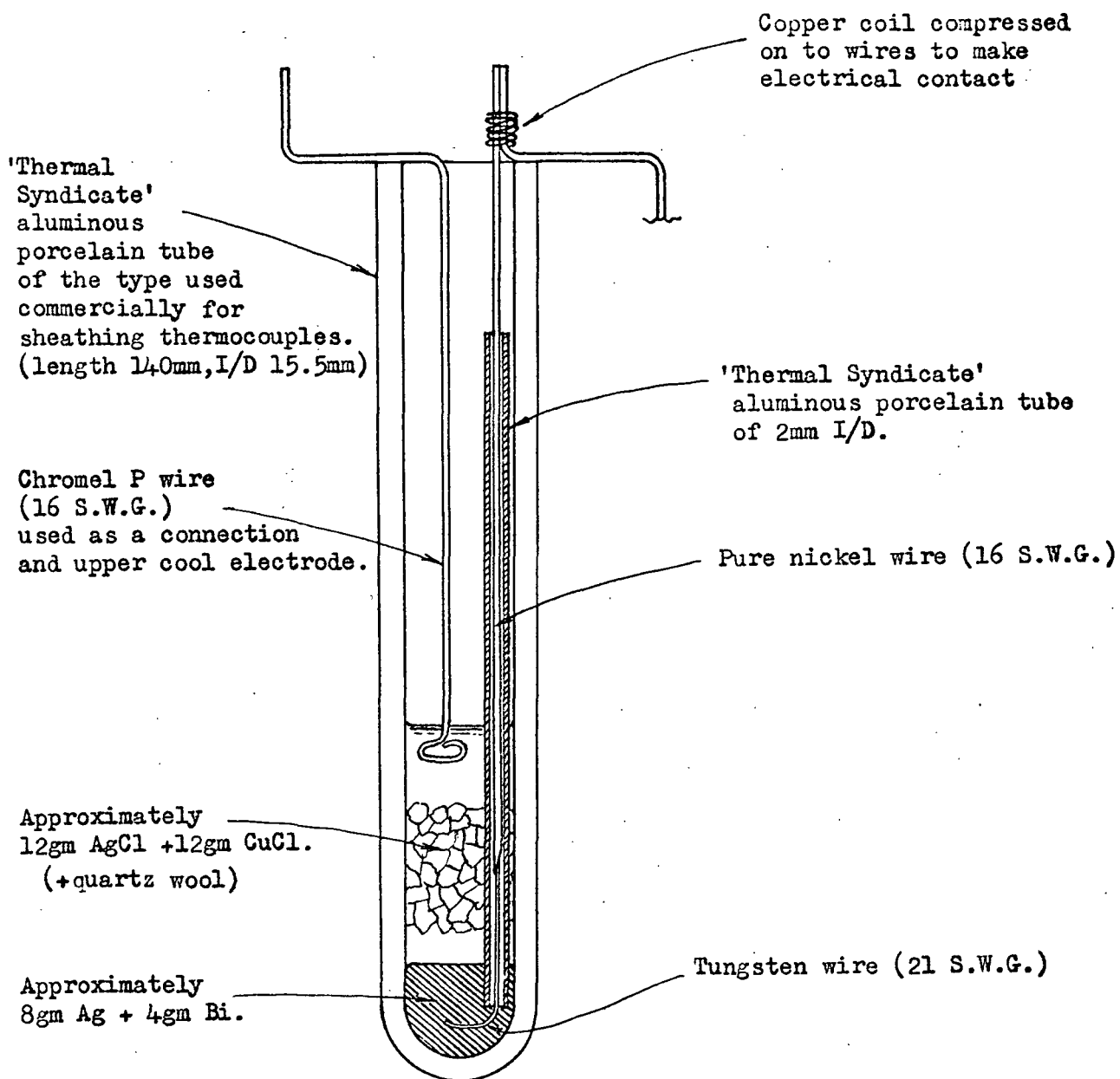


Figure 10.4 A thermocell used in the generator shown in fig.10.3.

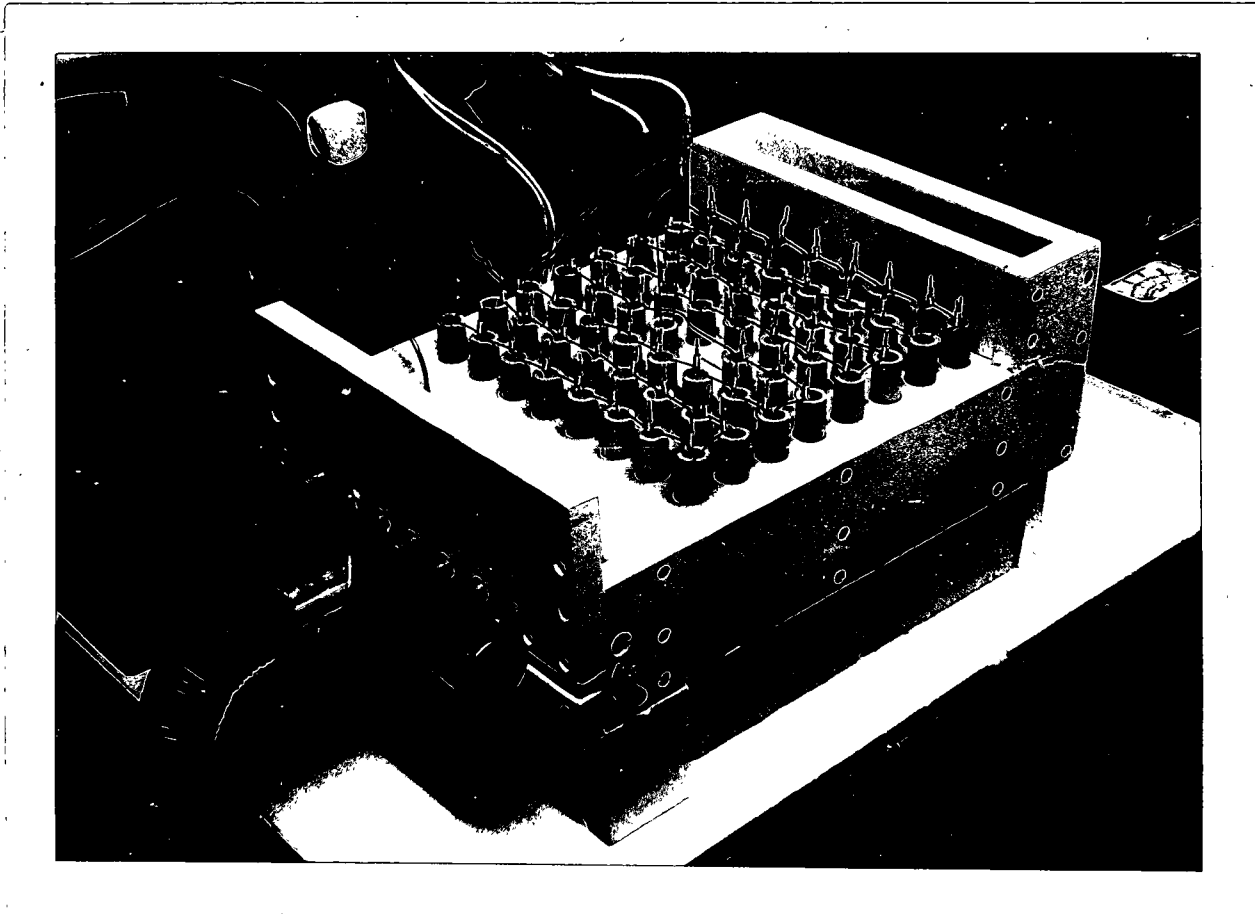
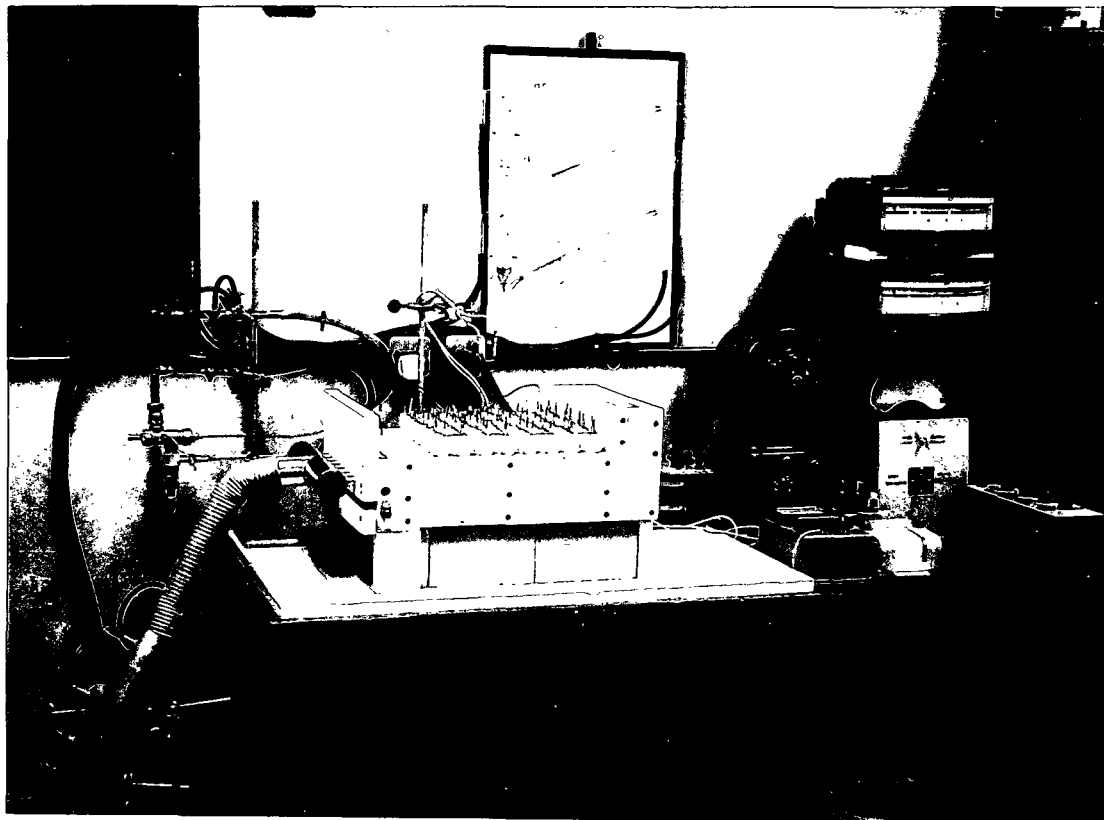


Figure 10.5 The thermocell generator.

Gas and air flow
manometers
(Energy supplied
about 1 kW)



Gas and forced
air supply

Air tube from
blower.

Temperature indicators

Blower control

Recorder for output
voltage, and load resistance

Figure 10.6 General view of generator ready for trial.

The salt mixture used in the cells was an equal weight mixture of AgCl and CuCl (41 mole % AgCl). This is considerably cheaper than the AgCl - AgI eutectic mixture and has a high thermoelectric potential, (-0.53 mV/K). A typical temperature distribution across the generator as measured at the internal base of each cell by a thermocouple probe was as follows, (in °C):

<u>Front</u>							<u>Back</u>
1000	----	----	740	----	----	----	505
1000	----	----	750	----	----	----	520
1010	----	----	755	----	----	----	525
1020	----	----	(760)*	----	----	----	530
1030	965	860	(---)*	705	645	600	545
1050	----	----	775	----	----	----	565
1070	----	----	785	----	----	----	570
1030	----	----	770	----	----	----	545

* cell not used for generation

The upper electrode temperature varied from 300°C at the front to about 270°C at the back. Hence the voltage per cell obtained from a cell situated in the middle of the second row (from the front) would be about $0.53 \times 10^{-3} \times (965 - 300)$ volts plus 0.01 volts for the metal wires yielding a total of 0.36 volts. A similar cell in the seventh row would produce 0.18 volts.

The test procedure involved filling the cells with the pre - weighed constituents in powder form, firing the gas and air burner and allowing the constituents to melt. The upper electrode wire could then be inserted and electrically connected to the next cell by pinching the copper coil (shown in figure 104) around the wires. In practice an unforeseen difficulty was found which prevented all the cells being filled. At the front of the generator, where the temperature was very high, the salt mixture melted quickly; but at the rear melting was much slower, and the solid salt powder was found to bake into a hard cake about half way up the cell. This cake could not generally be forced down the cell to the

high temperature region and it prevented further salt being added. Although 18 of the cells, (mainly situated in the 7th and 8th rows), were inoperative owing to this effect the reduction in the generator voltage was not as great as this number would imply because these cells, being at the cooler end of the generator, were only expected to yield a small voltage per cell.

The results of this test are shown in the following table:

no. of cells	V_{oc}		$V_{oc}/cell$	I_{sc}	Duration of test	Power	
	max.	mean	max.	max		total	per cell
22	7.6	6.5	0.355	0.78	5	1.48	67
44	13.2	13.0	0.30	0.615	2	2.03	46
	(volts)	(volts)	(volts)	(amps)	(hours)	(watts)	(mW/cell)

In the case of the test with 22 cells, (situated at the front of the generator), the mean open circuit potential over the period of the test, (column 3 in the table), was rather less than the maximum potential owing to experimentation with the burner during the test. The open circuit potential per cell compared favourably with the expected value of about 0.36 volts. When 44 cells were used the potential per cell dropped as the mean hot electrode temperature had decreased. The generator was restarted on two subsequent occasions and the potential was allowed to reach 5 volts before the heater was turned off. The final examination showed that one of the cells in the 4th row had fractured.

10.3. The prospects for thermocell generation.

10.3.1. The possibilities.

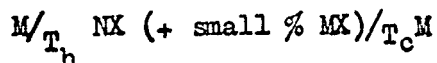
The molten salts used in this work have been silver halides or mixtures involving silver halides. It has been indicated in section 4.4 and 9.4 that certain alkali halides and common anion salt mixtures may have thermoelectric potentials in the order of 1 mV/K. With an electrical conductivity of about $5 \Omega^{-1} \text{cm}^{-1}$ and a thermal conductivity of 4×10^{-3} watts $\text{cm}^{-1} \text{K}^{-1}$ the $Z_S T$ value (at 1000°K) would be about 1.25. Operating between temperatures of 1000°C and 300°C this would yield a theoretical conversion efficiency (at $Z_C = 0.8 Z_S$) of 11%. It would therefore appear to be unlikely that after further development a thermocell generator will have a practical conversion efficiency in excess of 10%.

The power per unit electrode area of the above salt operating between the same temperatures and with an electrode spacing of 10 mm would be 0.625 watts/ cm^2 ($6\frac{1}{4}$ kW/ m^2). If the salt was predominantly a mixture of reasonably common alkali halides and the electrodes were of copper (rather than silver), the capital cost of a 10 - 100 kW generator would be in the order of £10 sterling per kW.

10.3.2. Proposals for future work.

Suggestions for future work have been made in appropriate places in the previous chapters. There are three main areas in which future work on thermocell generation must concentrate:

- 1) The cationic thermoelectric potential of alkali halides and their mixtures. (No values have been reported in the literature to date).
- 2) The cationic thermoelectric potential of common anion mixtures in cells of the type:



where M and N are metals and X is a halide, (see chapter 9).

- 3) Engineering development of cell containers which will allow the contents to be thermally recycled from below to above the melting point of the contents without cracking, for many hundreds of times.

It is worthy of note that each of these proposals may be studied experimentally without requiring specialised or expensive research equipment,

and would therefore provide admirable research topics for those employed in colleges of technology or other establishments where research is not the primary function.

It is unlikely that thermocell generation will ever be suitable for large scale power generation. A similar conclusion was reached for semiconductor thermoelectric power generation by Spring and Swift-Hook in 1962. It is also unlikely that thermocell generation will find application in the space exploration field owing to the part played by the force of gravity in the cell operation. But there is an area of application which may become of importance during the next few decades.

In July 1969 a contract was signed between John Player and Sons Ltd. and the East Midland Gas Board for the Board to supply the entire fuel and power needs for a new £6 million factory, (Anon, 1969). This 'total energy' scheme involved the use of eight gas turbine generator sets to meet the electrical power requirements of the factory. Gas turbines are notably inefficient but this was not important in this case as the heat energy rejected by the turbines was used to heat steam boilers for space heating. As 'North Sea Gas' becomes more widely available it is likely that an increasing number of industrial concerns may find it economical to utilise 'total energy' schemes. The capital cost of providing gas turbine generating sets for the electrical power and lighting requirements is high and this effectively limits the scheme to large firms. If a reasonably cheap (but low efficiency) device converting heat energy directly into electrical energy could be developed this could cause the 'total energy' scheme to become economical for smaller factories and even office blocks where the conversion device need only supply the lighting load.

10.4 Conclusion

The major achievement of this work has been to show that it is possible to generate electrical energy from heat energy using the thermoelectric effect of the flow of ions in a material. This method of generating electricity could find application in situations where the thermal efficiency is not the most important factor. Among minor achievements may be included the first complete review of the thermal conductivity and thermoelectric potential measurements made on molten salts, the measurements of these properties for certain halide salts and further development of the transient hot-wire thermal conductivity measurement technique. In addition, theory to the thermoelectric potential of thermocells with metal alloy electrodes and thermocells containing mixtures of ionic molten salts has been developed, and partially substantiated by experiment.

It has become evident that the techniques involved in thermoelectric generation using molten salts are very different from those used in solid-state electronic thermoelectric generation. In the former case the thermoelectric effect is predominantly dependent upon the electrodes and the main problems are concerned with these electrodes and the mass transfer between them. In the latter case the thermoelectric potential is dependent on the material itself and some of the problems are concerned with the brittleness and cost of the semiconductor material required. During this work the term 'thermocell generation' has sometimes been used as an abbreviation of 'thermoelectric generation using molten salts'. It is here suggested formally that, in future, generation of electrical energy from heat energy using the thermoelectric effect of the passage of ions in a material (solid or liquid) be termed 'thermocell generation' to distinguish it from solid-state thermoelectric generation due to the flow of electrons.

References

References

- ABELES, B., et al., 1962, *Phys. Rev.*, 125, 44.
- ALTENKIRCH, E., 1909, *Phys. Zeits.*, 10, 560.
- 1911, *Phys. Zeits.*, 12, 920.
- ANON. 1969, *Gas J.*, 339, 56.
- BARGEN, D. W., 1963, *Ad. Energy Conv.*, 3, 507.
- BECQUEREL, A. C., 1826, *Annales de Chimie*, 31, 371.
- 1829, *Annales de Chimie*, 41, 353.
- BLOOM, H., 1959, *Rev. Pure & Appl. Chem.*, 9, 139.
- BLOOM, H., & E. HEYMAN, 1947, *Proc. Roy. Soc. (London)*, A188, 392.
- BLOOM, H., et al., 1965, *Aust. J. Chem.*, 18, 1171.
- BOCKRIS, J. O' M. et al., 1960, *Proc. Roy. Soc. (London)*, A225, 558.
- BRIDGEMAN, P. W., 'The Physics of High Pressures', (Bell, London), 1949.
- CLARK, L., 1876, *I. E. E. Journal*, 5, 321.
- CORBETT, G., & S. WINBUSH, 1955, *J. Amer. Chem. Soc.*, 77, 3964.
- CUBICCIOTTI, D., 1964, 'The Encyclopedia of Electrochemistry', Ed. C. A. Hampel, (Reinhold, New York), p 635.
- CUMMING, J., 1823, *Trans. Camb. Phil. Soc.*, 2, 47.
- CUTLER, M., & C. E. MALLON, 1965, *J. Appl. Phys.*, 36, 201.
- DANCY, E. A., 1965, *Trans. Met. Soc. A. I. M. E.*, 233, 270.
- DELIMARSKII, I. U. K., & B. F. MARKOV, (Trans. by A. Peiperl), 1961, 'Electrochemistry of Fused Salts', (Sigma, Washington).
- DETIG, R. H., & D. H. ARCHER, 1963, *J. Chem. Phys.*, 38, 661.
- DISMUKES, J. P. & F. D. ROSI, 1965, *A. I. Chem. E. — I. Chem. E., Symposium Series*, 5, 53.
- DUPUY, J., 1964, *C. R. Acad.*, 258, 158.
- EPSTEIN, A. S., 1963, *J. Appl. Phys.*, 34, 3587.
- EWING, C. T., et al. 1962, *J. Chem. Engng. Data.*, 7, 246.
- FARADAY, M., 'Experimental Researches in Electricity' (Taylor & Francis, London), 1839, Vol. 1, Series 3, Para. 349.
- FISCHER, W., 1966, *Z. Naturf.*, 21a, 281.

- FLEISCHMANN, H., et al., 1959, Z.Naturf., 14a, 999.
 1961, Z.Naturf., 16a, 765.
 1963, Z.Naturf., 18a, 646.
- FRITTS, R.W., 1960, A.I.E.E. Trans., 78, 817.
- GAMBILL, W.R., 1959, Chem. Engng., 66, 129.
- GLAZOV, V.M., et al., 'Liquid Semiconductors', (Plenum Press, N.Y.), 1969.
- GOLDSMID, H.J., 'Applications of Thermoelectricity', (Methuen, London), 1960.
- GREGORCZYK, Z., 1960, Roczniki Chem., 34, 621.
- HAMER, W.J., et al., 1956, Electrochem. Soc. J., 103, 8.
 1965, Electrochem. Soc. J., 112, 750.
- HANSEN, M., 'Constitution of Binary Alloys', (McGraw-Hill, New York), 1958, (Ag-Bi diagram page 10).
- HEIKES, R.R. & R.W. URE, 'Thermoelectricity: Science and Engineering', (Interscience, N.Y.), 1961.
- HOLTAN, Jr. H., 1953, Proc. Kon. Ned. Ak. v. Wet., 56, 498.
- IOFFE, A.F., 'Semiconductor Thermoelements and Thermoelectric Cooling', (Infosearch: London), 1957.
- JAMIESON, D.T. & J.S. TUDHOPE, 1964, N.E.L. Report 137.
- JANZ, G.J., 'Molten Salt Handbook', (Academic Press, N.Y.), 1967.
- JOHANSEN, E.S., Ann. d. Physik., 33, 517, (1910).
- JOHNSON, E.W. and R.L. READAL, 1963, Adv. Energy Conv., 3, 407.
- JOULE, J., 1841, Phil. Mag., 19, 260.
- KELLY, C.M., 1962, A.I.E.E. Pacific Energy Conf. Proc.: Direct Conversion, Paper 26.
- KLEMM, A. 1964, in 'Molten Salt Chemistry', Ed. M. Blander, (Wiley, N.Y.), page 535.
- KUBASCHEWSKI, O., et al., 'Metallurgical Thermochemistry', 4th Ed., (Pergamon, London), 1967.
- KVIST, A., 1967, Goth. Studies Phys., 2, (38pp).
- KVIST, A., & A. RANDELA, 1966, Z.Naturf., 21a, 278.
- KVIST, A., et al., 1966, Z.Naturf., 21a, 184.

- LUBELL, M.S., & R. MASELSKY, 1965, *Solid State Electronics*, 8, 729.
- LUCKS, C.F. & H.W. DEEM, 1956, *Prepr. Amer. Soc. Mech. Engrs.*, 56-5A-31.
- MARKOV, B.F., 1956, *Doklady Akad. Nauk. S.S.S.R.*, 108, 115.
- MARKOV, B.F., & E.B. KUZYAKIN, 1967, *Ukr. Khim. Zh.*, 33, 1097.
- 1968a, *Dopov. Akad. Nauk. Ukr.*, Ser. B, 30, 138.
- 1968b, *Ukr. Khim. Zh.*, 34, 860.
- MAZUR, P., 1954, *J. Phys. Chem.*, 58, 700.
- MEISSNER, H.P. et al., 1956, *Adv. Energy Conv.*, 5, 205.
- MILNE, H.R., 1939, *Brit. Patent*, 510,410; and 501,411, (Feb. 24.).
- MOGILEVSKII, B.M., & O.U. USMANOV, 1967, *Elektrokhimiya*, 3, 1124.
- MÖNKEMEYER, K., 1906, *Neues Jahrb. Mineral Geol. Beilage Bd.*, 22, 1.
- MORSE, J.G., 1966, *U.K.A.E.A.-E.N.E.A. Proc. Sym. on Ind. Appl. for Isotope Powered Generators*, Harwell.
- MURGULESCU, G., et al., 1963, *Electrochim Acta.*, 8, 65.
- NICHOLS, A.R. Jr., & C.T. LANGFORD, 1960, *Electrochem Soc. J.*, 107, 842.
- PELTIER, J.C.A., 1834, *Annales de Chimie*, 56, 371.
- PEPPER, V.D., et al., 1964, *Am. Soc. Agric. Engrs. Trans.*, 7, 170.
- PITZER, K.S., 1961, *J. Phys. Chem.*, 65, 147.
- POINCARÉ, L., 1890, *Annl. Chim. Phys.*, 6, (21), 289.
- POOLE, M.J., 1967, *Brit. Nuclear Energy Soc. J.*, 6, 206.
- RAO, M.R., 1941, *Phys. Rev.*, 59, 212.
- RAYLEIGH, J.W., 1892, *Phil. Mag.*, 34, 481.
- REDDY, T.B., 1966, *J. Electrochem. Soc.*, 113, 117.
- REINHOLD, H., 1928, *Z. Anorg. Allgem. Chem.*, 171, 181.
- ROSI, F.D., et al., 1961, *R.C.A. Review*, 22, 82.
- ROSSTKOWSKI, A.P., 1929, *Zh. Russ. Fiz. Khim. Obsh.*, *Chast Khim.*, 61, 595.
- RUCH, J., & J. DUPUY, 1965, *C.R. Acad. Sc. Paris*, 261, 957.
- SANDONNINI, C., 1914, *Gazz. Chim. Ital.*, 44, 290.
- SCHNEEBaum, R. & B.R. SUNDHEIM, 1961, *Far. Soc. Disc.*, 39, 197.
- SEEBECK, T.J., 1822-3, *Abhandl. d. Berlin Akad.*, 10, 265. (Also called *Pogg.*, 4.).

- SENDEROFF, S., & R.I. BRETZ, 1962, *J. Electrochem. Soc.*, 109, 56.
- SINISTRÌ, C., 1965, *Z. Naturforsch.*, 20a, 1045.
- 1966, *Z. Naturforsch.*, 21a, 753.
- SINISTRÌ, C. & E. PEZZATI, 1967, *Ricerca Sci. (Italy)*, 37, 111.
- SPRING, K.H., Ed., 'Direct Generation of Electricity', (Academic Press, London), 1965.
- SPRING, K.H., & D.T. SWIFT-HOOK, 1962, *Brit. J. Appl. Phys.*, 13, 159.
- STONEBURNER, D.F., et al., 1959, *Trans. Met. Soc. A.I.M.E.*, 215, 879.
- 1965, *Trans. Met. Soc. A.I.M.E.*, 233, 153.
- SUNDHEIM, B.R., 1960, in 'Thermoelectric Materials and Devices', Eds. I.B. Cadoff & E. Miller, (Reinhold : New York), Chapter 14.
- SUNDHEIM, B.R., & J. ROSENSTREICH, 1959, *J. Phys. Chem.*, 63, 419.
- SUTTON, G.W., 'Direct Energy Conversion', (McGraw-Hill, New York), 1966.
- TAIT, P.G., 1873, *Nature*, 8, 86.
- TAIT, R.W.F., & B.A. HILLS, 1964, *Ind. & Engng. Chem.*, 56, 29.
- TELKS, M., 1947, *J. APPL. Phys.*, 18, 1116.
- TEMKIN, M.I., & A.V. KHOROSHIN, 1952, *Zh. Fiz. Khim.*, 26, 500.
- THOMSON, W., 1851, *Proc. R.S. Edin.*, 3, 91.
- TUBANDT, C., & E. LORENZ, 1914a, *Z. Phys. Chem.*, 87, 513.
- 1914b, *Z. Phys. Chem.*, 87, 543.
- TURNBULL, A.G., 1961a, *Austral. J. Appl. Sci.*, 12, 30.
- 1961b, *Austral. J. Appl. Sci.*, 12, 324.
- VARGAFTEK, N.B., 1952, *Bull. All. Un. Pwr. Engng. Inst.*, 21, 1.
- WAGNER, C., 'Thermodynamics of Alloys', (Addison-Wesley, Cambridge, Mass.), 1952.
- WALL, T.F., 1927, *Elect. Rev.*, page 847.
- WARE, R.M., & McNEILL, 1964, *Proc. I.E.E.*, 3, 178.
- WARTANOWICZ, T., 1964, *Adv. Energy Conv.*, 4, 149.
- WHITE, L.R., & H.T. DAVIS, 1967, *J. Chem. Phys.*, 47, 5433.
- WHITTAKER, E., 'History of the Theories of Aether and Electricity', (Nelson, London), 1951.

WRIGHT, D.A., 1965, in 'Direct Generation of Electricity', Ed.
K.H. Spring, (Academic Press, London), chapter 5.

ZUEV, K.P., 1960, Soviet Physics - Solid State, 1, 1007.
